Master of Science Thesis

The influence of core permeability on the stability of interlocking, single layer armour units

Physical model test

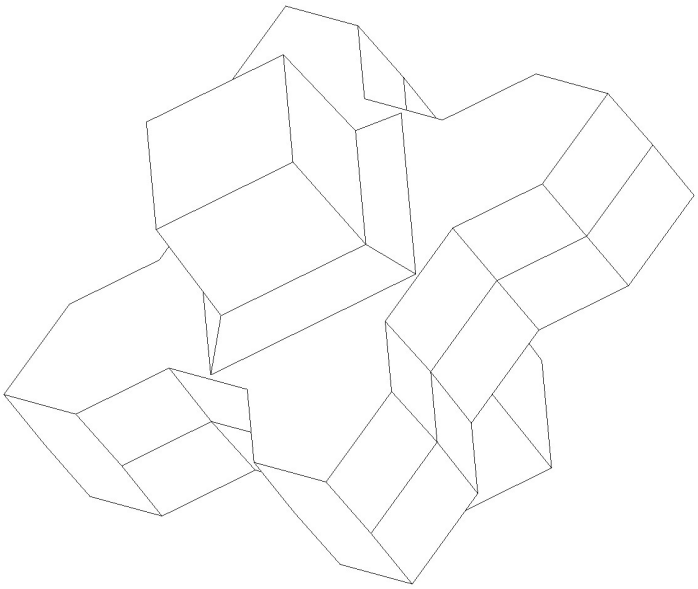

Author:
Ilse Verdegaal
May 2013

Delft University of Technology
Faculty of Civil Engineering and Geosciences
Section Hydraulic Engineering

Delta Marine Consultants
Department Coastal Engineering

Master of Science Thesis

The influence of core permeability on the stability of interlocking, single layer armour units

Supervisors:

Prof. dr. ir. W.S.J. Uijttewaal	(CITG, TU Delft)
ir. J.P. van den Bos	(CITG, TU Delft)
ir. A. van den Berg	(CITG, TU Delft)
ir. B.N.M. van Zwicht	(Delta Marine Consultants)

Delft University of Technology
Faculty of Civil Engineering and Geosciences
Section Hydraulic Engineering
Stevinweg 1
P.O. Box 5048
2600 GA Delft
The Netherlands

Delta Marine Consultants
Tradename of BAM Infraconsult bv
H.J. Nederhorststraat 1
P.O. Box 268
2800 GA Delft
The Netherlands

Master of Science Thesis

The influence of core permeability on the stability of interlocking, single layer armour units

List of trademarks used in this report:

- Accropode is a registered trademark of Sograh Consultants, France;
- Core-Loc is a registered trademark of US Army corps of Engineers, USA;
- Delta Marine Consultants (DMC) is a registered trade name of BAM Infraconsult bv, The Netherlands;
- Xbloc is a registered trademark of Delta Marine Consultants (DMC), The Netherlands;

The use of trademarks in any publication of Delft University of Technology does not imply any endorsement or disapproval of this product by the University.

PREFACE

This thesis has been performed to fulfill the requirements for the degree Master of Science in the field of Hydraulic Engineering at Delft University of Technology. The report contains the results of a study on the effect of core permeability on the hydraulic stability of single layer interlocking armour units.

This thesis can be seen as an extension on the current knowledge of the effect of core permeability on the stability of the armour layer. Besides the armour stability, the study gives insight in the physical background of the failure mechanisms and hereby provides a more complete overview of the effect of core permeability.

Physical model tests on the hydraulic stability of armour units took place in the Hydraulic Laboratory of the coastal department of BAM Infraconsult, which operate under the tradename Delta Marine Consultants. In addition to the model tests, experimental research on the permeability of rock gradings have been carried out at the Environmental Mechanics Fluid Laboratory of the Faculty of Civil Engineering Geosciences.

I would like to thank my graduations committee, professor dr ir W.S.J. Uijttewaal, ir. J.P. van den Bos, ir. A. van den Berg and ir. B.N.M. van Zwicht for their supervision and patience. Furthermore, I would like to thank all members of Delta Marine Consultants for their expertise and the nice work environment.

Finally, I would like to thank my mother and sister for their unconditional support throughout my study and I would like to thank especially my friends for their support during the last months of my thesis.

Ilse Verdegaal
Gouda, May 2013

SUMMARY

Introduction

Rubble mound breakwaters are used on many locations around the world. Their predominant function is to protect adjacent coastal areas against erosion and excessive wave action, by energy dissipation inside the structure. The permeability of the structure is therefore an important feature for the stability of the breakwater as a whole. However, different trade-offs exist between the costs and design of a breakwater. For financial or design reasons the core can be designed either more or less permeable. This affects the hydraulic stability of the armour layer to a certain extent. There is still lack of understanding about the balance between core permeability and the stability of armour units.

The focus of this thesis is to study the influence of core permeability on the stability of single layer interlocking armour units in general and Xblocs in particular. In this study, permeability is explained as the ease with which water flows through granular material. This means that low core permeability has a low water penetration into the core, increasing the flow forces on the armour units and thereby induces failure of the armour layer. The objective of this study can be defined as follows:

> *The goal of this thesis is to extend the knowledge on the failure mechanisms of the armour layer for different structural permeabilities and use this knowledge to define correction factors on the unit weight for single layer interlocking armour.*

Research method

For this study, the permeability of the core is of great importance. However, no straightforward theoretical method exists to determine the permeability of rock material. To overcome this problem and to assure differences in permeability of the rock gradings, the permeability of each individual rock grading is determined with a permeameter at the Environmental Mechanics Fluid Laboratory of the Faculty of Civil Engineering Geosciences.

The study of Burcharth & Andersen (1993) on core permeability indicates a great change in the water profile around the armour units, which affects the hydraulic stability. To analyse the influence of core permeability on the failure mechanisms of the armour layer and the physical background of these mechanisms, physical model tests have been performed in the Delta flume of Delta Marine Consultants in Utrecht. Three core permeabilities were used: an open core that has an equal size as the filter grading, an impermeable core that is represented by a wooden plank with small stones on top and a normal core following from Burcharth et al. (1999) for scaling core material of small scale model tests.

Conclusions

In this study the armour stability and water profile in the armour layer have been investigated. Damage of the armour layer was observed and the water level on and under the armour layer was recorded using two run-up gauges. The evaluation of the water level on and under the armour layer indicated the following changes in the water elevation, velocity and hydraulic gradient in the armour layer due to core permeability:

1 The maximum run-down level on the armour layer increases with decreasing permeability;

2 The hydraulic gradient in the armour layer at maximum rund-down increases with decreasing core permeability;

3 The maximum run-up level on the armour layer remains approximately the same;

4 The maximum run-up level on the filter layer increases with decreasing permeability;

5 The location of the maximum hydraulic gradient shifts towards the maximum run-down;

6 Larger flow accelerations near the maximum run-down increases with decreasing permeability;

7 The maximum uprush and downrush velocities on the armour layer remain approximately the same;

The observed key failure mechanisms for this physical model test are separated in lifting of the armour units, settling of the armour layer, rocking of units and collapsing waves. The individual contribution of the water elevation, velocity and hydraulic gradient in the armour layer could be linked to flow forces that might induce the failure mechanisms.

The maximum uprush velocity and the maximum downrush velocity [7] parallel to the slope remain approximately the same and cannot cause differences in failure mechanism. However to overcome the larger distance between the run-up and increased run-down for an impermeable core [1], leads to a larger average velocity. This means that the average force parallel to the armour layer is larger for an impermeable core than for an permeable core.
The run-down levels under the armour layer are smaller than on the armour layer, generating an hydraulic gradient in the armour layer [2]. This hydraulic gradient indicates the size and the direction of the out- and inflow. It has been confirmed that the outflow has an important role in the lifting of armour units. The force that contributes most to uplifting the armour layer is the turbulent acceleration force [6], which rotates the units in upward direction at maximum run-down. Measurements showed that the maximum hydraulic gradient during the run-down increases with an impermeable core. Larger hydraulic gradients in the armour layer indicate larger forces parallel to the slope. This increases flow accelerations during maximum run-down and thereby the lifting mechanism. Additional to the size of the hydraulic gradient, the shift of the maximum hydraulic gradient in time [5] for an impermeable core induces also the acceleration forces at maximum run-down. However, smaller hydraulic gradients in the armour layer indicate smaller forces but relative large forces in outward direction of the slope. These forces induce extraction of armour units out of the armour layer. .
Settling of the armour layer is caused by large downward forces and lost of friction forces between armour layer and under layer. Forces parallel to the armour layer are mainly induced by the flow velocity. Loss of friction between armour layer and under layer might be caused by the negligible inflow forces into the core [4], which increased the pore pressure in front of the core. The degree of settlement of the armour layer influences the space for movement between the armour units and thereby the rocking of armour units. This means that settling of the armour layer reduces the failure mechanism rocking. It is therefore concluded that some settling of the armour layer is not negative by definition.
A change of breaker type was observed for the impermeable core under attack of wind waves. This indicates a shift in the breaker type and can be explained by the fictitious steeper slope angle due to the water volume in the armour layer [2].

The observed key failure mechanisms for the physical model test are settling of the armour layer, rocking of units, lifting of the armour units and collapsing waves. The impact of the various failure mechanisms on the armour stability for the open, normal and impermeable are presented in table 0.1.

++	Great impact
+	Large impact
+/-	Moderate impact
-	Low impact
- -	No impact

Failure Mechanism	**Open core**	**Normal core**	**Impermeable core**
Settling of armour layer	-	+/-	++
Rocking	+	+/-	-
Lifting of armour units	-	+	++
Extraction of armour units	+	-	- -
Collapsing waves	- -	-	+

Fig. 0.1: Overview of the failure mechanism, impact and flow force for the open, normal and impermeable core.

Damage to the open core occurs mainly due to low interlocking forces inducing rocking and extraction of armour units out of the armour layer. Mainly rocking ensures that damage of the armour layer occurred earlier than normal. For the normal core, it is found that settling and lifting of armour units have a great impact on the damage progression. Both, lifting of armour units as settling of the armour layer ensures that damage and failure of the armour layer occurred earlier than normal.
It was found that both the open and impermeable core encounter a lower armour stability than the normal core. This is due to different failure mechanisms, illustrated in table 0.1. The result of the study showed that an open core is more sensitive for wind wave and the impermeable core for swell waves. The correction factors on the unit weight found for an impermeable and open core are 2.41 and 1.17. Table 0.1 contains an overview of the recommended correction factors based on the test results.

Correction factor		
Wave spectrum	Core	Unit weight
Xbloc guideline	Impermeable Open	2.00 -
Wind waves	Impermeable Open	- 1.2
Swell waves	Impermeable Open	2.5 -

Tab. 0.1: Correction factors

Discussion

Decades ago, the influence of structural permeability on the hydraulic stability of armour units has been indicated by Van der Meer (1988b) in a study on rock armour. The study avoided the complexity of rock material and introduced a new parameter called 'notional' permeabiltiy (P), which can be related to four breakwater cross-sections with different structural permeabilities.
It is generally assumed that the effect of decreased core permeability on the hydraulic stability of single layer armour units has the same effect as on the hydraulic stability of double layered rock armour. However, the stability mechanism of single layer interlocking armour units is different from gravity based rock units. Therefore, it can be expected that variations in the stability mechanism lead to different failure mechanisms and react differently on deviations in core permeability. For instance, Burcharth (1998) found a larger correction coefficient for a low permeable core than suggested by the P factor of Van der Meer (1988b). The hypothesis of this study is therefore:

The effect of core permeability on the stability of single layer interlocking armour units cannot be compared to that of rock armour units resulting in a different stability trend of the armour units than suggested by Van der Meer (1988b) with the structural permeability parameter P.

This hypothesis is confirmed for single layer interlocking armour units such as Xblocs. Van der Meer (1988b) suggested that for highly permeable structures the hydraulic stability of the armour layer increases. However, for a single layer interlocking armour units this is not the case. The stability factor of a single layer interlocking armour unit is based on interlocking forces between neighbouring units. The required interlocking forces between the units are achieved by initial settlements of the armour layer. The settlements of an armour layer on an open core are smaller than on a normal core increasing the probability of rocking. Furthermore, the flow forces in the armour layer are directed more perpendicular to the slope in case of an open core. This increases the outward forces and the probability of extraction of armour units out of the armour layer. Rock armour is not affected by these changes due to definition of damage and the larger unit weight.
For highly permeable breakwaters it is concluded that; the reduced settlements of the armour layer increase the potential occurrence of damage due to the rocking of armour units and increase the probability of extraction. It could not be confirmed that single layer interlocking armour units with a larger structural permeability have a higher hydraulic stability.

Van der Meer (1988b) suggests for an impermeable core a decrease in hydraulic stability of the armour layer. This study found a similar dependence between core permeability and the hydraulic stability of single layer interlocking armour units. However, the mechanism behind the decrease in armour stability of single layer interlocking armour units less straightforward than for rock armour. It can be confirmed that a similar trend occurs for single layer interlocking armour units as for rock armour in case of an impermeable core.

CONTENTS

Preface . . . iv

Summary . . . vii

List of symbols . . . xv

1. Introduction . . . 1
1.1 Breakwaters . . . 1
1.2 Armour layer . . . 2
1.3 Problem description . . . 3
1.4 Research objective . . . 4
1.5 Hypothesis . . . 4
1.6 Research approach . . . 5
1.7 Report outline . . . 5

2. Armour stability . . . 7
2.1 General . . . 7
2.2 Parameters . . . 8
2.2.1 Hydraulic parameters . . . 8
2.2.2 Structural parameters . . . 8
2.3 Wave-structure-interaction . . . 9
2.3.1 General . . . 9
2.3.2 Breaker type . . . 9
2.3.3 External water motion . . . 10
2.3.4 Internal water motion . . . 11
2.4 Forces . . . 12
2.4.1 Stabilisation forces . . . 12
2.4.2 destabilisation forces . . . 13
2.5 Description of armour stability . . . 14
2.6 Summary . . . 15

3. Core permeability . . . 17
3.1 General . . . 17
3.2 Forchheimer model . . . 17
3.2.1 Darcy flow . . . 18
3.2.2 Forchheimer flow . . . 18
3.2.3 Fully turbulent flow . . . 19
3.2.4 Non-stationary flow . . . 20
3.3 Wave induced pore pressure model . . . 21
3.4 Structural permeability in stability formulas . . . 23
3.4.1 General . . . 23
3.4.2 Correction factor . . . 24
3.4.3 Conclusion . . . 25

4. Permeability test . . . 27
4.1 General . . . 27
4.2 Rock samples . . . 27
4.3 Experimental set-up . . . 28
4.3.1 Permeameter . . . 28

4.3.2 Rock sample . . . 29
4.4 Testing procedure . . . 30
4.5 Test conducted . . . 31
4.6 Results . . . 32
4.6.1 Porosity . . . 32
4.6.2 Permeability . . . 32
4.7 Analyse . . . 33
4.7.1 Test data . . . 33
4.7.2 Theory . . . 34
4.8 Conclusion . . . 35

5. Physical scale model . . . 37
5.1 scaling . . . 37
5.1.1 scaling rules . . . 37
5.1.2 Scale effects . . . 38
5.2 Experimental set-up . . . 39
5.2.1 Wave flume . . . 39
5.2.2 Foreshore . . . 39
5.2.3 Armour layer . . . 39
5.2.4 First under layer . . . 40
5.2.5 core . . . 41
5.2.6 slope angle . . . 43
5.2.7 water level . . . 43
5.2.8 Crest height and width . . . 43
5.2.9 Toe . . . 44
5.2.10 Crest and rear slope . . . 44
5.2.11 Wave spectrum . . . 44
5.2.12 Measuring data . . . 45
5.2.13 Model layout . . . 46
5.3 Core gradings . . . 48
5.3.1 General . . . 48
5.3.2 Core configuration . . . 48
5.4 Test program . . . 50
5.4.1 Hydraulic parameters . . . 50
5.4.2 Test duration . . . 50
5.4.3 Programme . . . 51
5.5 Damage description . . . 51

6. Test results . . . 53
6.1 General . . . 53
6.2 Failure mechanisms . . . 53
6.3 Observations . . . 54
6.3.1 Swell waves . . . 55
6.3.2 Wind waves . . . 57
6.4 Data analyse . . . 59
6.4.1 Swell waves . . . 59
6.4.2 Wind waves . . . 61
6.5 Discussion . . . 63
6.5.1 Water motion around the armour layer . . . 63
6.5.2 Settlement . . . 66
6.5.3 Rocking . . . 69
6.5.4 Lifting of armour units . . . 70
6.5.5 Collapsing breaker . . . 70
6.5.6 Hydraulic stability . . . 71
6.6 Comparison with rock armour units . . . 72
6.7 Conclusion . . . 78

7. Conclusions and recommendations . . . 81
7.1 Conclusion . . . 81

7.2 Limitations for usage . . . 83
7.3 Recommendation . . . 84

References . . . 88

List of figures . . . 91

List of tables . . . 93

Appendix 95

A. Correction factors . . . 96

B. Rock properties . . . 97

C. Rock gradings . . . 99

D. Shape coefficients . . . 100
D.1 Experiments . . . 100
D.2 Previous research . . . 104

E. Core configurations . . . 107

F. Wave data . . . 109
F.1 Naming of test series . . . 109
F.2 Calibration . . . 109
F.3 Wave distribution . . . 110

G. Start and 100% photos . . . 115

H. Damage observations test series . . . 125
H.1 Open core . . . 125
H.2 Normal core . . . 127
H.3 Impermeable core . . . 128

I. Relative placement densities . . . 130

J. Data analyse . . . 132
J.1 General . . . 132
J.2 Accuracy and reliability . . . 132
J.3 Run-up and run-down level . . . 135
J.4 Hydraulic gradient . . . 139
J.5 Velocity . . . 144
J.6 Wave reflection . . . 145

LIST OF SYMBOLS

ROMAN SYMBOLS

Symbol	**Description**	**Unit**
a	Laminar Forchheimer term	[-]
b	Turbulent Forchheimer term	[-]
c	Time dependent Forchheimer term	$[T^2/L]$
C_f	Reflection coefficient	[-]
D	Armour unit height	[L]
d	sieve size	[L]
d_{50}	Median sieve size	[L]
d_n	Nominal grain diameter	[L]
d_{n50}	Median nominal grain diameter depending on W_{50}	[L]
Fr	Froude number	[-]
F_D	Drag force	[F]
F_G	Gravitational force	[F]
F_I	Inertia force	[F]
F_L	Lift force	[F]
g	Gravitational acceleration	$[L/T^2]$
H	Wave height	[L]
H_d	Design wave height	[L]
H_i	Incoming wave height	[L]
H_r	Reflected wave height	[L]
H_s	Significant wave height	[L]
I	Hydraulic gradient	[-]
KC	Keulegan-Carpenter number	[-]
K	Hydraulic conductivity	$[L/T]$
K_d	Stability parameter	[-]
L	Characteristic length	[L]
L_{op}	Deep water wave length of the peak period	[L]
L_x	Average horizontal length	[L]
L_y	Average vertical length	[L]
L'	Wave length inside the core	[L]
N	Number of waves	[-]
N_{od}	Damage definition for this thesis	[-]
N_s	Stability number	[-]

N_x	Number of Xbloc in the x-direction	[-]
N_y	Number of Xbloc in the y-direction	[-]
n	Porosity	[-]
P	Notional permeability (Van der Meer, 1988b)	[-]
p	Pressure	[F/L^2]
p_o	Reference pressure	[F/L^2]
Q	Discharge	[L^3/T]
Re	Reynolds number	[-]
R_u	Run-up level	[L]
S	Damage level (Van der Meer, 1988b)	[-]
s	Wave steepness	[-]
s_{op}	Fictitious deep water steepness with peak period	[-]
T	Wave period	[T]
T_p	Peak period	[T]
T_m	Mean period	[T]
t	Time	[T]
u	Pore velocity	[L/T]
V	Average velocity	[L/T]
W	Weight of block	[M]
W_{50}	50% value on the mass distribution curve	[M]

GREEK SYMBOLS

Symbol	**Description**	**dimension**
α	Slope angle	[degree]
α	Laminar shape factor Forchheimer flow	[-]
α'	Laminar shape factor Fully turbulent flow	[-]
α"	Laminar shape factor Darcy flow	[-]
β	Turbulent shape factor Forchheimer flow	[-]
β'	Turbulent shape factor Fully turbulent flow	[-]
Δ	Relative density	[-]
δ	Damping coefficient	[-]
ξ_E	Ration between laminar and turbulent flow	[-]
ξ_m	Surf similarity parameter using mean wave period	[-]
ξ_p	Surf similarity parameter using peak wave period	[-]
ν	Kinematic viscosity	[L^2/T]
μ	Friction coefficients	[-]
ρ_s	Density rock	[-]
ρ_w	Density water	[-]

1. INTRODUCTION

The focus of this Master thesis is a study on the influence of core permeability on the stability of single layer interlocking amour units. The results of the study are presented in this thesis.
First the relevance of core permeability will be explained in a short introduction on breakwaters. Thereafter the motive and the goal of this research will be given in the problem description and the objective.

1.1 Breakwaters

Breakwaters are used on many locations around the world. Their predominant function is to protect adjacent coastal areas against erosion and excessive wave action, by reflecting the wave energy and turbulent dissipation. There are two main types of breakwaters; monolithic and rubble mound breakwater. Monolithic breakwaters provide a sheltered area by reflection of waves while on the other hand rubble mound breakwaters dissipate energy by turbulent flow inside the structure. This study focusses in particular on the rubble mound breakwater that basically consists of a mound of loose elements.
The general lay-out of a rubble mound breakwater consists out of various layers, such as an armour layer, one or multiple filter layers and the core. The core generally contains the largest volume of material that can range from sand to quarry-run. The core material in general is too small to resist wave forces during adverse weather conditions, therefore it is armoured by a layer of larger elements (so called armour layer) to assure the stability of the entire structure. The filter consist one or multiple layers of rock placed between the core and armour layer, preventing the core from washing out through the pores of the larger armour stones. Figure 1.1 illustrates a typical cross-section of a rubble mound breakwater.

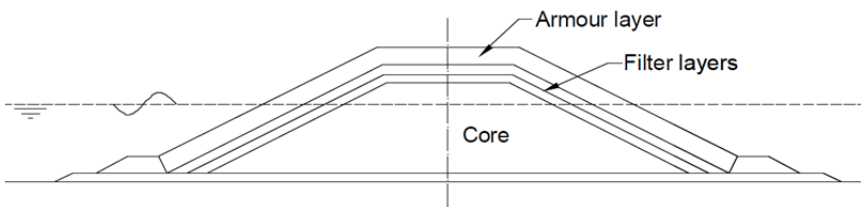

Fig. 1.1: Cross-section of a rubble mound breakwater

The size of the core material, and thereby the permeability of the core, is an important feature in the stability of a rubble mound breakwater as a whole. The effect of core permeability on the stability of the armour layer is explained in general by water penetration into the core of the structure. Higher permeability reduces the reflection and the loads on armour units. However, some predominant reasons might motivate engineers to use low permeable material over conventional quarry- run for a rubble mound structure as (i) economical reasons and (ii) zero per cent transmission requirements in the area behind the breakwater by the client. Although the economical and zero-transmission requirements are fulfilled with an impermeable core, the stability of the armour layer is not always guaranteed.
A good illustration of a damaged breakwater where the effect of an impermeable core has been misjudged, is the breakwater at IJmuiden, the Netherlands, where on multiply occasions concrete elements of 45 tons have been swept away. The cross-section of the breakwater of IJmuiden is presented in figure 1.2. The breakwater was constructed with a stone asphalt layer, which turned out to be insufficient, mainly because of the water pressure inside the core. Soon after construction large heavy concrete cubes were placed on top of the entire asphalt stone layer. After almost 40 years an increased damage level was observed possibly caused by the impermeable asphalt stone layer under the heavy blocks.

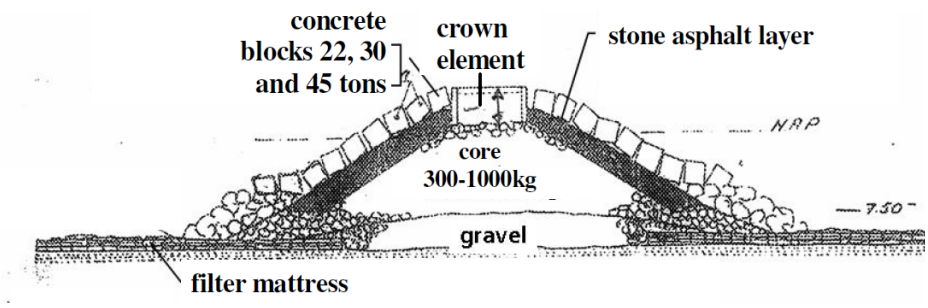

Fig. 1.2: Cross-section of the breakwater of IJmuiden (Reedijk et al., 2008)

1.2 Armour layer

The armour layer of a breakwater has two main functions being; providing overall stability of the entire construction by preventing washing out of smaller material and energy dissipation by wave breaking and turbulent flow.
The armour layer can be constructed from either rock or concrete armour units, depending on both the availability of the required rock dimensions in the local quarry and the wave conditions. Armour units can be classified by shape, stability factor and placement as shown in table 1.1. Influencing the slope roughness and energy dissipation on the breakwater. The main difference between the various types of armour elements is the variation in stability mechanism.
The stability of rock armour stones is mainly caused by gravitational forces. This means that the weight of the unit provides the stability of the armour layer. Gravity based armour layers are typically placed in a double layer to allow some damage. Armour units based on friction, gain their stability from friction with neighbouring units and under layer. The armour layer is uniformly placed to generate maximum contact area and thereby friction forces. The stability of interlocking armour units is mainly based on interlocking with surrounding units but increase their stability by gravity forces. This means interlocking units can be designed lighter than non-interlocking units under similar design conditions generating a more economical concrete armour unit. An advantage of slender, randomly placed elements is an increased energy dissipation by turbulence due to the very open structure.

Both friction and interlocking based armour units are placed in a single layer. The main disadvantage of a single layer is that less energy will be dissipated by turbulent flow and that displaced armour units will immediately lead to exposure of the under layer to the waves. An exposed under layer might lead to washing out of rock material and progressive damage. These armour units are designed for zero-damage.
Since 2001, Delta Marine Consultants (DMC) developed a single layer interlocking armour unit called the Xbloc. The unit was designed to increase the hydraulic stability and structural integrity resulting in a slender but robust structure with a large economical advantage.

This research focused on stability of single layer interlocking concrete armour units in general and Xblocs in particular.

Placement pattern	**Number of layers**	**Shape**	**Stability factor(main contribution)**		
			Gravity	**Interlocking**	**Friction**
Random	Double layer	Simple	Antifer Cube, Modified Cube		
			Tetrapod, Alkmon, Tripod		
		Complex		Stabit, Dolos	
	Single layer	simple	Cube		Cube
		Complex		Stabit, Accro-pede, Core-loc, Xbloc	
Uniform	Single layer	simple	Haro		Seabee, Haro
		Complex			Cob, Shed, Tribar, Diode

Tab. 1.1: Armour unit classified by shape, placement and stability factor (CIRIA, 2007).

1.3 Problem description

An important design objective for rubble mound breakwater is to decrease the construction cost, which can be achieved by using less permeable material or impermeable material for the core, such as sand cores or geotextile containers. Although on the one hand the costs for the core reduces, larger armour elements might be required, increasing the costs for the armour layer on the other hand. Understanding of the balance between core permeability and the stability of armour units is of great importance for the design of an economical breakwater. The relation between core permeability and the increase of the armour size is therefore of importance to practical usage.

However, a straightforward relation between core permeability and the armour size is difficult to define due to the complexity of permeability. Van der Meer (1988b) suggested to avoid the complexity of rock material by comparing four breakwater cross-sections with different structural permeabilities. The four breakwater cross-sections are defined with a 'notional' permeability parameter as illustrated in figure 1.3. Configuration P=0.1, represents the lower boundary with an impermeable core, thin filter layer and armour layer. The upper boundary is a homogeneous structure of armour stones, indicated with P=0.6. The 'notional' permeability parameter is incorporated in the formula of van der Meer (1988b) (equation 1.1 and equation 1.2) to calculate the stability of a rock armour layer. For the preliminary design of the breakwater the cross section can be compared with the four different configurations, resulting in an estimation of P for the design formula.

$$\frac{H_s}{\Delta D_{n50}} = c_{pl} P^{0.18} (\frac{S}{\sqrt{N}})^{0.2} \xi_m^{-0.5} \qquad \text{Plunging waves} \qquad (1.1)$$

$$\frac{H_s}{\Delta D_{n50}} = c_s P^{-0.13} (\frac{S}{\sqrt{N}})^{0.2} \sqrt{\cot \alpha} \xi_m^{P} \qquad \text{Surging waves} \qquad (1.2)$$

Here, ξ is the surf similarity, S the level of damage, N the number of waves, D_{n50} the nominal diameter and H_s the significant wave height.

No guidelines are available on the effect of core permeability on the stability of armour units in the design of a single layer interlocking armour layer. DMC suggest a correction factor on the unit weight similar to the influence of structural permeability founded by Van der Meer (1988b). However, the stability mechanism of interlocking units differs from natural blasted rock armour and might therefore respond differently to deviations in structural permeability. Furthermore the thickness and porosity of the armour layer affects the energy dissipation in the armour layer, inducing the uncertainty in the stability of single layer interlocking armour units on an impermeable core.

In addition to the study of Van der Meer (1988b), Burcharth (1998) conducted a study on the effect of core permeability on single layer interlocking armour units. From these tests can be concluded that the single layer interlocking armour units are more sensitive to the permeability of the core than rock armour units. This means that the effect of structural permeability on single layer interlocking armour units might be higher than assumed in the proposed correction factors for Xblocs.

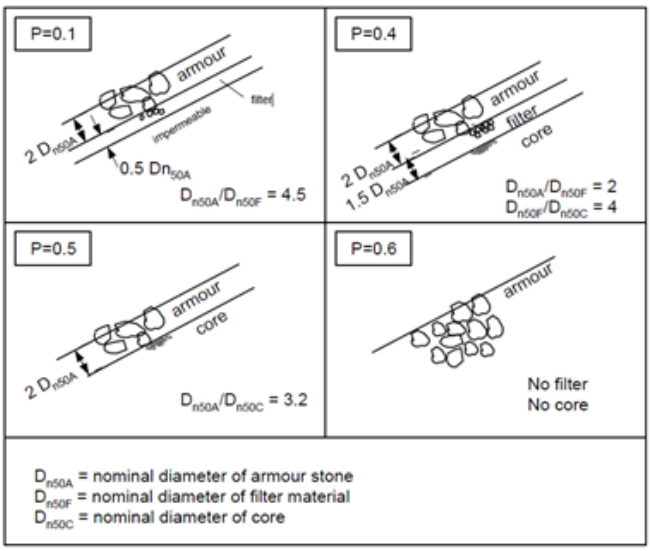

Fig. 1.3: Notional permeability configurations (Schiereck, 2001)

1.4 Research objective

The influence of the core permeability on the stability of single layer interlocking armour units is of both academic and practical importance. Knowledge on the relation between core permeability and single layer interlocking armour units will give a better understanding of the differences between rock amour units and single layer interlocking units, which is of academic importance and it will optimize the construction costs in practice. The ultimate goal is a to generate a complete overview of the effect of core permeability on the key destabilization forces and thereby on the failure mechanism of the armour layer. With this overview an extension of the current stability formulas for armour units can be deduced. This study will contribute to this goal by evaluating the stability of single layer interlocking armour units on a relative open core, normal core and impermeable core. The objective of this study can be defined as follows:

The goal of this thesis is to extend the knowledge on the failure mechanisms of the armour layer for different structural permeabilities and use this knowledge to define correction factors on the unit weight for single layer interlocking armour.

1.5 Hypothesis

In addition to the research objective, a hypothesis is set-up regarding the differences between rock armour layers and single layer interlocking armour units. In the past, several researchers performed physical model experiments on the effect of core permeability on the armour layer. The two most relevant studies are by Van der Meer (1988b) and Burcharth (1998) respectively describing the influence of core permeability on rock armour units and on single layer interlocking units. Van der Meer describes the influence of structural permeability with the factor P in the stability formula for rock armour layers, also known as the 'notional' permeability parameter. The rock armour stability formula is based upon a large amount of physical model tests with various variables such as wave period, wave height, slope angle and structural permeability. It is in general assumed that the trends in armour stability found by Van der Meer (1988b) are also valid for other armour units.

However, the stability mechanism of single layer interlocking armour units is different from gravity based rock units. Therefore it can be expected that variations in the stability mechanism lead to different failure mechanisms and thereby different correction factors for the structural permeability. For instance, Burcharth (1998) found a larger correction coefficient than suggested by the P factor of Van

der Meer (1988b).

The main hypothesis of this study is:

The effect of core permeability on the stability of single layer interlocking armour units cannot be compared to that of rock armour units resulting in a different stability trend of the armour units than suggested by Van der Meer (1988b) with the structural permeability parameter P.

1.6 Research approach

A literature study on the stability of the amour layer and effect of structural permeability has been conducted. In the literature study it was concluded that the stability of the armour layer depends on both the water motion around the units (loads) and the stability mechanism (strength). Structural permeability influences the water motion around the slope of the breakwater being the run-up and internal set-up. Changes in the water motion lead to an increase in forces on the units decreasing the hydraulic stability.
In order to study the influence of core permeability on the armour stability and flow profile, different core configurations have been tested. The main challenge in designing these configurations is that they must vary sufficiently in permeability so that changes in hydraulic stability of the armour layer can be assigned to core permeability. For this reason, it was decided to test the permeability of the rock material available using a permeameter at the Delft University of Technology. These test results have been used to validate the outcome of the physical model test.

The armour stability for the various configurations has been examined using physical model tests in the wave flume of Delta Marine Consultants, Utrecht. This is a widely used method in hydraulic engineering and is considered to be the base of many engineering formulae. The observed damage has been translated into damage levels and stability numbers, using visual observations, video and photo analysis.

In literature, the water profile in the armour layer is indicated to be important for the failure mechanisms. Therefore the water motion has been examined using data on the water motion along the slope, which was obtained during the physical model tests. Two run-up gauges were placed on and under the armour layer, measuring the water level continuously. The obtained data has been combined with observations of failure indicating the failure mechanism and empirical formulae of run-up and run-down levels and hydraulic gradient in the armour layer for rock armoured breakwaters.

1.7 Report outline

The literature is separated into two topics:

- Armour stability
- Core permeability

These topics are discussed in chapter 2 and chapter 3. The permeability tests are conducted prior the model tests in chapter 4. The model set-up is presented in chapter 5 of this report. The results of the experiments are processed and compared to the hypothesis in chapters 6 and 7. The final chapter elaborates on recommendations for improvements for further research. The outline is illustrated in the flow chart in figure 1.4.

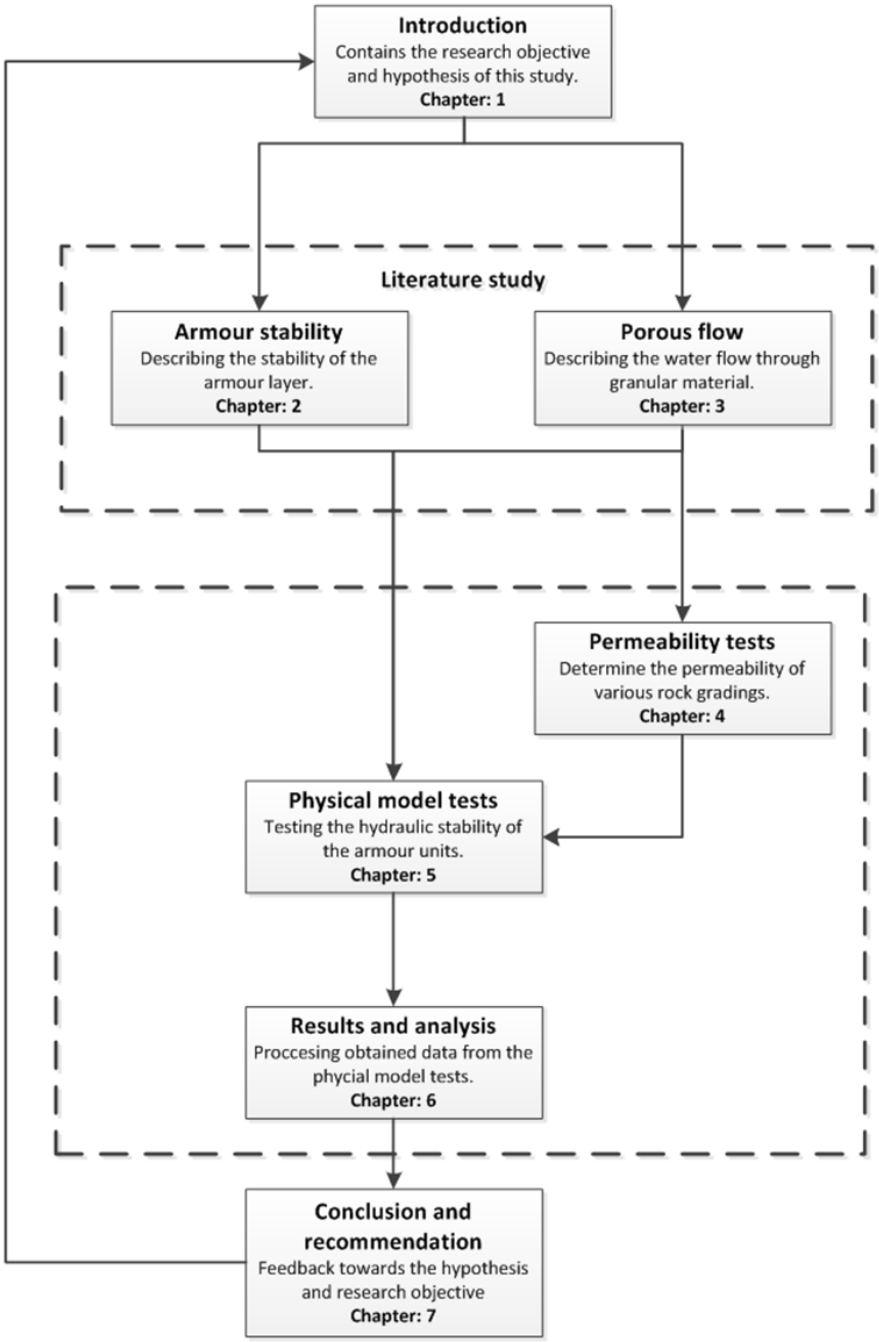

Fig. 1.4: Report outline

2. ARMOUR STABILITY

2.1 General

This chapter describes the effects of structural permeability on the stability of armour units on a breakwater slope under wave attack. Primarily, it is important to have an understanding of the processes which occur in a breakwater and the impact of the forces on the armour layer. Figure 2.1 shows a flow chart of the wave structure interaction of a coastal structure under wave attack. The figure is further explained in subsequent sections.

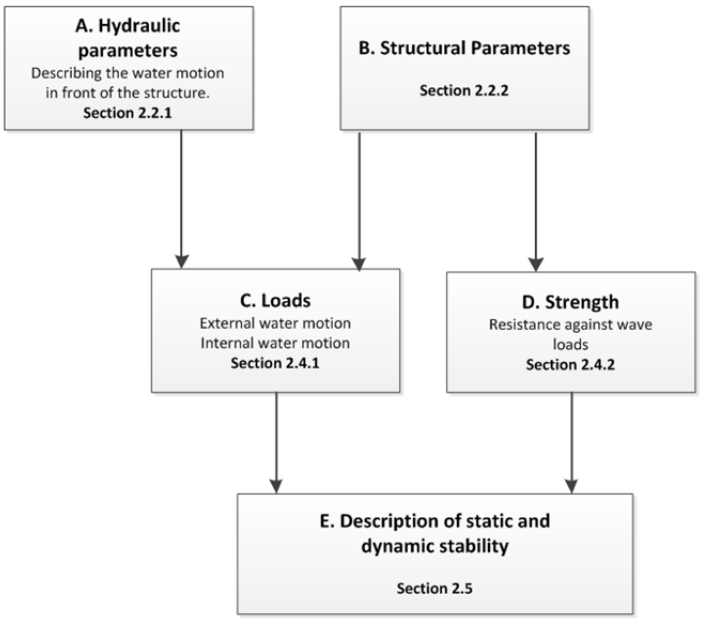

Fig. 2.1: Scheme of coastal structure under wave attack from Van der Meer (1995)

The key parameters that are important for the armour stability can be divided in hydraulic and structural parameters. Both hydraulic and structural parameters influence the wave-structure-interaction, the combination of these parameters determine the load on the structure as a whole and on the single elements of the structure. Hydraulic parameters (A) are related to the description of the wave action in fron of the structure (hydraulic response of the breakwater) described in section 2.2.1. The structural parameters (B) are covered in section 2.2.2.
Based on the main hydraulic parameters, the external and internal water motion are described in section 2.3 being wave run-up, run-down and reflection. The strength or stabilisation forces of the armour layer against wave forces (D) are described in section 2.4.1. The loads (C) on the structure are described by both hydraulic and structural parameters in section 2.4.2. The final section combines the loads on the armour layer and the strengths of the armour layer (E), resulting in stability formulae for the hydraulic stability of the armour layer under wave attack. These formulae are used during the first phase of a breakwater design and are the basis for this research.

It must be noted that in this report the wave-structure-interaction is focused on the influence of core permeability on the armour stability. Therefore only topics of relevance will be discussed extensively, whereas others will only be mentioned.

2.2 Parameters

2.2.1 Hydraulic parameters

Hydraulic parameters or wave parameter are wave related parameters such as wave height, wave period and the dimensionless surf similarity parameter.

The majority of the relationships are described with the in incident significant wave height (H_s) at the toe of the structure, usually as the significant wave height H_s, which is the average of the highest 1/3 of the waves. The wave period is often expressed as the mean period T_m or peak period T_p. It can be assumed that the peak and the mean wave period can be converted into each other $T_p = 0.8 \cdot T_m$. The fictitious deep water wave steepness (s_0) can be calculated using the relation for the wave length (L_0) on deep water (Schiereck, 2001).

$$L_0 = \frac{gT^2}{2\pi} \tag{2.1}$$

$$s_0 = \frac{H}{L_0} = \frac{2\pi H}{gT^2} \tag{2.2}$$

2.2.2 Structural parameters

There are various structural parameters that influence the stability, such as the slope angle, relative freeboard or water depth at the toe. However most of them are therefore irrelevant for this research and are not disregarded in this thesis. The two categories which are relevant and adopted in subsequent section are:

- Armour layer
- Filter and core material

The purpose of an armour layer is to be a robust but porous structure providing overall stability of the structure by preventing out-wash of smaller rock grading and energy dissipation by porous flow. Overall stability of the structure can only be guaranteed with minor damage to the armour layer, increasing the importance of hydraulic stability. Both the porosity as the thickness of the armour layer affect the energy dissipation in the core and therewith the velocity and reflection forces on the armour elements. The focus of this research is on interlocking armour units which are placed in a high porous single layer.

The grading of the core and filter material affect the structural permeability and contribute to the wave reflection and loads on the armour layer. Rock gradings are commonly indicated by the mean nominal diameter d_{n50} and width of the grading. The nominal diameter depends on to the weight W_{50}, which is the 50% value on the mass distribution curve, and the density ρ_s.

$$d_{n50} = (\frac{W_{50}}{g \cdot \rho_s})^{1/3} \tag{2.3}$$

Small particles (less than 200 mm) are distinguished with a sieve analysis. The median sieve size on the passing cumulative curve (indicated as d_{50}). The relation between d_{n50} and d_{50} is general adopted to be d_{n50}=0.84d_{50} (Schiereck, 2001).
The grading of rock can be expressed as a value of the sieve curve d_{85}/d_{15} or mass distribution d_{n85}/d_{n15}. The width of the grading is an important parameter for both the internal stability and to determine permeability, see chapter 3. Table 2.1 shows ranges of grading widths according to CIRIA (2007):

	$(W_{85}/W_{15})^{1/3}$	W_{85}/W_{15}
Narrow grading or "single-sized"	< 1.5	1.7-2.7
Wide grading	1.5-2.5	2.7-16.0
Very wide grading or "quarry run"	> 2.5	> 16.0

Tab. 2.1: Ranges of grading widths

2.3 Wave-structure-interaction

2.3.1 General

The water motion in and on the breakwater is depends by both hydraulic and structural parameters. For describing the shape of the wave with respect to the structure, the dimensionless breaker parameter or surf similarity parameter ξ is typically used. This parameter indicates the breaker type and is of crucial importance for the energy dissipation on the slope and thereby for the water motion in and on the breakwater.

In subsequent subsections the breaker type and water motion in and on the structure will be discussed regarding structural permeability. Due to the complexity of the wave-structure-interaction, the water motion in and on the structure is simplified by separating it in two processes; external and internal motion. The external process is mainly described by the hydraulic response parameters of the breakwater. The internal motion is the water movement under influence of a certain external water movement.

2.3.2 Breaker type

The breaker type on a slope is generally described by the surf similarity parameter. The function of the surf similarity parameter is given by:

$$\xi = \frac{tan\alpha}{\sqrt{H/L_0}} \tag{2.4}$$

where α is the slope angle and H/L_0 is the fictitious deep water wave steepness with L_0 as the deep water wave length. The different breaker types with associated surf similarity numbers are presented in figure 2.2.

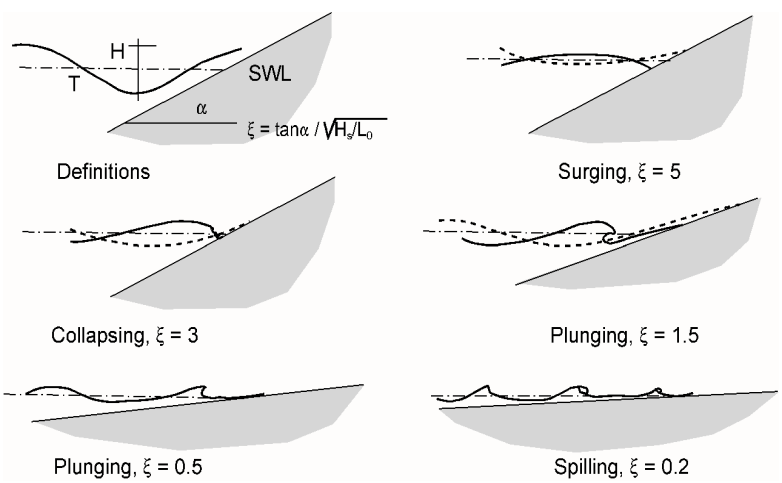

Fig. 2.2: Wave shape relative to the slope angle described with the surf similarity parameter; from Schiereck (2001)

The breaker types can be divided in breaking ($\xi < 2.5 - 3$) and non-breaking waves ($\xi > 2.5 - 3.0$). Breaking waves dissipate energy on the slope by turbulence surface rollers or a yet-like impact on the slope. A jet acts locally on the bed inducing pore pressures at the specific location, especially with an impermeable core. Although the slope encounters locally a heavy loading, much energy is dissipated reducing the run-up and run-down levels and associated destabilisation forces, which will be discussed in the next subsection.
Surging waves dissipate less energy on the slope of the structure due absence of breakage, resulting larger run-up and run-down level. The larger run-up levels influence the water flow and thereby the forces on the armour layer. The explanation of the water motion on the structure in the following subsections is based on non-breaking was as surging waves.

2.3.3 External water motion

Wave action on a rubble mound structure will cause the water surface to oscillate over the slope of the structure. The oscillation movement is generally greater than the incident wave height. The oscillating movement on the slope of the structure is called run-up and run-down of the wave (shown in figure 2.3). Wave run-up R_u and run-down R_d are defined as the upper and lower water level reached on the slope relative to Still Water Level (SWL).
The run-up height will decrease with increasingly structural permeability. Water percolates more easily through a high permeable core than through a low permeable core. Therefore, within a fixed time period, more water will flow into a permeable core than in a less permeable core. For a low permeable core the water inflow is limited and accumulation of water occurs in the armour layer. The concentrated flow in the armour layer induces the wave run-up and run-down accompanied by higher velocities and larger forces on the armour units. Figure 2.3 illustrates the difference of the velocity vector for permeable and impermeable slopes.
During the downrush the external water motion is in downward direction. This induces the water outflow from the core of the structure due the increased difference in water level between the in- and outside of the structure. The maximum run-down level is found to be of great importance for the stability of armour units in combination with the outflow velocity as the size and direction of the maximum outflow velocity affect the destabilizing forces on a single armour unit. During uprush the velocity parallel to the slope reaches its maximum around SWL where the inflow is still relative low. The maximum flow velocity has a large impact when it strikes an amour unit. Upslope, the inflow increases and the parallel velocity is minimized reducing the forces on the armour layer.

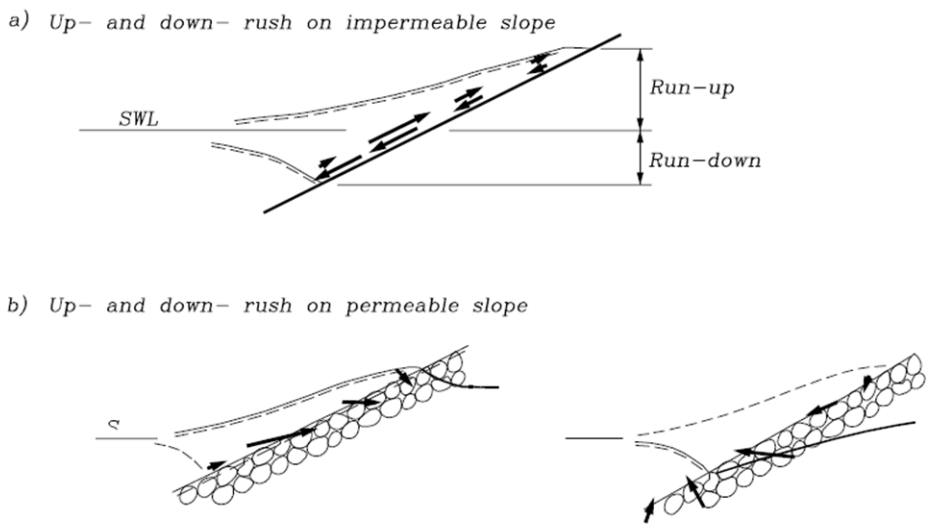

Fig. 2.3: Up and down flow on impermeable slope (upper figure); Up and down flow on permeable slope (lower figure) (Burcharth & Andersen, 2007)

There are several formulae available to determinate the maximum run-up. Run-up formula are generally based on the formulae introduced by Hunt (1959). The formula is based on the relation between the surf similarity parameter and the wave height, which can be described as:

$$\frac{R_u}{H} = 1.0\xi_0 \tag{2.5}$$

Van der Meer and Stam (1992) analysed measured data and proposed prediction formulae incorporating the permeability of the structure. Formulae 2.6 and 2.7 present the average trend through the large scatter data based upon the 'notional' permeability parameter, which was discussed in chapter 1. Formula 2.8 presents the upper bound for the run-up level for a permeable core. These three formulae have been used to compare the run-up level of a rock armoured breakwater with the run-up level of a breakwater with X-blocs for an open and impermeable core in the analysis phase of this thesis.

$$R_{un\%}/H_s = a\xi_m \qquad \text{for } \xi_m \leq 1.5 \tag{2.6}$$

$$R_{un\%}/H_s = b\xi_m^c \qquad \text{for } \xi_m \geq 1.5 \tag{2.7}$$
$$R_{un\%}/H_s = d \qquad \text{for P>0.4} \tag{2.8}$$

When the run-up has reached its highest level on the slope of the structure the flow direction reverses and the water flows downward along the slope till the lowest level has been reached. The downward water motion downrush, creates a wave towards the sea, which is called the reflective wave. Most of the structures reflect some proportion of the incident wave energy. The proportion of reflection depends on the slope of the structure, wave steepness and permeability of the whole structure. Reflection is described by a reflection coefficient, C_r, incident wave height H_i and reflected wave height H_r.

$$C_r = \frac{H_r}{H_i} = \sqrt{\frac{E_r}{E_i}} \tag{2.9}$$

The basic approach to describe the reflection is to relate the reflection coefficient to the surf similarity parameter (Batjes, 1974).

$$C_r = a\xi^b \tag{2.10}$$

Postma (1989) analysed the datasets of van der Meer (1988b) and Allsop and Channell (1989) and presented an alternative equation based on equation 2.10 including the effect of structural permeability.

$$C_r = \frac{0.081}{P^{0.14}(cot\alpha)^{0.78}s_{op}^{0.44}} \tag{2.11}$$

where P is the notional permeability factor and s_{op} is the deep water wave steepness. The reflection coefficient indicates the energy dissipation in the armour layer for an impermeable core. Formula 2.11 has been used to compare the energy dissipation inside the rock armour layer with the energy dissipation inside the Xbloc layer in the analysis phase of this thesis.

2.3.4 Internal water motion

During the period of downrush the water level outside the breakwater becomes lower than inside the breakwater. This is due the penetration delay, creating a hydraulic gradient which induces the outflow of water from the core. During the uprush it is the other-way around, inducing the inflow of water into the core. Figure 2.4 illustrates the wave motion through the structure plotted against time.

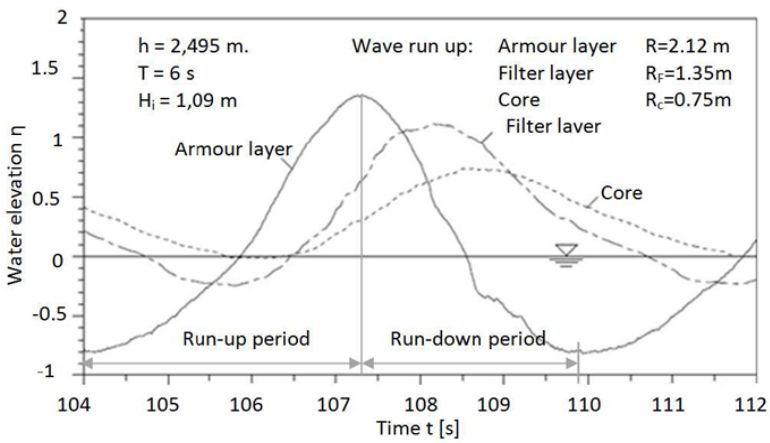

Fig. 2.4: Phase difference in the armour layer, filter layer and core by Muttray (2000)

Wave attack does not only influence the outflow and inflow velocity but also the internal water level and therefore the mean pore pressure (hydrostatic pressure). This is called internal set-up and can be explained by the fact that higher water levels are reached during the run-up than during the run-down, resulting in a larger inflow surface than outflow surface.

Furthermore, it is observed that the average flow path for inflow is shorter than for outflow (illustrated in figure 2.5) causing more water to flow into the structure than outflow. The imbalance of water inflow and outflow results in an elevation of the internal water level above the sea water level outside of the breakwater (set-up), leading to an increase in hydrostatic pressure. The increase in hydrostatic pressure lead to a larger hydraulic gradient at maximum run-down inducing the hydrostatic pressure forces in outward direction. Furthermore, a large difference in the hydraulic pressure induces the outflow velocity and the associated destabilisation forces.

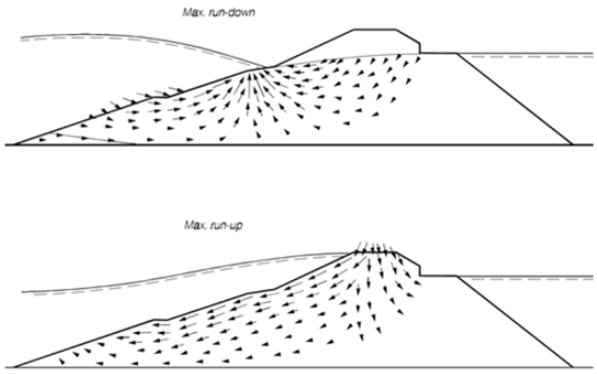

Fig. 2.5: Internal water motion according to Abbott & Price (1994)

2.4 Forces

The forces on an armour layer can be divided in stabilisation forces in destabilisation forces by the wave motion on the structure. Stabilisation forces acting in the positive direction increasing the hydraulic stability, these forces are in other words the strength of the amour layer. The destabilisation forces are typically dynamic loads.

2.4.1 Stabilisation forces

The stabilisation forces are related to the stability mechanisms namely, gravity, friction and interlocking. The gravitational force (F_G) is defined by the weight of the unit, the gravitational acceleration (g) and density of te water (ρ_w) in case the unit is located under water. The gravitational force can be decomposed in a force parallel and perpendicular to the slope, illustrated in figure 2.6.
The friction (F_W) and interlocking (F_i) forces are the response of the imbalance of the individual force balance in the horizontal and vertical direction. The size of the friction and interlocking force depends mainly on the contact area and placement.

$$\begin{aligned} F_G &= (\rho_s - \rho_w) \cdot D_n^3 \cdot g, \\ F_W &= \mu(F_G) cos\alpha, \end{aligned} \tag{2.12}$$

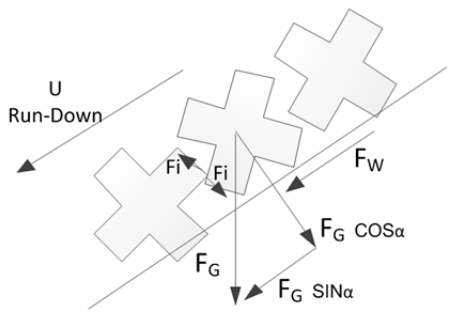

Fig. 2.6: Static loads on an Xbloc armour layer

2.4.2 destabilisation forces

Destabilisation forces on the armour layer are induced by the flow around the armour unit. Since the flow around the armour is not stationary, the size and direction vary in time. Figure 2.7 illustrates the destabilisation forces on a single unit during wave run-up and run-down.

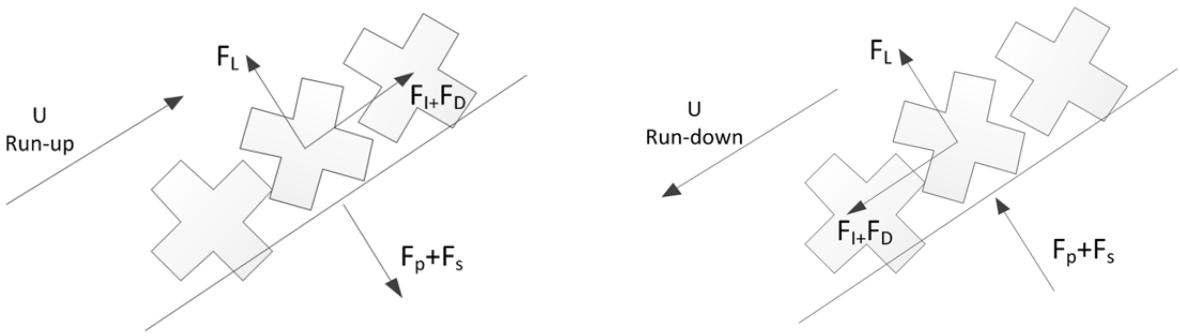

Fig. 2.7: loads on a grain during run-up

The forces in the figure are:
F_L =Lift force
F_D =Force force
F_I =Inertia force
F_s =In- and outflow
F_p =Pressure force

The flow velocity generates a drag force (F_D) and lift force (F_L). The drag force acts in the direction of the fluid motion and is caused by pressure and viscous skin friction. The lift force (F_L) acts always perpendicular to the drag force and is caused by the curvature of the streamlines.

The oscillated wave motion on the slope of the structure generates an additional load due acceleration. The so called inertia force (F_I) works in the direction of the fluid motion.

$$F_D = 0.5 \cdot C_d \cdot \rho_w \cdot V^2 \cdot A_d, \tag{2.13}$$
$$F_L = 0.5 \cdot C_l \cdot \rho_w \cdot V^2 \cdot A_l, \tag{2.14}$$
$$F_I = C_m \cdot \rho_w \cdot V \frac{du}{dt} \tag{2.15}$$

The fluctuating hydraulic gradient in the armour layer induces the in- and outflow forces (F_s) and a pressure force (F_p). This gradient acts parallel to the slope in outward direction.

2.5 Description of armour stability

Various empirical and semi-empirical stability formulae were derived for an armour layer for example Hudson (1959), Van der Meer (1988b) and the Xbloc design formula. The stability of the armour layer is generally expressed with the stability number N_s that represents the ratio between the loads on an armour unit (drag and lift force) and the resistance force (gravitational force).

$$\frac{F_D + F_L}{F_G} \approx \frac{\rho_w V^2}{g(\rho_s - \rho_w)d_n} K_{d1}, K_{d2}... \tag{2.16}$$

In the formula above, the d_n is nominal diameter (explained in section 2.2.2), ρ_s and ρ_w are the stone and water density, u is the velocity and g is the gravitational acceleration. Rewrite the formula using the relative buoyancy density ($\Delta = \frac{(\rho_s - \rho_w)}{\rho_w}$) and the velocity as $V = \sqrt{H \cdot g}$, one obtains:

$$\frac{H}{\Delta \cdot D_n} = f(K_{d1}, K_{d2}...) \tag{2.17}$$

Hudson (1959)

Hudson (1959) suggested a basic semi-empirical formula that is written in its original form as:

$$W_{50} = \frac{\rho_s g H^3}{K_d \Delta^3 \cot \alpha} \qquad \text{which can be rewritten to} \qquad \frac{H}{\Delta d_{n50}} = (K_d \cdot \sqrt{cot\alpha})^{1/3} \tag{2.18}$$

Δ is the relative buoyant density of the stone(-), ρ_s is the stone density (kg/m^3), α is the slope angle(-) and K_d is the dimensionless stability coefficient (K_d) to account for all other influences that are not described in the formula. Recommended values for K_d for different types of armour units, breaker types or core permeability can be found in (CIRIA, 2007).

Stability of Xbloc

The hydraulic stability of the Xbloc armour layer is determined after several model tests. The stability is expressed by the stability number $H_s/\Delta d_n$. The start of damage is concluded to be from a N_s= 3.5 and failure may occur from N_s=4.0, illustrated in figure 2.8. The design value of an Xbloc armour layer is set on N_s=2.77 fulfilling the zero-damage requirement of single layer armour layers.

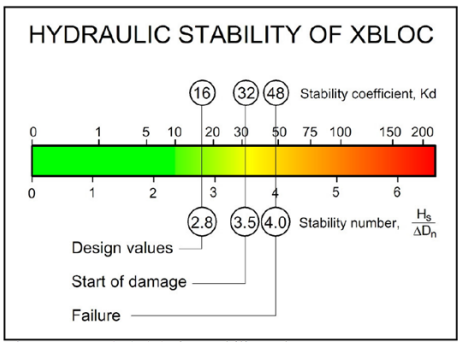

Fig. 2.8: Xbloc design values (P. Bakker et al., 2006)

The stability values of the Xbloc armour units correspond to a stability coefficient of 16 in the adjusted Hudson formula, which neglects the slope angle. The slope angle is neglected due to the application of comparable slope angles, namely a slope angle of 3V:4H and 2V:3H.

$$\frac{H}{\Delta d_{n50}} = (K_d)^{1/3} \tag{2.19}$$

2.6 Summary

The stability of the armour layer can be explained by the water motion around the structure. The rather complex process is influenced by various variables including the structural permeability (P). Figure 2.9 shows a flow chart describing the influence of the hydraulic and structural parameter, discussed in this chapter, on the armour stability. The stability of an armour unit can be given in it general form using the stability number (N_s):

$$\frac{H_s}{\Delta d_n} = f(K_{d1}, K_{d2}....P) \tag{2.20}$$

Fig. 2.9: Flow chart of the stability of armour units

The stability formulae of Hudson (1959), Van der Meer (1988b), which is presented in chapter 1, and the Xbloc formula make use expression 2.20. However, the remaining part of the stability formulae differ from each other. The key differences between the Hudson (1959), Xbloc and Van der Meer (1988b) are summarised below.

- All variable in the Van der Meer (1988b) formula are permanent present. For the Hudson (1959) and Xbloc formulae, the variable can be incorporated into the formula when required.
- Relation between various variable are indicated in the Van der Meer (1988b) formula while the Hudson (1959) and the Xbloc formula use a single correction factor for each phenomena.
- The Van der Meer (1988) formula is difficult to adjust due to the complexity of the formulae. This is in unlike the Hudson (1959) and Xbloc formulae, which can be easily adjusted.

3. CORE PERMEABILITY

3.1 General

Porous flow through granular material as in the core a breakwater differs from groundwater flow. Higher flow velocities occur in coarse material than in sand body changing the flow characteristics. This chapter describes the flow characteristics for the core of the breakwater.
The focus in the first part of this chapter is on the flow characteristics at different velocities explained with Forchheimer model. The Forchheimer model describes the relation between the pressure gradient and the average velocity in granular material. This model is an indication of the permeability of rock material and is used to describe the water flow in the core in chapter 4. The Forchheimer model can be coupled to the wave induced pore pressure model to calculate the flow velocity in the core for a specific wave. The wave induced pressure model is a description of the exponential pore pressure attenuation inside the core of the breakwater.

The last section of this chapter describes on the stability relation between armour units and core permeability found by various researchers. Finally, the suggested correction factors on the stability number by van Gent et al. (2004), Van der Meer (1988b), Burcharth (1998) and DMC are be compared with each other.

3.2 Forchheimer model

Forchheimer (1901) suggested the following type of model for an uniform stationary flow, existing out of two terms:

$$I = aV + b|V|V \tag{3.1}$$

where V is the filter velocity, I is the hydraulic gradient and a and b are constants for a specific fluid and material. The linear term in equation 3.1 presents the contribution of the laminar flow depending of the viscosity. The quadratic or non-linear term presents the contribution of the turbulent flow, which is independent on the viscosity. The characteristics of the flow depend on the Reynolds number related to the nominal grain size and filter velocity.

$$Re = \frac{V \cdot d_{50}}{\nu} \tag{3.2}$$

Different flow regimes can be described depending on the Reynolds number, i.e. creeping flow, laminar flow with non-linear convective inertia forces and fully turbulent flow. These flow regimes are called respectively; Darcy flow, Forchheimer flow and turbulent flow (figure 3.1).

The transition between various flow regimes is studied by Dybbs and Edwards (1984), which described the different flow regimes depending on the Reynolds number Re_p based upon the pore diameter d_p and pore velocity u. In this research is the Reynolds number used based on the grain size, similar as in the Forchheimer model.
According to Bakker (1989) it can be assumed that the Reynolds number based on grain size is roughly 1.5 times the Re_p since the filter velocity is approximately 0.4 times the pore velocity and the grain size is 4 a 5 times the pore diameter. The flow regimes with associated Reynolds numbers are summarized in table 3.1.

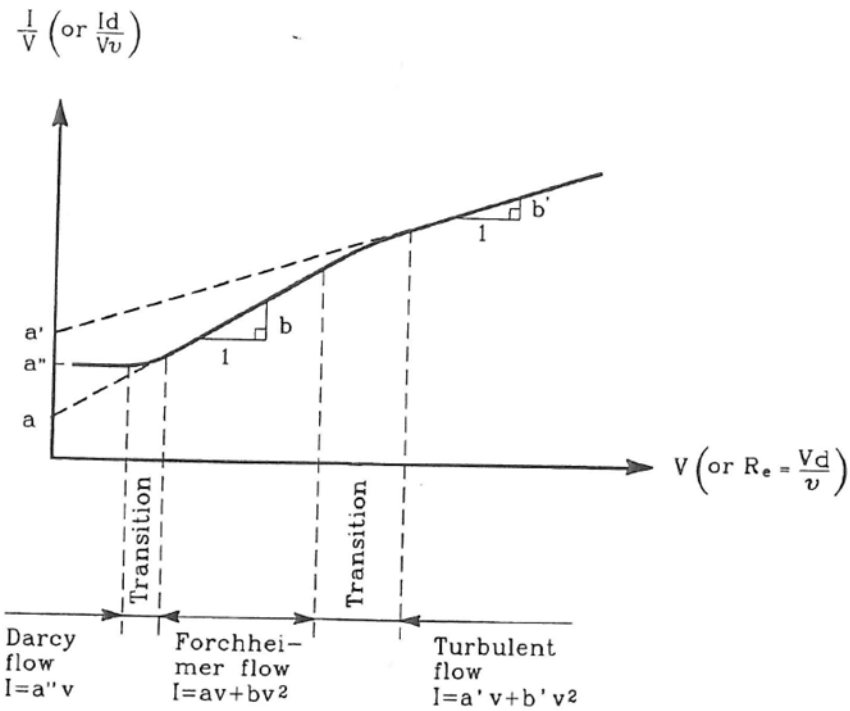

Fig. 3.1: A representation of flow regimes, from Burcharth (1991)

Flow regime	Re_p	Re
Darcy flow regime	$Re_p <$ 1-10	1.5-15
Forchheimer regime	1-10 $< Re_p <$ 150	1.5-15 $<$ Re $<$ 225
Fully turbulent flow	300 $< Re_p$	450 $<$ Re

Tab. 3.1: Reynolds number ranges for different flow regimes according to Dybbs and Edwards (1984).

3.2.1 Darcy flow

The Darcy flow is dominated by viscous forces and is well-examined by Darcy in 1856. When the non-linear term of the Forchheimer model is neglected for stationary flow, we obtain the Law of Darcy:

$$I = a"V \tag{3.3}$$

where V is the filter velocity; $a"$ is the hydraulic conductivity and I is the hydraulic gradient.

The Darcy flow occurs for low velocities and is not relevant for flow through coarse material and therefore not relevant for this research.

3.2.2 Forchheimer flow

If larger velocities occur, but the flow is still laminar, the flow can be described with the Forchheimer equation (equation 3.1). The non-linear term represents inertia forces caused by an additional pressure drop over curvatures.

In the Forchheimer equation two friction coefficients (a and b) are proposed. Many researchers have tried to develop an empirical or semi-empirical definition for a and b. The expressions can be solved partly using the Navier-Stokes equation for stationary flow condition in granular material.
However, the rational approach is the dimensional analysis leading to the following expressions (Ergun (1952), Lindquist (1933)

$$a = \alpha \frac{(1-n)^2}{n^3} \frac{\nu}{gd^2} \tag{3.4}$$

$$b = \beta \frac{1-n}{n^3} \frac{1}{gd} \tag{3.5}$$

$$\tag{3.6}$$

Coefficient α depends on gradation and β depends both on gradation and relative roughness. Inserting the expression in the Forchheimer equation 3.1, we obtain

$$I = \alpha \frac{(1-n)^2}{n^3} \frac{\nu}{gd^2} V + \beta \frac{1-n}{n^3} \frac{1}{gd} V^2 \tag{3.7}$$

where n presents the porosity; ν presents the kinematic viscosity; V is the filter velocity and α and β are coefficients depending on grain shape and grading.

The flow in the core of a small scale model is expected to be in the Forchheimer flow range.

3.2.3 Fully turbulent flow

For high velocities turbulent flow will occur. In fully turbulent flow the inertia forces will dominate over the viscous forces. The linear term in equation 3.13 can be neglected in this case, obtaining the equation of the form:

$$I = b'|V|V = \beta' \frac{1-n}{g} \frac{V^2}{D} \tag{3.8}$$

In principle equation 3.1 can be used for turbulent flow. In this case the laminar term has no physical meaning and is only a fitting term.

It is theoretical not correct to describe fully turbulent flow with the Forchheimer equation existing out of a linear and a non-linear term. Burchartah 1991 proposes a critical Reynolds number for the lower boundary of the turbulent flow regime, replacing the fitting term (figure 3.2).

$$I = I_c + b(V - V_c)^2 \tag{3.9}$$

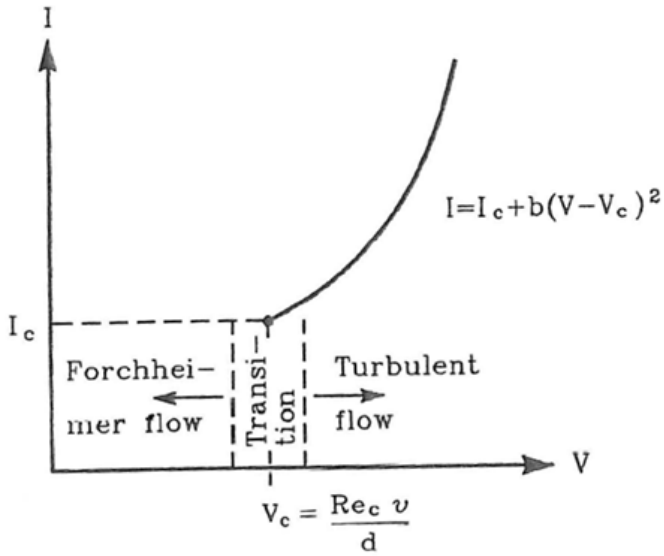

Fig. 3.2: suggested representation of the turbulent flow regime (Burcharth & Andersen, 1993)

The critical Reynolds number is the transition between Forchheimer flow and turbulent flow. For stone samples, the critical Reynolds number to be used is approximately Re_c=450 (tabel 3.1). However, for the fully turbulent flow it is assumed that the laminar part of the Forchheimer equation is negligible to the turbulent part. Englund (1953) suggested to express the ratio between the two terms as follows:

$$\xi_E = \frac{\beta Re_c}{\alpha(1-n)} \tag{3.10}$$

Using the critical Reynolds number of 450, α of 3.6, β of 360 and porosity (n) of 0.4 in equation 3.10 result in a value of 7.5, corresponding to a lower value of the turbulent flow regime. The fully turbulent flow regime starts higher around a Re_c of 600.

The critical Reynolds number corresponds to a critical average velocity V_c obtained by equation 3.11.

$$V_c = \frac{Re_c \cdot \nu}{d} \tag{3.11}$$

Inserting equation 3.11 in equation 3.7, we obtain the equation for the critical hydraulic gradient

$$I_c = Re_c \alpha_F \frac{(1-n)^2}{n^3} \frac{\nu^2}{gd^3} + Re_c^2 \beta_F \frac{(1-n)}{n^3} \frac{\nu^2}{gd^3} \tag{3.12}$$

Fully turbulent flow in the core will only occur in large scale models and in the prototype breakwater. Its is not feasible to obtain this flow regime in small scale models.

3.2.4 Non-stationary flow

An extended Forchheimer model for non-stationary flow is proposed by Polubarinova Kochina [1962]. By adding a time dependent term to the Forchheimer model the following equation is generated:

$$I = aV + b|V|V + c\frac{\partial V}{\partial t} \tag{3.13}$$

where 'c' is a dimensional coefficient (s^2/m). The time dependent term represent the resistance of the core material against acceleration (inertia) of the flow. In the paper of Burcharth & Christensen (1991) is the inertia force evaluated and the following expression of C is suggested.

$$C = \frac{1 + C_m(\frac{1-n}{n})}{g} \frac{dV}{dt} \tag{3.14}$$

where C_m is expected to depend on the Reynolds number, shape, surface roughness and relative water motion. The relative water motion is determined by Keulegan-Carpenter number (KC number), which describes the turbulent resistance relative to the inertial resistance. The KC factor is defined as UT/D where T is the wave period, D is the characteristic diameter and U is the characteristic velocity. The magnitude of the inertial resistance relative to the laminar resistance is described with Re/KC= D^2/Tν.

The figure below shows different regions with different dominant resistance. Small scale model tests are placed in figure 3.3 between a Re/KC of 10^3 - 10^4 and Reynolds numbers in the Forchheimer flow 15-225, illustrated with the red area. Van Gent (1993) and Smith (1991) researched the influence of the time dependent part of equation 3.13. Van Gent researched the α and β values of the stationary Forchheimer equation for relative large grain material and concluded that the values are deviating for the non-stationary flow.
The β coefficient could be determined by assuming the time dependent part of 3.13 to be equal to zero at the peak velocity. Van Gent suggests that the coefficient β exist out of a stationary part β_c and an extra contribution by the non-stationary flow β' ($\beta = \beta_c + \beta'$).

The suggested expression for β in the Forchheimer equation by Van Gent becomes $\beta_c(1 + \frac{7.5}{KC})$. When no experimental research is conducted to determine the β_c of a grain sample α of 1000 and β of 1.1 is

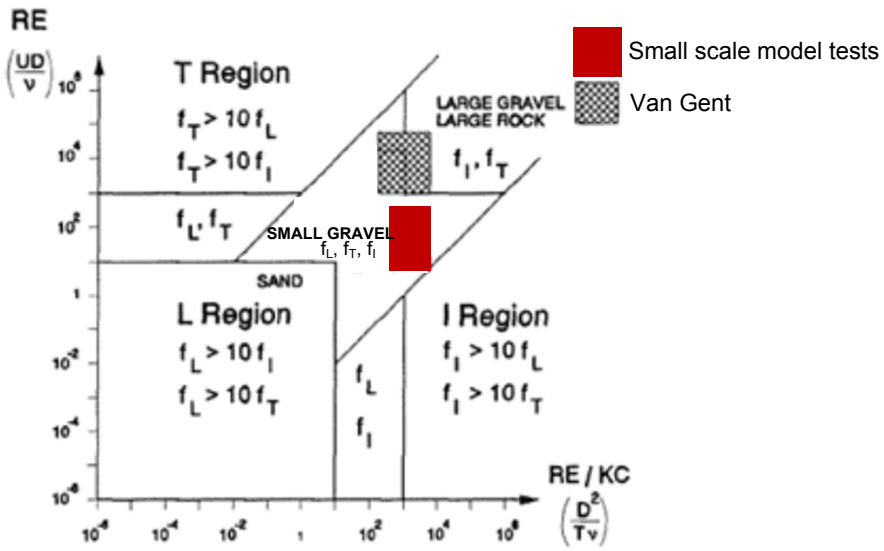

Fig. 3.3: Regions with different dominant resistance, from Van Gent (1993) adapted by author

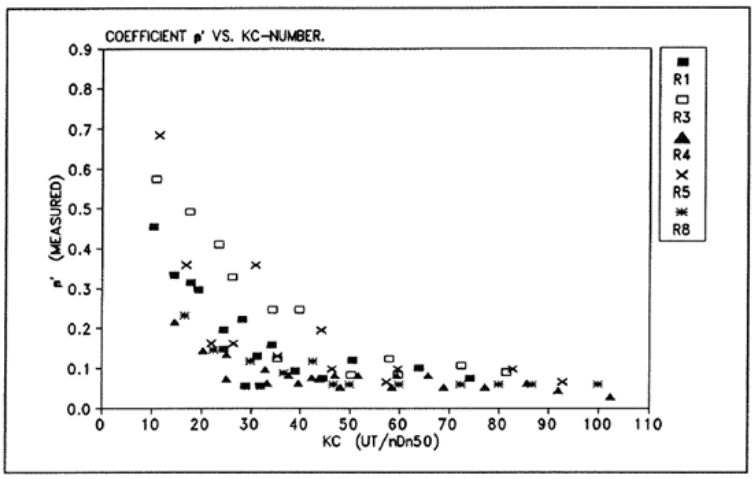

Fig. 3.4: β' extra contribution by the non-stationary flow (van Gent, 1993)

suggested by Van Gent taken into account that D=D_{n50} is applied.
The proposed expression for the time dependent term (C) by Van Gent is as follows:

$$C = \frac{1 + \frac{1-n}{n}(0.85 - \frac{0.015}{A_c})}{ng} \qquad \text{for} \qquad A_c > \frac{0.015}{\frac{n}{1-n} + 0.85} \tag{3.15}$$

where A_c is the acceleration number and n the porosity. The influence of the C-term becomes smaller for high porosity values. From a theoretical point of view this seems reasonable. High porosity structures have a high permeability, increasing the ease of the water to flow into the structure. The effect of fluctuating water motion on the water inflow decreases with an increase in porosity as described in equation 3.15.

3.3 Wave induced pore pressure model

Oscillatory flow along the slope of the breakwater (run-up and run-down movement) causes a non-stationary flow in the pores of the breakwater core. The flow in the core shows laminar and turbulent characteristics.
The total pressure in the core can divided in a hydrostatic part and a hydrodynamic part caused by

wave motion. The hydrodynamic pore pressure decreases in the direction of the incident wave (pressure attention).
Pore pressure is of great importance when studying the hydraulic stability of the armour layer since it affects the energy dissipation on and inside the breakwater structure. Based on theoretical derivations from Biesel (1950), Le Mehaute (1957) and Oumeraci et al. (1990) the following simple expression for the amplitude of maximum pressure oscillation in a porous body under wave attack is suggested.

$$p_{max}(x) = p_0 e^{-\delta \frac{2\pi}{L'} x} \tag{3.16}$$

where
- x =horizontal coordinate (x=0 corresponds to the interface between core and filter layer)
- p_0 =reference pressure at the interface between core and filter layer
- δ =damping coefficient
- L' =wave length in the core (L'=L/$\sqrt{D}$ for d/L<0.5)
- L =length of the incidental wave
- D =coefficient to account seepage length as a result of the deviation of the flow path caused by the grains. Emperical value found by Mehaute (1957) of 1.4. Theoretical value found by Biesel (1950) of 1.5.

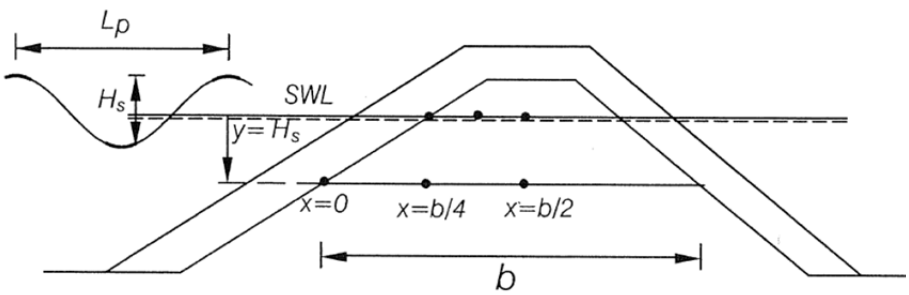

Fig. 3.5: Pore pressure distribution along the breakwater (Burcharth (1999))

Here it is assumed that the reference pressure p_0 is constant along the slope between under layer and core. Burcharth et al. (1999) found a simple relation between wave height and reference pressure.

$$p_0 = p_w g \frac{H_s}{2} \tag{3.17}$$

The relation is evaluated with the dataset from the large scale model tests of Burger et al. (n.d.) and the Zeebrugge project. The results showed that is was reasonable to estimate the reference pressure as proposed in equation 3.17 ((Burcharth et al., 1999)).

Damping coefficient

The damping coefficient δ in equation 3.16 accounts for the rate of energy dissipation in the direction of wave propagation. An empirical expression for the damping coefficient is determined by Burcharth (Burcharth et al. (1999)) after evaluating the trend-line of several variable in the dataset

$$\delta = a_\delta \frac{\sqrt{n} L_p^2}{H_s \cdot b} \tag{3.18}$$

where n is the core porosity, b the width of the breakwater at a given depth and H_s and L_p are the wave height and length. The coefficient a_δ is determined by the least square fitting of the δ values resulting in 0.0141.

From the equation of the damping coefficient Δ we can observe the following trends:

- Increase of the damping coefficient with an decrease in breakwater width;
- Increase of the damping coefficient with an decrease in wave height;

- Increase of the damping coefficient with an increase in wave length;
- Increase of the damping coefficient with an increase on core porosity;

3.4 Structural permeability in stability formulas

3.4.1 General

The effect of core permeability on the stability of armour units is acknowledged by various researchers either in words or in a formula. Both the formulae of Hudson (1953) as the formula of van der Meer (1988b) include the effect of core permeability on rock stability. Van der Meer, through the 'notional' permeability P and the Hudson formula by the empirical determined correction factors K_D. For single layer armour layer, no design guidelines are available on the effect of core permeability on the stability of armour units. However, Burcharth (1998) conducted a research on the effect of core permeability on single layer interlocking armour units.

In the subsequent part a comparison is made between the various proposed or empirical founded correction coefficients on the stability number. This comparison provides an indication for the expected results of the model tests.

Van der Meer (1988b)

The effect of structural permeability on the stability of armour units can easily be distinguished in the formulae of Van der Meer (equation 1.1 and equation 1.2), as exponent of P. The relation between armour stability and structural permeability differs between the formula for plunging waves and surging waves. This indicates a dependence of the armour stability on the wave steepness. The following relation of the core permeability on the stability number are suggested by van der Meer (1988b):

$$\text{Plunging waves} = \frac{\text{Normal core}}{\text{Open or impermeable core}} = \frac{P^{0.18}}{P^{0.18}} \tag{3.19}$$

$$\text{Suring waves} = \frac{\text{Normal core}}{\text{Open or impermeable core}} = \frac{P^{-0.13}\xi_m^P}{P^{-0.13}\xi_m^P} \tag{3.20}$$

The reduction factor on the stability number for surging waves depends on the wave length. For P=0.1 and ξ_p between 6.3 and 9.3 the reduction factor is between 0.74 and 0.65. Using the plunging formula of Van der Meer, the obtained reduction factors on the stability number for configuration P=0.1 and P=0.5 are 0.78 and 1.04, respectively.

Husdon (1953)

The data set of Van Gent (2004) and van der Meer (1988b) are gathered by Van Gent and evaluated for the formula of Hudson (equation 2.18). Two curves were derived through a large scatter of data; being K_D=1 and K_D=4.
The following stability coefficients are recommended in the CIRIA (2007) for the Hudson formula.

- The impermeable core was described with K_D=1, which is comparable with P=0.1.
- The permeable core was described with K_D=4, which is comparable with P=0.4.

The reduction factor on the stability number N_s becomes 0.63.

Burcharth

Burcharth (1998) conducted model a test with single layer interlocking armour units, namely Accropodes. The paper describes the effect of two grain gradings, fine and coarse material, and two wave steepness on the stability of the armour layer. The fine material was sharp sand with the gradation 2-3 mm. Coarse

material was crushed stones with the gradation 5-8 mm. The permeability or structural permeability of the core materials are not specified in the paper.
Although the effect of core permeability was not included in the stability for Accropode by Burcharth (1995). The relative influence can be derived from the stability numbers found in the model tests (table 3.2). The paper indicates that it is acceptable to define the coarse material, used during the model tests, with P=0.4 and the fine material with P=0.2.

	P=0.4	P=0.2	Reduction factor on N_s
ξ_p=3.75	3.5	2.4	0.69
ξ_p=5.00	>3.9	2.1	<0.54

Tab. 3.2: Stability numbers found corresponding to zero damage

Xbloc armour units

The basis of the stability formula for Xblocs is the stability number $(H_s/(\Delta \cdot d_n))$. Correction factors are recommended on the unit weight of the Xbloc for situations that lead to a reduced hydraulic stability. The correction factors recommended by DMC are presented in appendix A.

For situations with a decreased core permeability, two correction factors are defined in case of a low permeable core or impermeable core. The correction factors represent the estimated influence of core permeability on the stability of the armour layer based upon model tests conducted for projects. The correction on the unit weight of 1.5 for a low permeable core can be compared with P=0.2 and the correction on the unit weight of 2 on the unit weight for an impermeable core can be compared with P=0.1. The correction factors are rewritten in terms of stability number reduction factor:

Low permeable core =0.87
Impermeable core =0.80

3.4.2 Correction factor

This section shows a summary of the correction factors for low (P=0.2) and impermeable (P=0.1) cores. The correction factors above are given in terms of a reduction value on the stability number $H_s/\Delta \cdot D_n$. The values are illustrated in figure 3.6. The red bars in the bar graph present the low permeable core and blue the impermeable core. The colour variations between the red bars indicate the difference in ξ_p.

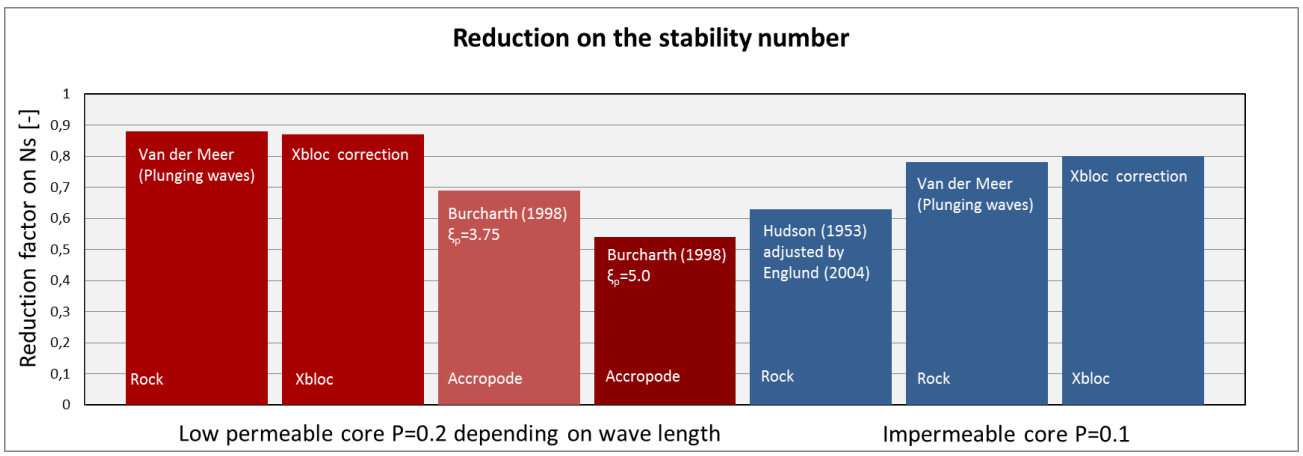

Fig. 3.6: Reduction factor on the stability number; red being for low permeable core and blue being for impermeable core

From figure 3.6 can be observed that Van der Meer (1988b) and Delta Marine Consultants expect a similar effect of core permeability on the stability number. This is in contrast to the finding of Burcharth

(1998), who found larger reduction factors on the stability number for Accropode armour units.
The reduction factor on the Hudson formula is partly based on the experimental data of van der Meer (1988b). However, a lower value is proposed by Van Gent (2004) that represents the largest reduction factor regardless of the wave period. Both Burcharth (1998) and Van der Meer (1988b) illustrate the effect of the wave period on the influence of structural permeability. The suggested dependence between wave length and armour stability is that swell wave experience a larger decrease in armour stability than wind waves.

The Xbloc reduction factors on the stability number are estimated values and have never been confirmed with a physical model tests. This thesis will verify the estimated correction on the unit weight for low permeable cores. Based on the research of Burcharth et al. (1998) it is expected that core permeability will have a larger effect on the armour stability than proposed by DMC.

3.4.3 Conclusion

Studies on the effect of core permeability on the stability of the armour layer show a decreasing stability trend for low core permeabilities. The two most relevant studies for Xblocs are by Van der Meer (1988b) and Burcharth (1998) respectively describing the influence of core permeability on rock armour units and on single layer interlocking units. van der Meer (1988b) proposed stability formulae incorporating the 'notional' permeability (P) and Burcharth et al. (1998) tested two structures, which can be compared with P=0.4 and P=0.2.
Burcharth et al. (1998) found larger decrease of armour stability between P=0.4 and P=0.2 than suggested by the formulae of van der Meer (1988b). Based on the research of Burcharth et al. (1998) it is expected that core permeability will have a larger effect on the stability of single layer interlocking armour units than for rock armour. The expected result for a Xbloc armour layer is as follows: A larger decrease of armour stability is expected for low permeable cores than for rock armour and a larger increase of armour stability is expected for very open cores than for rock armour.
An additional trend found by van der Meer (1988b) and Burcharth et al. (1998) is a larger decrease in armour stability for longer waves than for shorter waves. This indicates that swell waves are more affected by the permeability of the core. A larger decrease of armour stability is expected for swell waves than for wind waves.

It can be concluded that the relation between core permeability and armour stability remains underexplored. Especially when it concerns single layer interlocking armour units.

4. PERMEABILITY TEST

4.1 General

In order to assess the influence of core permeability on the hydraulic stability single layer interlocking units, it is important to know that the permeability of the gradings differ sufficiently. The permeability depends amongst other on the rock properties, namely d_{n50}, stone shape, grading width and the packing. The influence of rock properties on the permeability of a material makes a simple definition of permeability quite complex, until now no general accepted equation has been set-up to determine rock permeability. For this reason it is chosen to determine the permeability of several rock materials in the fluid mechanics laboratory of Delft University of Technology (DUT). These rock gradings will be used to build up the core for the hydraulic model test to access the influence of core permeability to the armour stability.

4.2 Rock samples

Permeability is influenced by various rock properties. More details on rock properties can be found in appendix B. The rock properties are; grain size, sorting, packing and grain shape. It is chosen to vary only one of the rock properties the other rock properties will be handled as follows:

- **Grain size; the size of the grains is used as variable in the rock samples, table 4.1 illustrates the available and tested gradings;**
- Sorting; core material in medium scale models are generally modelled with narrow graded material d_{85}/d_{15} of 1.27;
- Packing; the packing of the material is expected to be differ and must be checked by measuring the porosity;
- Grain shape; the material is of crushed stones as often used in practice. Photos of the available in appendix C on rock gradings.

Available gradations [mm]	d_{50}	**Density** $[kg/m^3]$	**tested**
31.5- 22.4	27.0	Approx. 2650	√
22.4- 16	19.2	Approx. 2650	√
16- 11.2	13.6	Approx. 2650	√
11.2- 8	9.6	Approx. 2650	√
8- 5.6	6.8	Approx. 2650	
5.6- 4	4.8	Approx. 2650	√

Tab. 4.1: Available stone gradations

4.3 Experimental set-up

4.3.1 Permeameter

The permeability of the rock materials is determined using a permeameter at the DUT. By measuring the discharge through a sample at constant head, the permeability could be determined using equation 4.1.

$$K = V \cdot I = \frac{Q * \Delta L}{A * \Delta H} \tag{4.1}$$

Where:

K	=Hydraulic conductivity	$[m/s]$
Q	=Discharge	$[m^3/s]$
ΔL	=Height of the rock sample	$[m]$
A	=Surface of the rock sample	$[m^2]$
Δ H	= Water level difference between the basin and the container at a specific discharge	$[m]$

The permeameter is constructed as a container in a large basin filled with water. A schematic cross section is presented in figure 4.1. A constant volume of water was pumped through the pipes into the basin. The discharge of this pump was calculated from the flow-meter on the pipes above the basin. The water levels were electronic measured with two wave gauges, one in the basin and one in the container. The water level difference was be read from the computer.

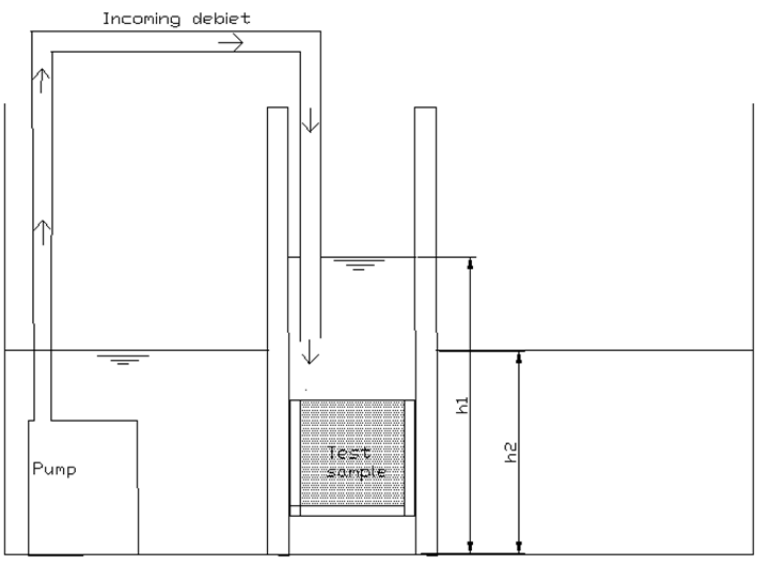

Fig. 4.1: Schematic lay-out of the permeameter at the DUT

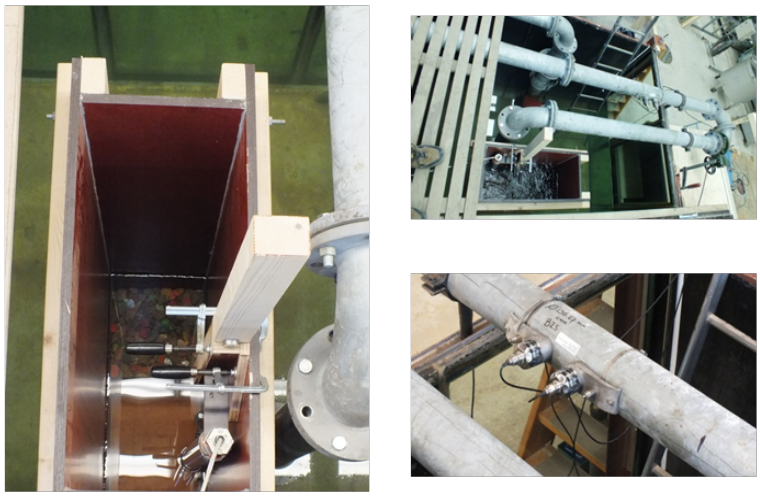

Fig. 4.2: Top of the container in the basin (left); the top of the basin (upper right); the flow-meter (lower right).

4.3.2 Rock sample

The container exists out of two compartments which are connected. The first compartment is closed at the lower side with a wooden plank, the other compartment was open and designed in such a way that the rock sample fitted on top of the open part.
The rock sample was placed inside a mobile bucket that could be lifted in- and out of the container with a crane (figure 4.3). The dimensions of the bucket were approximately 26*26*30 cm, which is large enough to generate sufficient accuracy for the test samples. The bottom of the bucket is covered with gauze ensuring that the stones cannot slip through the gauze. Three different buckets are available with different wire mesh for the various rock gradings minimizing the influence from the gauze on the measurements.

Fig. 4.3: Pictures of the bucket without rock material and the crane.

4.4 Testing procedure

The testing procedure in presented in a flow chart shown in figure 4.4.

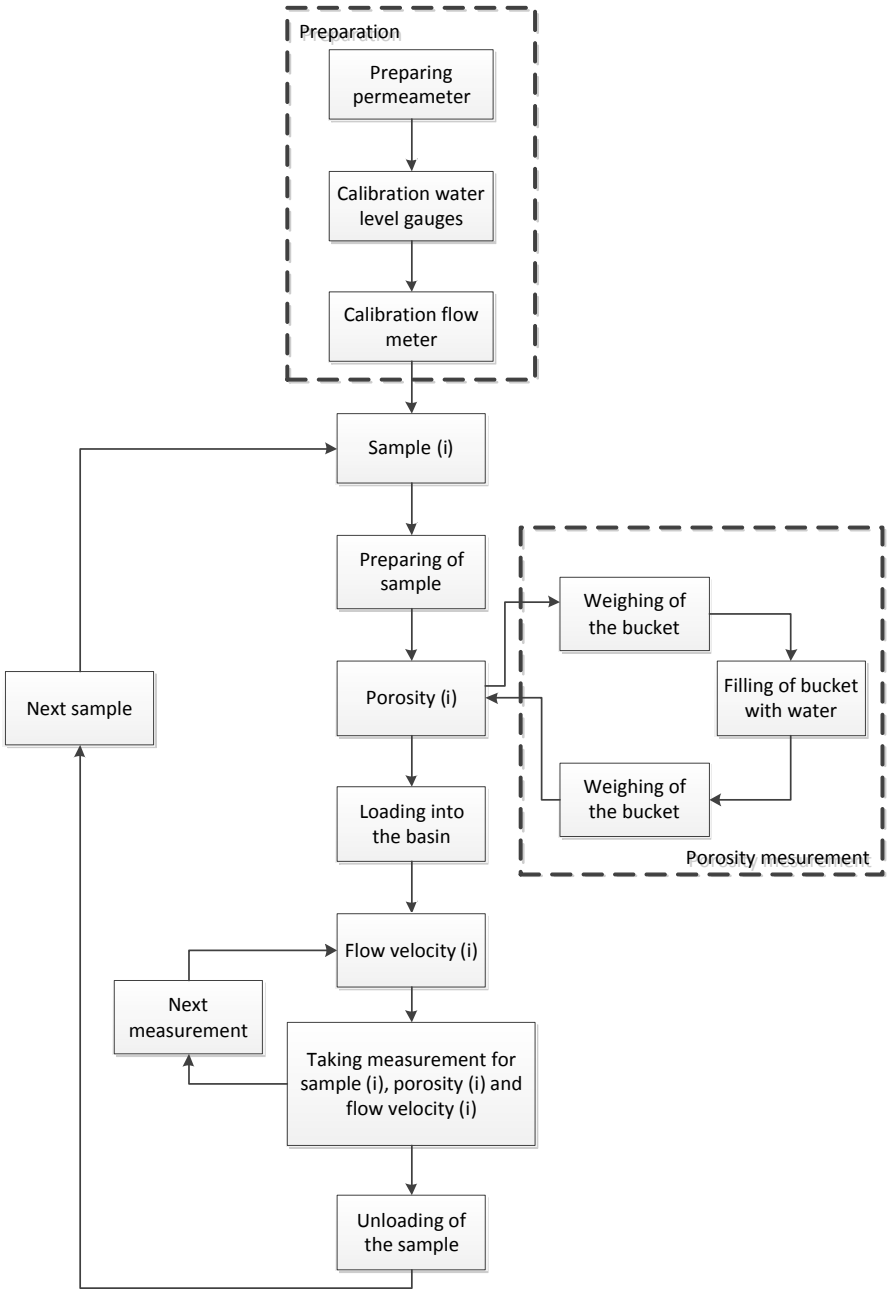

Fig. 4.4: Flow chart testing procedure

Preparation permeameter

The calibration of the wave gauges and flow meter were conducted according to the prescribed method of the Laboratory of Delft University of Technology.

Preparing of sample

Each sample used in the test was sieved and the density was determined by weighing several stones above and under water. The dry stone sample was placed in the bucket and compacted if necessarily. Compaction of the sample was reached by dropping the bucket several times on the ground till the settlement of the rock was negligible. In case of the sample with loose material this process was neglected.

Porosity measurements

Before starting with a new test the empty bucket was made watertight by fixation of a wooden plank on the underside of the bucket with clamps. The empty bucket was weighted and subsequently the bucket with rock sample was weighted. The bucket was filled with water and weighted again. The porosity was obtained twice; once by the weight of the stones and once by the weight of the water. The most reliable method was found by the weight of the added water in the bucket as the density of the rock samples remain uncertain. The used equation was for calculating the porosity is illustrated below

$$n = \frac{V_b * \rho_w}{W_w} \tag{4.2}$$

Where:

n	=Porosity	$[-]$
V_b	=Volume of the bucket	$[m^3]$
W_w	=weight of the water	$[kg]$
ρ_w	=Density of water	$[kg/m^3]$

Loading into the basin

The sample was not re-packed after the porosity measurement. The water was let out of the bucket and lifted carefully with a crane into the container. Some compaction may have occurred due to the handling of the sample. However, the compaction is expected to be relatively small and therefore similar porosity in the model set-up is assumed as the measured porosity.

Measurements

For each sample (i) and porosity (i) approximately 15 flow velocities with associated water level difference is measured. The filter velocity in the sample differed between 0.25 and 0.07 m/s. The greatest filter velocities were measured for largest gradings while the lowest filter velocities were measured for smallest gradings.

4.5 Test conducted

General

From chapter 3 follows that the permeability is closely related to the porosity of a sample. A dense packed sample have a lower permeability than loose packed material. Each sample has been tested twice; once with the sample compacted and once with the sample loose in the bucket. This covers the full range of permeabilities of the tested rock sample. In section 4.2 the available and tested rock samples are presented. It is expected that the densely packed samples show a lower permeability compared to the loose sample of an individual rock grading.

Limitations

The achievable filter velocities were restricted by the model set-up.

Upper boundary of the velocity was limited by the maximum water level difference between the basin and the container or, in other words, the hydraulic gradient. The maximum water level in the container was restricted by the height of the container. The minimum water level in the basin was restricted by the fact that the bucket should remain under water.

Lower boundary of the velocity is limited by accuracy of the flow-meter at low velocities and the minimum hydraulic gradient. The flow-meter cannot measure velocities below 1 m/s in the pipes very accurately. Furthermore, quite low hydraulic gradient lead to a turbulent overflow from the first to the second compartment resulting in inaccurate measurements for the permeability.

The limitation regarding the velocities during the test results into a restriction of the occurred Reynolds numbers. In chapter 3 three flow regimes were distinguished depending on the Reynolds number. From the theory on the Forchheimer model follows that each regime has its own shape factors describing the permeability, being α" for creeping flow, α and β for Forchheimer flow and β' for fully turbulent flow. The different flow regimes would make it difficult to compare the permeability of different samples with each other.

4.6 Results

4.6.1 Porosity

The porosity is an important variable for the permeability of the sample. Both the turbulent part (b) as the laminar part (a) of the Forchheimer equation are affected by the porosity. During the tests the porosity was measured with two methods; mass of the sample combined with density of the stones and mass of the water combined with the density of the water. However, the density of rocks is an uncertain factor in the calculations and therefore it is chosen to continue in this research with the porosity obtained by the weight of the water, presented in table 4.2.

Grading [mm]	4- 5.6	5.6-8.0	8.0- 11.2	11.2-16.0	16.0- 22.4	22.4- 31.5
Loose sample						
	0.48	-	0.48	0.46	0.46	0.48
Compacted sample						
	0.42	-	0.40	0.41	0.41	0.43

Tab. 4.2: Porosity measurements

4.6.2 Permeability

The obtained data from the experiments is presented in figure 4.5. In this figure the filter velocity is set-out against the hydraulic gradient. The figure shows that the velocity increases with the larger stones and lower porosity for the various rock gradings with comparable hydraulic gradient. Although the filter velocity of adjacent rock gradings overlap each other for different porosities, the filter velocities deviate for similar porosities. It can concluded that the rock gradings have a different permeability.

From figure 4.6 is observed that each sample has a different angle with horizontal axis differ indicating differences in flow regimes. A steep line represents larger laminar forces and a gentle line larger turbulent forces. Figure 4.6 illustrates that samples with smaller grain diameter or with lower porosity have a more laminar character than larger or loose samples of rock gradings.

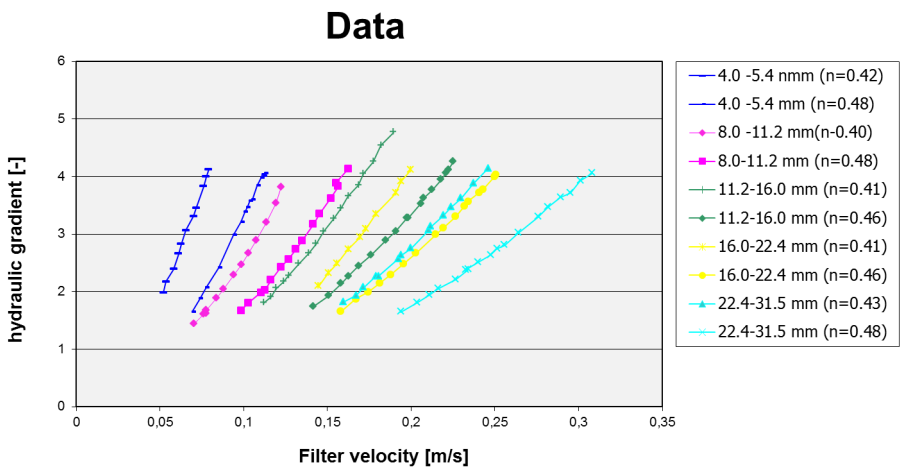

Fig. 4.5: Experimental data

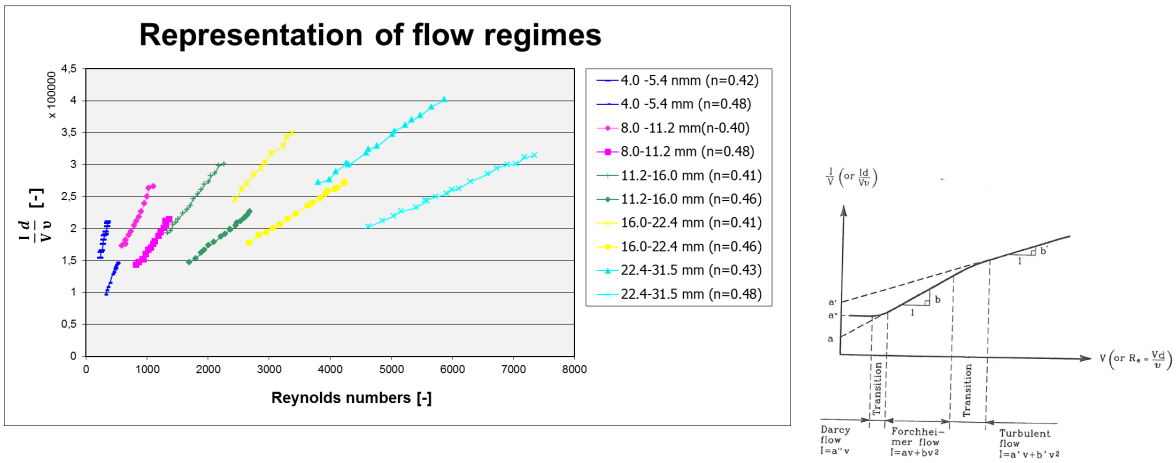

Fig. 4.6: Representation of the measured data similar as the conventional representation of flow regimes

4.7 Analyse

4.7.1 Test data

The permeability or the ease of the water to flow through the samples can be described with the Forchheimer equation. The expressions of Ergun (1952) is used to determinate 'a' and 'b' coefficients, which are formulated as $a = \alpha\frac{(1-n)^2}{n^3}\frac{\nu}{gD^2}$ and $b = \beta\frac{1-n}{n^3}\frac{1}{gD}$. The coefficients α and β can be evaluated by rewriting the Forchheimer equation to a linear line called regression line; α+βx (equation 4.3). The obtained regression lines show a good linear fit for each test. The coefficients are illustrated in figure 4.8 and the regression graphs can be found in appendix D.

$$\frac{I}{V}\frac{gd^2}{\nu}\frac{n^3}{(1-n)^2} = \alpha + \beta\frac{1}{(1-n)}\frac{Vd}{\nu} \tag{4.3}$$

The coefficient β' is idem evaluated by an regression analysis depending on the Reynolds number (equation 3.8). The turbulent flow equation neglects the laminar part of the Forchheimer equation and assumes fully turbulent flow. Figure 4.7 show stabilizing trend-line with increase of Reynolds numbers indicating a fully turbulent flow in the permeameter. For Reynolds numbers lower than approximately 600 show an exponential increase in the β' coefficient indicating that from this point the β' coefficient show great deviations with the Reynolds number. This indicates that the transition line of Re=450 between

the Forchheimer flow and fully turbulent (suggested by Dybbs and Edwards, 1984) is relative at the low end. Upward of Re=2000, the β' coefficients remain approximately similar for each individual rock grading.

$$\frac{I}{V^2}\frac{n^3 gd}{(1-n)} = \beta' \tag{4.4}$$

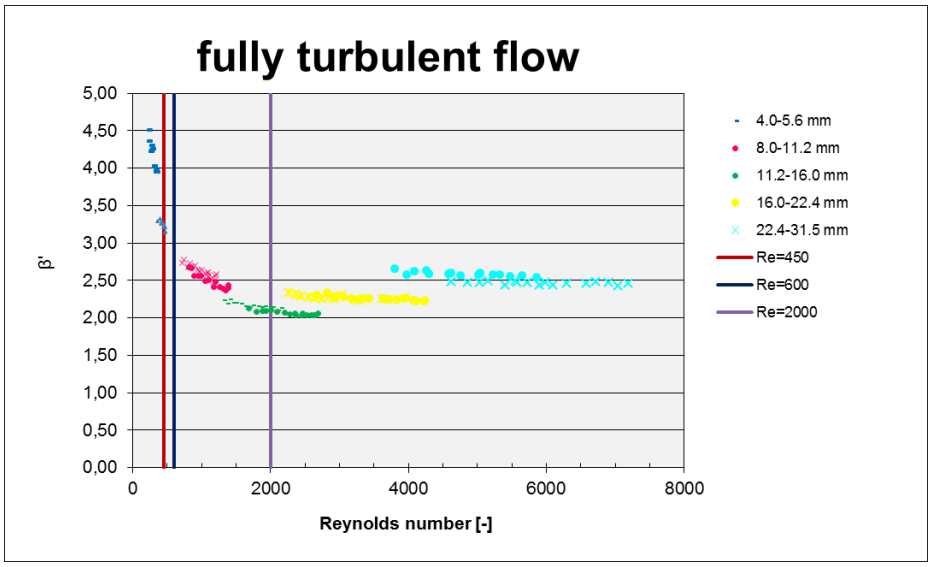

Fig. 4.7: Experimental data: fully turbulent equation

The shape coefficients calculated for the Forchheimer flow (equation 4.3) and for fully turbulent flow (equation 4.4) are presented in figure 4.8 for various d_{50}. From the figure can be observed that the β coefficient and β' coefficient for fully turbulent flow show good resembles indicating the relative importance of the α coefficient is minor.
However, from grading 8.0-11.2mm the beta coefficient shows discrepancies between the β coefficient for the Forchheimer flow and β' coefficient for the fully turbulent flow. It is likely that the laminar part of the Forchheimer model is still of great importance for rock grading of 4.0-5.6mm. Upward of 11.2-16.0mm the laminar part of the Forchheimer model is of minor importance and can be neglected.

It is concluded that the laminar part is not negligible for Reynolds numbers lower than 600. For Reynolds numbers upward of Re=1000, the flow can be described with only the turbulent part of the Forchheimer equation. The transition regime between the Forchheimer flow and Fully turbulent flow is Reynolds numbers of 600- 1000 .

4.7.2 Theory

In appendix D, the shape coefficients are compared with the values found by van Gent (1993), Englund (1953) and Shih (1990) and Williams (1992). Following from the comparison, it is concluded that the shape coefficients α and β depend the model set-up and shape of the grains. Van Gent (1993) conducted permeability tests with horizontal flow resulting in lower coefficients than vertical flow. The difference are rather large and therefore important to note.
Englund (1953) conducted permeability tests with uniform spherical, uniform rounded and irregular sand grains, mainly in the Forchheimer regime. For irregular sand grains shape coefficient $\alpha > 360$ and $\beta >3.6$ are found for the Forchheimer flow, which do not correspond with the values for 4.0-5.6mm.

Shih (1990) and Williams (1992) conducted tests within the fully turbulent flow regime, which is indicated with β'. The β' coefficients found for fully turbulent flow for narrow graded samples are summarised in the table below. The gradings width of the studies in table 4.3 are similar to the samples of the conducted permeability test.

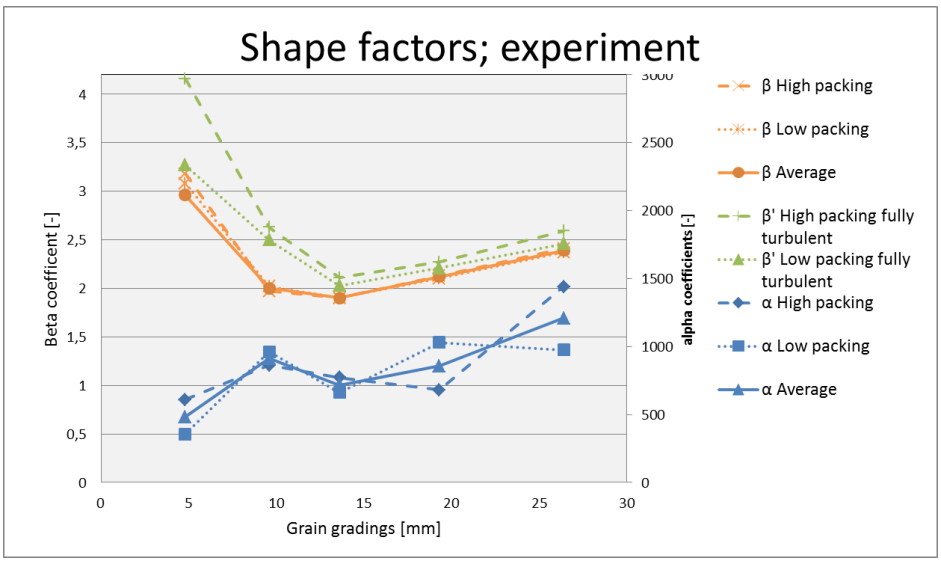

Fig. 4.8: Shape factors obtained from the experimental data

Material	**Sorting** d_{85}/d_{15}	β'	**Study**
Round rock	1.3	1.9	Williams (1992)
Semi-round rock	1.3	2.4	Williams (1992)
Irregular rock	1.3-1.4	2.5-2.9	Shih (1990)
	1.3	3.7	Williams (1992)

Tab. 4.3: Coefficients for fully turbulent flow (Burcharth & Andersen, 1993)

Comparing table 4.3 with the obtained from the permeability tests, it can be argued if grading 11.2-16.0mm is irregular rock and not semi-round rock. It is a subjective observation and can be argued. However, it can be concluded that the values found by Shih (1990) and Williams (1992) show good resembles with the test data.

4.8 Conclusion

The permeability of the rock gradings is described using the relation between hydraulic gradient (I) and the filter velocity, illustrated in figure 4.5. Although large differences in porosity leads to an overlap in permeability it can be concluded that the rock gradings deviate in permeability. This means that during the physical model tests deviating filter velocities will be obtained for identical hydraulic gradients in the core of the breakwater, assuming same porosity due to constant construction method.
Observing the water level difference during the permeability tests and the scale of the model test it is expected that lower hydraulic gradients will occur in the model tests and less differences in te filter velocity. It is recommended that the applied rock gradings in the model test are not sequent gradings. In this way it is ensured that the difference in permeability remains significant.

The obtained shape coefficients of the permeability tests can be used to calculate the velocity for a certain hydraulic gradient in the core. The relation between velocity and hydraulic gradient is used to scale core material in section 5.3. Unfortunately, the application of the shape coefficients for scaling of core material is limited due to different flow regime. The fully turbulent flow regime is tested during the permeability tests instead of the Forchheimer flow, which is expected in the core of the breakwater. This means that most part of the obtained data of the shape coefficients cannot be used for small scale models. However, it is possible that the smallest rock grading might be applied in the model tests. This depends on the Reynolds number in the core of the model test.

5. PHYSICAL SCALE MODEL

5.1 scaling

5.1.1 scaling rules

It is important that the physical model behaves in the same manner as the prototype. In order to achieve this the scale of the model is determined theoretically by geometric, kinematic and dynamic similarity.

Geometric similarity exists when all geometric lengths L_p in a prototype have a constant relation with the geometric lengths L_m in the model.

$$n_L = \frac{L_p}{L_m} \tag{5.1}$$

Kinematic similarity exists when all time depended processes in a model have a constant relation with the process in nature. This is achieved when the horizontal and vertical scale geometric do not differ. Dynamic similarity exists when the forces in the model have a constant relation with the force in nature. Thus for geometrical similar models dynamic similarity is necessary.

For wave models, the relevant forces are the gravity, surface tension, viscosity and inertia forces which are represented by the Froude (Fr), Weber (We) and Reynolds (Re) scaling numbers.

$$Fr = \frac{V}{\sqrt{g \cdot L}} \qquad \text{(ratio inertia- gravitation)} \tag{5.2}$$

$$Re = \frac{V \cdot L}{\nu_k} \qquad \text{(ratio inertia- viscosity)} \tag{5.3}$$

$$We = \frac{\rho_w \cdot V^2 \cdot L}{\sigma} \qquad \text{(ratio inertia- surface tension)} \tag{5.4}$$

$$\tag{5.5}$$

The Weber similarity can be neglected when the wave length is much larger than 2 cm and when wave periods larger than 0.35 sec (Hughes, 1993). The surface tension for larger waves is relative small and thereby negligible.
This leaves the gravity and viscosity as the most important forces. However, it is not possible to find a fluid that fulfils both the Froude and the Reynolds requirement.

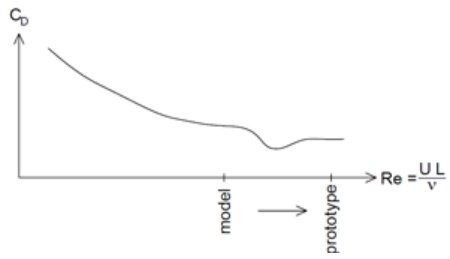

Fig. 5.1: Drag variation with the Reynolds number (Burcharth & Andersen, 2007)

The Reynolds number is an important indicator for the laminar forces (drag forces) which become relative high in low flow velocities. Induced drag forces in the scale model lead to unrealistic high resistance force

in the core (scale effects). Figure 5.1 shows that the increase of the drag coefficient, and therewith scale effects, is limited when the Reynolds number is in the turbulent flow range.
The Froude scale law is used for breakwater scale models in most cases. This is to ensure that the wave resistance of the gravity waves is correctly scaled. The Reynolds number is chosen such that the reduction of the drag coefficient is limited. Table 5.1.2 gives an overview of both the Reynolds and Froude scaling methods.

Parameter	**Froude**	**Reynolds**
Force ratio	$\frac{Inertia}{Gravity}$	$\frac{Inertia}{Viscosity}$
Equation	$\frac{V}{\sqrt{g \cdot L}} = const.$	$\frac{V \cdot L}{\nu} = const.$
Geometric		
Length [m]	N_L	N_L
Kinematic		
Time [s]	$N_t = \sqrt{N_L}$	$N_t = \frac{N_L^2}{N_\nu}$
Velocity [m/s]	$N_u = \sqrt{N_L}$	$N_u = \frac{N_\nu}{N_L}$
Acceleration $[m/s^2]$	$N_a = 1$	$N_a = \frac{N_\nu^2}{N_L^3}$
Overtopping $[\frac{m^3}{s \cdot m}]$	$N_q = N_L^{1.5}$	$N_q = N_\nu$
Dynamic		
Structural mass [kg]	$N_m = N_L^3 \cdot N_\rho$	$N_m = N_\rho \cdot N_L^3$
Pressure [Pa]	$N_p = N_\rho \cdot N_L$	$N_p = \frac{N_\rho \cdot N_\nu^2}{N_L^2}$
Force [N]	$N_F = N_\rho \cdot N_L^3$	$N_F = N_\rho \cdot N_\nu^2$

Tab. 5.1: Overview of scaling methods by Froude and Reynold

5.1.2 Scale effects

Scale effects are the result from the scaling assumption that gravity is the dominating force resisting the inertia forces. A consequence of the Froude model is disproportion of viscosity and surface tension.

viscosity scale effect

Viscosity scale effects are related to the Reynolds number and the drag coefficient illustrated in figure 5.1. Small scale models encounter much lower Reynolds numbers and thereby larger drag coefficients in the core than the prototype. The increased drag coefficient in small scale models generates an additional force, which is not present in the prototype.

A coarse granular prototype encounters a turbulent flow while the flow in a small scale model might be laminar when geometrical scaling of core material is used. The consequence of the larger drag coefficient is reduced in- and outflow of the water into the core. This will affect the energy dissipation, armour stability and run-up height on and in the armour layer.
To compensate for the low penetration rate and energy dissipation in the core, Burcharth (1999) proposed to use a larger diameter of the core material than calculated by Froude's model law. The method proposed is described more detailed in section 5.3

Inertia forces are of minor importance in small water depths, the flow resistance is dominated by the drag force. This can be explained by the fact that when the run-up thickness is several times the roughness of the armour units, water will flow over obstacles. But when the thickness of the flow is less than the roughness as in the upper part of the run-up, the flow will go around obstacles.
In order to avoid viscous scale effects during run-up the flow type in the model must similar to that of the prototype; rough turbulent. In the upper part of the run-up wedge of the model the run-up velocity relative low and are not necessarily rough turbulent. Smaller velocities result in lower Reynolds number; $Re = V \cdot d/\nu$, V being the run-up velocity, d the characteristic width of the armour layer and ν the viscosity. The reduction in the Reynolds number has a larger effect on the drag force when Re reduces from $\leq 10^5$ (sub critical flow) than for $\geq 10^6$ (supercritical flow).

The effect of larger drag forces in small scale models is smaller run-up velocities, run-up heights and less overtopping. This scale effect is more significant for small overtopping rates than for larger ones.

Friction scale effects

Surface roughness of rock of armour units may not be similitude between the prototype and small scale model, which increases the friction forces between units and between units and the slope. It is therefore common to reduce the surface friction in small scale model. Scale effects due surface friction is considered to have minimum influence on result of the experiment.

Surface tension scale effect

Surface tension is relative much larger in small scale models than in the prototype causing damping of the waves in the model that does not occur in the prototype. This effect is negligible for waves larger than 0.35 sec and water depth larger than 2 cm (Hughes, 1993).
Furthermore, the relative large surface tension causes large air bubbles in breaking waves on the rubble mound breakwater. Energy dissipation will be relative larger and the run-up level and overtopping lower.

5.2 Experimental set-up

5.2.1 Wave flume

The hydraulic test have been carried out in the wave flume of Delta Marine Consultants (DMC) in Utrecht, the Netherlands. The flume has a length of 25 meter, a width of 0.60 m and a height of 1.05 m. The water level can varies between 0.40 and 0.70 m for physical model testing. The maximum wave height, which can be generated by the wave generator, is 0.30 m (depending on the water depth).

The wave generator in the flume is a Edinburgh Designs piston, which can generate irregular waves. It corrects the paddle motion to absorb reflective waves resulting in a fully predicted wave field. Te generator is capable to generate predefined sea states such as the JONSWAP wave spectrum used in this research.

5.2.2 Foreshore

The foreshore in a physical model test represent the bathymetrie in front of the prototype. Waves might be transformed by the rising slope of the foreshore influencing the stability of the breakwater. This physical model test is not related to an actual prototype, it is conducted to evaluate the influence of the permeability of the core on the armour stability. Influence of the steepness of the foreshore on the armour stability is omitted to compared the research parameters.

5.2.3 Armour layer

The research is conducted with Xbloc armour units. The main dimensions of an unit are shown in figure 5.2. The volume of a block corresponds with 1/3 of the cube volume ($V = 1/3 \cdot D^3$) with the same unit weight.
The block size depends on the wave height and can be calculated with the general design formula for Xblocs, which is based on the Hudson formula for slope angles of 3V:4H with a stability number (N_s) of 2.77.

$$V = \left[\frac{H_s}{2.77 \cdot \Delta}\right]^3 \tag{5.6}$$

The size of the armour units, and thereby the geometrical scaling is restricted by the maximum wave height in the wave flume. This research focussed on the stability of the armour layer for different permeability of the core. This aspect is evaluated by testing till Start of Damage (SoD) of even failure

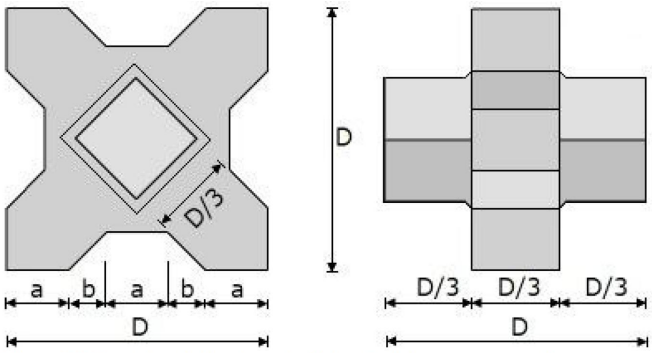

Fig. 5.2: The geometry of the Xbloc

occurs. SoD and failure might not occur for the normal wave conditions and therefore overload conditions are tested. An overload condition of approximately 180% provides enough information of the armour stability for this study.
The physical model tests are conducted with a Xbloc unit of 49 gram with a unit height (D) of 40 mm and an average density of 2270 kg/m^3. The associated design wave height, calculated with the design formula, is 99.8mm.

placement

The Xbloc armour units are placed on a staggered grid with a certain packing density. Research on the packing density has shown that a tighter placement than $1.18/D^2$ leads to a better hydraulic stability. For lower placement densities the hydraulic stability stay constant but significant, undesirable, settlements will occur. Settlements cause a gap in the armour layer near the crest, exposing the under to waves.
The prescribed packing density by DMC is $1.20/D^2$ that is described by a vertical and horizontal distance regarding the unit height, being $d_x = 1.33D$ and $d_y = 0.63D$. The actual placing density may deviate from 2% below till 5 % above this value. The packing is normally expressed as percentage of the recommended packing density, called relative packing density (RPD) and can be calculated with equation 5.7.

$$RPD = \frac{(N_x - 1)(N_y - 1) \cdot D_x \cdot D_y \cdot D^2}{L_x \cdot L_y} \cdot 100\% \tag{5.7}$$

$N_x N_y$	= number of units in the x-direction and y-direction
$D_x D_y$	= distance between the centre of gravity of two neighbouring units in the x-direction and y-direction
D	= the width of the unit
$L_x L_y$	= the measured length in the x-direction and y-direction

5.2.4 *First under layer*

For the first under layer, in this research called filter layer, is recommended to use the standard gradings from the CIRIA (2007). The design for the under layer is based on the specific weight of an armour unit. Ten Oever (2011) proposes the following requirements for the under layer:

$$W_{15} \geq (\frac{1}{15})W_{bloc}, \tag{5.8}$$
$$(\frac{1}{11})W_{Xbloc} \geq W_{50} \geq (\frac{1}{9})_{Xbloc},$$
$$W_{85} \leq (\frac{1}{7})W_{bloc}$$

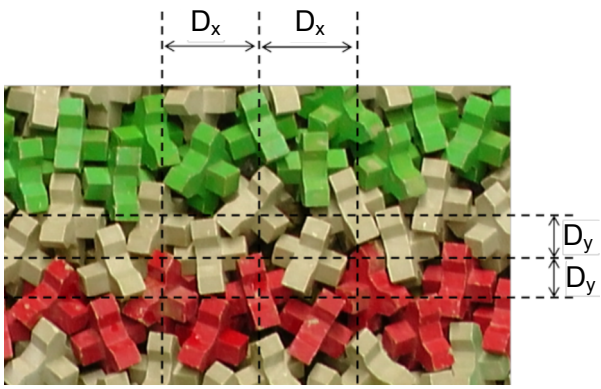

Fig. 5.3: Distance between horizontal and vertical neighbouring units

In which:

W_{Xbloc} = weight of the Xbloc;
W_{85} = rock weight that is exceeded by 15% of the rocks in the under layer;
W_{50} = rock weight that is exceeded by 50% of the rocks in the under layer;
W_{15} = rock weight that is exceeded by 85% of the rocks in the under layer;

Applying the filter rules on the 49 grams Xblocs units that are used in this study, the following values are valid for the filter grading.

Criteria	**Weight [gramm]**	**Size [mm]**
$W_{Xbloc}/7$	7.0	10.75
$W_{Xbloc}/9$	5.5	11.90
$W_{Xbloc}/11$	4.5	12.74
$W_{Xbloc}/15$	3.3	13.85

The best fit to the filter requirements using the available sieve gradings, is the grading 11,2 -16 mm. Larger grain sizes for the filter layer are not recommended because this will result in large irregularities. Research on the tolerance of the filter layer by Monster (2010) showed that large deviations in the under layer result in lower interlocking coefficients. The tolerance of the filter is limited to $+0.75D_{n50}$ and $-0.5D_{n50}$ without losing interlocking between the units. The filter layer is held constant during the test to focus on the effect of core permeability and to neglect the effect of placement and permeability of the filter layer.

5.2.5 core

The rock grading for the core in a prototype depends on the filter grading using the filter rules of Terzaghi for a geometrical open filter. The filter rules of Terzahi ensure the total stability by preventing outflow of small material, internal stability by preventing large settlements and permeability by requirements to the d_{15} of the core. These filter rules are presented below.

$$\begin{aligned} \text{stability} \quad & \frac{d_{15F}}{d_{85C}} < 5 \\ \text{Internal stability} \quad & \frac{d_{60}}{d_{10}} < 10 \\ \text{permeability} \quad & \frac{d_{15F}}{d_{15C}} > 5 \end{aligned} \tag{5.9}$$

The core of the breakwater can be scaled in three ways geometric similarity, Froude similarity and Burcharth method. For scale models with a fully turbulent flow regime in the core can be scaled geometrical. This is the case for Reynolds number is larger than of 40,000 according to (Hughes, 1993). Below this value the effect of induced viscous forces must be taken into account. It is important for the armour stability to have similarity of flow velocity in the core. This suggest to use the Froude scaling law as described in table 5.1.2. The linear geometric scaling of material diameters which follow from the Froude scaling may also lead to much too large viscous forces in the core for small scale models. Burcharth (1999) proposed a scale model incorporating the effect of large viscous forces corresponding to small Reynolds numbers.

Burcharth scaling

Burcharth (1999) proposed an empirical formula for the wave induced pressure gradient in the core. Together with the Forchheimer equation (explained in chapter 3) this can be used for estimation of the pore velocities in the core. Burcharth (1999) presents a method that the Froude scale law holds for the characteristic pore velocity. The method is based on the principle that the hydraulic gradients I in geometrically similar points in the core must be the same:

$$I_P = I_M \tag{5.10}$$

Where the I_P and I_M refer to the hydraulic gradient of the prototype and model, respectively.

Horizontal pore pressure gradient
The pore pressure in time is described by the wave-dampings-model described in section 3.3. Burcharth (1999) assumes an harmonic oscillation of the pore pressure at a fixed point in cores and neglecting the internal water set-up (illustrated in figure 5.4).

$$p(x,t) = p_{max}(x)cos(\tfrac{2\pi}{L'} + \tfrac{2\pi}{T_p}t) \tag{5.11}$$

$$= p_w g \tfrac{H_s}{2} e^{-\delta \frac{2\pi}{L'} x} cos(\tfrac{2\pi}{L'} + \tfrac{2\pi}{T_p}t) \tag{5.12}$$

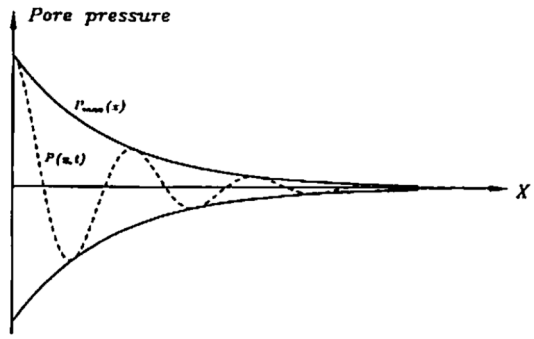

Fig. 5.4: Assumed pore pressure fluctuation in the core Burcharth (1999)

Inserting equation 5.11 in the horizontal pressure gradient, we obtain

$$I_x = \frac{1}{\rho g}\frac{dp}{dx}$$
$$= -\tfrac{\pi H_s}{L'} e^{(} - \delta \tfrac{2\pi}{L'} x)[\delta cos(\tfrac{2\pi}{L'} + \tfrac{2\pi}{T_p}t) + sin(\tfrac{2\pi}{L'} + \tfrac{2\pi}{T_p}t)] \tag{5.13}$$

With the pressure gradient the pore velocity in the core can be calculated using the Forchheimer equation.

$$I = \alpha \frac{(1-n)^2}{n^3}\frac{\nu}{gd^2}V + \beta \frac{1-n}{n^3}\frac{1}{gd}V^2 + c\frac{\partial V}{\partial t} \tag{5.14}$$

The main problem related to scaling of the core is that the hydraulic gradient and flow velocity varying from time and space. This makes it impossible to generate an accurate scale model of core material. Burcharth proposes to use the average flow velocity in the most relevant areas, which are around sea water level.

5.2.6 slope angle

Interlocking, single layer armour units benefit from gravity forces. The relation between the slope angle and interlocking forces and gravity are illustrated in figure 5.5. The effect of the interlocking forces increase with increasing slope angle while the gravity forces decreasing with the slope angle. Delta Marine Consultants recommends slope steepness from 2V:3H to 3V:4H to ensure complete usage of the interlocking capacity and gravity forces. The practical standard slope 3V:4H as it is in general the cheapest solution due to less volume. A slope of 2V:3H or flatter may be applied in areas with seismographic activities.
This research has been performed with the commonly used slope angle of 3V:4H.

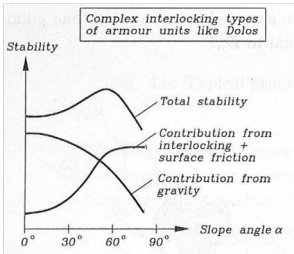

Fig. 5.5: Influence of the slope angle on the stability, from Abbott & Price (1994)

5.2.7 water level

The maximum water level in the wave flume is 70 cm. The maximum water level has been used during the model tests to generate the maximum wave height in the wave flume.

5.2.8 Crest height and width

The crest height of the breakwater is an important parameter which determines, in combination with the water level, the relative freeboard. The relative freeboard is the area between the Still Water Level (SWL) and crest that determines the amount of wave overtopping for a certain wave height.

To limit the possible settlement the maximum rows of Xblocs is set on 20. Settlement induces undesirable failure of the armour layer. However, it also increases the residual force parallel to the slope that increases the interlocking forces. The residual forces occurs due to an imbalance in forces on a single unit. Many rows in the model may increase the interlocking forces between the units and increase the armour stability unrealistic.
Model tests from Koppel (2012), show that till 25 rows does not show any significant influence on the interlocking forces. The model tests will be conducted with 22 rows. The required slope length is calculated with formula 5.15 prescribed by DMC, resulting in a length of 58.3 cm. The associated vertical length, in case of a 3V:4H slope, is 35 cm.

$$L_{armourlayer} = N_y \cdot d_y + 1/2D \tag{5.15}$$

Where N_y is the number of rows, d_y is the up-slope distance between the Xblocs and D is the Xbloc height.
The rows are situated following the damage expectation for Xbloc armour units. The area where damage can be expected lies between SWL +0.5 H_d and -1.5 H_d according to De Rover (2008) and is confirmed

by Van Zwicht (2009). The Xbloc rows are situated from SWL -20.0 cm till SWL +15.0 cm.

The crest width determines the wave penetration through a breakwater. This might be important by the demand of limited waves on the rear side of the breakwater. The minimum crest width requirement is 2.28 times D_{Xbloc}. With the chosen model units the design minimum crest width is 9.12 cm.

5.2.9 Toe

The toe of the breakwater is the foundation basis for the whole structure and must not influence on the wave propagation. The toe is normally constructed on the bottom in front of the armour layer and consist generally of large stones.
The model is dimensioned with a SWL of 70cm and 20cm of armour layer under the SWL leaving 50cm of the slope to be filled up by the toe. Minimizing the influence of the toe on the wave propagation the toe will partly be constructed with epoxy tiles. Epoxy tiles exist out of large stones (22.4-31.5mm) that are glued together with elastocoast. The stones are permeable enough to prevent collapsing waves on top of the breakwater and are small enough to guarantee a geometrically closed layer. The bottom of the epoxy tiles are supported by stones > 31.5mm.

5.2.10 Crest and rear slope

This study focusses on the hydraulic stability of the armour layer on the front slope of the breakwater. It is important that other failure mechanisms are prevented. During the model test overtopping of the breakwater is expected. Overtopping might lead to instability of the crest and rear side of the breakwater. The crest is therefore constructed with a crown wall and the rear side of the breakwater with similar epoxy tiles similar to the toe of the structure.

5.2.11 Wave spectrum

The model tests are performed with an irregular wave spectrum or random waves. Random waves present natural conditions and are chosen to obtain a realistic design situation. It is accepted for general application to describe irregular waves by a spectrum that indicates the amount of energy of waves at difference frequencies, also known as Energy-density spectrum. For coastal area the Joint North Sea Wave Project (JONSWAP) spectrum is often used to describe waters where the fetch is limited. However, many studies have confirmed that the JONSWAP spectrum is relative universal, not only for waters with limited fetch but also for deep water conditions including storms.

$$E_{JONSWAP(f)} = \alpha g^2 (2\pi)^{-4} f^{-5} exp[-\frac{5}{4}(\frac{f}{f_p})^{-4}]\gamma^{exp[-\frac{1}{2}(\frac{f/f_p-1}{\sigma})^2]} \tag{5.16}$$

where

E	The variance density;
α	Scale parameter;
g	gravitation;
f	The frequency;
f_{peak}	The peak frequency;
γ	Shape parameter with as general value;
σ	Scale parameter.

$$\begin{aligned} \alpha &= 0.0081; \\ \gamma &= 3.3. \end{aligned}$$

$$|\sigma| = \begin{cases} f \leq f_{peak} & 0.07 \\ f > f_{peak} & 0.09. \end{cases}$$

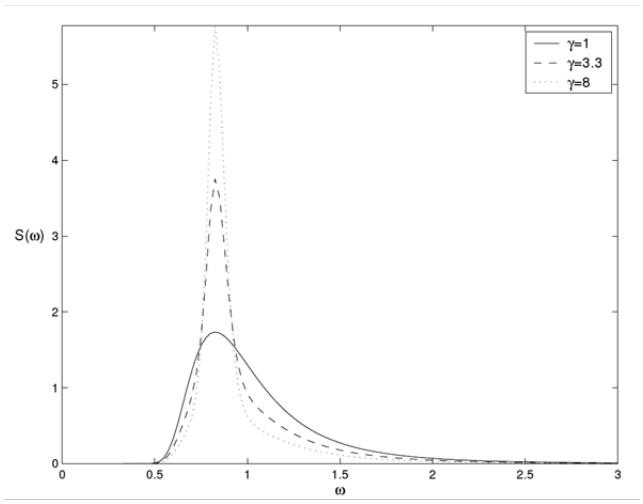

Fig. 5.6: The JONSWAP spectrum for γ=1 (dashed line), γ=5 (dotted line), γ=10 (solid line) with f_0 =0.1 Hz and α =0.0081; from Holthuijsen (2007).

The shape parameter γ influenced the peakedness and the width of the band. This difference in peakedness and the band width can be observed in figure 5.6.

The distribution of wave heights can be described with a Rayleigh distribution in water deeper than $\sim 3H_s$. In shallower water waves will break and the distribution deviates. The Rayleigh-distribution is valid for the wave height distribution in the physical experiments of this research.

$$P\underline{H} > H = \exp[-2(\frac{H}{H_s})^2] \tag{5.17}$$

5.2.12 Measuring data

The most important outcome of the experiments is the damage progression of the armour layer. With regards to the underlying physics the run-up on and under the breakwater will be measured and the wave height before the breakwater is measured.
The damage is measured by visual observations during the experiments. Two cameras has been used to record the armour layer from above and from the side which can be assessed to analyse the failure mechanisms. In addition photos are taken of armour layer before and after the wave series.

The wave height is measured with a set of wave gauges, existing out of three gauges. The distance between the gauges is related to the wave length (0.5-1.0L). The distance between of the wave gauges is taken constant on 0.3m and 0.4m. During testing a set of wave gauges is placed in front of the breakwater for measuring the wave height and wave reflection. The method of Mansard and Funke (1980) is used to separate the incoming wave from the reflective wave. This method is applicable for gentle sloping foreshores and uni-directional wave.
The wave gauge consist of two wire resistance probes that are simple and reliable, illustrated schematic in figure 5.7. The measurement method of the wave gauges is based on electricity conduction through water. The conductivity of water changes with temperature and therefore calibration of the wave gauges is of great importance. After calibration the wave gauge shows an error of less than 0.1 percent.

The water motion on the slope is measured using a run-up gauge, which is similar as the wave gauge with longer wires. Studies (Van Boekhoven, 2011) on core permeability showed that the wave run-up is an important parameter in the physical background of the effect of core permeability. Van Boekhoven (2011) recommends in his thesis to measure the run-up height under the armour layer as it is more affected by the core permeability. It is chosen to measure the run-up height both on and under the armour layer during the model tests using two run-up guages. Figure 5.8 show the run-up gauges as applied during the model test.

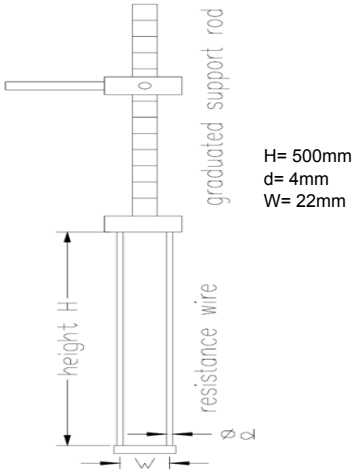

Fig. 5.7: Schematic overview of a wave gauge

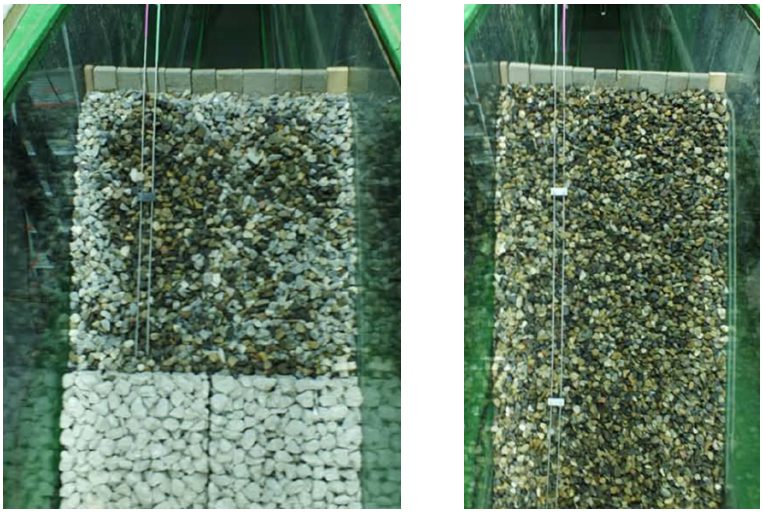

Fig. 5.8: Photos from the run-up gauge under the armour layer

Calibration of the wave gauges and run-up gauges is required to ensure reliable measurements. This is done before every test series to minimize the influence of temperature fluctuations. Besides gauge calibration the wave spectrum must be calibrated to ensure that the desired waves are released on the breakwater. Calibration of the wave record is done without a structure ensuring no effect of the structure on the measured wave height. The method of Mansard and Funke (1980) has been applied to measure the wave height.

5.2.13 Model layout

The general flume lay-out with the locations of the gauges is presented in the figure 5.9. The distance between the wave generator is long enough for a wave to fully develop. Behind the breakwater, the transmitted wave is damped by bottom friction or by a wave absorber (designed as an porous parabolic sponge). These measurements prevent that the transmitted wave influenced model tests.

The cross section of the breakwater is presented in figure 5.10. This figure illustrate the details and dimensions explained in this chapter. The crown wall on the crest must be placed to the rear side of the slope to allows for the run-up gauge underneath the armour layer.

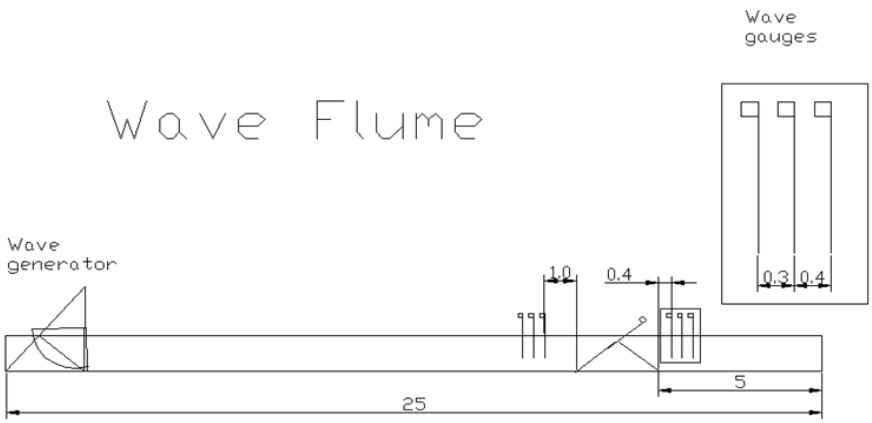

Fig. 5.9: Cross-section of the flume with two sets of gauges

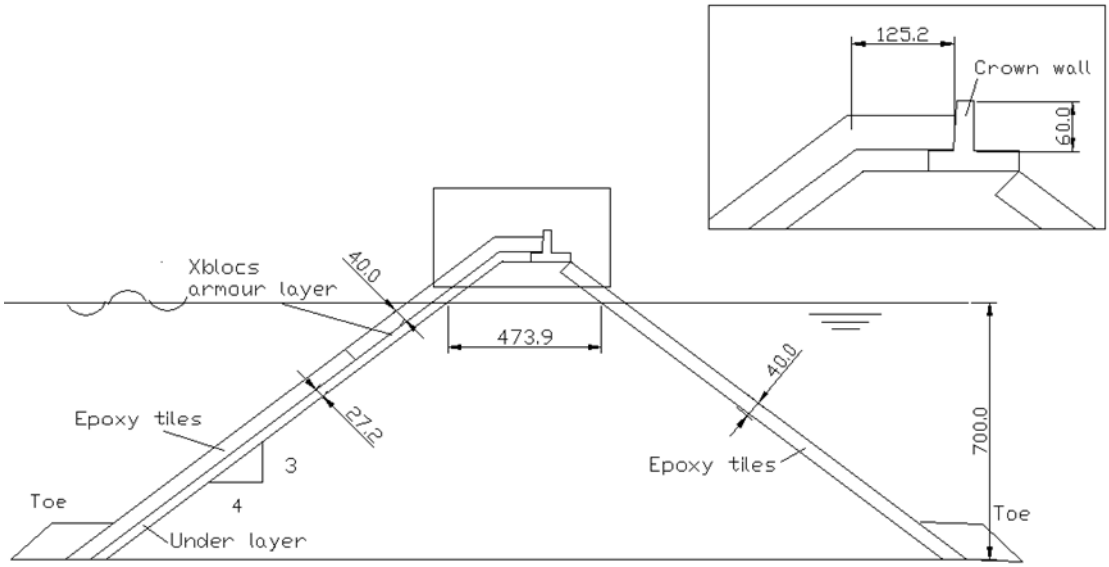

Fig. 5.10: Cross-section of the physical model

Armour lay-out

The width of the flume did not match an integer number of units. Therefore the width of the flume is adjusted with a small wooden strip placed against the glass.

Armour units near the wall lack interlocking from adjacent units on one side. The lack of interlocking is countered by the weight of a chain, see figure 5.11.
The glass and the run-up gauge also influence the flow and the stability of the armour units. The vertical Xbloc row next to the glass and run-up gauge are therefore not included in the damage observations. The observation area is marked with coloured units. This makes it easy to indicate the damaged area on the slope. The run-up gauges are located 15 cm from to wall to prevent boundary effects in the measurements of the gauge.

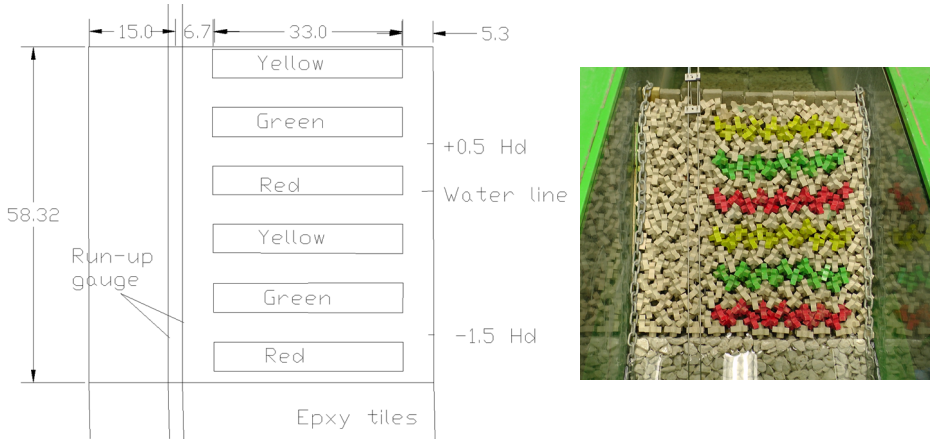

Fig. 5.11: Schematic front view of the armour layer

5.3 Core gradings

5.3.1 General

The core configurations are chosen such that the results of the permeability tests can be assigned to the permeability of the core. The permeability of various rock gradings is tested in the hydraulic laboratory of the Delft University of Technology. The permeability test and results are described in chapter 4 of this report. The filter layer was kept constant for two reasons; (i) the under the armour units is prescribed by Delta Marine Consultants and (ii) the filter layer affects the stability of armour layer.

The results of the filter velocity between the rock material varied for comparable hydraulic gradient and porosity. However, deviations in porosity can lead to overlapping in te filter velocity. It is also assumed that the hydraulic gradient in the core is smaller than during the test resulting in a smaller deviation in filter velocity and therefore it was recommended not to use two neighbouring rock gradings in the physical model test.
Furthermore, the test could not be executed for all Reynolds numbers as explained in chapter 4. For this reason shape factors of the Forchheimer model (section 3.2) are derived for a limit Reynolds range.

5.3.2 Core configuration

The initial test program consisted of three core configurations, it was decided to use the largest rock grading (31.5-22.4mm), filter material (16.0-11.2mm) and the smallest rock grading (5.6-4.0mm) in the physical model tests creating a large difference in permeability. Although the filter rules of Terzaghi were applied between the largest rock grading and filter material (16.0-11.2mm) the grains of the filter were forced into the core by the wave force and the total breakwater settled during testing. It was concluded that a larger core grading than the filter grading is not applicable.

Available gradations [mm]	d_{50}	**Tested**	**Initially chosen**
31.5- 22.4	27.0	√	√
22.4- 16	19.2	√	-
16- 11.2	13.6	√	-
11.2- 8.0	9.6	√	√
8.0- 5.6	6.8	-	-
5.6- 4.0	4.8	√	√

Tab. 5.2: Tested and initially chosen rock gradings

The test program was adjusted by using a core grading equal to the filter layer, an impermeable and a core grading in between being; the upper boundary, lower boundary and 'normal' core, respectively. The core grading for the middle configuration must fulfils the following two requirements:

- The Reynolds number in core should exceed the critical value of 1.5- 15 of the laminar flow. The flow should be in the Forchheimer flow regime.
- The core grading should skip a rock grading between two core consecutive model tests.

The following core gradings are tested:

Core 1 Core grading 16- 11.2mm.
Core 2 Core grading 8.0- 5.6mm.
Core 3 Core as impermeable layer.

Core 2 can be up-scaled using the Burcharth (1999) scaling method for core material. The core will be scaled using a fictitious breakwater with a D of 2.47m, a D_n of 1.71 m.
The scaling method uses the α and β coefficients calculated in chapter 5. The values variate with Reynolds number and can be determined for the scale model from i.e. the conducted tests or Burcharth (1995). It is important to check whether the used shape coefficients are valid in the Reynolds range, calculated from the average velocity of the method of Burcharth. The flow in the fictitious breakwater is fully turbulent, the coefficients are chosen similar as the breakwater of IJmuiden α is 0 and the β is 3.6 (Burcharth, 1999).

α and β coefficients

In chapter 4, the shape coefficients for the core gradings are calculated using a permeameter. The average calculated value from the permeability measurements are:

Gradation	Re	α	β
4.0- 5.6	app. 200- 300	∼600	∼3.0
4.0- 5.6	app. 300- 450	∼350	∼3.0
8.0- 11.2	app. 600-1,000	∼820	∼2.0
11.2- 16.0	app. 1,800- 2,700	∼716	∼1.9
16.0- 22.4	app. 2,000- 4,500	∼856	∼2.1
22.4- 32.5	app. 3,500- 7,200	∼1208	∼2.4

The Reynolds number in a small scale model remain generally below the fully turbulent boundary of Re< 600. The Reynolds range is only achieved by one rock grading (4.0- 5.6mm) due to limitations in the experimental set-up, as discussed in section 4.5.

- A characteristic prototype rock diameter of 0.25 m is obtained using α=350 and β=3.0 with a Reynolds number of 65 which is lower than the evaluated range.
- A characteristic prototype rock diameter of 0.14 m is obtained using α=600 and β=3.0 with a Reynolds number of 39 which is lower than the evaluated range. It cannot be confirmed that both coefficients are valid in this Reynolds range.

The estimated values of the α an β coefficients by Burcharth (1995) are in common used if no experimental research is conducted. The suggested values for irregular rock material are as follows:

Gradation	Re	α	β
narrow	5-600	360	3.6
wide	>600	13,000	3.6
very wide	>600	13,000	4.0

The rock gradings are narrow graded (d_{85}/d_{15}) and will be in the Reynolds range of 5-600.

-A characteristic prototype rock diameter of 0.22 m is obtained using α=360 and β=3.6 with a Reynolds number of 57 justifying the choice of α and β.

Conclusion

From the scaling method of Burcharth (1999), we obtain the prototype core gradings between 0.14m and 0.25m, which correspond to a standard coarse grading of 90mm- 250mm and a light grading of 5kg- 40kg (CIRIA, 2007). Using the filter rules (equations 5.8 and equations 5.9) for the fictitious breakwater with armour units of D_n of 1.71m, it can be concluded that the rock grading is in the range of the normal core. The core configurations will called further in this research refered to "open core", "normal core" and "impermeable core". Photos of the scale models can be found in appendix E.

The upper and lower boundary of the core configurations are comparable to P=0.5 and P=0.1 of the tests of Van der Meer (1988b). It is assumed assumption that the normal core is comparable to P=0.4. This assumption is not based on the prescribed configurations by Van der Meer (1988b) but on the common use in practise to apply P=0.4 for a normal core.

5.4 Test program

5.4.1 Hydraulic parameters

The model tests are set-up such that an overload condition of 180% of the design wave height can be achieved. Each test starts with a small wave conditions allowing the structure to settle. The model tests are performed with a wave height from 40% or 60% till 180% of the design wave height with in between steps of 20%. The design wave is calculated based on the stability formula for Xblocs with a stability number of (N_s) of 2.77.

Together with the wave height, the wave period is increased maintaining a similar surf similarity during the individual test series and therewith a similar breaker type. The breaker type is indicated to be important for the energy dissipation on the slope of the structure, determine the impact of the wave forces on the armour units. In this study the surf similarity represents the wave steepness s_{0p} due the fixed slope in the model test.

$$\xi_{op} = \frac{tan\alpha}{\sqrt{s_{op}}} \tag{5.18}$$

The influence of the wave length will be researched by performing the tests with two different surf similarities. The requirement of non-breaking waves is fulfilled when a surf similarity parameter larger than 3.5 is chosen. Table 5.3 shows the wave steepness during the tests.

Surf similarity	**Wave steepness**	**Type**
3.75	0.040	Wind wave
5.0	0.023	Swell wave

Tab. 5.3: Surf similarity parameter with associated wave steepness during testing

5.4.2 Test duration

Van der Meer (1988b) analysed the data and came up with a linear function from N=0 till N= 500 or 1000 if only high wave groups cause the first damage. After the first damage, the increase of damage will be reduced, partly due to the changed slope. The damage is limited by 1.3 times the damage at 5000

waves.
Te tests in this research are conducted with a test duration of 1000 waves

5.4.3 Programme

The physical model test is performed with two different surf similarities and three core configurations. Each test will be repeated at least three times to increase the reliability of the outcome. The test programme for this research is summarized in table 5.4. The repetition numbers will be indicated with a number behind the two characters presented in table 5.4.

	Open core	**Normal core**	**Impermeable core**
Wind waves	CA	BA	FA
Swell waves	CB	BB	FB

Tab. 5.4: Test programme

The significant wave height and wave period are calibrated without the structure near the intended structure. This is to make sure that the structure has no effect on the incident calibrated wave height. The allowable deviation from the design wave height was set on 5%. In appendix F the recorded and desired wave height are summarized and additional information on the wave spectra is reported. The impermeable core showed large settlements during the 60% wave height. Therefore it was chosen to start the repetition tests with a wave height that is 40% of the design wave height for the impermeable and normal core. The 40% wave height is less carefully calibrated with the result a deviation above the 5%.

5.5 Damage description

General

During physical model tests the hydraulic stability of the breakwater under wave attack is tested. Breakage of armour units can be the starting point for breakwater failure and must therefore be prevented, structural integrity. As known from breakwater history, the combination of hydraulic stability and structural integrity of armour units is important for the stability of the armour layer.

Structural integrity and Hydraulic stability

Structural integrity can be explained as the robustness or strength of a single unit against breakage. In other words: the resistance of an armour unit against forces due handling, placement and movement under extreme wave attack.
The structural integrity of the Xbloc has been determined by Finite Element (FE) calculations and a prototype drop test to validate the FE calculation made with standard load cases.
The drop test conducted in 2003 consist of four test series respectively overturning on the nose, overturning on the leg, hammer drop test and the free fall drop test. In the overturning tests it was found that the edges of the concrete will crush, leading to a negligible decrease of the unit mass. Larger fall heights resulted in a broken nose of leg depending on the orientation of te drop test.
Hydraulic stability is the ability of an armour unit to withstand wave forces. The hydraulic stability is general studied during hydraulic model tests. In the final design phase the breakwater should always be tested with a physical model test.

Damage definition

De Rover (2008) researched the effect of broken single layer armour units on the damage progression. It was expected that loss of unit mass reduces the gravitational force and inducing the damage progression. The used definition of start of damage was the displacement of more than four armour units. Damage

was defined as the displacement of units from the armour layer leading to exposure of the filter layer (approximately 25 units). The outcome of the research was that a breakage of an individual units has a negative effect on the displacement of units but has no significant influence on the displacement of the units from the armour layer. However breakage of several units close to each other has a slight negative effect on the start of failure (figure 5.12). Furthermore, the detached parts did not move or even tended to dig themselves in the filter layer. It is therefore unlikely that rapid damage progression occurs due to broken parts.

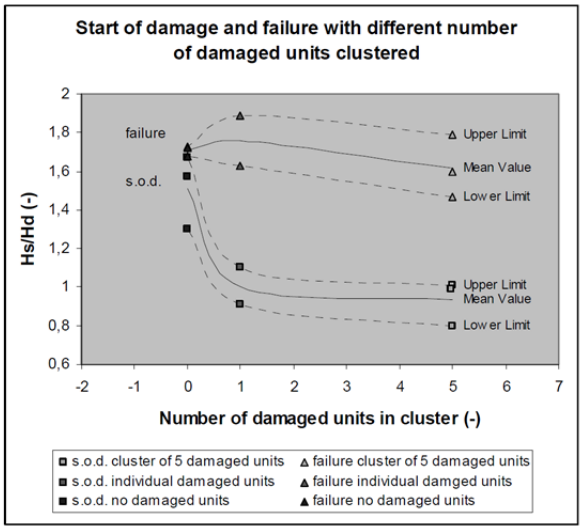

Fig. 5.12: Start of damage and failure with clustered damaged units (de Rover et al., 2008)

From the report of De Rover can be concluded that broken units have a significant impact on displacement or start of damage of units and therefore it can be said that breakage of a unit is the start of damage for this research. Although breakage will not be observed during model tests with plastic model units, movements of units can be observed. The probability of breakage to a certain movement can be estimated on the basis of the prototype drop tests. The research concluded furthermore that interlocking units have a high ability of self repairing but multiply broken units in the same area show a rapid damage development due loss of interlocking. Breakage of several units will eventually lead to failure.

For this research it is chosen to use the degree of movement of units for the damage definition. Damage can be presented as percentage of the total amount of units but if the amount of units differ for each design the result of various model test can hardly be compared. For this research is chosen to define damage as a percentage of units in horizontal direction, similar as Van der Meer. The damage progression of the slope is defined as the number of moved units within a width of strip of breakwater slope with the nominal diameter.

$$N_{od} = \frac{Numberofmovedunits}{widthofthelayer/D_n} \tag{5.19}$$

The contribution of a moving unit to the damage development depends on the probability that it initiates breakage of the unit. This is corporate in formula 5.19 as follows:

$$N_{od} = \frac{N_{0<0.5} > 2\% \text{ of the waves}}{\text{Width layer}/D_n} + \frac{N_{0>0.5}}{\text{Width layer}/D_n} \tag{5.20}$$

$N_{0>0.5}$=number of units moved more than $0.5D_n$.

$N_{0<0.5}$=number of units moved less than $0.5D_n$.

N_{od} = definition for damage.

6. TEST RESULTS

6.1 General

This section presents and discusses the observed damage results for each of the considered core permeabilities. Each experiment was repeated three times, increasing the reliability of the experiments. During testing various failure mechanisms were observed namely rocking, lifting of armour units and settling of the armour layer, which will be explained below.

6.2 Failure mechanisms

Rocking single unit

Rocking is the result of a combination between limit interlocking of a unit and high flow forces upwards. The mechanism behind rocking is that the velocity force during rushup rotates the unit in upward direction. The rushdown force of the same wave pulls the unit back down in position. This principle is defined as rocking and is illustrated in figure 6.1. A unit will start with rocking when the unit is not sufficient interlocked by neighbouring units. In other words, a unit might rock when there is enough space above the unit for rotation.

Generally, rocking of a single unit occurs around sea water level where the packing density is reduced by settlements of lower-lying Xblocs rows. Low packing density of the armour layer results in less interlocking between neighbouring units. Furthermore, the run-up velocity is at its maximum around SWL increasing the probability of rocking.

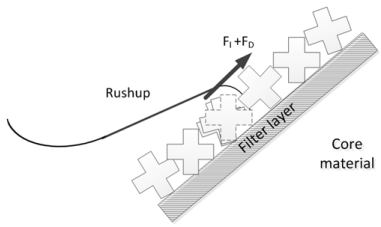

Fig. 6.1: Rocking of a single unit around SWL.

Lifting of units from the slope

Lifting of units from the slope has two appearances; lifting of multiple rows at once or lifting of single units. Lifting of units is initiated by a high wave in series of higher waves with large run-up heights and a deep rushdown. At maximum run-down is the flow direction downwards in outward direction along with the hydraulic gradient. The higher pore pressure inside the structure pushes the units in outward direction. At the same time a new incident wave overtakes the previous wave at lowest point resulting in a turbulent breaker in upward direction. The flow in downward direction in the armour layer must turn suddenly 180 degrees in upward direction pushing the units in outward direction and successively upwards (lifting the armour units).

Units that are insufficiently interlocked around the maximum run-down are lifted by drag and inertia forces. The unit tend to move till it is sufficiently interlocked. The unit will come back in place when the gravity force of the unit exceeds the inertia and drag force. This event occurs each time when the forces exceeds the gravity force till the unit is replaced and has no space for movement. The unit will be extracted when its not interlocked by neighbouring units during the uplift.

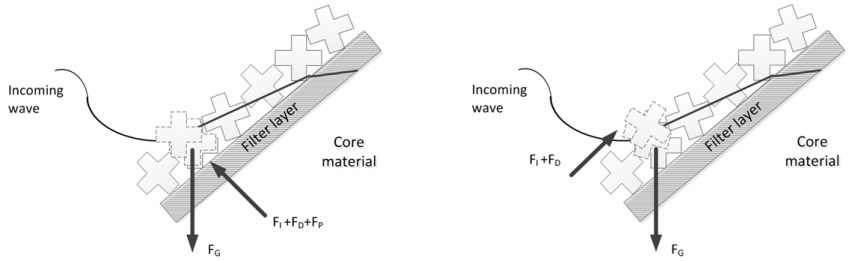

Fig. 6.2: Lifting of a single unit

Lifting of multiple rows at once occur when the hydraulic gradient in the armour layer is less steep and the inertia forces are relative low. The units are not pushed out of the pattern by turbulence and stay interlocked but do come loose from the under layer.

Settlement

Settlement is it suddenly or gradually sliding down of unit on the filter layer resulting in a higher packing density and therewith interlocking with neighbouring units. Although the settlement has a positive effect on the hydraulic stability of lower laying rows, it has a negative effect on the upper part of the slope. The higher rows experience a lower packing density or even gaps between units decreasing interlocking forces and exposing the under layer.

During testing two main mechanism were distinguished which cause settling of the armour layer.

1. The drag force exceeds the gravity and interlocking forces during the uprush. This part of the mechanism is similar to that of rocking but occurs on the entire width of the slope. The downrush pushes the units down generating a large force on the lower rows that exceeds the friction forces between the under layer and neighbouring units. This results in sliding down of units so called settlement.
2. Friction forces between armour layer and under layer are reduced by high pore pressure inside the structure and outflow velocity. The combination of limited friction force and a downward drag force results in settling of the armour layer.

6.3 Observations

During testing the armour layer was observed. This section will summarize the observation of the individual wave series. In appendix G is the start photo and the photo after the design wave height presented. These photos give a good representation of the relative impact of the waves on the armour layer.

6.3.1 Swell waves

The breaker type observed during testing was mainly a surging wave during with occasionally a collapsing waves.

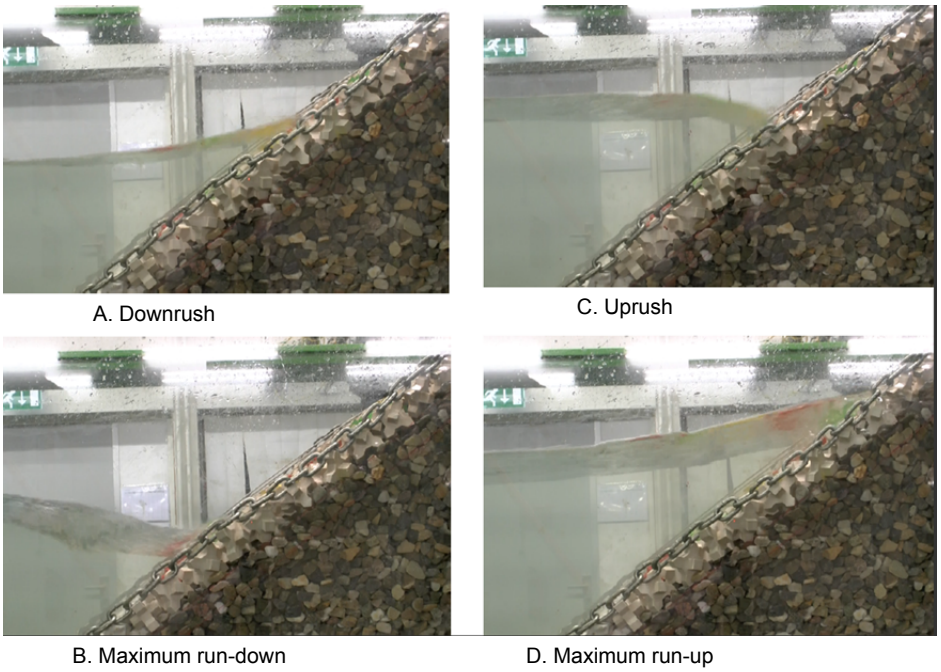

Fig. 6.3: The wave motion on the breakwater

Settlement

The test series with swell waves showed large settlements with respect to wind waves. The occurrence of the settlements varied with core configurations, the largest settlements occurred with an impermeable core and minimum settlement with an open core. A summary of the observations regarding settlement of the armour layer are presented below.

Open core

- The total armour layer settled slowly.
- At the 100%-120% wave height larger settlements were observed.

Normal core

- During the 60% wave height of repetition 1 the armour layer settled. It was chosen to perform repetition 2 and 3 with additional wave series with a 40% wave height to minimize the probability of abrupt settlement of the armour layer.
- Settlement has not been observed during the 40% wave height. Relative large armour settlement occurred at the 60% wave height for repetition 2 and 3.
- From the 80% wave height the armour rows at the upper part of the breakwater move downwards (settle).
- At the 160% wave height the armour layer have been settle so that overtopping waves transported armour units over the breakwater.

Impermeable core

- At the 40% wave height small initial settlements of the armour layer have been observed.
- During the 60% wave height the armour layer settled greatly.
- Rows at the upper part over the breakwater moved along downwards with the settlements at the 60% wave height preventing units to rock. Till +1.0 H_d the armour stays tightly packed.
- At the 160% wave height the armour layer have been settle so that overtopping waves transported armour units over the breakwater.

Rocking

The test series showed a great deviation in the amount of rocking for each configuration. The amount of rocking is partly related to the degree of settlement of the armour layer as the interlocking increased for higher packing densities of the armour layer.

Open core

- During the 80%- 100% wave height rocking occurred. The location of rocking armour units were mainly from SWL to crest.

Normal core

- At the 80% wave height occasional rocking of armour units located from the SWL till crest by lack of interlocking.
- Wave heights larger than the 100% wave height cause rocking armour units below SWL.

Impermeable core

- Rocking was negligible during the tests.
- Large uprush and downrush have been observed along the slope during the test series. The low degree of rocking might therefore been assigned to the high packing density of the armour layer.

Lifting of units from the slope

The degree that units were lift from the slope depended on the core configuration and wave height, showing different type of lifting mechanism.

Open core

- At the 120%-160% wave height single units are occasional lifted a bit around -1,0 H_s of the wave series.
- The degree of movement was relative low and can be compared with rocking of armour units.

Normal core

- From the 100% wave height single units were lifted form the slope around -1.0 H_s.
- From the 120% wave height multiply rows are lifted from the slope at maximum run-down.

Impermeable core

- From the 100% wave height wave height units are lifted from the slope around -1.0 H_s. The increased interlocking due high packing of the armour layer allows minimal lifting of single units.
- At the 120% wave height an incoming wave with a breaking character was observed.
- From the 160% wave height the lowest wave retreat occurs under the armour layer reducing the lifting force on the armour units.

Overview

The observation with respect to settling, rocking and lifting of units, described above are summarized in the table 6.1. A complete overview of the damage progression can be found in appendix H.

	Large settlements	Rocking	Lifting of units
Open core	100%-120%	80%-160%	120%-160%-
Normal core	60%	100%-120%	120%-160%
Impermeable core	60%	>140% crest	100%-140%

Tab. 6.1: Overview of the occurrence of the failure mechanisms

It was overall observed that the large settlements for an impermeable core leads to a dense packed armour layer and only little rocking of armour units. This is in contrast to an open core, which encounter less settling of the armour layer and more rocking of armour units. Furthermore, lifting of armour units at the 80% wave height for an impermeable core indicate an increase in forces on the armour layer with a decrease in core permeability. A more detailed analysis of the failure mechanisms regarding core permeability can be found in section 6.4.

6.3.2 Wind waves

The breaker type observed during testing was mainly a surging wave with turbulent breaker and occasionally a collapsing wave. The collapsing wave happened for the impermeable core.

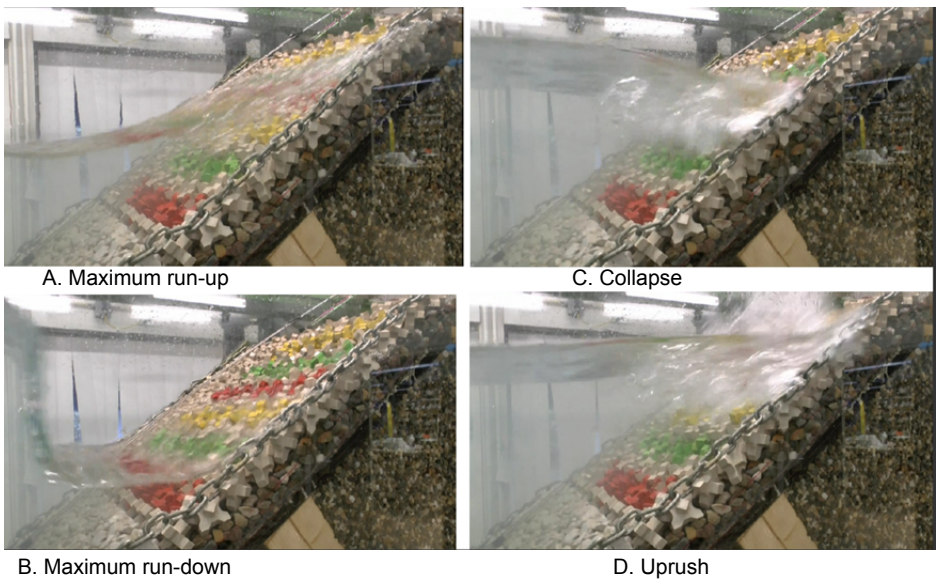

Fig. 6.4: A wave collapsing on a breakwater

Settlement

The occurrence of the settlements varied with core configuration. The largest settlements occurred with an impermeable core and minimum settlement with an open core, which corresponds with swell waves. A summary of the observations regarding settlement of the armour layer is presented below.

Open core

- Negligible initial settlement of the armour layer has been observed.

Normal core

- During the 60% wave height of repetition 1 settling of the armour layer occurred. Though repetition 2 and 3 are conducted from the 40% wave height, large settlements remain at the 60% wave height.
- The armour layer settles gradually.

Impermeable core

- At the 40% wave height small initial settlement of the armour layer.
- At the 60% wave height the armour layer settled at once.
- From the 100% wave height waves with breaking character have been observed. The impact of the breaker wave resulted in settlement of the armour layer.

Rocking

The test series showed a great deviation in the amount of rocking for each configuration. The amount of rocking is partly related to the degree of settling of the armour layer as the interlocking forces increases for higher packing densities of the armour layer.

Open core

- From the 80% wave height rocking occurred mainly from SWL till maximum run-up.

Normal core

- From the 100% wave height occasional rocking of armour units.

Impermeable core

- Low degree of rocking due the relative high packing density of the armour layer.

Lifting of armour units

Open core

- From the 100% wave height single and multiply units are easily lifted from the slope at the maximum run-down of the wave.
- Test CB1 experienced a sudden extraction of an armour unit during the 100% wave height.
- Test CB4 experienced extraction of several armour units with the result that the total breakwater failed.

Normal core

- From the 100% wave height multiply rows are lifted, in varying degrees, from the armour slope at lowest wave retreat.

Impermeable core

- At the 100% wave height waves with breaking character have been observed.
- From the 120% wave height armour units from lowest run-down till SWL are pushed a tiny bit out of the armour layer and pulled upward with the incoming wave.

Overview

The observation with respect to settling, rocking and lifting of units, described above are summarized in the table **??**. A complete overview of the damage can be found in appendix H.

	Large settlements	Rocking	Lifting of units
Open core	>180%	80%-180%	100%-180%
Normal core	60%-100%	100%-160%	100%-180%
Impermeable core	60%-100%	> 140% crest	100%-160%

Overall, the failure mechanisms of wind waves regarding core permeability show a similar trend as for swell waves. Only an additional failure mechanism was observed for wind waves, being a collapsing waves. The largest waves started to collapse for the impermeable core increasing the damage to the armour layer. A more detailed analysis of the failure mechanisms regarding core permeability can be found in section 6.4.

6.4 Data analyse

The description of the observed damage in section 6.3 does not show the relation between the core permeability and the armour stability. The influence of the core permeability will be described on the basis of the damage definition defined in section 5.5 of this thesis. The damage level N_{od} will be set out against the stability number N_s for the test series. The results are analysed by comparison of the damage level N_od with the normal core for the individual tests series.

The damage levels obtained from the test results with the normal core should show good resembles with the stability numbers for start of damage, prescribed by DMC. It is expected that the open core is more stable and the impermeable less stable than the normal core. First the damage level of the normal core tests will be discussed in order to compare the open and impermeable core with the results of the normal core.

In addition to the damage levels, the standard deviation is determined for each individual wave height. The graph on the right hand of figure 6.5 till figure 6.10 show the mean value (μ) and the 90% confidence levels of N_{od}. The 90% confidence level is based on the Gaussian distribution, which is defined with $\mu \pm 1.64 \cdot \sigma$, were σ is the standard deviation illustrated in the figure at the bottom.

6.4.1 Swell waves

From the damage curves for swell waves it becomes clear that damage occurs for higher wave loads by the normal than for the open and impermeable core. Furthermore, it can be concluded that the damage progression is lower for the open core compared to the normal and impermeable core. The uncertainty surrounding the occurrence of damage is indicated with the standard deviation of each core configuration. It is concluded that the damage level for the open core is higher than for the normal and impermeable.

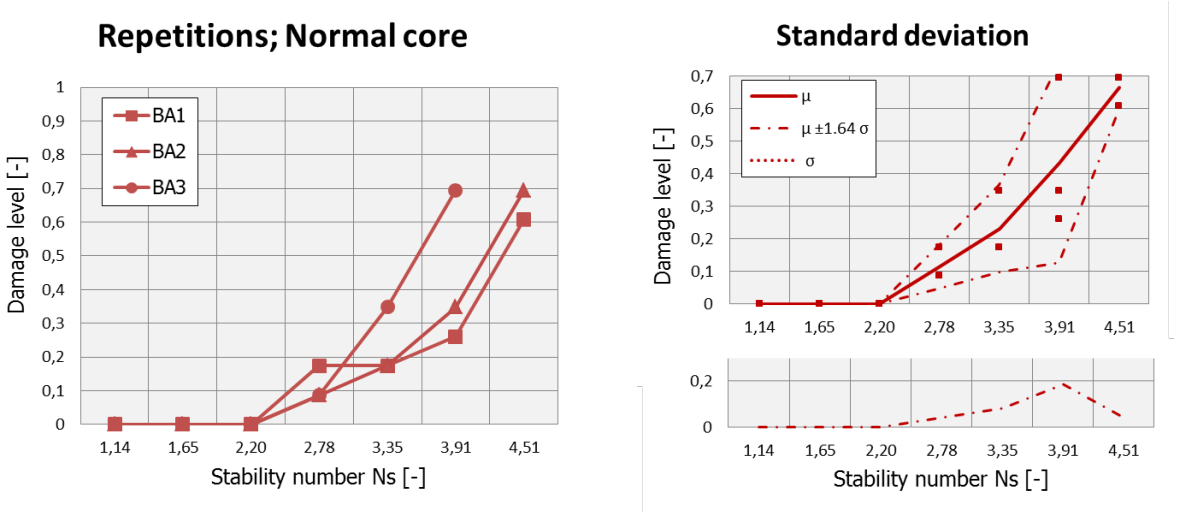

Fig. 6.5: Damage number versus armour stability number for the normal core; swell waves

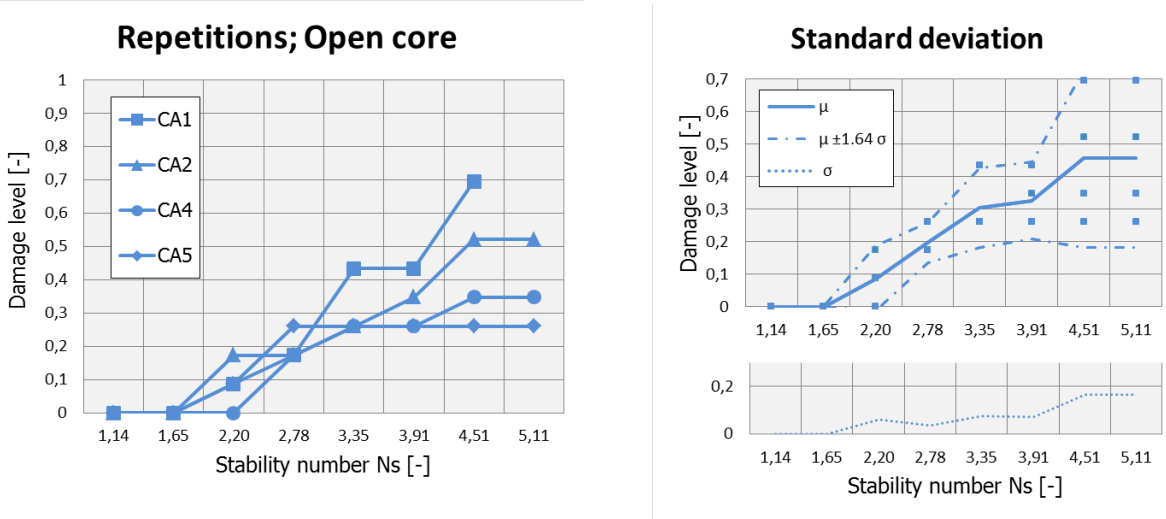

Fig. 6.6: Damage number versus armour stability number for the open core; swell waves

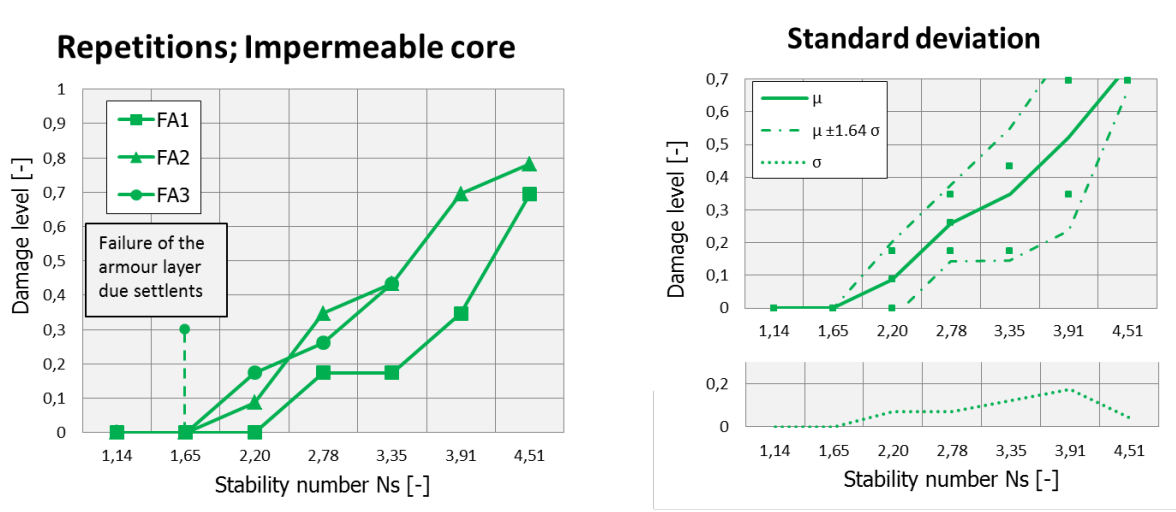

Fig. 6.7: Damage number versus armour stability number for the impermeable core; swell waves

Normal core
The tests results for the normal core are presented in figure 6.5. The tests series show a good resemblance in start of damage and damage progression. However start of damage occurs due rocking or armour units, the amour layer fails due rocking and movement of the armour units larger than $0.5d_n$.

The standard deviation for the open core is low for small wave heights and increases with the wave height till failure of the armour layer is guaranteed.

Open core
It is expected that the tests results for the open core show a higher stability of the armour layer than the normal core. The damage levels for the test series with the open core are presented in figure 6.6. The three test series show a good resemblance in the trend-line of the damage levels. The trend-line is more gradually than for the normal core and starts at a lower stability number than for the normal core. The damage level increases gradually till the maximum wave height of 180% except repetition CA1, which fails at the 160% wave height while for the other repetitions no failure occurs.
The standard deviation of the damage level for each individual wave height remains relative low till failure of repetition CA1 occurs. From there on the standard deviation increases a till the highest relative wave height (180%).

The expected increase in hydraulic stability cannot be confirmed from the damage observations.

Impermeable core
It is expected that the test results for the impermeable core show a lower stability of the armour layer than the normal core. The tests series for the impermeable core are presented in figure 6.7. The three test series show a good resemblance in start of damage. The lower stability of the amour layer is confirmed with the start of damage at low stability numbers for repetition FA2 and FA3.
The damage progression is in first instance slowed down by tight packing of the armour layer due great settlements. This results finally in a comparable stability number for failure as the normal core.

However, the settlements at the 60% wave height are such large that the upper armour rows move more than $0.5d_n$ and are accounted in the damage definition. This results in failure of the armour layer at the 60% wave height for the impermeable core.

6.4.2 Wind waves

From the damage curves for wind waves it becomes clear that the start of damage occurs at similar wave height for all three of the core configurations. The damage progression decreases with the permeability of the core. The standard deviation works opposite, it increases with the permeability of the core. This means that low damage levels are expected with high waves for the open core but a large uncertainty must be encountered with this prediction.

Normal core
The tests with the normal core are presented in figure 6.8. The tests series show large deviation for the wave height where the armour layer fails. This can be observed from the increasing standard deviation for higher wave heights.

The fast damage progression of repetition BB3 can be explained by the low placing density of the armour layer. It seems that failure is not influenced by the low packing density. The sudden increase of damage level of repetition BB1 cannot be explained.

Open core
It is expected that the open core has a higher armour stability than the normal core. Figure 6.9 presents the test with the open core. The three tests in the graph show a comparable start of damage. The damage progression deviates for the three the repetition. During repetition CB4, extraction of single

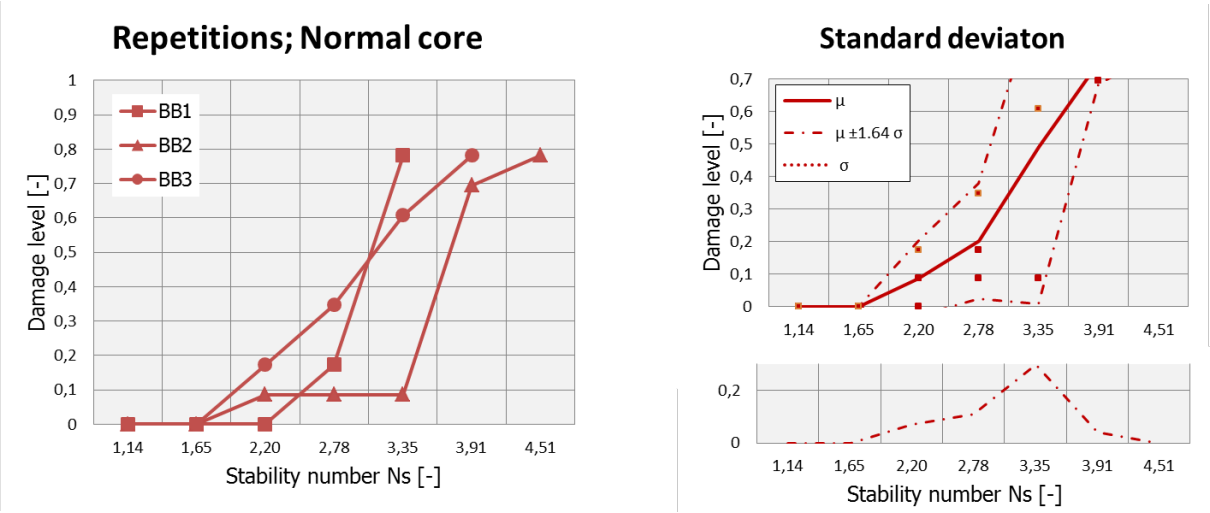

Fig. 6.8: Damage number versus armour stability number for the normal core; wind waves

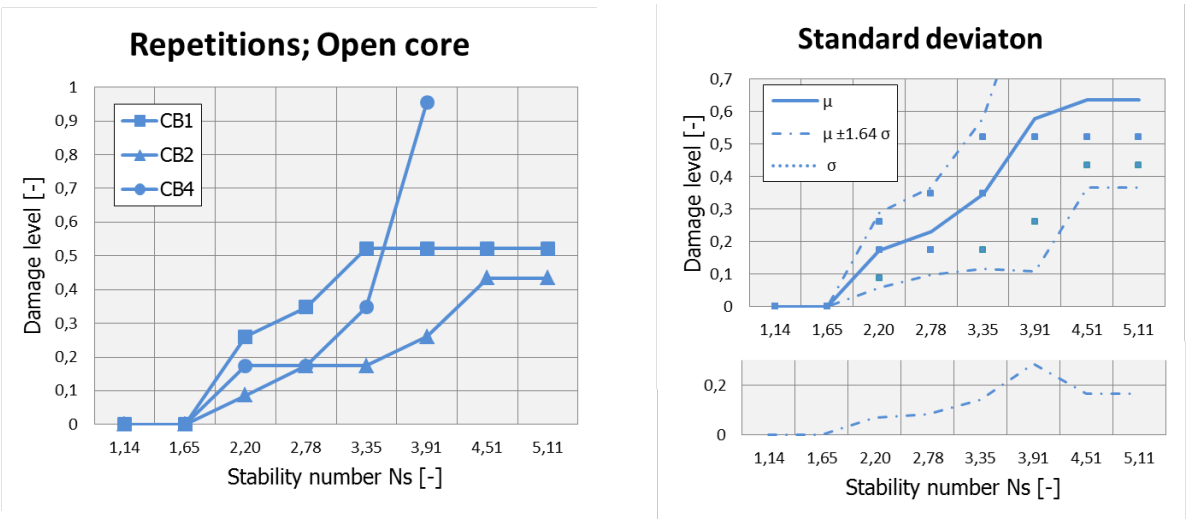

Fig. 6.9: Damage number versus armour stability number for the open core; wind waves

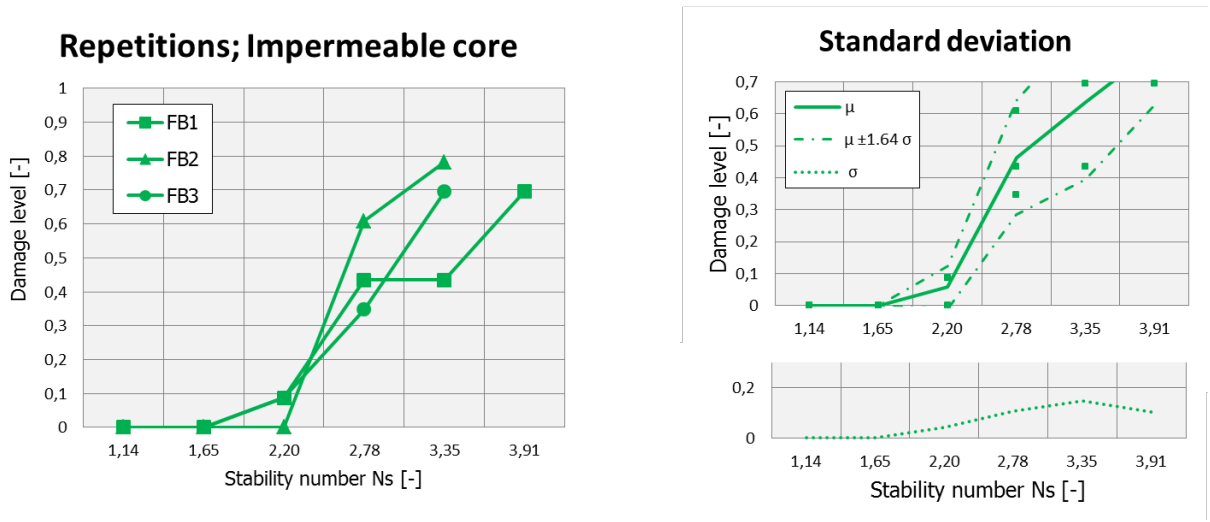

Fig. 6.10: Damage number versus armour stability number for the impermeable core; wind waves

units occurred where after the whole armour layer failed. The extraction of the armour layer can be explained by the low packing density of the armour layer, reducing the interlocking forces between the armour units.
During repetition CB1 a single armour units was extracted from the slope due low interlocking forces. However, progressive damage development was withheld higher armour packing preventing failure of the armour layer.

The standard deviation is relative large due the great differences in the damage progression curves. This means that a large uncertainty is encountered with the test results of the open core.

Impermeable core
It is expected that an armour layer on an impermeable core has a lower stability than with of a normal core. The tests with the impermeable core are presented in figure 6.10. The three tests in the figure shows a good resembles in damage progression. From the graph it becomes clear that the start of damage occurs at similar wave heights as the normal core. The damage progression is larger for the impermeable core than for the normal core confirming a lower armour stability for the impermeable core than for the normal core.

The damage progress is relative consequent resulting in low standard deviations compared to the open and normal core. This means that the damage levels are assured for a certain wave height.

6.5 Discussion

The observed failure mechanisms can be related to the water motion in the structure. An attempt has been made to find the cause of each failure mechanism.
The water motion around the armour layer influenced the failure mechanism of the armour units. The water flow in the armour layer was studied by analysing the video's and data of the run-up gauges. The observations were linked to the measured data of the water level around the armour layer to obtain an overview of the water levels in the specific time period. This analysis was performed in order to gain an overview of the water motion around single units, which is of great importance for the dynamic stability of the armour layer. The change in water profile in the armour layer with an impermeable core affects the flow forces and the stability of armour units.

The results and implications of the analysis that are worked out in detail in appendix J will be discussed. Hereafter, the failure mechanisms will be discussed in relation to the water motion.

The observed damage levels are translated into damage and failure numbers resulting in correction factors on the unit weight for primarily design. In the final part of this section the difference between the influence of the core permeability on rock armour layer and single layered interlocking armour units is discussed. The difference is obtained by a comparison of the empirical formulae for the run-up level, hydraulic gradient, reflection coefficient and damage level with the measured data.

6.5.1 Water motion around the armour layer

This section discusses the data analyse in appendix J, which elaborates on the water motion around the armour layer. The water motion as a whole will be treated and in specific the differences between an open and impermeable core.

The water movement on the slope will be described by four phases, being the downrush, maximum run-down, uprush and maximum run-up. The water motion around the armour layer will be explained on te basis of these phases in subsequent subsection. In addition, the most important differences in water motion between an impermeable core and open core will be explained using the conclusions of the data analysis in appendix J. Figure 6.11 till figure 6.13 illustrate the water motion around the slope of the breakwater. The explanation of the water motion below refers to these figures.

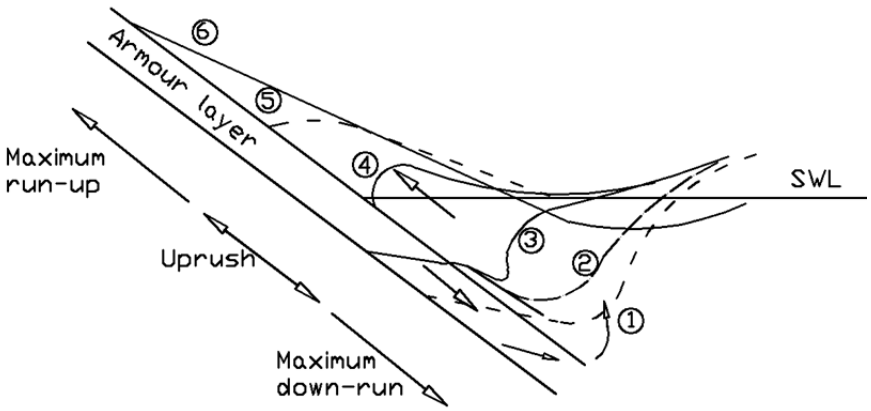

Fig. 6.11: Water motion on the armour layer; maximum run-down, uprush and maximum run-up

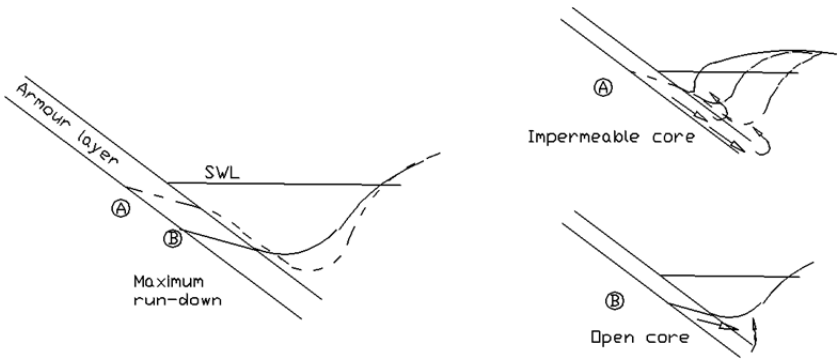

Fig. 6.12: Difference in water motion at maximum run-down between an open (B) and impermeable core(A)

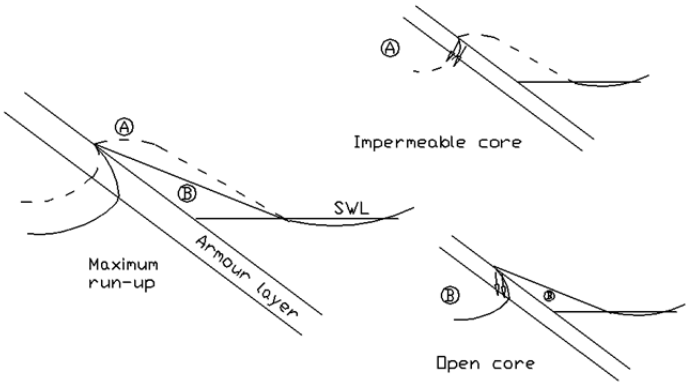

Fig. 6.13: Difference in water motion at maximum run-up between an open (B) and impermeable core(A)

Before the effect of the core permeability on the water motion and associated flow forces around the armour layer will be discussed, several flow situations will be explained:

Outflow:	Water flow in outward direction of the structure.
Backflow:	Water flow in the armour layer of the structure due outflow from the core during downrush.
Inflow:	Water flow into the structure.

Downrush During the downrush the external water motion is in downward direction inducing the water outflow from the core of the structure. The downrush is followed by backwash in the armour layer leading to dominating parallel forces. The amount of backflow depends on the outflow rate from the core, which depends on the permeability of the material combined with the hydraulic gradient in the core. Low core permeability decreases the outflow rate that increases the hydraulic gradient in the core, which increases the outflow rate again. The relation between permeability, hydraulic gradient and average velocity has been proven with the permeability tests in chapter 4.

consequence of a low permeable core is a low outflow rate of water from the core, which increases the phase lag of the water motion between the top of the Xbloc layer and the filter layer. This results in a large hydraulic gradient in the armour layer as the external water level continues to decrease. The water outflow area from the core increases increasing the backflow in the armour layer as shown in figure 6.12.

Maximum run-down At lowest point of wave retreat the backflow meets the incident wave resulting in a complex flow situation with forces directed in outward direction from the slope (line 1+2 in figure 6.11). The main difference between an open and impermeable core at maximum run-down are illustrated in figure 6.12 and can be described as follows:

i The level of maximum run-down decreases with core permeability.

ii The maximum hydraulic gradient in the armour layer increases with decreasing core permeability indicating a large flow parallel along the slope.

iii The maximum hydraulic gradient shifts in time toward the location of maximum run-down for an impermeable core. This is possibly caused by the water volume in the armour layer that pushes the incoming water back into seaward direction.

iiii More abrupt rotation at the maximum run-down of the backflow to turn from downward into upward direction. This is indicated by a peaked line in the water motion on the slope.

The forces on a single unit around maximum run-down depend on the combination between flow velocity, flow acceleration and the duration that the water flow is directed in outward direction. Two forces are of importance for destabilizing a single unit at maximum run-down, being the drag force due flow velocity and inertia forces due flow acceleration. The inertia force increase with the size of the backflow (iii), rotation angle of the backflow (ii) and the duration of the turning moment of the backflow (iiii). However, great accelerations during the maximum down-run shortens the moment that the flow forces are directed in outward direction reducing the total force on a single unit. In other words, flow acceleration has a negative effect on the size of the force on the armour units but shortens the duration of the forces in outward direction.

Besides the water motion in the structure, the armour stability is influenced by the wave steepness. Steep waves have a steeper front side forcing the backflow rapidly in upward direction. This fast change in flow direction is accompanied by larger accelerations and inertia forces.
Nevertheless, steep waves contain a smaller volume of water than gentle waves in case of similar wave heights. The lower water volume and smaller wave period for wind waves lead to lower hydraulic gradients in the armour layer for the normal and impermeable, which have a positive effect on the armour stability.

Uprush Upslope, the uprushing wave meets the backflow in the armour layer resulting in a similar situation as at maximum run-down, as presented in line 3+4 in figure 6.11. The backflow volume in the armour layer and the acceleration of the water flow during uprush is significant larger for an impermeable core than for an open core, resulting in great negative forces on the armour layer. This is illustrated in figure 6.12.
Although the flow acceleration increases, the maximum flow velocity on the slope of the structure remains unaffected by the processes inside of the structure.

Maximum run-up Further upslope, the inflow increases and the parallel velocity reduces at line 5+6 in figure 6.11). The reduction of the parallel forces depends on the water penetration into the structure, which is affected by the permeability of the core.
The permeability of the core is reflected in the run-up level on the core and in this study on the filter layer, illustrated in figure 6.13. The run-up level on the filter layer increase with low

core permeability, indicating a large water accumulation in the armour layer and larger forces on the armour units. Armour units on an impermeable core encounter larger hydrodynamic and hydrostatic pressure forces on the armour units.

To summarise, armour units on an impermeable core encounters a different water motion around the armour units than armour units on an open core. This results in a change in size and direction of the forces on the armour layer. This is illustrated in table 6.2.

Change in water motion for an impermeable core compared to an open core.	**Cause of the change in water motion**	**Effect of the change in water motion**
Larger maximum run-down level.	Large backflow volume pushing the wave toward the sea.	- Larger hydraulic gradients in the armour layer
Larger hydraulic gradient in the armour layer at maximum run-down.	Low outflow velocity from the core in combination with a large run-down level and internal set-up in the core.	- Larger backflow volume - Flow parallel to the slope increasing the angle of rotation for the backflow - Larger outflow velocities
The maximum hydraulic gradient shifts in time toward the location of maximum run-down.	Large backflow volume pushes the wave toward the sea causing a delay.	- Larger hydraulic gradients in the armour layer - Larger forces near the incident wave
More abrupt change in flow direction at maximum run-down indicated by a peaked line in the water motion.	Large backflow that is suddenly abrupt by the incident wave.	-Shorter rotation moment for the backflow results in larger acceleration forces.
Constant maximum flow velocity parallel to the slope	The maximum velocity is bounded by the maximum vertical velocity	-Negigible increase of maximum drag force parallel to the slope. -Longer large flow velocities to overcome a larger distance.
Larger run-up levels on the filter layer	Small inflow velocity results in low water penetration into the core.	-Larger parallel forces and pressure forces on the armour units.
Larger reflection coefficient for an impermeable core	Absence of wave transmission increasing the backflow volume.	-Large force on the armour units.

Tab. 6.2: Change in water motion in the armour layer and the cause and effect of this change

6.5.2 Settlement

The packing density of the armour layer is of great importance for the interlocking forces between the amour units and the concrete usage for an area. The armour layer encountered large settlements during wave series with low wave height increasing the packing density of the armour layer. The settlement of the armour layer is expressed in the packing density relative to the prescribed placing density by Delta Marine Consultants, which relates to the unit height $1.2/D^2$. The relative packing density (RPD) is measured after completion of placing of the armour layer and after each wave series during testing and from photos. The average RPD was calculated from a rectangular surface by measuring five times the horizontal distance and seven times the vertical distance, illustrated in figure 6.14.

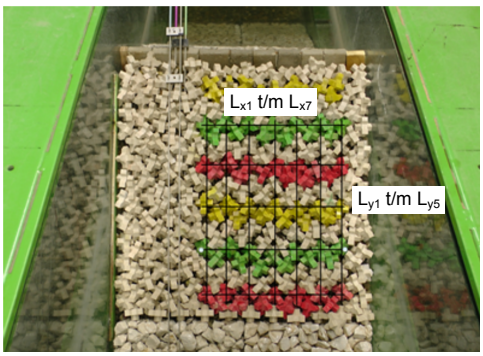

Fig. 6.14: Area within RPD is measured

The RPD showed a relative large difference. Therefore, it is concluded that RPD calculations are sensitive toward the point of view, which influences the measurement results. Despite the differences in RPD both measurements showed a similar trend-line presented in figure 6.15. The different colours in the figure illustrate the different core configurations and the zero wave height is placing density of the armour layer.

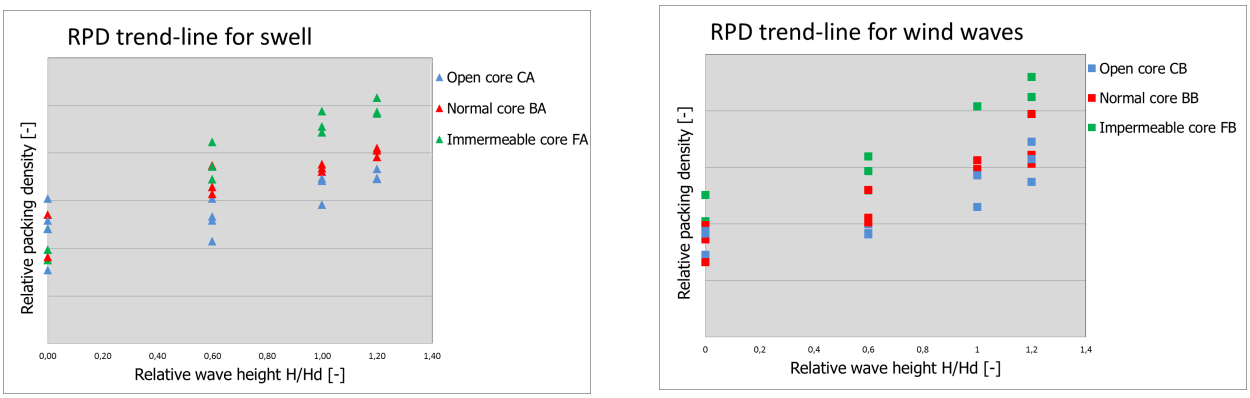

Fig. 6.15: Trend-line of the relative packing density plotted against the relative wave height

Settlement of the armour layer was observed by three mechanism:

1 Units move suddenly downwards with the downrush after a high wave in series of higher waves.

2 A large down-rush pushes the units downwards resulting in gradual settling of the armour layer.

3 Collapsing waves turn units out of there position and result in a sudden settling of the armour layer.

Settling of the armour layer by phenomena 1 occur mainly during the 60% wave height and is called initial settling of the armour layer. However, from figure 6.15 can be observed that the impact of the initial settlement differs with the steepness of the waves or water volume within the wave. Swell waves encounter larger settlements than wind wave. However, the impact of the settlements differs for the core configuration.
The open core settles slightly during the 60% wave height of both test series. The normal core encounters larger settlements than the open core and the impermeable core the largest settlements. The settlement occur over the whole width of the armour layer suggesting a sudden lost of friction between the armour units and under layer, caused by structural or hydraulic differences. The structural variable, placing density, as hydraulic variable, the water motion in the armour, are covered in subsequent sections.

Settling by phenomena 2 is mainly due a large backflow volume in the armour layer in combination with large forces parallel to the slope. The increased average downward load on the lowest armour row for an impermeable core was confirmed in the thesis of Koppel (2012), which researched the static and dynamic loads on the lowest row. Koppel (2012) found an increase of 260% of the average load for an impermeable core compared with a normal core using 20 rows of armour units.

The settling mechanism of collapsing waves (phenomena 3) is based on the loss of friction between armour units and under layer by high pore pressure. At the moment of high pore pressure the backflow is still in downward direction while the water flow on top of the armour layer moves in upward direction. The top of the armour units are pushed in upward direction and the bottom part in downward direction, inducing settling of the armour layer. Figure 6.16 illustrates the water motion for collapsing waves on an impermeable core.

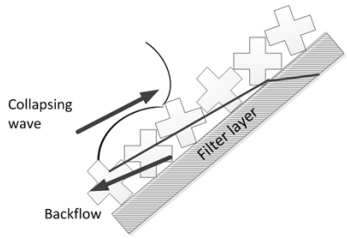

Fig. 6.16: Settling mechanism caused by collapsing waves on an impermeable core.

Relative placing density

The prescribed placing density by DMC is $1.2/D^2$ and may deviate between 98% and 105%. The relative placing density is measured after completion of placing of the armour layer and from photos. Both measurements deviated significant and are not accurate to use the exact numbers in data processing. The average relative placing density is calculated in appendix I for the test series and is summarized in table 6.3.

Open core		**Normal core**		**Impermeable core**	
Repetition	**Placing RPD** [%]	**Repetition**	**Placing RPD** [%]	**Repetition**	**Placing RPD** [%]
CA1	105.2	BA1	102.3	FA1	101.5
CA2	102.9	BA2	100.6	FA2	101.1
CA4	99.2	BA3	104.0	FA3	103.4
CA5	103.8				
CB1	99.9	BB1	103.1	FB1	103.8
CB2	99.9	BB2	99.5	FB2	101.9
CB4	100.5	BB3	98.3	FB3	101.7

Tab. 6.3: Relative placing density (RPD) Tests

The relative placing density of the open core is similar to the relative placement density of the normal and impermeable core. The great settlements of the armour layer with an impermeable can therefore not be attributed to the placing density.
Furthermore all repetitions for a single test tend to go to the same value independent of its placing density. From this is concluded that the placement has a minor influence on the packing density during testing. The difference in settlement is not caused by a structural difference but by a change in hydraulic forces.

Hydraulic forces

The force parallel to the slope is influenced by the flow velocity parallel to the slope and the water inflow into the structure. The force from the inflowing water can be separated in a force perpendicular and parallel to the slope, which contributes to the drag force on the armour units. This is illustrated in figure 6.17.

The flow velocity parallel to the slope is calculated from the wave motion on the slope of the structure that is measured with the wave gauges. Based on the data analysis on the flow velocity in appendix J is concluded that the maximum velocities parallel to the slope are not influenced by structural permeability.

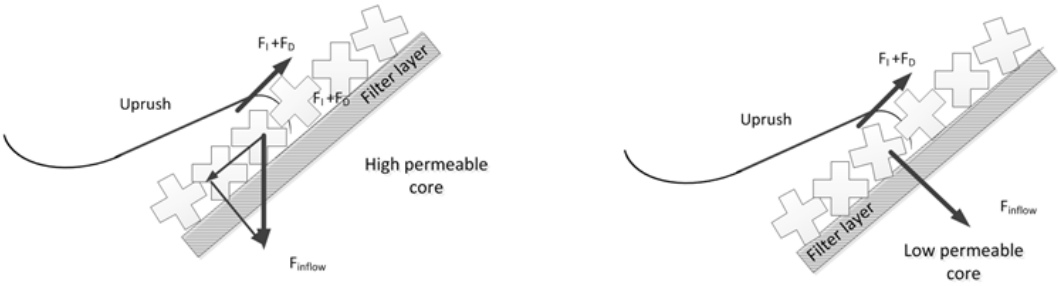

Fig. 6.17: Flow velocity vector parallel to the slope

However, the maximum run-down level on the armour layer is lower for an impermeable core than ofr an open core indicating a larger average force parallel on the slope.
Figure 6.17 illustrates that a low hydraulic gradient and thereby low inflow rates increases the force parallel to the slope. The hydraulic gradient is determined by the run-up level on and under the armour layer. However, due to the comparable run-up levels on the armour layer for the three core configurations, the hydraulic gradient depends only on the run-up level on the filter layer. Analysis of the run-up level on the filter layer in appendix J showed that the run-up level on the filter layer is larger for an impermeable than open core. This indicates smaller hydraulic gradients in the armour layer during the run-up and larger parallel forces on the armour units.
Furthermore, the decreased water inflow into the structure leads to an increase in pore pressure. This pore pressure during the upper part of the run-up reduces the friction between armour unit and filter layer and thereby the strength of the armour layer.

Settling of the armour layer is induced by upward forces on the armour units in combination with smaller friction forces between the armour and filter layer. The smaller hydraulic gradients in the armour layer during the run-up of an impermeable core increases the upward force in the armour layer. Furthermore, decreased water inflow into the core lead to larger pore pressure reducing the friction forces between the armour and filter layer. It can be concluded that a reduction of the strength of the amour layer and increasing forces lead to settling of the armour layer.

6.5.3 Rocking

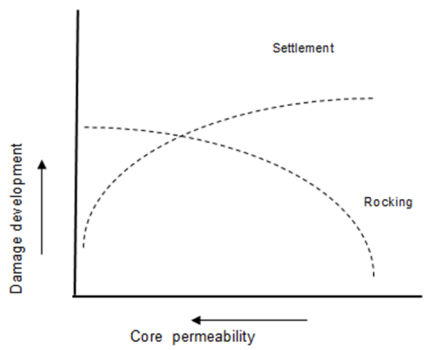

Fig. 6.18: Damage progression due rocking and armour settlement.

During testing a clear relation could be observed between the degree of rocking and relative packing density. Settling of the armour layer results in a closer packing of the armour layer increasing interlocking and decreasing the freedom of movement for each unit. It can therefore be concluded that settling of the armour layer and rocking of armour units are related to each other. Figure 6.18 presents the global observed trend regarding the failure mechanisms, namely rocking and armour settlements.

6.5.4 Lifting of armour units

Lifting of armour units has two extreme appearances; lifting of the whole armour layer from the slope or lifting of individual armour units. The second mechanism is mainly observed for the impermeable core. Typical features of the wave motion for this phenomena is a large downward backflow and short rotation moment. This results in large flow accelerations at maximum run-down and large forces on the armour units. The flow accelerations at maximum run-down limit the duration that the forces are directed outward of the slope (described in section 6.5.1.
Lifting of several armour rows at once from the slope is observed for the open core under influence of wind waves. The gradual movement suggest negligible turbulence around the armour units (indication of small flow acceleration). It is expected that this mechanism is caused by a large outward velocity and mainly by drag forces. The movements of the armour rows and thereby the damage level remain low for this lifting mechanism. The small movement can be adjusted to the large weight of the total armour layer, which can be taken into account due to the interlocking between the armour unit.

Lifting by acceleration under turbulent flow has a more damaging impact on the armour layer than the outflow velocity. From section 6.5.1 can be concluded that an impermeable core encounters larger acceleration forces at maximum run-down. This means that reduced core permeability results in more damage due to lifting of armour units from the slope.

6.5.5 Collapsing breaker

Observations made during model testing show that the breaker type change with the permeability of the core. The breaker type of waves is assumed to depend on the ratio between slope angle and wave steepness expressed as the surf similarity parameter (section 2.2.1). According to literature surging waves occur from a surf similarity parameter of $\xi_{0p} = 3.5$, which is smaller than the surf similarity parameter of the conducted tests; being ξ_{0p}= 3.75 and ξ_{0p}=5.0.

However, van der Meer (1988b) incorporated the structural permeability in the transition equation 6.1 that determines the use of the surging or collapsing formula for the stability of rock armour. Table 6.4 illustrates the varying transition parameter ξ_p between surging and plunging waves for P=0.1, P=0.4 and P=0.5.

$$\xi_{cr} = [\frac{6.2}{P}^{0.31} \sqrt{tan\alpha}]^{\frac{1}{P+0.5}} \qquad \text{transition equation} \qquad (6.1)$$

For $\xi_m < \xi_{cr}$ waves are plunging and the plunging wave equation applies.
For $\xi_m \geq \xi_{cr}$ waves are surging and the surging wave equation applies.

	$\xi_{cr} = \xi_m$	Converted to ξ_p
P=0.5	4.3	5.4
P=0.4	4.7	5.9
P=0.1	5.0	6.3

Tab. 6.4: Transition ξ for plunging and surging waves.

Collapsing waves were observed during the tests with the impermeable core . A collapsing wave was initiated by the highest wave in series of higher waves with large run-up levels and a deep downrush. Collapsing waves were not present during the test series of the normal and open core. This observation suggests that the surf similarity for which only surging waves occur shift with a low in core permeability. The observed physical change that might cause the collapsing wave for an impermeable core was the change in backflow volume and direction, which was almost parallel to the slope during outflow of water. It is presumed that the incoming wave falls over the high outflow and collapse on the slope of the structure. This assumption can be confirmed by research on the change in outflow velocity, direction and the backflow volume in seaward direction. Both the change in outflow velocity and the backflow volume will be discussed in subsequent part.

The outflow velocity and direction are influenced by the hydraulic gradient in the armour layer. From the analyse in appendix J it is be concluded that the hydraulic gradient in the armour layer increases with decreasing core permeability. In addition to the increased hydraulic gradient, it is observed that the water flows parallel to the slope in downward direction. This observation can be interpreted as a decreased slope angle.
The increased water level difference for the impermeable core indicates that the outflow is directed almost parallel to the slope and that the outflow velocity is larger than for an open core. The location of maximum hydraulic gradient is found to be shifted towards the maximum run-down confirming large flow forces from the backflow on the incident wave, pushing the wave in the seaward direction. This results in a steeper waves in front of the slope.

A breakwater with a low or even impermeable core will experience negligible wave transmission through the breakwater and low energy dissipation in the core. This results in large upward water movement along the slope that moves downward again causing a great reflective wave. Data analyse in appendix J confirmed that the impermeable core reflects a significant larger proportion of the wave than the normal and open core.

It can be concluded that collapsing waves are caused by large flow forces in combination with a large backflow. The lower section of the incoming wave front is pushed into the direction of the sea by the large backflow forces causing the wave to lean over and to collapse on the slope of the structure. This phenomena is illustrated with the sketch below.

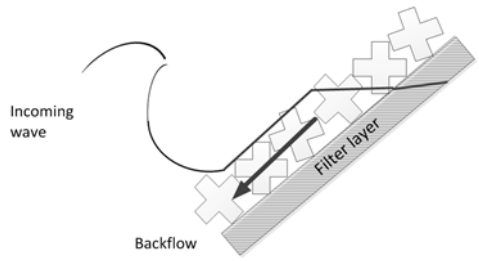

Fig. 6.19: Breaking wave

6.5.6 Hydraulic stability

The failure mechanisms has been converted into damage levels in section 6.4, presented in figure 6.5 till figure 6.10 according to the damage criterion 5.5. These damage levels have been converted to allowable damage (start of damage) for Xblocs and failure of the armour layer. The start of damage is defined by DMC with the following requirement: 2% of the units may rock more than 2% of the waves. This requirements correspond to a damage number of N_{od}= 0.2. Failure is defined with N_{od} = 0.7 corresponding to eight moving units.
Figure 6.20 illustrate the start of damage and start of failure of the three core configurations and damage progression.

Start of damage is normally expected to be between N_s=3.3 and 5.5 corresponding with wave height ≥120%. Failure of the armour slope occurs between N_s=3.7 and 6.0 corresponding with wave height ≥150%. Figure 6.20 shows that this is not the case experiments performed with wind waves. However, the experiments are performed in relative deep water with a larger maximum wave height, which induce the damage of the armour layer according to the study of Zwanenburg (2012. The Xbloc design guideline recommends a correction factor of 2 on the unit weight for $3.5H_s < h$. The H_s used in the model was kept below 0.2m for a water depth of 0.7m. Applying the correction factor for deep water on the unit weight, we obtain figure 6.21.

Figure 6.21 shows that correction factors must be applied for lower and for higher core permeability than the normal core to guarantee armour stability. The exact correction factor that should be applied on the stability number for the impermeable core following from this research is for swell waves 0.75 and none

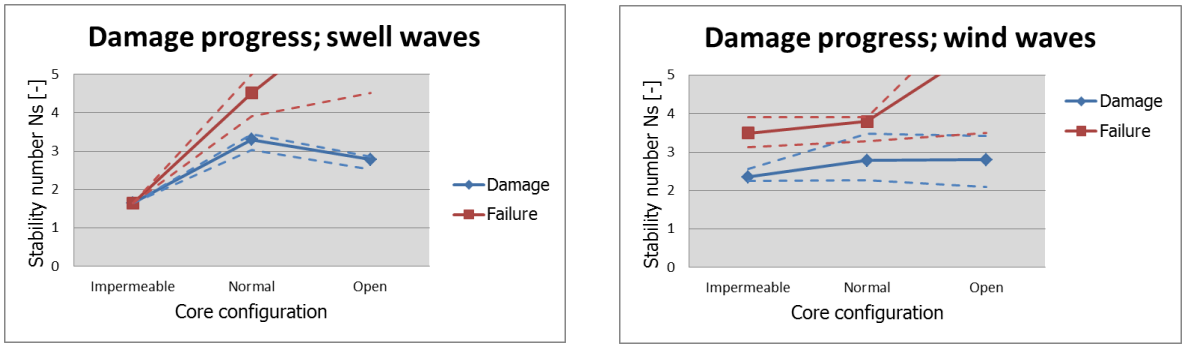

Fig. 6.20: Damage development

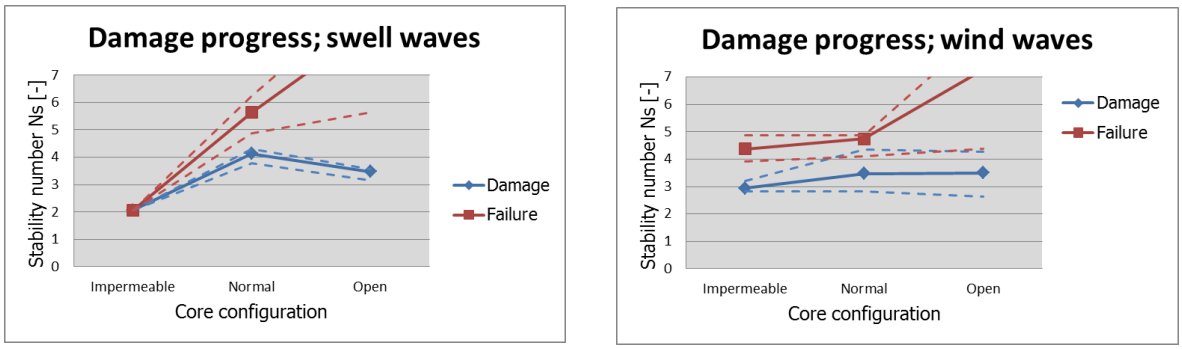

Fig. 6.21: Damage development for deep water

for wind waves. For a higher permeable core is also a correction factor required due to rocking of single armour units at low wave heights. The correction factors on the stability number for high permeable cores following from the model test is for wind 0.97 and none for swell waves. The correction factors on the stability number can be rewritten in terms of a correction factor on the unit weight using the design value of N_s=2.77, illustrated in table 6.5.

Correction factor			
Wave spectrum	Core	$H_s/\Delta D_n$	Unit weight
Xbloc guideline	Impermeable	0.80	2.00
	Open	-	-
Wind waves	Impermeable	-	-
	Open	0.97	1.17
Swell waves	Impermeable	0.75	2.41
	Open	-	-

Tab. 6.5: Correction factors

6.6 Comparison with rock armour units

In appendix J of this thesis the run-up levels, run-down levels, velocities, hydraulic gradient in the armour layer and reflection coefficient of the model tests are analysed. Data on the water profile in the armour layer following from the analysis is used to obtain an overview of the differences in water motion between a rock armour layer and single layer interlocking layer. This is done by comparing the data of the model tests with empirical formulae for rock armour units. From this comparison conclusions are drawn on the differences in energy dissipation in the structure and flow forces.
This section contains a summary of the analysis, the whole analysis can be found in appendix J. In

addition to the analysis on the water motion, the armour stability of single layer interlocking units has been compared with the stability formulae of Van der Meer (1988b) for rock armour.

It must be noted that several empirical formulae contain the 'notional' permeability of Van der Meer (1988b). In this section is assumed that the impermeable core is equivalent to P=0.1, the normal core is equivalent to P=0.4 and the open core is equivalent to P=0.5. The assumption that the normal core is equivalent to P=0.4 is not based on the prescribed configurations by Van der Meer (1988b) but on the common use in practise to apply P=0.4 for a normal core.

Run-up levels

The run-up level has been compared with the formulae of Van der Meer and Stam (1992), which proposes values for i.e. 0.1%, 1%, 2% run-up level. Two formulae are proposed for the run-up level (equation 6.2 and equation 6.2) and an additional formula for the upper boundary of permeable structures (equation 6.4). The upper boundary found for permeable structures by Van der Meer and Stam (1992) is not confirmed by the measured data from the model test as mentioned in section 6.5.1. Therefore, equation 6.4 is neglected and only expression 6.3 is used as all tests are conducted with a surf similarity parameter (ξ_m) larger than 1.5. Analysis of the run-up level using both equation 6.3 and equation 6.4 has also been done and is presented in appendix J.

$$R_{u.n\%}/H_s = a\xi_m \qquad \text{for}\xi_m \leq 1.5 \tag{6.2}$$

$$R_{u.n\%}/H_s = b\xi_m^c \qquad \text{for}\xi_m \geq 1.5 \tag{6.3}$$

$$R_{u.n\%}/H_s = d \qquad \text{Upper boundary for P}\geq 0.4 \tag{6.4}$$

Run-up level n%	a	b	c	d
0.1	1.12	1.34	0.55	2.58
1	1.01	1.24	0.48	2.15
2	0.96	1.17	0.46	1.97
5	0.86	1.05	0.44	1.69
10	0.77	0.94	0.42	1.45
Significant	0.72	0.88	0.41	1.35
Mean	0.47	0.60	0.34	0.82

Tab. 6.6: Coefficients for equation 6.2, 6.3 and 6.4 CIRIA (2007)

The coefficients for a, b and c are expressed in table J.2. The maximum measured run-up levels are plotted in figure 6.22 against the theoretical run-up level Van der Meer and Stam (1992). The solid black line in the figure represents the theoretical 0.1% run-up level, which is equivalent to the maximum run-up level of the model tests.

From the figures can be observed that the trend-line of theoretical values show great resembles with the measured run-up levels. However, the values of the measured data differs significantly from the expected values for the 0.1% run-up level, which follow from the formulae of Van der Meer and Stam (1992) for n=0.1%. This observation suggest that less wave energy is converted into potential energy for single layer interlocking armour units than for rock armour units.
It is possible that the water motion on the slope of the structure encounter more energy dissipation on the Xbloc layer than on a rock armour due to the larger surface roughness. The overtopping method of TAW (CIRIA, 2007) on impermeable structures uses such slope roughness factors (γ_f) and specifies this value for rock units and Xblocs units on 0.4 and 0.45. A larger surface roughness leads to more energy dissipation and less energy conversion from kinetic energy into potential energy. This explains the lower run-up levels for Xblocs than for rock armour layers found by Van der Meer and Stam (1992).

The left hand of figure 6.22 presents the run-up of swell waves, in which the black dotted line presents the theoretical n=5% values from equation 6.3. From this figure can be observed that the measured maximum run-up levels show a better fit with the theoretical 5% run-up level than 0.1% run-up level

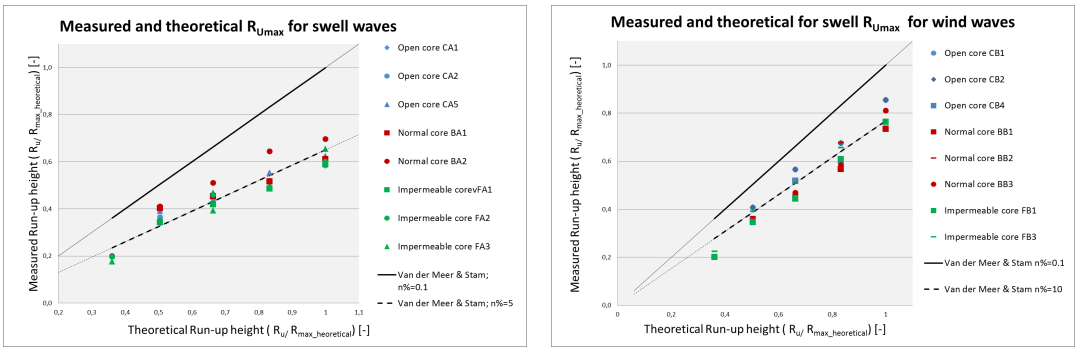

Fig. 6.22: The R_{u_max} for s=0.023 (left figure) and s=0.04 (right figure) with formula 6.3

exept for repetition BA2. The apparent trend of repetition BA2 can be attributed to calibration failure of the run-gauge. The right figure presents the data of wind waves, in which the black dotted line presents the theoretical n=10% values from equation 6.3. It can be observed that the measured run-up levels for wind waves show a better fit with the theoretical 10% run-up level.
It can be concluded that the maximum run-up levels of wind waves show a larger deviation from equation 6.3 than swell waves. This observation suggests that the run-up level for single layered armour units are more affected by the wave steepness than the run-up level for a doubled layer rock armour.

Run-down levels

The run-down level is found to be equally important for the forces on the armour layer as the run-up level. Van der Meer (1988b) suggested the following relation between slope angle α, 'notional' permeability P, and fictitious wave steepness s_{om}

$$R_{d2\%}/H_s = 2.1\sqrt{tan\alpha} - 1.2P^{0.15} + 1.5exp(-60s_{om}) \tag{6.5}$$

The theoretical values following from equation 6.5 are plotted against the measured $R_{d2\%}$ in figure 6.23. The black solid line in both figures present the theoretical data. From the figures can be observed that the theoretical values show resembles with the measured run-down levels. The run-down levels for wind waves are slightly overestimation for the normal and impermeable core but fits the values of the open core quite well.
The run-down levels on the armour layer for swell waves are presented in the left graph of figure 6.23. It can be observed that for the normal core larger run-down levels occur than expected from equation 6.5 while the impermeable and the open core show good resembles with the theoretical values. Omit the normal core of swell was and it can be concluded that equation has a good fit with the measured data.

The deviating result for the normal core between the measured data and equation 6.5, suggests that the run-down level for single layered concrete armour units are more affected by the wave length than double layered rock armour units. However, Van der Meer (1988b) performed no physical model test with P=0.4. This means that no data was available of configuration P=0.4 and therefore the statement cannot be confirmed.

Hydraulic gradient

According to the literature is the hydraulic gradient in the armour layer is an important parameter to indicate the size and the direction of the water flow in the armour layer. However, the hydraulic gradient in the armour layer has not been researched very often by researchers. An indication of the hydraulic gradient in a rock armour layer is given by Muttrray (2000) for regular waves.
Muttray (2000) related the hydraulic gradient ($\Delta\eta/\Delta x$) in the armour layer to the horizontal particle velocity in shallow water, which corresponds to Rgk/ω with $R = H_i(1 + C_r)$. A dimensionless number was obtained by multiply the relation with $\sqrt{gd_{n50}}$.

$$\kappa_r = H_i(1 + C_r)\frac{k}{\omega}\sqrt{\frac{g}{d_{n50}}} \tag{6.6}$$

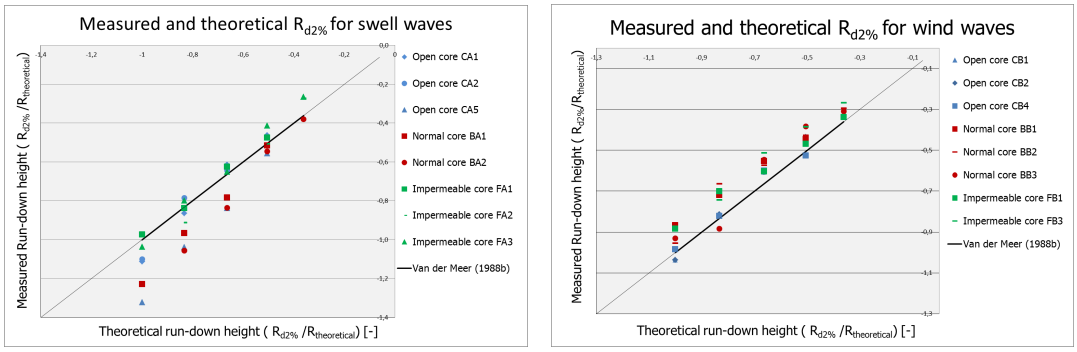

Fig. 6.23: The $R_{d2\%}$ for s=0.023 (left figure) and s=0.04 (right figure) with formula 6.5

The relation found by Muttrray (2000) between the hydraulic gradient and the κ_r of equation 6.6 is $\arctan(\Delta\eta/\Delta x)2/\pi$=0.129$\kappa_r$. The relation of Muttray has been compared with the maximum hydraulic gradient in the armour layer during the run-down of this study. This comparison cannot be justifiable entirely because a regular spectrum is applied by Muttrray (2000) and a JONSWAP spectrum is applied in this study. Larger waves in the spectrum will induce the hydraulic gradient in the armour layer and therefore it chosen to perform the comparison with the highest waves of the spectrum in combination with the largest hydraulic gradient. If the hydraulic gradient in the armour layer is similar for rock armour as for single layer interlocking units, lower values of the hydraulic gradient are expected than calculated from the relation found by Muttray (2000).
The theoretical value is calculated using the wave period and reflection coefficient related to the H_{max}. The hydraulic gradient for the model test is calculated using the shortest distance between the run-up gauges, which is measured on 45 mm.

Figure 6.24 presents both the relation of Muttrray (2000) and the data of the model tests. From the figure can be observed that the theoretical trend-line for the hydraulic gradient show a good resembles with the measured values. However, the size of the theoretical and measured values show large differences. This might be adjusted to a key parameter in the equation 6.6, which is the relation between wave length and wave height or wave steepness (s).
The model tests of Muttrray (2000) were conducted with three wave steepness between s=0.04 and s=0.1 on a slope of 1V:2H. This results in surf similarity parameters between ξ=2.5 and ξ=1.6, which are lower than the surf similarity parameter of the maximum wave height in this study, which are ξ=3.4 for swell waves and ξ=2.4 for wind waves.

In figure 6.24 are the values related to swell waves illustrated with black borders around the marks. These marks fall outside the range in which the relation of Muttrray (2000) is applicable. This might explain the great difference between measured and theoretical gradient in the armour layer for ξ=3.4. The values related to swell waves hereafter omitted from the analysis.
The values related to wind waves are also presented in figure 6.24 without a black border. It can be observed that the measured values are larger than theoretical values. The measured hydraulic gradients for the permeable core shows a better fit with 0.15κ_r instead of 0.129κ_r, which means an increase of approximately 20%. The impermeable structure shows a better with 0.17κ_r instead of 0.129κ_r, which is an increase of approximately 30%.

The hydraulic gradient can be a good indication of the size and the direction of the forces. The size and direction of the flow forces are important for the failure mechanism of the armour layer. An increase of the hydraulic gradient means an increase in flow velocity and flow forces. This means that single layer interlocking armour units encounter larger flow forces. However, the relative direction of this force is even of greater importance for the armour stability. The relative direction of the force on the armour units depend on the relation between slope angle and hydraulic gradient. The slope used in this study was 3V:4H, which is 40% steeper than used by Muttrray (2000). This means that the slope angle increases more than the hydraulic gradient for single layer interlocking armour units. It is therefore not possible to draw any conclusions on the difference in the relative direction of the flow forces between rock and interlocking armour units.

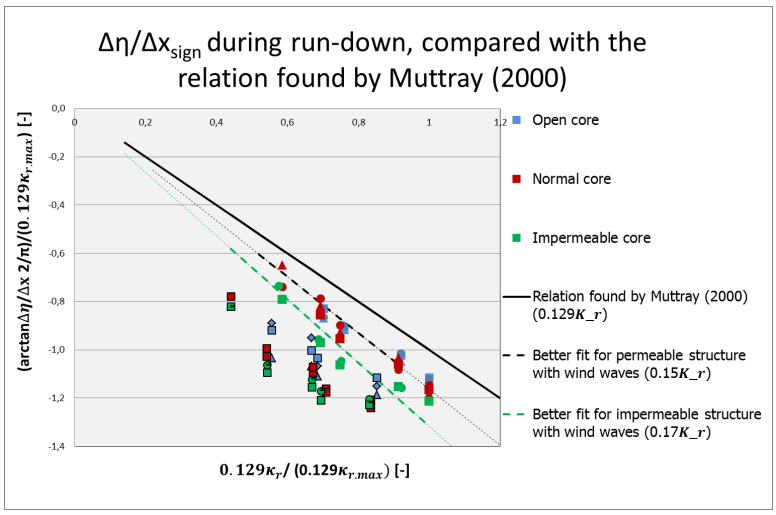

Fig. 6.24: Measured significant hydraulic gradient in the armour layer during run-down compared with the equation found by Muttrray (2000) for rock armoured breakwaters under regular wave attack.

Overall, it can be concluded that a single layer armour units encounters larger hydraulic gradients in the armour layer during the run-down than rock armour units. This means that larger flow velocities occur and thereby larger flow forces on the armour units. However, it cannot be confirmed that the relative direction of the flow force on the armour units change due to the increased slope angle for single layer interlocking armour units.

Reflection coefficient

The reflection coefficient regarding core permeability has been studied by Postma (1989) (CIRIA, 2007). According to Postma (1989), the reflection coefficient depends on the slope angle (α), fictitious wave steepness (s_{op}) and permeability of the construction (P). The parameters are related to each other as in the following formula.

$$C_r = \frac{0.081}{P^{0.14}(cot\alpha)^{0.78}s_{op}^{0.44}} \tag{6.7}$$

The theoretical and measured reflection coefficients are presented in figure 6.25 against the relative wave height. The horizontal lines illustrate the theoretical coefficients for P=0.1 (green), P=0.4 (red) and P=0.5 (blue) obtained from equation 6.7. From figure 6.25 and equation 6.7 can be observed that the Postma (1989) suggest a constant reflection coefficient for an individual wave steepness, which is not valid for the measured reflection coefficient. However, the size of the reflection coefficient following from equation 6.7 shows a reasonable fit with the 100% and 120% wave height of the measured data. This suggest similar energy dissipation in the structure during the most important wave heights. This observation suggests that the equation is usable for the design criteria but not for research.

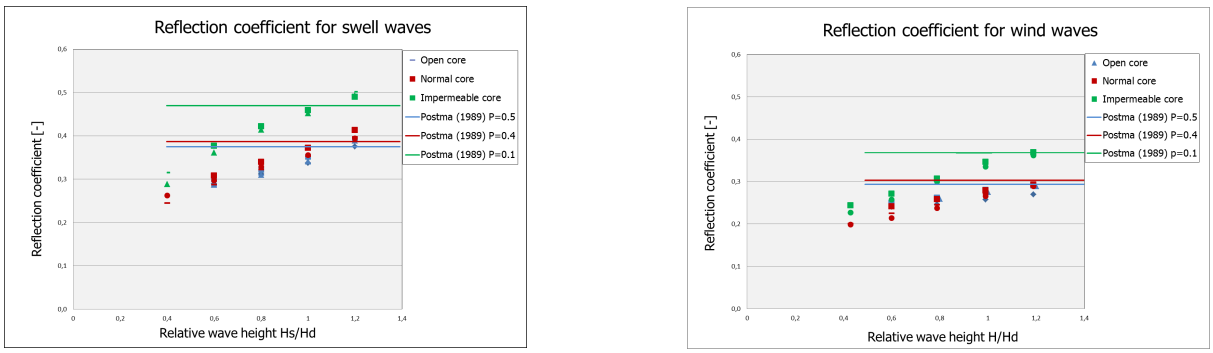

Fig. 6.25: Reflection coefficient versus percentage of the design wave height

Armour stability

The formulae of Van der Meer (1988b) is a commonly used formula for rock armour stability due to the large variety of parameter including the 'notional' permeability parameter (P). The contribution of the structural permeability is tested with physical model test. Based on a large variety of model tests, a small increase in armour stability was suggested for high core permeabilities and a large decrease in armour stability for an impermeable cores.
The armour stability of single layer interlocking units show a similar trend with the formulae of Van der Meer (1988b) for an impermeable core as for rock armour. However, the increased armour stability for high permeable cores suggested by Van der Meer (1988b) was not observed for single layer interlocking units. This difference in stability trend is due to the difference in stability mechanism. Interlocking units gain a part of its stability from interlocking forces, which increases with larger packing density of the armour layer. The packing density depends on the placing density and settlements of the armour layer. Observations showed that damage of the open core starts in case of negligible settlements combined with large parallel forces resulting into rocking of armour units.
Furthermore, the direction of the flow forces is more perpendicular to the slope increasing the force in outward direction. The probability of armour extraction is must higher for relative open cores with wind waves than for the normal core reducing the armour stability. Rock armour units are less affected by this change in flow direction due to the larger mass of the units.

Summary

The run-up level, run-down level, hydraulic gradient, reflection coefficient and armour stability are compared with empirical formulae, which are based on model tests with rock armoured breakwaters. The key difference between single layered concrete armour units and double layered rock armour units following from this comparison are :

Phenomena	**Difference between rock and single layer amour units**
Run-up level	Lower run-up levels are observed in the model tests than suggested by Van der Meer and Stam (1992). This is due to the difference slope roughness between Xblocs and rock armour units.
Run-down level	The formula showes good resembles with the formula of Van der Meer (1988b) exept for the normal core. However, Van der Meer (1988b) performed no physical model tests with configuration P=0.4 and therefore no conclusion can be drawn regarding the energy dissipation in the breakwater.
Hydraulic gradient	Larger hydraulic gradients were measured in the armour layer for single layer interlocking armour units than suggested by the formula of Muttrray (2000) during the run-down. This indicates larger flow velocities and thereby larger forces on the armour layer. No conclusions could be drawn on the relative direction of the flow forces on the armour units due to the difference in slope angle.
Reflection coefficient	The constant reflection coefficient for an individual wave steepness suggested by Postma (1989) is not observed for single layer interlocking armour units. The reflection coefficient increases with the length of the wave for single layer interlocking armour units. However, the values of Postma (1989) showed great resembles with the measured values for the 100% and 120% wave height, which indicates similar energy dissipation in the structure during the most important wave heights. It can also be concluded that the impact of core permeability on the energy dissipation in the breakwater is similar for rock and single layer interlocking armour units for these wave heights.
Armour stability	The suggested decrease in armour stability by Van der Meer (1988b) for rock is also valid for single layer interlocking armour units. However, the increase in armour stability for a increased core permeability suggested by Van der Meer (1988b) for rock armour, appears not to be valid for single layer interlocking armour units. A lower stability number is found for single layer interlocking units on a relative open core.

6.7 Conclusion

The various failure mechanisms described in this chapter react differently for the three the core configurations used in the model test. The failure mechanisms were analysed using the data on the water motion in the armour layer. The key changes in the water profile and thereby flow forces were indicated for the three core configurations and linked to the failure mechanisms. Table 6.7 gives a summary of the failure mechanism and its impact on the armour stability.
From the table can be observed that damage to the open core occurs due to low interlocking forces inducing rocking and extraction of armour units out of the armour layer. Mainly rocking causes damage at lower wave heights than normal. For the impremeable core, it is found that settling and lifting of armour units have a great impact on the damage progression. Both, lifting of armour units as settling of the armour layer causes damage and failure of the armour layer at lower wave heights than normal.

++ Great impact
+ Large impact
+/- Moderate impact
- Low impact
- - No impact

Configuration	**Configuration**	**Impact**	**Destabilization factor**
Open core	Settlement	-	Low interlocking force
	Rocking	+	
	Lifting of armour units	-	
	Removal of armour units	+	
	Collapsing waves	- -	
Normal core	Settlement	+/-	Combination of drag and inertia force
	Rocking	+/-	
	Lifting of armour units	+	
	Removal of armour units	-	
	Collapsing waves	-	
Impermeable core	Settlement	+ +	Large inertia force
	Rocking	-	
	Lifting of armour units	+ +	
	Removal of armour units	- -	
	Collapsing waves	+	

Tab. 6.7: Overview of the failure mechanism, impact and flow force for the open, normal and impermeable core.

Following from the damage observations and damage criteria, the start of damage and failure of the armour layer is defined. A lower stability number was obtained for both the open and impermeable core than the design stability number for Xblocs, which is set on 2.77. It is therefore recommended to apply correction factors on the unit weight in case of a relative open or impermeable core. The maximum correction factors on the unit weight following from this study for an impermeable core is 2.41 and for a relative open core is 1.17. Additional, it was observed that the armour layer is less stable on an impermeable core for swell waves than for wind waves while a relative open core reacts less stable for wind waves than for swell waves. The Xbloc guideline recommends only a single correction factor independent of the wave length. The recommended correction factor on the unit weight for an impermeable core is 2.5 and for a relative open core 1.2.

In addition to the analyse on the water profile in the armour layer and armour stability, the result has been compared with empirical formulae for rock armour units. This comparison provided knowledge on the fundamental difference between the run-up levels, run-down levels, hydraulic gradient and reflection coefficients of rock armour units and single layer interlocking armour units. Lower run-up levels are found for single layer interlocking armour units than suggested by Van der Meer and Stam (1992). This is plausible given that the overtopping method of TAW (CIRIA, 2007) on impermeable structures indicates a larger surface roughness of for Xblocs than for rock armour. Run-up levels and overtopping are closely related to each other, meaning that lower overtopping rates imply lower run-up levels.
However, for the run-down levels great resembles is found between the run-down formulae of Van der Meer (1988b) and the data obtained from the model tests. This observation suggests a similar energy

dissipation in the structure at maximum run-down for breakwaters with a rock armour layer and single layered interlocking units.
Furthermore, it was concluded that the maximum hydraulic gradient during the run-down is larger for single layer interlocking armour units than for a rock armour using the empirical formula of (Muttrray, 2000). This means larger flow velocities and forces in the armour layer. In contrast to the size of the forces, no conclusion could be drawn on the relative direction of the forces on the armour units due to difference in slope angle.
The reflection coefficient is also compared with a empirical formula. Postma (1989) suggested a constant value for the reflection coefficient, which was not observed in measured reflection coefficients. However, the formula of Postma (1989) shows good resembles of the relative contribution of the structural permeability on the reflection coefficient and size for the design wave height. From this observation can be concluded that the impact of core permeability on the energy dissipation in the breakwater is similar for rock and single layer interlocking armour units.
Finally, a comparison has been made between the stability trend of the interlocking armour layer with the stability formula of Van der Meer (1988b) for rock armour. It is concluded that rock and single layer interlocking armour units have a resembled stability trend for impermeable cores but show a great difference in stability for relative open core. This difference in stability trend is mainly due to the difference in stability mechanism.
It can be concluded that the permeability of the core has a large impact on the stability of the armour layer. Incorrect scaling of core material has a large effect on the failure mechanism and on the reliability of the model tests. This conclusion confirms the importance of a good scaling method which is complex for core material. The method prescribed by Burcharth (1999), based on Froude similarity, Forchheimer model and the wave induced pore pressure model, seems to be the most reliable method for scaling of core material. However, due varying hydraulic gradient in time and location in the core it is difficult to fulfil the Froude similarity during a single wave motion on the slope.
Furthermore, the shape coefficients α and β in the Forchheimer model are not constant with changing velocity (or Reynolds numbers). The appropriate shape coefficients for the specific scaling situation are difficult to define for small scale models with flow velocities in the Forchheimer flow regime in the core.
All together it can be concluded that proper scaling of the core remains rather uncertain in small scale models where the flow in the core is not fully turbulent. It is important to understand the scaling method and to know the shape factors of the used grain material in the specific Reynolds range.

7. CONCLUSIONS AND RECOMMENDATIONS

In this chapter a reflection on the research objective and hypothesis stated in chapter 1 is presented. The research objective of this study was:

The goal of this thesis is to extend the knowledge on the failure mechanisms of the armour layer for different structural permeabilities and use this knowledge to define correction factors on the unit weight for single layer interlocking armour.

In order to achieve the objective, permeability tests and physical model tests have been conducted to investigate the influence of core permeability on the hydraulic stability of a Xbloc armour layer. The conclusions of the research are presented in this chapter. Furthermore, the limitations of the research and recommendations for further research are discussed in this chapter.

7.1 Conclusion

Main conclusions on the armour stability

The key failure mechanisms for this physical model test are settling of the armour layer, rocking of units, lifting of the armour units and collapsing waves. Failure mechanisms can be explained by differences in water motion for different structures tested. The individual contribution of the water elevation, velocity and hydraulic gradient in the armour layer were evaluated. The main conclusions on the difference in water profile between a breakwater with a highly permeable core and an impermeable core are:

1 The maximum run-down level on the armour layer increases with decreasing permeability;

2 The hydraulic gradient in the armour layer at maximum rund-down increases with decreasing core permeability;

3 The maximum run-up level on the armour layer remains approximately the same;

4 The maximum run-up level on the filter layer increases with decreasing permeability;

5 The location of the maximum hydraulic gradient shifts towards the maximum run-down;

6 Larger flow accelerations near the maximum run-down increases with decreasing permeability;

7 The maximum uprush and downrush velocities on the armour layer remain approximately the same;

The observed key failure mechanisms for this physical model test are defined as lifting of the armour units, settling of the armour layer, rocking of units and collapsing waves. The individual contribution of the water elevation, velocity and hydraulic gradient in the armour layer could be linked to flow forces that might induce the failure mechanisms.

The maximum uprush velocity and the maximum downrush velocity [7] parallel to the slope remain approximately the same and cannot cause differences in failure mechanism. However to overcome the larger distance between the run-up and increased run-down for an impermeable core [1], a larger average velocity is expected. This means that the average force parallel to the armour layer is larger for an impermeable core than for an permeable core.
The run-down levels under the armour layer are smaller than on the armour layer, generating an hydraulic gradient in the armour layer [2]. This hydraulic gradient indicates the size and the direction of the out- and inflow. It has been confirmed that the outflow has an important role in the lifting of armour units. The force that contributes most to uplifting the armour layer is the turbulent acceleration force [6], which rotates the units in upward direction at maximum run-down. Measurements showed that the

maximum hydraulic gradient during the run-down increases with an impermeable core. Larger hydraulic gradients in the armour layer indicate larger forces parallel to the slope. This increases flow accelerations during maximum run-down and thereby the lifting mechanism. Additional to the size of the hydraulic gradient, the shift of the maximum hydraulic gradient in time [5] for an impermeable core induces also the acceleration forces at maximum run-down. However, smaller hydraulic gradients in the armour layer indicate smaller forces but relative large forces in outward direction of the slope. These forces induce extraction of armour units out of the armour layer. .
Settling of the armour layer is caused by large downward forces and lost of friction forces between armour layer and under layer. Forces parallel to the armour layer are mainly induced by the flow velocity. Loss of friction between armour layer and under layer might be caused by the negligible inflow forces into the core [4], which increased the pore pressure in front of the core. The degree of settlement of the armour layer influences the space for movement between the armour units and thereby the rocking of armour units. This means that settling of the armour layer reduces the failure mechanism rocking. It is therefore concluded that some settling of the armour layer is not negative by definition.
A change of breaker type has been observed for the impermeable core under attack of wind waves. This indicates a shift in the breaker type and can simplified be explained by the fictitious steeper slope angle due to the water volume in the armour layer [2].

The impact of the various failure mechanisms on the armour stability for the open, normal and impermeable are presented in table 7.1. From the table can be observed that each individual failure mechanisms shows a clear trend with core permeability, which is either positive or negative with decreasing permeability.

++ Great impact
+ Large impact
+/- Moderate impact
- Low impact
- - No impact

Failure Mechanism	**Open core**	**Normal core**	**Impermeable core**
Settling of armour layer	-	+/-	++
Rocking	+	+/-	-
Lifting of armour units	-	+	++
Extraction of armour units	+	-	–
Collapsing waves	–	-	+

Tab. 7.1: Overview of the failure mechanism, impact and flow force for the open, normal and impermeable core.

Damage to the open core occurs mainly due to low interlocking forces inducing rocking and extraction of armour units out of the armour layer. Mainly rocking ensures that damage of the armour layer occurred earlier than normal. For the normal core, it is found that settling and lifting of armour units have a great impact on the damage progression. Both, lifting of armour units as settling of the armour layer ensures that damage and failure of the armour layer occurred earlier than normal.
It is found that both the open and impermeable core encounter a lower armour stability than the normal core. From the study followed that an open core is more sensitive for wind wave and the impermeable core for swell waves. The correction factors on the unit weight found for an impermeable and open core are 2.41 and 1.17. Table 7.2 contains an overview of the recommended correction factors following from the test results.

Correction factor		
Wave spectrum	Core	Unit weight
Xbloc guideline	Impermeable Open	2.00 -
Wind waves	Impermeable Open	- 1.2
Swell waves	Impermeable Open	2.5 -

Tab. 7.2: Correction factors

Comparison with rock armour units

The hypothesis regarding the difference between rock armour units and single layer interlocking armour units was:

The effect of core permeability on the stability of single layer interlocking armour units cannot be compared to that of rock armour units resulting in a different stability trend of the armour units than suggested by Van der Meer (1988b) with the structural permeability parameter P.

This hypothesis is confirmed for single layer interlocking armour units such as Xblocs. Van der Meer (1988b) suggested that for high permeable structures (P=0.5) the hydraulic stability of the armour layer increases. However, for a single layer interlocking armour units this is not the case. The stability factor of a single layer interlocking armour unit is based on interlocking forces between neighbouring units. The required interlocking forces between the units are achieved by initial settlements of the armour layer. The settlements of an armour layer on an open core are smaller than on a normal core increasing the probability of rocking. Furthermore, the flow forces in the armour layer are directed more perpendicular to the slope in case of an open core. This increases the outward forces and the probability of extraction of armour units out of the armour layer. Rock armour is not affected by these changes due to definition of damage and the larger unit weight.
For P=0.5 the conclusion is; the reduced settlements of the armour layer increase the potential occurrence of damage due to the rocking of armour units and increase the probability of extraction. It cannot be confirmed that single layer interlocking armour units with a larger structural permeability have a higher hydraulic stability.

Van der Meer (1988b) suggested a decrease in armour stability for an impermeable core as P=0.1. In addition, an relation between the correction factor and wave length was suggested by Van der Meer (1988b). This study found a similar dependence between core permeability, wave length and the hydraulic stability of single layer interlocking armour units. From the results of this study, it can be confirmed that a similar trend occurs for single layer interlocking armour units as for rock armour in case of an impermeable.
However, in contrast to rock armour layers the reduced stability of single layer interlocking armour units are not straightforward. Although settling of the armour layer generates additional strengths, it can also cause failure pf the armour layer. Furthermore, the increased forces on the interlocking armour units counteracts the positive effect of the increased interlocking forces.

7.2 Limitations for usage

This study focussed on the influence of the permeability of the core on the stability of armour units. Insight were obtained into the change of water motion around the armour layer, which influences the stability of the armour layer. Both the impermeable core and the open core have been compared with each other and to the so-called *normal* core. The *normal* core was obtained using the scaling method of Burcharth (1999) and the shape coefficients recommended by Burcharth (1998). In chapter 4 on the permeability tests, its illustrated that the shape coefficients differ greatly in the Forchheimer flow regime. This means an uncertainty is entailed in the definition *normal* core.

One should be aware that the presented conclusions for the 'normal' core are based on the specific configurations in which the physical model tests were executed. However, the scaling method for the impermeable and open core are correct and therefore the correction factors derived from the physical model tests can be deemed reliable.

7.3 Recommendation

Breakwater design

Two recommendations can be formulated for the design of future breakwaters. The first recommendation is dedicated to the safety factors for the primarily design. The correction factor on the armour weight for units on an impermeable core must increase from 2.0 to 2.5 in the Xbloc guidelines. Furthermore, a correction factor on the unit weight must be applied for an open core, being 1.2 as found for the tested grading.
The second recommendation is dedicated to physical model tests. The final design of each breakwater is normally tested in a small scale model on hydraulic stability. The physical model tests in this study showed that both larger core permeabilities and lower core permeabilities have a negative effect on the occurrence of damage of the Xbloc armour layer. Therefore it is recommended to scale the core accurate by using proper shape coefficients for the Forchheimer model in the scaling method of Burcharth.

Future research

Following the limitations, an important recommendation can be given for further research on this topic. Research should be conducted with a larger scale model to minimize the uncertainties following from scale effects. It is recommended to perform scale model tests with fully turbulent flow in the core of the breakwater (Re$>$ 600), where the turbulent part (b) of the Forchheimer model is dominant and the β remains rather constant. This will improve the reliability of the Burcharth (1998) scaling method for a *normal* core material or it might even be possible to use the Froude scaling law for large scale models.

Future model tests on core permeability can be done on:

- This research has been conducted with a large water depth with small wave asymmetry and a Rayleigh distributed wave spectra. It is recommended to repeat the tests with a water level below than $2.5H_s$, which normally occurs in coastal areas. Between a deep and shallow wave spectra, two key differences influence the failure mechanism significantly; the shape of the wave (or non-linearities) and the Rayleigh distribution of the wave height, which is not valid in shallow waters.

- The armour layer on the impermeable core settled greatly in this study. Research on the stability mechanism found that slope angle is responsible for the gravitation force distribution. A lower slope angle would increase the forces perpendicular to the slope that reduces uplifting of armour units and decreases the parallel forces, which induces settling. It is recommended to perform a research on the optimum slope angle for a breakwater with impermeable core.

- The geometry of the breakwater was kept constant during the research. It is recommended to investigate the influence of the geometry, such as the breakwater width, of the breakwater on stability of the armour layer. The wave-induced pore pressure model indicates the width of the breakwater as a variable for the hydraulic gradient in the breakwater under wave attack. Besides the influence of the grain diameter, it is assumed that the width of the breakwater around SWL has also an impact on the permeability of the scale model.

- It is recommended to improve the scaling method of Burcharth (1998) for core material. In specific more attention must be paid to the influence of the wave length on the size of the rock grading. The current scaling model recommend smaller rock grading for longer waves, which is in contrast to the general assumption that core permeability decreases towards longer waves. From this perspective the recommended rock grading in the scale model must increase with a increase in wave length.

The 'notional' Permeability parameter

Problems have been experienced in practice around the subjective definition of the 'notional' permeability parameter of Van der Meer (1988b). In case of doubt the most the most conservative value is chosen for the stability formulae of Van der Meer (1988b) resulting in larger armour units, which increases unnecessarily the construction costs. However, more accurate method to describe core permeability are complex or incomplete, namely the Forchheimer model and the stability formula of Van Gent (2004).

It is suggested that the following aspects must be incorporated to incorporate the core permeability into a stability formula:

- The hydraulic gradient in the armour layer; this is influenced by the slope angle, armour thickness, wave energy, energy dissipation and water inflow into the core.
- The stability factor of the armour unit.
- Water inflow into the core; this is determined by the relative permeability of the core regarding the wave height. The core permeability might be described with the d_{15} of the material as this is a better indication for the permeability.

It is recommended to obtain the relation from large scale models with fully turbulent flow in the armour layer, where β'_{core} is valid. The relation can be applied on prototype breakwaters and large scale models. For small scale models the core grading must be scaled using an appropriate scaling method after application of the stability relation.

REFERENCES

Abbott, M. B., & Price, W. A. (Eds.). (1994). *Coastal, estuarial and harbour engineers' reference book.* Londen: Chapman and Hall.

Bakker, K. (1989). Klassieke theorie leidt tot kostbare filterconstructies. *Land + Water nu*, 35-47.

Bakker, P., Klabbers, M., Mutrray, M. O., & van den Berge, A. (2006). Hydraulic performance of xbloc armour units. *DMC*.

Burcharth, H. F., & Andersen, L. T. (2007). Scale effects related to small scale physical modelling of overtopping of rubble mound breakwaters. In *Coastal structures 2007: Proceedings of the 5th international conference* (Vol. 2, p. 1532-15741). Venice, Italy: World Scientific Publishing Co Pte Ltd.

Burcharth, H. F., & Andersen, O. H. (1993, Februari). *On the one-dimensional unsteady porous flow equation* (Tech. Rep.).

Burcharth, H. F., & Andersen, O. H. (1995). *On the one-dimensional unsteady porous flow equation* (Vol. 24).

Burcharth, H. F., & Christensen, C. (1991). *On stationary and non-stationary porous flow in coarse granular materials.* Aalborg University, Department of Civil Engineering. (European Community, MAST G6-S: Project 1, Wave Action on and in coastal structures)

Burcharth, H. F., Christensen, M., Jensen, T., & Frigaard, P. (1998). Influence of core permeability on accropode armour layer stability. *International Conference coastlines, structures and breakwater, Institution of Civil Engineers*, 34-45.

Burcharth, H. F., Liu, Z., & Troch, P. (1999, April). Scaling of core material in rubble breakwater model tests. *Coastal and Port Structures*, 1518-1528.

Burger, W., Oumeraci, H., & Partenscky, H. W. (n.d.). Geohydraulic investigations of rubble mound breakwaters. In *Coastal engineering.*

CIRIA. (2007). Rock manual. the use of rock in hydraulic engineering. In (2nd ed.). London: C683, CIRIA.

de Rover, R., Verhagen, H. J., van den Berge, A., & Reedijk, B. (2008). Breakwater stability wiht damaged single layer armour units. *International Conference Coastal Engineering (ICCE).*

Dybbs, A., & Edwards, R. (1984). Fundamentals of transport phenomena in porous media. In (chap. A new look at posous media fluid mechanics). Mokjpff Publishers.

Englund, F. (1953). *On the laminar an dturbulent flow of ground water through homogeneous sand* (Tech. Rep.). Danish academy of Technical sciences.

Ergun, S. (1952). Fluid flow through packed columns. *Chem. Engrg. Progress*, *48*(2), 89-94.

Holthuijsen, L. H. (2007). *Waves in oceanic and coastal waters.* Camebridge University Press: publisher.

Hudson, R. Y. (1953). Wave forces on breakwaters. In *Trans am soc civ engrs* (Vol. 118, p. 653-674).

Hudson, R. Y. (1959). Laboratory investigation of rubble mound breakwaters. In *J. waterway and port division, am soc civ engrs* (Vol. 85, p. 93-121).

Hughes, S. (1993). *Physical models and laboratory techniques in coastal engineering, advanced series on ocean engineering.* Coastal Engineering.

Koppel, M. A. a. (2012). Static and dynam loads on the first row of interlocking, single layer armour units. *Coastal Engingeering*.

Mansard, E. P. D., & Funke, E. R. (1980). The measurement of incident and reflected spectra using a leas squares method. In (p. 154-172). Coastal Engineering.

Monster, H., & Philipsen, K. (2010). *Underlayer tolerances xbloc breakwater unis.*

Muttrray, M. O. (2000). *Wellenbewegung an und in einem geschutteten wellenbrecher.* Unpublished doctoral dissertation, Technischen Universitt CaroloWilhelmia, Braunschweig.

Reedijk, B., Muttray, M., van den Berge, A., & de Rover, R. (2008). *Effect of core permeability on armour layer stability.*

Schiereck, G. J. (2001). *Introduction to bed, bank and shoreline protection.* The Netherlands: Delft University Press.

Shih, R. W. K. (1990). Permeability characteristics of rubble material- new formulae. In (Vol. 2, p. 1499-1512). ICCE.

Smith, G. (1991). *Comparison of stationary and oscillatory flow through porous media.* Unpublished master's thesis, Queen's University, Canada.

ten Oever, E. (2011). *Specifications for the application of xbloc* (Tech. Rep.). Gouda, Netherlands: Delta Marine Consultants.

van Broekhoven, P. J. M. (2011). *The influence of armour layer and core permeability on the wave run-up.* Unpublished master's thesis, Delft University of Technology, Netherlands.

van der Meer, J. W. (1988b). *Rock slopes and gravel beaches under wave attack.* Unpublished doctoral dissertation, Delft University of Technology.

van Gent, M. R. A. (1993, June). *Stationary and oscillatory flow through coarse porous media* (Tech. Rep. No. 93-9). Delft: Delft University of Technology, Faculty of Civil Engineering.

van Gent, M. R. A., Smale, A. J., & Kuiper, C. (2004). *Stability of rock slopes with shallow foreshores.* Portland: ASCE. (Proceedings 4th International Coastal Structures Conference)

van Zwicht, B. N. M. (2009). *Effect of the concrete density on the stability of xbloc armour units.* Unpublished master's thesis, Delft University of Technology, The Netherlands.

Zwanenburg, S. A. A. (2012). *The influence of the wave height distribution on the stability of single layer concrete armour units.* Unpublished master's thesis, Delft University of Technology.

LIST OF FIGURES

0.1 Overview of the failure mechanism, impact and flow force for the open, normal and impermeable core. . . . viii

1.1 Cross-section of a rubble mound breakwater . . . 1
1.2 Cross-section of the breakwater of IJmuiden (Reedijk et al., 2008) . . . 2
1.3 Notional permeability configurations (Schiereck, 2001) . . . 4
1.4 Report outline . . . 6

2.1 Basic scheme of a coastal structure under wave attack . . . 7
2.2 Surf similarity parameter . . . 9
2.3 Up and down flow on an impermeable an permeable structure . . . 10
2.4 Phase shift in the water motion in the structure . . . 11
2.5 Internal water motion . . . 12
2.6 Static loads on an Xbloc armour layer . . . 13
2.7 loads on a grain during run-up . . . 13
2.8 Xbloc design values (P. Bakker et al., 2006) . . . 14
2.9 Flow chart of the stability of armour units . . . 15

3.1 A representation of flow regimes, from Burcharth (1991) . . . 18
3.2 Fully turbulent flow . . . 19
3.3 Regions with different dominant resistance, from Van Gent (1993) adapted by author . . . 21
3.4 Non-stationary part of the β coefficient by Van Gent (1993) . . . 21
3.5 Pore pressure distribution along the breakwater (Burcharth (1999)) . . . 22
3.6 Reduction factor on the stability number by various researchers . . . 24

4.1 Schematic lay-out of the permeameter at the DUT . . . 28
4.2 Photos permeameter: flow-meter and basin . . . 29
4.3 Photos permeameter: crane and bucket without rock material . . . 29
4.4 Flow chart testing procedure . . . 30
4.5 Experimental data . . . 33
4.6 Representation of the measured data . . . 33
4.7 Experimental data: fully turbulent equation . . . 34
4.8 Shape factors obtained from the experimental data . . . 35

5.1 Drag variation with the Reynolds number (Burcharth & Andersen, 2007) . . . 37
5.2 The geometry of the Xbloc . . . 40
5.3 Distance between horizontal and vertical neighbouring units . . . 41
5.4 Assumed pore pressure fluctuation in the core Burcharth (1999) . . . 42
5.5 Influence of the slope angle on the stability, from Abbott & Price (1994) . . . 43
5.6 JONSWAP spectrum . . . 45
5.7 Schematic overview of a wave gauge . . . 46
5.8 Photos from the run-up gauge under the armour layer . . . 46
5.9 Cross-section of the flume with two sets of gauges . . . 47
5.10 Cross-section of the physical model . . . 47
5.11 Schematic front view of the armour layer . . . 48
5.12 Start of damage and failure with clustered damaged units (de Rover et al., 2008) . . . 52

6.1 Rocking of a single unit around SWL. . . . 53
6.2 Lifting of a single unit . . . 54
6.3 The wave motion on the breakwater . . . 55

6.4 A wave collapsing on a breakwater . . . 57
6.5 Damage number versus armour stability number for the normal core; swell waves . . . 60
6.6 Damage number versus armour stability number for the open core; swell waves . . . 60
6.7 Damage number versus armour stability number for the impermeable core; swell waves . . 60
6.8 Damage number versus armour stability number for the normal core; wind waves . . . 62
6.9 Damage number versus armour stability number for the open core; wind waves . . . 62
6.10 Damage number versus armour stability number for the impermeable core; wind waves . . 62
6.11 Water motion on the armour layer; maximum run-down, uprush and maximum run-up . . 64
6.12 Difference in water motion at maximum run-down between an open (B) and impermeable core(A) . . . 64
6.13 Difference in water motion at maximum run-up between an open (B) and impermeable core(A) . . . 64
6.14 Area within RPD is measured . . . 67
6.15 Trend-line of the relative packing density plotted against the relative wave height . . . 67
6.16 Settling mechanism caused by collapsing waves on an impermeable core. . . . 68
6.17 Flow velocity vector parallel to the slope . . . 69
6.18 Damage progression due rocking and armour settlement. . . . 69
6.19 Breaking wave . . . 71
6.20 Damage development . . . 72
6.21 Damage development for deep water . . . 72
6.22 The R_{u_max} for s=0.023 (left figure) and s=0.04 (right figure) with formula 6.3 . . . 74
6.23 The $R_{d2\%}$ for s=0.023 (left figure) and s=0.04 (right figure) with formula 6.5 . . . 75
6.24 Comparison with Muttrray (2000) . . . 76
6.25 Reflection coefficient versus percentage of the design wave height . . . 76

A.1 Correction factors on the unit weight recommended by DMC on primarily design. . . . 96

B.1 Influence of the grain size . . . 97
B.2 Influence of the degree of sorting . . . 98
B.3 Influence of the packing of the material . . . 98
B.4 Influence of the gain shape . . . 98

C.1 Available rock samples . . . 99

D.1 Regression line of rock sample: 22.4- 31.5 mm . . . 101
D.2 Regression line of rock sample: 16.0- 22.4 mm . . . 101
D.3 Regression line of rock sample: 11.2- 16.0 mm . . . 102
D.4 Regression line of rock sample: 8.0- 11.2 mm . . . 102
D.5 Regression line of rock sample: 4.0- 5.4 mm . . . 103
D.6 Test set-up of Van Gent (1993) . . . 105
D.7 Shape factors compared with the formula of Shih (1990) . . . 105

E.1 Cross-section of a rubble mound breakwater with rock grading 22.4-32.5 mm . . . 107
E.2 Cross-section of a rubble mound breakwater with impermeable core . . . 107
E.3 Photo of the breakwater with open and normal core . . . 108

F.1 Raleigh distribution of the 40% wave height of ξ=5.0 . . . 110
F.2 Raleigh distribution of the 60% wave height of ξ=5.0 . . . 111
F.3 Raleigh distribution of the 80% wave height of ξ=5.0 . . . 111
F.4 Raleigh distribution of the 100% wave height of ξ=5.0 . . . 111
F.5 Raleigh distribution of the 120% wave height of ξ=5.0 . . . 111
F.6 Raleigh distribution of the 140% wave height of ξ=5.0 . . . 112
F.7 Raleigh distribution of the 140% wave height of ξ=5.0 . . . 112
F.8 Raleigh distribution of the 180% wave height of ξ=5.0 . . . 112
F.9 Raleigh distribution of the 40% wave height of ξ=3.75 . . . 113
F.10 Raleigh distribution of the 60% wave height of ξ=3.75 . . . 113
F.11 Raleigh distribution of the 80% wave height of ξ=3.75 . . . 113
F.12 Raleigh distribution of the 100% wave height of ξ=3.75 . . . 113
F.13 Raleigh distribution of the 120% wave height of ξ=3.75 . . . 114

F.14 Raleigh distribution of the 140% wave height of ξ=3.75 . . . 114
F.15 Raleigh distribution of the 140% wave height of ξ=3.75 . . . 114
F.16 Raleigh distribution of the 180% wave height of ξ=3.75 . . . 114

G.1 Test CA repetition 1; start and 100% picture . . . 115
G.2 Test CA repetition 2; start and 100% picture . . . 116
G.3 Test CA repetition 4; start and 100% picture . . . 116
G.4 Test CA repetition 5; start and 100% picture . . . 117
G.5 Test CB repetition 1; start and 100% picture . . . 117
G.6 Test CB repetition 2; start and 100% picture . . . 118
G.7 Test CB repetition 4; start and 100% picture . . . 118
G.8 Test BA repetition 1; start and 100% picture . . . 119
G.9 Test BA repetition 2; start and 100% picture . . . 119
G.10 Test BA repetition 3; start and 100% picture . . . 120
G.11 Test BB repetition 1; start and 100% picture . . . 120
G.12 Test BB repetition 2; start and 100% picture . . . 121
G.13 Test BB repetition 3; start and 100% picture . . . 121
G.14 Test FA repetition 1; start and 100% picture . . . 122
G.15 Test FA repetition 2; start and 100% picture . . . 122
G.16 Test FA repetition 3; start and 100% picture . . . 123
G.17 Test FB repetition 1; start and 100% picture . . . 123
G.18 Test FB repetition 2; start and 100% picture . . . 124
G.19 Test FB repetition 3; start and 100% picture . . . 124

I.1 Area within RPD is measured . . . 130

J.1 Influence of water temperature on the calibration . . . 133
J.2 Data accuracy with 3% deviation lines. . . . 134
J.3 Data analyse . . . 134
J.4 The R_{u_max} on the armour layer. . . . 135
J.5 The R_{u_max} under the armour layer. . . . 135
J.6 The R_{d_max} on the armour layer . . . 136
J.7 Water motion on the slope of the structure during the 100% wave height. . . . 136
J.8 The R_{u_max} for s=0.023 (left figure) and s=0.04 (right figure) using equation J.4 and equation J.5 . . . 137
J.9 The $R_{d2\%}$ for s=0.023 (left figure) and s=0.04 (right figure) with formula J.6 (Green= impermeable core, Red= normal core and blue= open core) . . . 138
J.10 Water level difference around the armour layer at maximum run-down . . . 139
J.11 Water level difference around the armour layer at maximum run-up . . . 139
J.12 Representation of the measurement of the hydraulic gradient during the run-up. . . . 140
J.13 Maximum water level difference during run-down . . . 140
J.14 Maximum water level difference during run-up . . . 140
J.15 The water level difference versus wave run-up for the open, normal and impermeable core. 141
J.16 Hydraulic gradient in the armour layer found by Muttrray (2000) for rock armoured breakwaters . . . 142
J.17 Measured significant hydraulic gradient in the armour layer during run-down compared with the equation found by Muttrray (2000) for rock armoured breakwaters under regular wave attack. . . . 143
J.18 Water level difference around the armour layer at maximum run-up . . . 144
J.19 Water level difference around the armour layer at maximum run-up . . . 144
J.20 Flow velocity and water motion on the slope of the structure. The red line represents the rate that the flow velocity changes in time (60% wave height). . . . 145
J.21 Reflection coefficient versus percentage of the design wave height . . . 146
J.22 Reflection coefficient versus the deep water wave length . . . 146
J.23 Fit between equation J.9 and data from the model tests . . . 147

LIST OF TABLES

0.1 Correction factors ix

1.1 Armour unit classified by shape, placement and stability factor (CIRIA, 2007). 3

2.1 Ranges of grading widths 8

3.1 Reynolds number ranges for different flow regimes. 18
3.2 Stability numbers found corresponding to zero damage 24

4.1 Available stone gradations 27
4.2 Porosity measurements 32
4.3 Coefficients for fully turbulent flow (Burcharth & Andersen, 1993) 35

5.1 Overview of scaling methods by Froude and Reynold 38
5.2 Tested and initially chosen rock gradings 48
5.3 Surf similarity parameter with associated wave steepness during testing 50
5.4 Test programme 51

6.1 Overview of the occurrence of the failure mechanisms 57
6.2 Change in water motion in the armour layer and the cause and effect of this change . . . 66
6.3 Relative placing density (RPD) Tests 68
6.4 Transition ξ for plunging and surging waves. 70
6.5 Correction factors 72
6.6 Coefficients for the run-up equation of Van der Meer and Stam (1992) 73
6.7 Overview of the failure mechanism, impact and flow force for the open, normal and impermeable core. 78

7.1 Overview of the failure mechanism, impact and flow force for the open, normal and impermeable core. 82
7.2 Correction factors 83

D.1 Obtained shape coefficients of from experimental data 100
D.2 Expressions for the a- and b-coefficients 104
D.3 Shape factors of Englund (1953) 104
D.4 Shape coefficients for stationary flow by (Van Gent, 1993) 105
D.5 Experimental data compared with Shih (1990) 106

F.1 Test programme 109
F.2 Explanation example test code BA32 109
F.3 Calibration data ξ=5.00 109
F.4 Calibration data ξ=3.75 110

J.1 Measuring errors 133
J.2 Coefficients for the run-up equation of Van der Meer and Stam (1992) 137

APPENDIX

A. CORRECTION FACTORS

Phenomenon	Effect on Armour Stability	Correction factor on unit weight
Units are placed on a breakwater head or on curved sections	Accurate placement in a staggered grid is complicated by the breakwater geometry and wave impact is affected by the geometry, therefore the stability is reduced.	1.25
Frequent occurrence of near-design wave height during the lifetime of the structure	Rocking of units, which can occur for a small percentage of the armour units during the design event of a breakwater, can occur frequently during the lifetime of the structure. Therefore rocking should be carefully assessed during the physical model tests.	1.25
The foreshore in front of the structure is steep	A steep foreshore can lead to adverse wave impact against the armour layer.	1.1 for a steepness between 1:30 and 1:20 1.25 for a steepness between 1:20 and 1:15 1.5 for a steepness between 1:15 and 1:10 2 for a steepness greater than 1:10
The structure is low crested	Armour units placed on the horizontal crest and high on the slope are less stable than units placed lower on the slope, where interlocking is increased by gravity and the above-lying units. In case of a low breakwater, the crest area sustains significant wave impacts and as a consequence a larger unit size is applied.	2 for a relative freeboard < 0.5 1.5 for a relative freeboard < 1
The water depth is large	For typical nearshore breakwater cross sections, the ratio between the highest wave heights in the spectrum and the significant wave height is in the order of 1.2 - 1.4. For breakwaters in deep water, this ratio can be up to 1.8 - 2. As the largest waves in the spectrum cause the largest loads on the armour layer, the stability of the armour layer is reduced compared to breakwaters in lower water depths. Furthermore a breakwater cross section in deep water typically contains a high rock toe which can affect the wave impacts on the armour slope. Therefore rocking should be carefully assessed during the physical model tests.	1.5 for a water depth > 2.5 x H_s 2 for a water depth > 3.5 x H_s
The core permeability is low	A low core permeability can lead to large pressures in the armour layer and reduce the stability of the armour layer. The permeability of the core depends on the materials used and the distance at the water line between the armour layer and the impermeable layer.	1.5 for a low core permeability 2 for an impermeable core
The armour slope is mild (<1:1.5)	On a mild slope, the interlocking of armour units is less effective and as a consequence the stability is reduced.	1.25 for a slope milder than 1V: 1.5H 1.5 for a slope milder than 1V:2H

Fig. A.1: Correction factors on the unit weight recommended by DMC on primarily design.

B. ROCK PROPERTIES

General

The amount of flow through the core of the breakwater, this is related to energy dissipation, plays an important role on the stability of the armour layer. Flow through the pores of granular material is influenced by many factors in practice. Therefore, it is interesting to realize that some parameters, such as the shape and size of the particle affect the passing flow. The properties of a particle determine the ease of a flow to pass the material. This chapter will focus on the contribution of various rock properties on the permeability of the material.

The properties of a rock that influence the permeability are defined as grain size, sorting, packing density and grain shape. The porosity which is, in most of the permeability formula's, an important parameter is not mentioned below as it is influenced by the same parameters.

grain size

The size of the median grain (d_{50}) often presents the characteristics of the grain and is used in several permeability formula's. Figure B.1 shows two different grain sizes by constant sorting, packing density and grain shape. While grain size has a negligible effect on the porosity of rock, it has a large effect on the size of the pores. Smaller pores result in more surface friction and higher permeability for the same volume of rock.

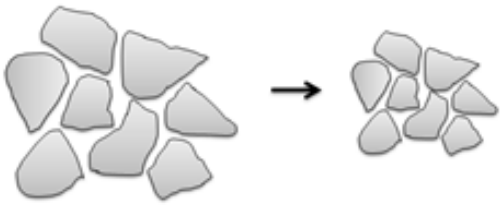

Fig. B.1: Influence of grain size on the size of the pores by constant porosity

Sorting

Sorting is a measure of deviation from the median diameter, showing the width of the distribution. Both large and small grains are present determine the porosity. For permeability the smallest grains will be more significant because they lead to smaller pore size and enlarge the resistance forces. It can be concluded that the median grain size will determine the dominant grain size by well-sorted material. The greater the deviation, the effect of smaller grain sizes will increase and the permeability will be lower.

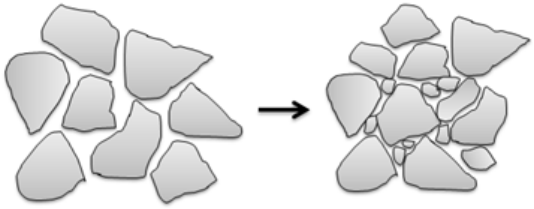

Fig. B.2: Left well-sorted material and right poorly-sorted material

Packing

Packing can be explained by the rate of pore volume around each grain. Therefore, different packings have different porosities. The maximum randomly packing is limited by a porosity of $\geq$0.399 depending on the material. In practise loose packings can change into tight packing resulting into unwanted settlements.

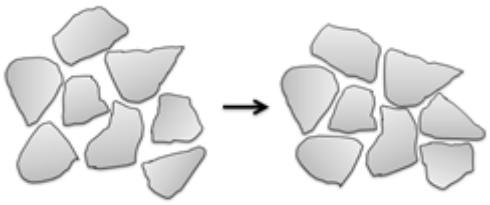

Fig. B.3: Difference in pore size with different packing densities

Grain shape

The shape of a grain is expressed in sphericity and roundness. Roundness describes the degree of angularity of the particle. Sphericity describes the degree to which the particle approaches a spherical shape.
Most grains are not spherical nor round as in an ideal situation. It is expected that the permeability might decreases with sphericity because spherical grains may be more tightly packed than low spherical ones. Angular grains might decrease the permeability as the surface friction will increase with the pore surface see figure B.4.

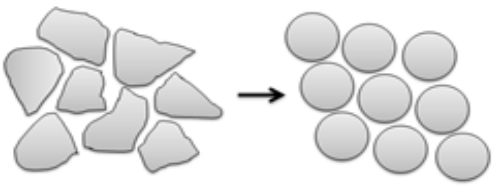

Fig. B.4: Influence of grain shape on the shape of the pore

C. ROCK GRADINGS

Fig. C.1: Available rock samples

D. SHAPE COEFFICIENTS

D.1 Experiments

Grading [mm]	4- 5.6	5.6-8.0	8.0- 11.2	11.2-16.0	16.0- 22.4	22.4- 31.5
Forchheimer equation						
α coefficient						
High packing	608.9	-	862.2	772.1	682.1	1441.6
Low packing	355.3	-	961.0	661.5	1030.7	974.9
Average	482.1	-	911.6	716.8	856.4	1208.3
β coefficient						
High packing	3.18	-	1.97	1.90	2.13	2.41
Low packing	3.08	-	2.02	1.90	2.10	2.37
Average	2.96	-	2.00	1.90	2.12	2.39
Fully turbulent						
Experiment $\beta_{\text{Compact sample}}$	4.16	-	2.63	2.11	2.27	2.59
Experiment $\beta_{\text{Loose sample}}$	3.27	-	2.50	2.03	2.21	2.46

Tab. D.1: Obtained shape coefficients of from experimental data

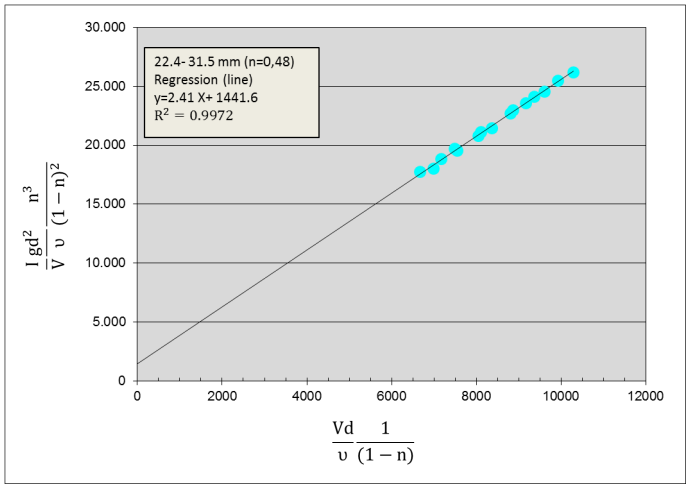

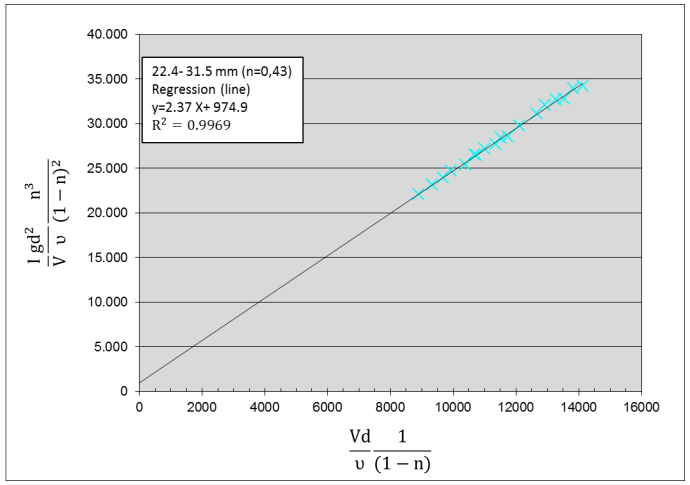

Fig. D.1: Regression line of rock sample: 22.4- 31.5 mm

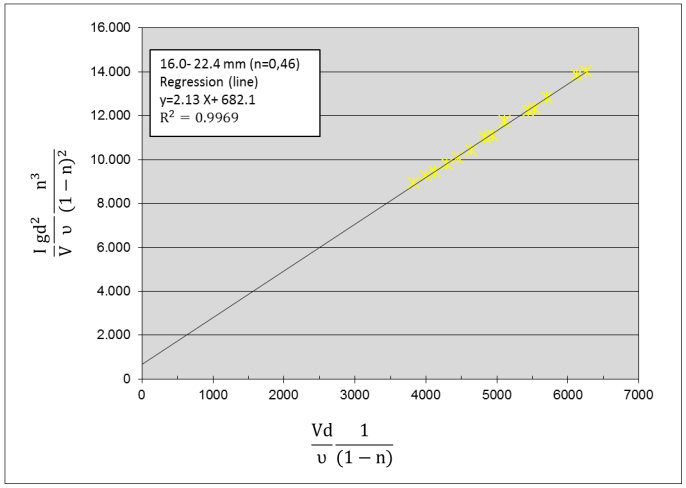

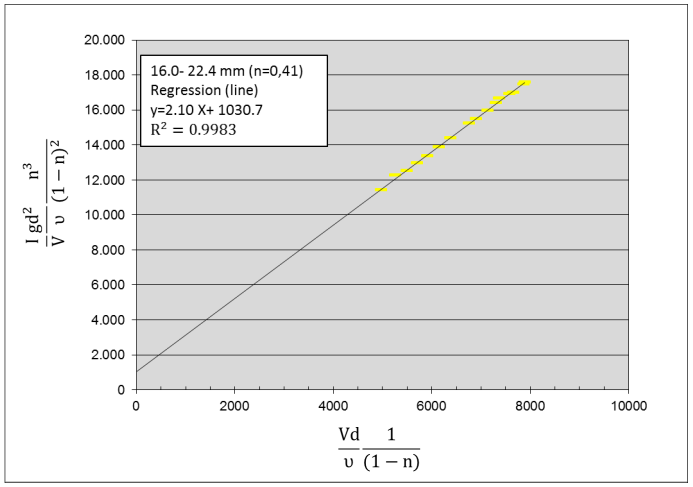

Fig. D.2: Regression line of rock sample: 16.0- 22.4 mm

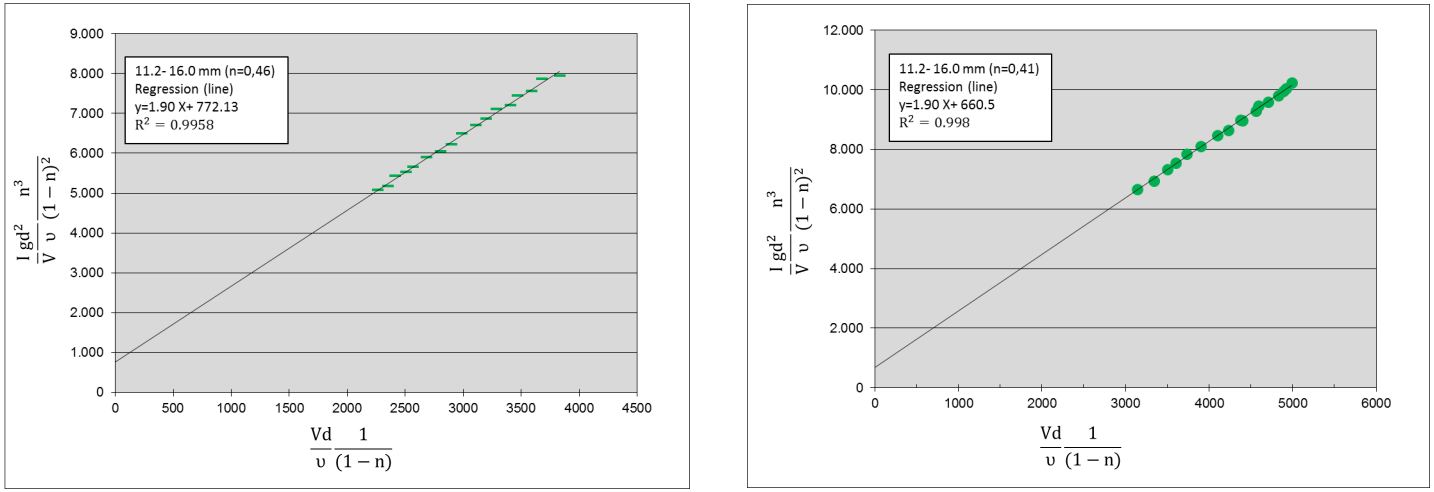

Fig. D.3: Regression line of rock sample: 11.2- 16.0 mm

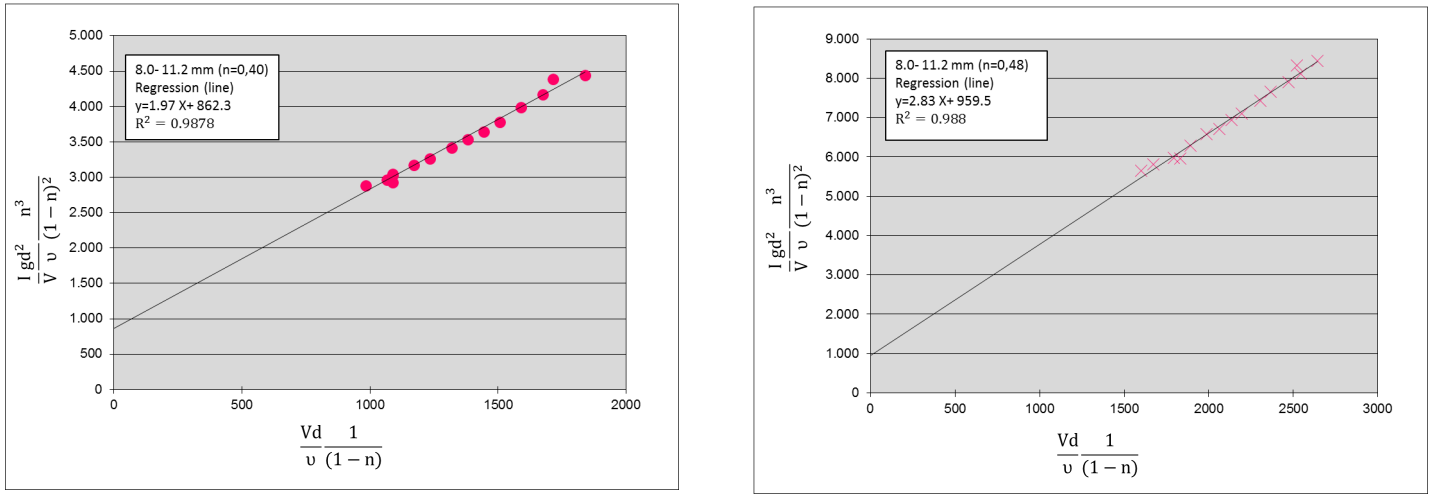

Fig. D.4: Regression line of rock sample: 8.0- 11.2 mm

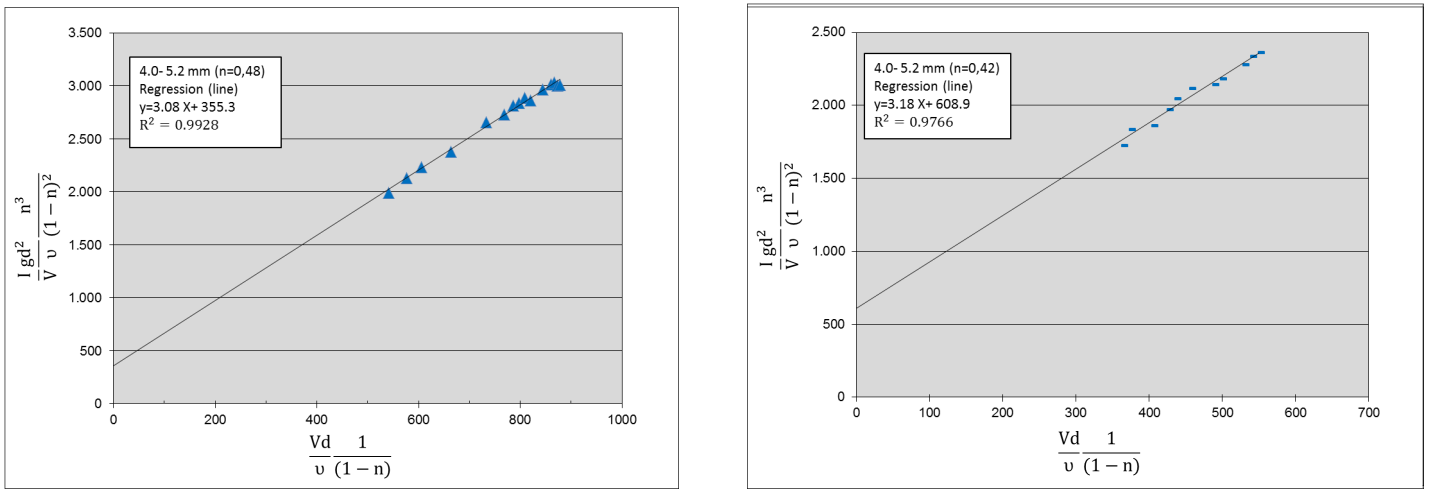

Fig. D.5: Regression line of rock sample: 4.0- 5.4 mm

D.2 Previous research

Chapter 3 elaborates on the Forchheimer model that describe the permeability of a material under various flow velocities and can be described as; $I = aV + bV^2$. Results from stationary and unsteady flow tests confirmed the validity of the Forchheimer model but leaded also to a discussion on the laminar and turbulent coefficients 'a' and 'b'. The coefficients a and b are dimensional and are defined by several researchers, three expressions are illustrated in table D.2.

a	b	Source
$\alpha_{Erg}\frac{(1-n)^2}{n^3}\frac{\nu}{gD^2}$	$\beta_{Erg}\frac{1-n}{n^3}\frac{1}{gD}$	Ergun(1952)
$\alpha_{Eng}\frac{(1-n)^3}{n^2}\frac{\nu}{gD_{eq}^2}$	$\beta_{Eng}\frac{1-n}{n^3}\frac{1}{gD_{eq}}$	Englund(1953)
$\alpha_s = 1684 + 3.12 \cdot 10^{-3}(\frac{g}{\nu^2})^{3/2}D_{15}^2$	$\beta_s = 1.72 + 1.57exp[-5.10 \cdot 10^{-3}(\frac{g}{\nu^2})^{1/3}D_{15}]$	Shih (1990)

Tab. D.2: Expressions for the a- and b-coefficients

All three the expressions lead to different values for the shape factors $'\alpha'$ and $'\beta'$ but none of all found a clear dependency between shape factors and rock properties as described above. However, it is generally that 'α' depends on the gradation and $'\beta'$ depends on both the relative surface roughness and the gradation.

Shih (1990)

In the paper of **?** an expression for α and β is proposed, based on test results for single size crushed limestone with stone diameters (d_{15}) between 5mm and 55mm, and an average d_{50} of 40 mm. Shih suggested the D_{15} is characteristic for the $'\alpha'$ and $'\beta'$ values and used it as representative grain length in the formula. The tested range for the formula is respectively $d_{85}/d_{15} \simeq 1.3$, mainly in the fully turbulent range. The shape of the stone and porosity of the used samples are not further specified in the paper. The tested Reynolds range is approximately 50$\leq$ Re $\leq$ 6,000, mainly fully turbulent range.
Shih derived the formula from test data by a linear regression method using the expression of Englund for the 'a' and 'b' coefficients (table D.2).

Englund (1953)

The expression of Englund deviates not significant from the expression of Ergun (1952) in the porosity range for rubble-mound structures (n=0.37-0.48). The coefficients obtained by the expression of Englund can be transformed by multiplying the coefficients with (1-n)/n $\approx$0.24. Table D.3 shows both coefficients derived by Englund (1953).

Gent (1993)

van Gent (1993) conducted stationary and non-stationary flow tests in the horizontal direction. The used expression for 'a' and 'b' in the data analyse is the one of Ergun (1952) described in table D.2. The results are summarized in table D.4. Note that Van Gent used the nominal diameter as characteristic grain length D_{n50} instead of median sieve diameter D_{50} that is normally used in the Forchheimer model. The tests set-up of Van Gent is illustrated in figure D.6.

Material	α_{Eng}	β_{Eng}	α_{Erg}	β_{Erg}
Uniform spherical grains	$\sim$780	$\sim$1.8	$\sim$190	$\sim$1.8
Uniform rounded grains	$\sim$1000	$\sim$2.8	$\sim$240	$\sim$2.8
Irregular, angular grains	1500 or larger	3.6 or larger	360 or larger	3.6 or larger

Tab. D.3: α and β factors derived by Englund (1953) and rewritten into shape factors fitting the expression of Ergun (1952)

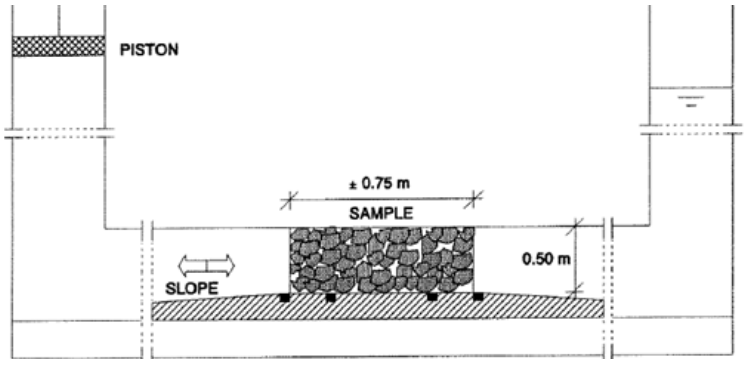

Fig. D.6: Test set-up of Van Gent (1993)

Stationary flow data from Van Gent (1993) with a flow angle of 0 degree					
Test	Material	D_{n50}	D_{n85}/D_{n15}	α	β
R5	Irregular	0.020	1.03	1662	1.07
R8	Irregular	0.031	1.74	1007	0.63
R1	Irregular	0.061	1.27	1791	0.55
R3	Semi-round	0.048	1.27	0	0.88
R4	Very round	0.048	1.26	1066	0.29

Tab. D.4: Shape coefficients for stationary flow by (Van Gent, 1993)

Comparison

In this section the obtained coefficients α and β are evaluated with the coefficients of Shih (1990), van Gent (1993) and Englund (1953). For the comparison with Shih (1990) the α and β coefficients for D_{15} are used. Figure D.7 illustrates the coefficients calculated using the expression of Englund for a and b, similar as Shih (1990), and D_{15}. The coefficient can be found be found in table D.5.

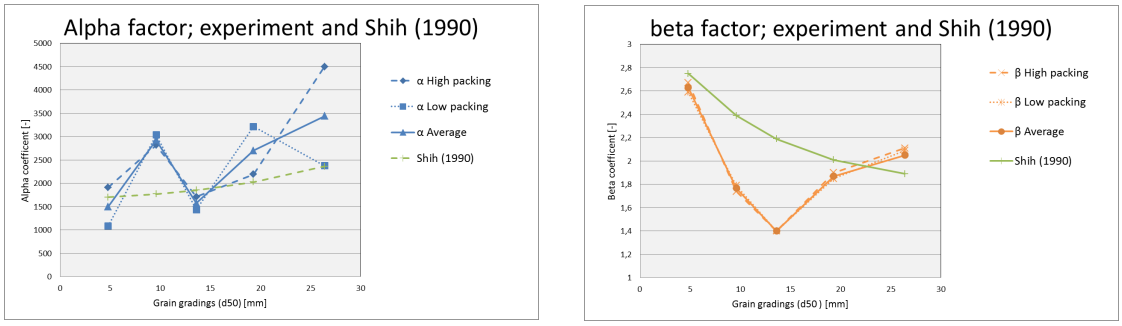

Fig. D.7: Shape factors compared with the formula of Shih (1990)

Comparing the test result with the prediction formula of Shih (1990) it can be concluded gives rather reliable results for both the α as β coefficients. Shih suggests further that the β coefficients consistently decreases with increase in d_{15} till a specific value is reached. This could not be obtained from the results. This might be attributable to the surface roughness between the various rock gradings.

The obtained values of α and β have been compared with the transformed values of England in table D.3 and the values of van Gent (1993) in table D.4. The values for the β coefficient of Englund for irregular material is larger than obtained from the current tests. This difference might also be adjusted to the shape of the material. Englund conducted permeability tests with sand grains that have a larger surface roughness than rock material.
The tests of Van Gent show on the other hand a consequent lower results for the β coefficient. Van Gent assigned the difference to set-up of the experiments as the tests of Van Gent were performed with a horizontal flow (illustrated in figure D.6) while current research and many other researches, were performed with a vertical flow (figure D.6). The main conclusion is that the β and α coefficients are larger in case of a vertical flow instead of horizontal slope.

Grading [mm]	4- 5.6	5.6-8.0	8.0- 11.2	11.2-16.0	16.0- 22.4	22.4- 31.5
D_{50} [mm]	4.8	6.7	9.6	13.6	19.2	27
d_{85} **[mm]**	5.4	7.64	10.7	15.28	21.4	30.1
d_{15} **[mm]**	4.2	6.0	8.5	11.9	17.0	23.8
Coefficients from Shih (1990)						
α	1705.2	1726.7	1770.7	1854.6	2031.0	2364.1
β	2.75	2.58	2.39	2.19	2.01	1.89
α **coefficient from the experiments** d_{15}						
High packing	1913.8	-	2816.6	1724.4	2192.8	4503.3
Low packing	1089.3	-	3037.1	1435.5	3217.0	2379.0
Average	1501.6	-	2926.9	1573.9	2704.9	3441.5
β **coefficient from the experiments** d_{15}						
High packing	2.67	-	1.74	1.40	1.9	2.11
Low packing	2.59	-	1.79	1.40	1.85	2.09
Average	2.63	-	1.76	1.40	1.87	2.05

Tab. D.5: Experimental data compared with Shih (1990)

Conclusion

The β' coefficients obtained from the tests show a great resembles with the formula of **?** for narrow gradings. The β' value is validated and as reliable assumed. The reliability of the α coefficients is more difficult to verify as the value differs greatly for the conducted tests and is a fitting value for turbulent flow.
Furthermore, it can be concluded that the α and β value depend on the direction of the flow. Permeability tests with horizontal flow direction result in lower coefficients than vertical flow. The difference are rather large and therefore important to note. Overall, the test results show a clear overview from fully turbulent flow (high Reynols numbers) to Forchheimer flow where laminar forces a gain more influence.

E. CORE CONFIGURATIONS

Fig. E.1: Cross-section of a rubble mound breakwater with rock grading 22.4-32.5 mm

Fig. E.2: Cross-section of a rubble mound breakwater with impermeable core

Fig. E.3: Cross-section of a rubble mound breakwater; left photo rock grading 11.2-16 mm and the right photo rock grading 5.4-8.0 mm

F. WAVE DATA

F.1 Naming of test series

	Open core	**Normal core**	**Impermeable core**	**Without a core**
Wind waves	CA	BA	FA	ZA
Swell waves	CB	BB	FB	ZB

Tab. F.1: Test programme

First character indicates the core configuration:

Open core	= Filter and core consist of the same material	C
Normal core	= Core consist of smaller material than filter layer (conventional breakwater)	B
Impermeable core	= Wooden board with small grains	F
Calibration	=Without a breakwater	Z

Second character indicates the wave steepness:

Swell waves	ξ=5.0	s=0.023	A
Wind waves	ξ=3.75	s=0.040	B

The repetition numbers will be indicated with a number behind the two characters followed by another number indicating the wave height of the test series. For example test BA32 in table F.2.

Code	**Explanation**	**Example**
B	Core configuration	B presents core 2
A	Wave steepness	A presents steepness 0.04
3	The repetition	3 is repetition 3
2	The wave height	2 is the 80% wave height

Tab. F.2: Explanation example test code BA32

F.2 Calibration

	Design wave height of 98mm for wave series ξ=5.0			
Series	percentage of H_d	Wave height [mm]		Relative deviation [%]
		desired	measured	
ZA0	40%	39.36	39.81	1.1%
ZA1	60%	59.04	57.34	2.9%
ZA2	80%	78.72	75.91	3.6%
ZA3	100%	98.40	96.67	1.8%
ZA4	120%	118.08	117.00	0.9%
ZA5	140%	137.76	139.10	0.9%
ZA6	160%	157.44	162.00	2.9%
ZA7	180%	177.12	185.10	4.4%

Tab. F.3: Calibration data ξ=5.00

	Design wave height of 98mm for wave series ξ=3.75			
Series	percentage of H_d	Wave height [mm]		Relative deviation [%]
		desired	measured	
ZB0	40%	39.36	42.25	7.3%
ZB1	60%	59.04	59.06	0.0%
ZB2	80%	78.72	77.55	1.5%
ZB3	100%	98.40	97.40	1.0%
ZB4	120%	118.08	117.00	0.9%
ZB5	140%	137.76	136.80	0.7%
ZB6	160%	158.44	158.70	0.8%
ZB7	180%	177.12	179.7	1.5%

Tab. F.4: Calibration data ξ=3.75

F.3 Wave distribution

The distribution of wave heights can be described with a Rayleigh distribution in water deeper than $\sim 3H_s$. In shallower water waves will break and the distribution deviates. The Rayleigh-distribution is valid for the wave height distribution in the physical experiments of this research.

$$P\underline{H} > H = \exp[-2(\frac{H}{H_s})^2] \tag{F.1}$$

The extreme wave height within a certain duration can be derived as the probability that a arbitrarily chosen wave height does not exceed the wave height in the wave record is then $1 - (Q_H)$.

$$Pr\underline{H}_{max} > H_D = 1 - (1 - Q_H)^N \tag{F.2}$$

where $Q_H = Pr\underline{H} > H$. The maximum value of this probability density function is called the mode H_{max}.

$$mod(\underline{H}_{max}) \approx H_{m0}\sqrt{1/2 \ln N} \tag{F.3}$$

For 1000 waves a the value H_{max}/H_{m0} is 1.86. Designing on this maximum is not wise as the actually occuring maximum wave height has a probability of 0.63 of exceeding the $mod(\underline{H}_{max})$.

Although the JONSWAP spectrum can be described with a Rayleigh distribution, the measured wave height show deviating wave heights. The maximum wave height observed for an individual wave spectrum exceeds the value of H_{max}/H_{m0}= 1.86. This is mainly the case for low wave heights.

ξ=5.0

ZA0	
H_{m0}	39.81 mm
T_p	1.07 sec.
s_{0p}	0.022
ξ	5.0
H_{max}	87.42 mm
$\frac{H_{max}}{H_{m0}}$	2.22
$T_{H\,max}$	0.90

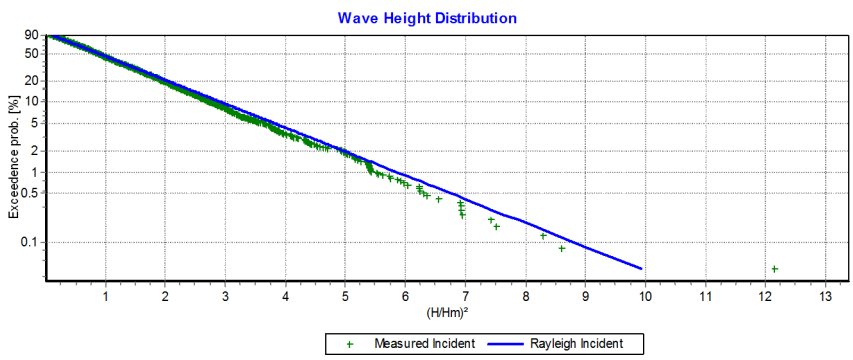

Fig. F.1: Raleigh distribution of the 40% wave height of ξ=5.0

ZA1	
H_{m0}	57.3 mm
T_P	1.3 sec.
s_{0p}	0.022
ξ	5.1
H_{max}	109.6 mm
$\frac{H_{max}}{H_{m0}}$	1.92
$T_{H\,max}$	1.18

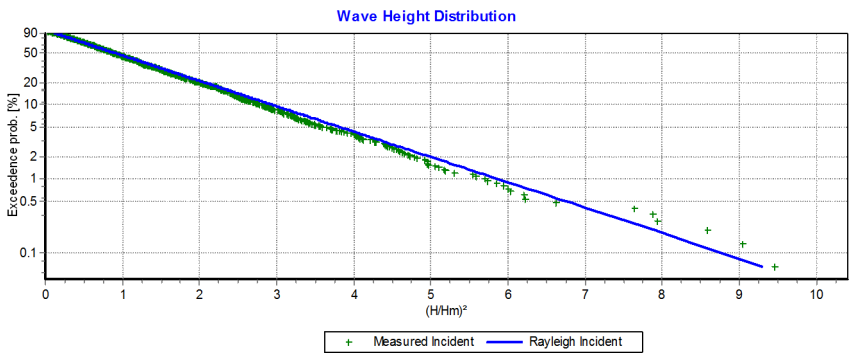

Fig. F.2: Raleigh distribution of the 60% wave height of ξ=5.0

ZA2	
H_{m0}	75.9 mm
T_P	1.6 sec.
s_{0p}	0.020
ξ	4.9
H_{max}	143.7 mm
$\frac{H_{max}}{H_{m0}}$	1.89
$T_{H\,max}$	1.31

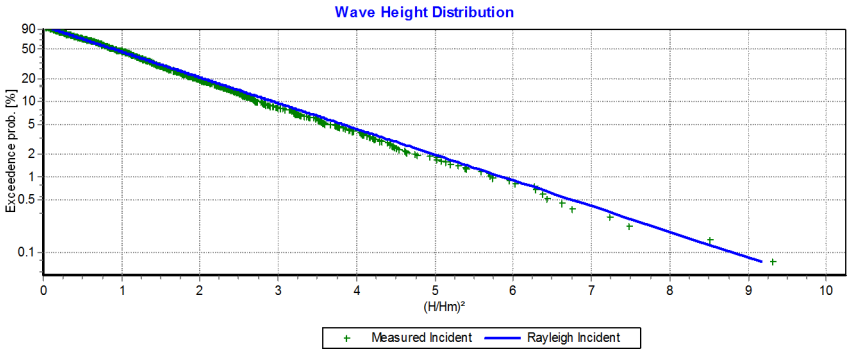

Fig. F.3: Raleigh distribution of the 80% wave height of ξ=5.0

ZA3	
H_{m0}	96.7 mm
T_P	1.6 sec.
s_{0p}	0.023
ξ	4.9
H_{max}	157.3 mm
$\frac{H_{max}}{H_{m0}}$	1.64
$T_{H\,max}$	1.58

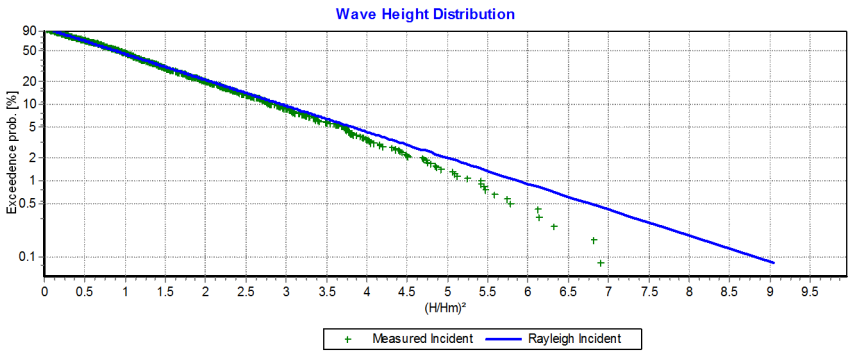

Fig. F.4: Raleigh distribution of the 100% wave height of ξ=5.0

ZA4	
H_{m0}	117.0 mm
T_P	1.9 sec.
s_{0p}	0.022
ξ	5.0
H_{max}	198.8 mm
$\frac{H_{max}}{H_{m0}}$	1.72
$T_{H\,max}$	1.70

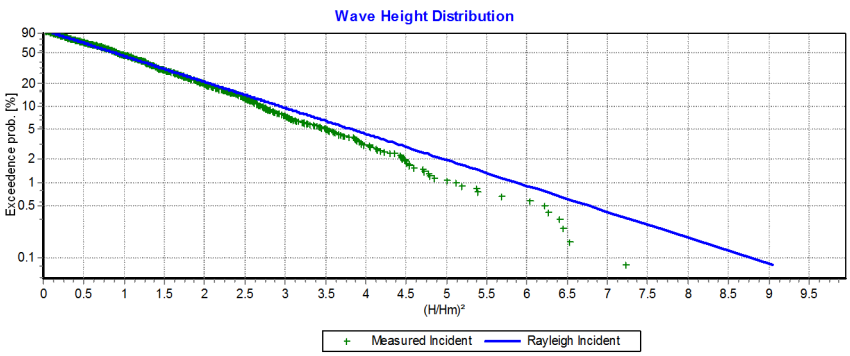

Fig. F.5: Raleigh distribution of the 120% wave height of ξ=5.0

ZA5	
H_{m0}	139.1 mm
T_P	2.0 sec.
s_{0p}	0.022
ξ	5.0
H_{max}	225.8 mm
$\frac{H_{max}}{H_{m0}}$	1.64
$T_{H\,max}$	1.78

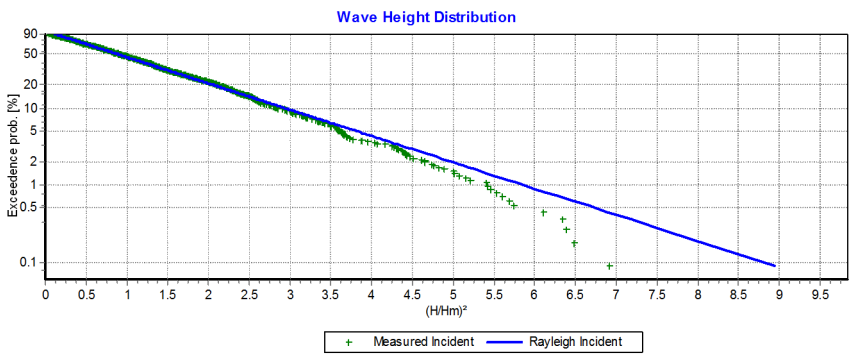

Fig. F.6: Raleigh distribution of the 140% wave height of ξ=5.0

ZA6	
H_{m0}	162.0 mm
T_P	2.2 sec.
s_{0p}	0.021
ξ	5.1
H_{max}	264.5 mm
$\frac{H_{max}}{H_{m0}}$	2.23
$T_{H\,max}$	

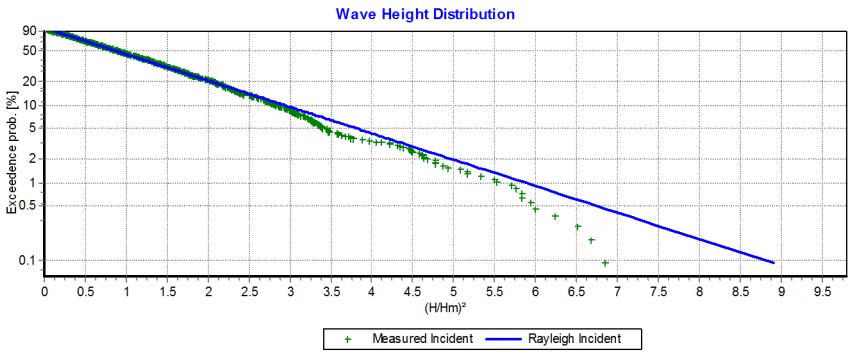

Fig. F.7: Raleigh distribution of the 140% wave height of ξ=5.0

ZA7	
H_{m0}	185.1 mm
T_P	2.2 sec.
s_{0p}	0.024
ξ	4.8
H_{max}	302.6 mm
$\frac{H_{max}}{H_{m0}}$	1.64
$T_{H\,max}$	2.29

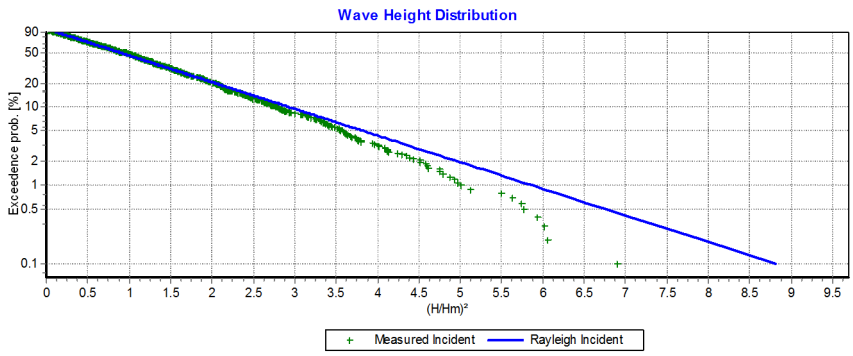

Fig. F.8: Raleigh distribution of the 180% wave height of ξ=5.0

ξ=3.75

ZB0	
H_{m0}	42.25 mm
T_p	0.8 sec.
s_{0p}	0.042
ξ	3.64
H_{max}	92.6 mm
$\frac{H_{max}}{H_{m0}}$	2.33
$T_{H\,max}$	0.76

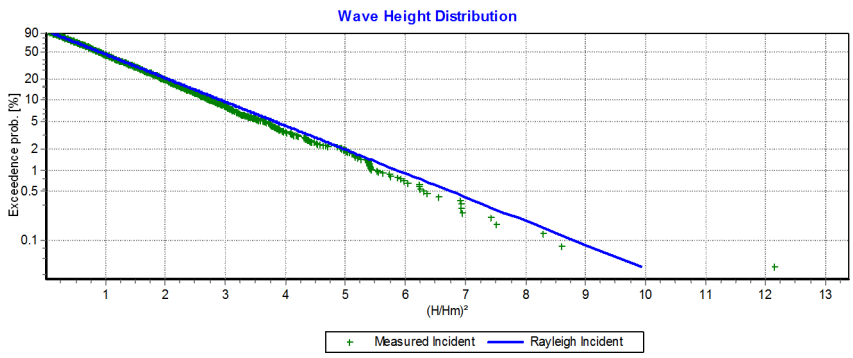

Fig. F.9: Raleigh distribution of the 40% wave height of ξ=3.75

ZB1	
H_{m0}	59.1 mm
T_P	1.0 sec.
s_{0p}	0.038
ξ	3.9
H_{max}	121.5 mm
$\frac{H_{max}}{H_{m0}}$	1.02
$T_{H\,max}$	0.88

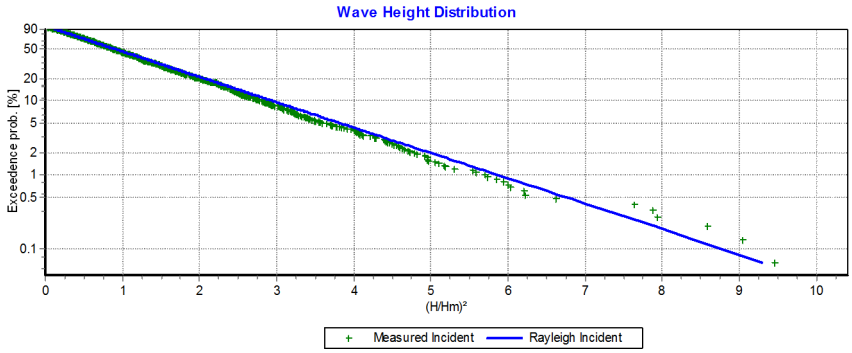

Fig. F.10: Raleigh distribution of the 60% wave height of ξ=3.75

ZB2	
H_{m0}	77.6 mm
T_P	1.1 sec.
s_{0p}	0.038
ξ	3.9
H_{max}	144.3 mm
$\frac{H_{max}}{H_{m0}}$	1.85
$T_{H\,max}$	1.02

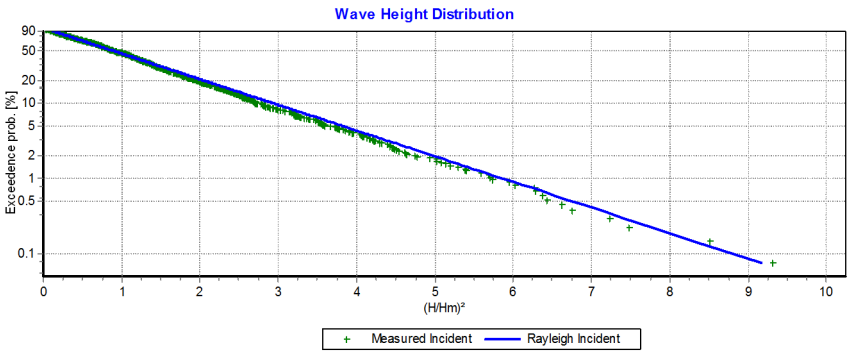

Fig. F.11: Raleigh distribution of the 80% wave height of ξ=3.75

ZB3	
H_{m0}	97.4 mm
T_P	1.2 sec.
s_{0p}	0.048
ξ	3.4
H_{max}	189.5 mm
$\frac{H_{max}}{H_{m0}}$	1.92
$T_{H\,max}$	1.13

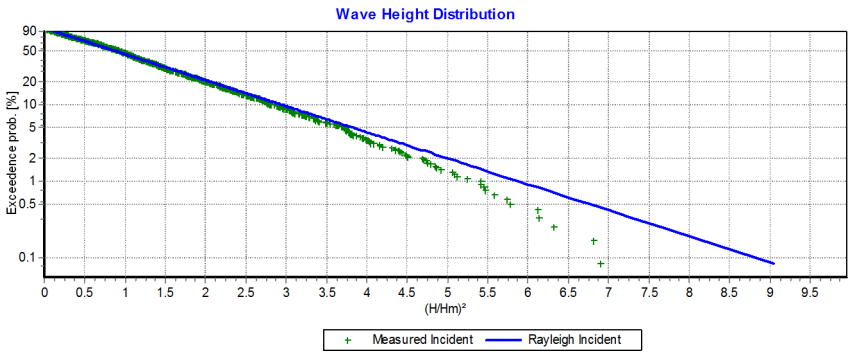

Fig. F.12: Raleigh distribution of the 100% wave height of ξ=3.75

ZB4	
H_{m0}	117.0 mm
T_P	1.2 sec.
s_{0p}	0.049
ξ	3.7
H_{max}	231.5 mm
$\frac{H_{max}}{H_{m0}}$	1.96
$T_{H\,max}$	1.30

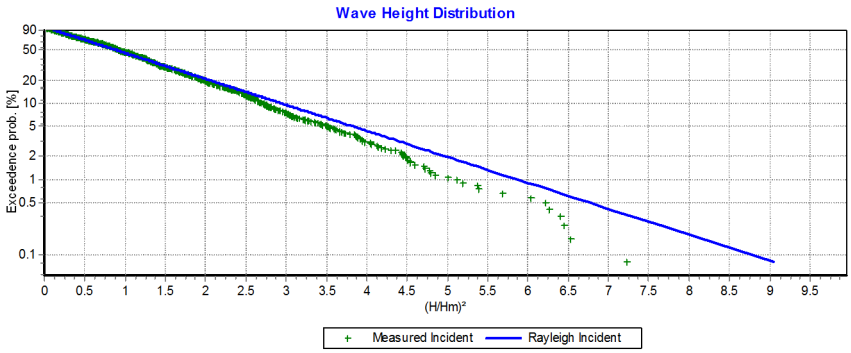

Fig. F.13: Raleigh distribution of the 120% wave height of ξ=3.75

ZB5	
H_{m0}	136.8 mm
T_P	1.5 sec.
s_{0p}	0.041
ξ	3.7
H_{max}	242.6 mm
$\frac{H_{max}}{H_{m0}}$	1.75
$T_{H\,max}$	1.31

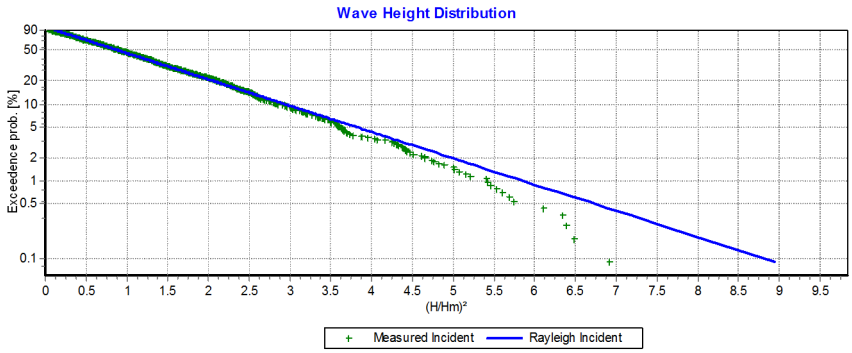

Fig. F.14: Raleigh distribution of the 140% wave height of ξ=3.75

ZB6	
H_{m0}	158.7 mm
T_P	1.6 sec.
s_{0p}	0.042
ξ	3.7
H_{max}	254.7 mm
$\frac{H_{max}}{H_{m0}}$	1.50
$T_{H\,max}$	1.42

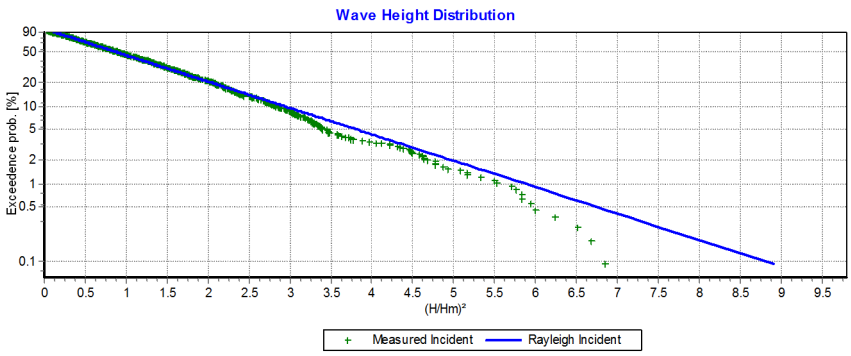

Fig. F.15: Raleigh distribution of the 140% wave height of ξ=3.75

ZB7	
H_{m0}	179.7 mm
T_P	1.6 sec.
s_{0p}	0.043
ξ	3.6
H_{max}	270.3 mm
$\frac{H_{max}}{H_{m0}}$	1.70
$T_{H\,max}$	

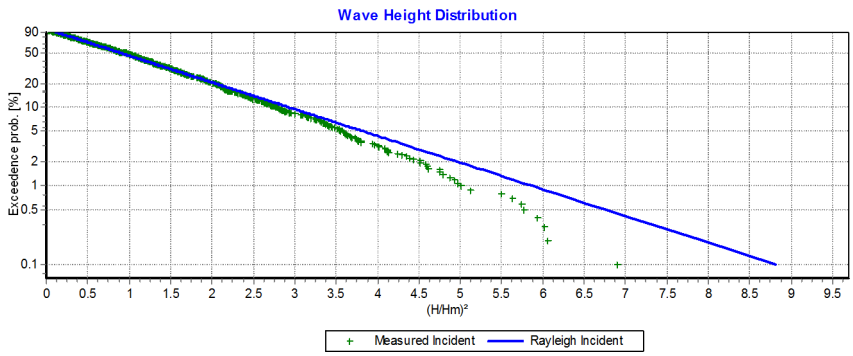

Fig. F.16: Raleigh distribution of the 180% wave height of ξ=3.75

G. START AND 100% PHOTOS

An overview of the start photos and the photo after the 100% wave height of all test series can be found below.

	Open core	**Normal core**	**Impermeable core**
ξ=5.0	CA	BA	FA
ξ=3.75	CB	BB	FB

Open core

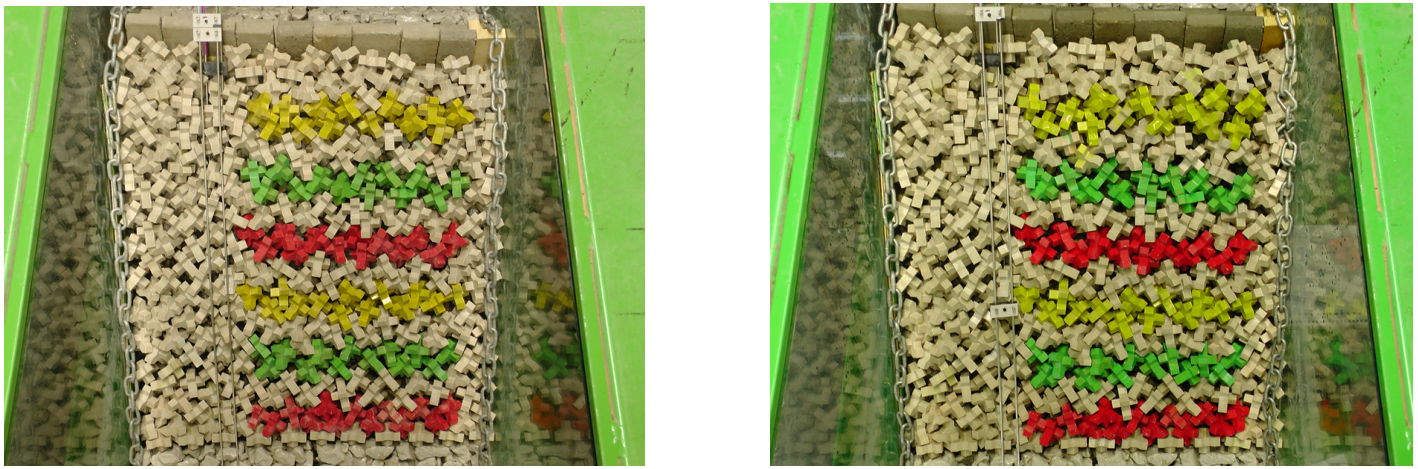

Fig. G.1: Test CA repetition 1; start and 100% picture

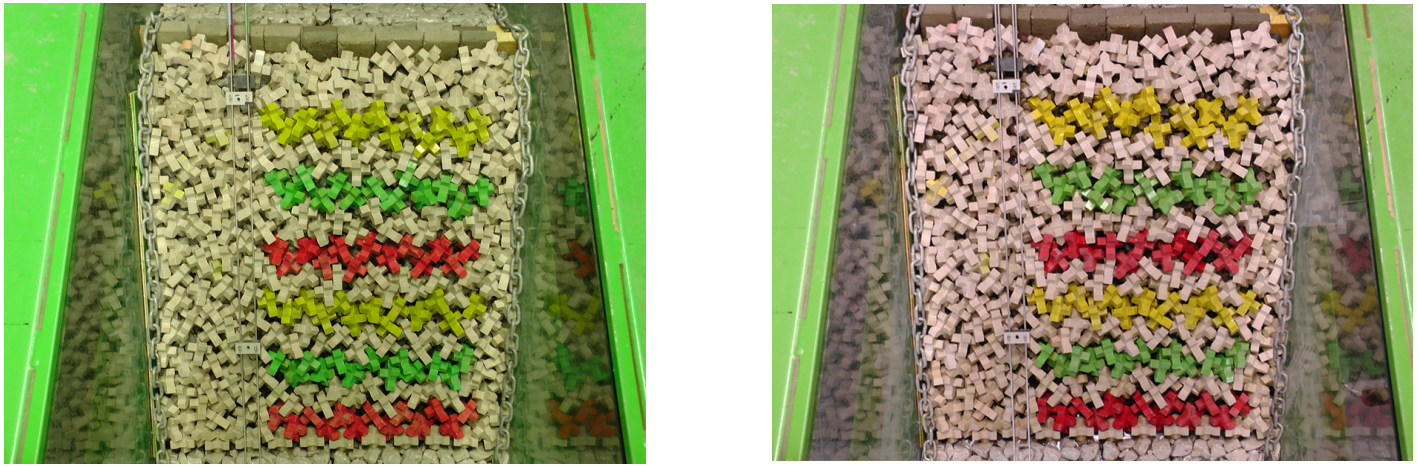

Fig. G.2: Test CA repetition 2; start and 100% picture

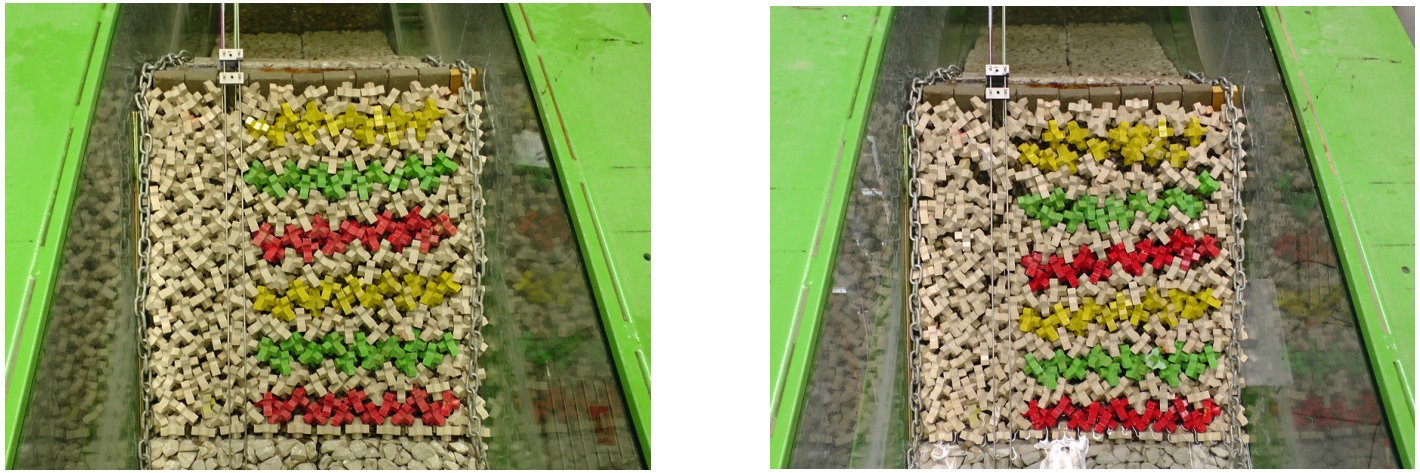

Fig. G.3: Test CA repetition 4; start and 100% picture

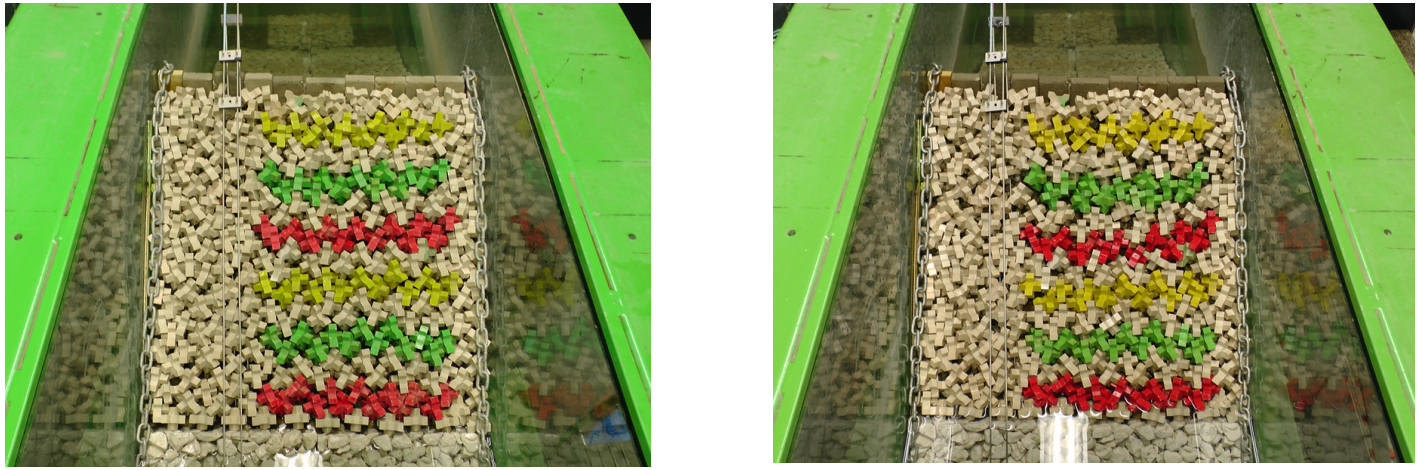

Fig. G.4: Test CA repetition 5; start and 100% picture

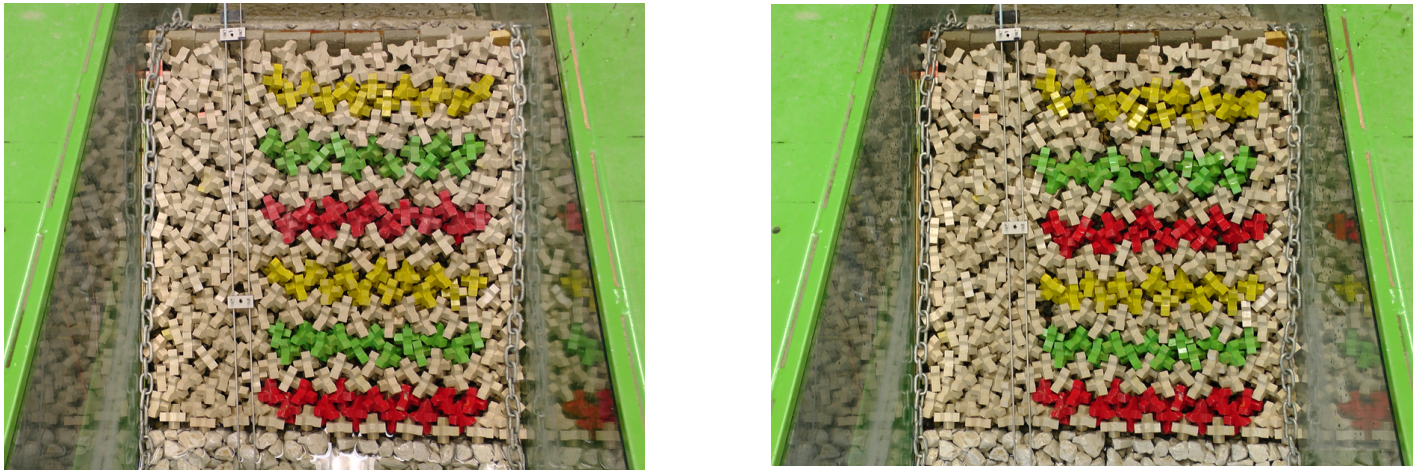

Fig. G.5: Test CB repetition 1; start and 100% picture

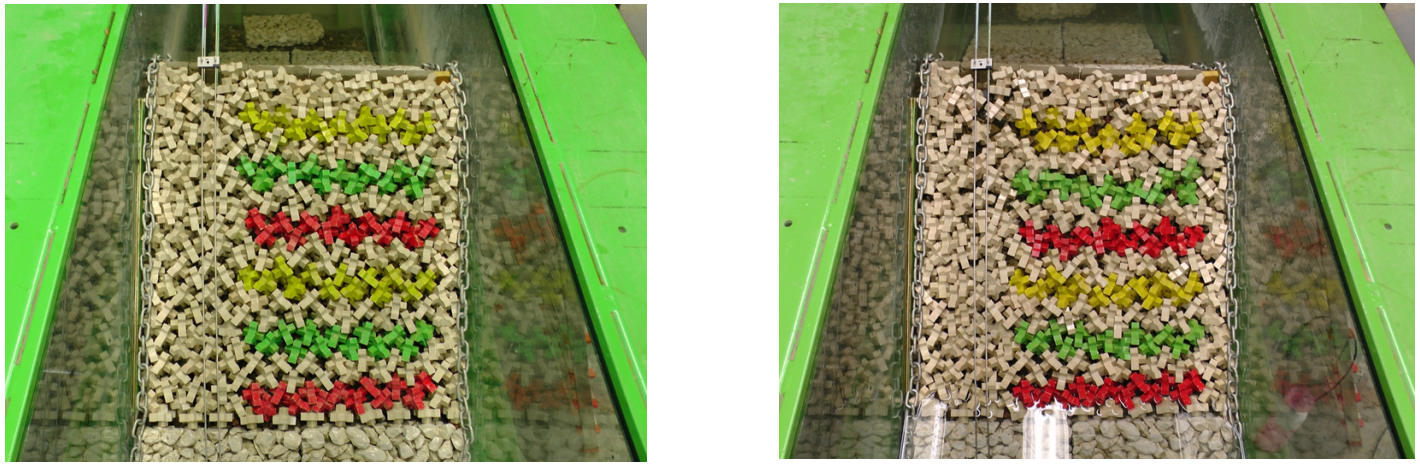

Fig. G.6: Test CB repetition 2; start and 100% picture

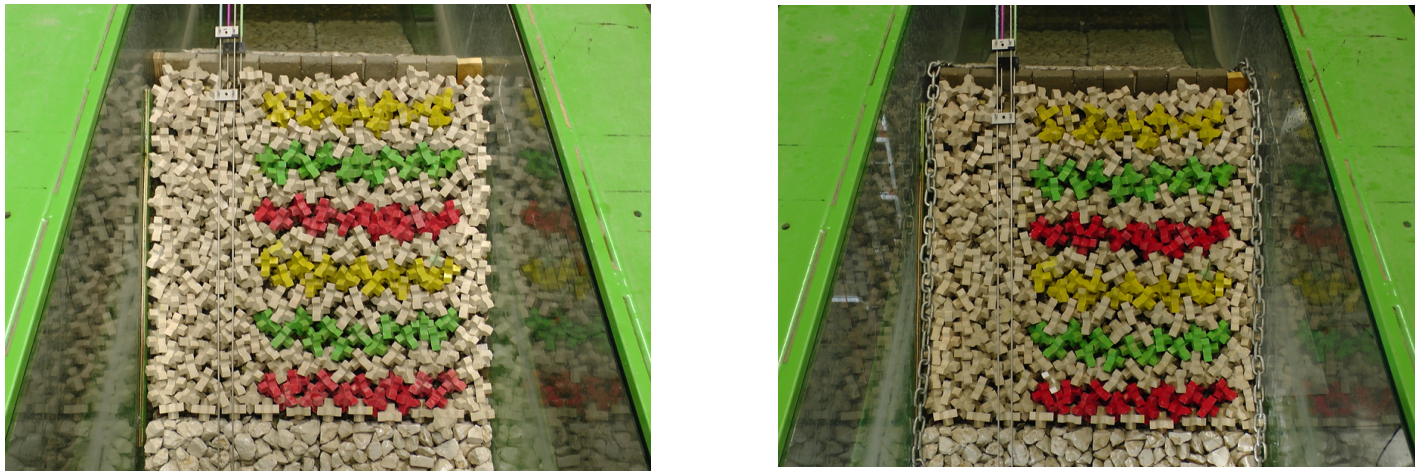

Fig. G.7: Test CB repetition 4; start and 100% picture

Normal core

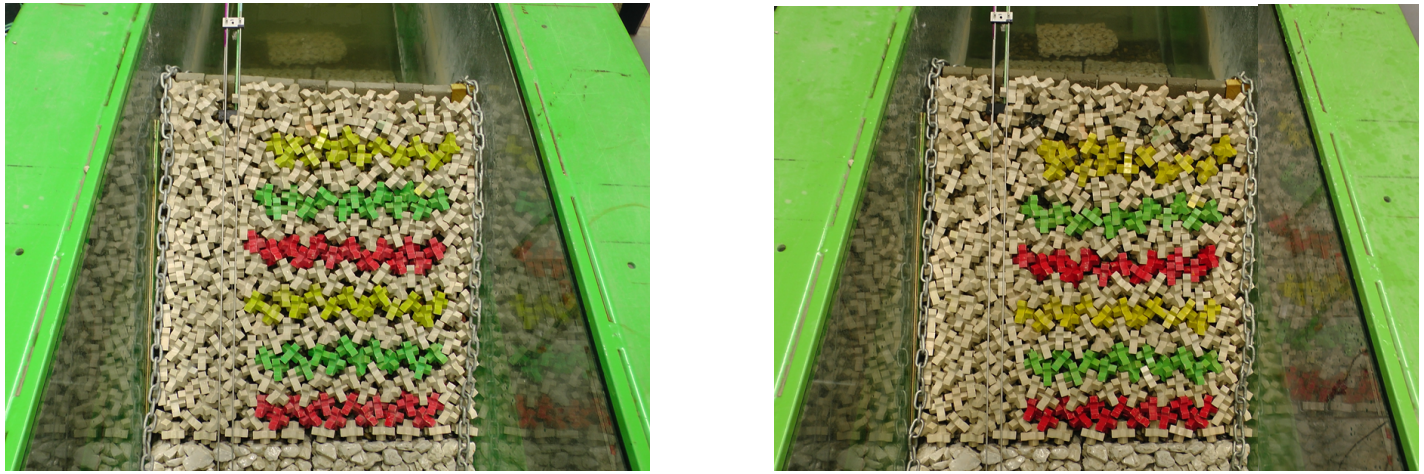

Fig. G.8: Test BA repetition 1; start and 100% picture

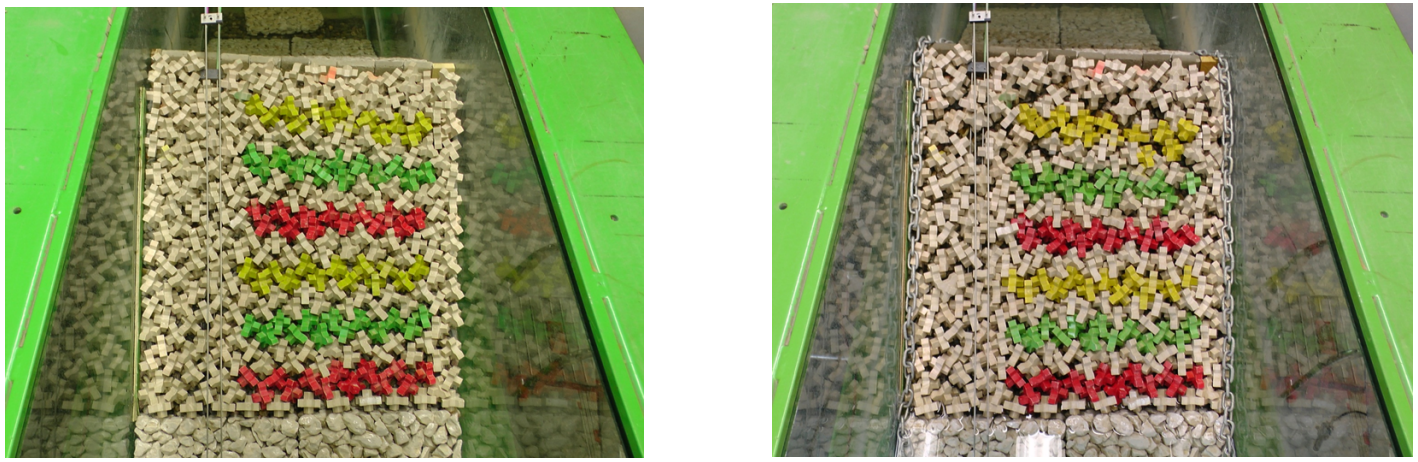

Fig. G.9: Test BA repetition 2; start and 100% picture

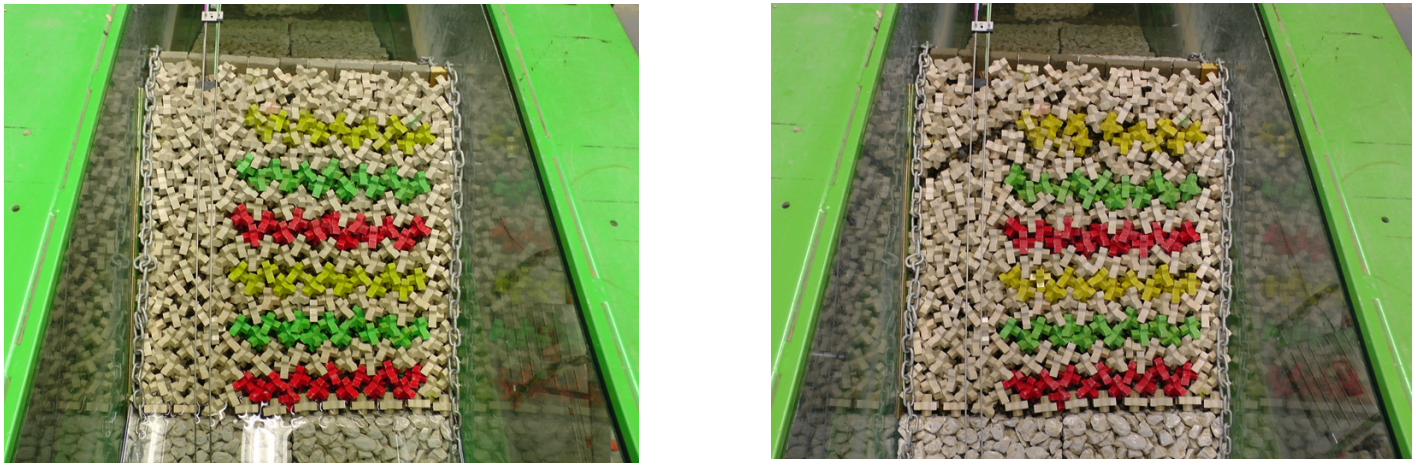

Fig. G.10: Test BA repetition 3; start and 100% picture

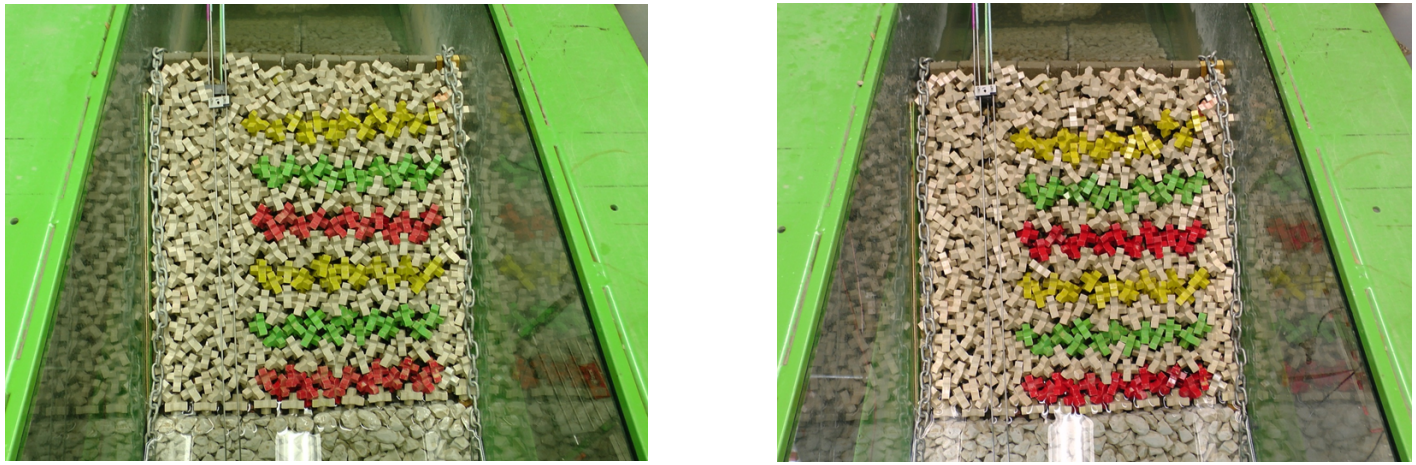

Fig. G.11: Test BB repetition 1; start and 100% picture

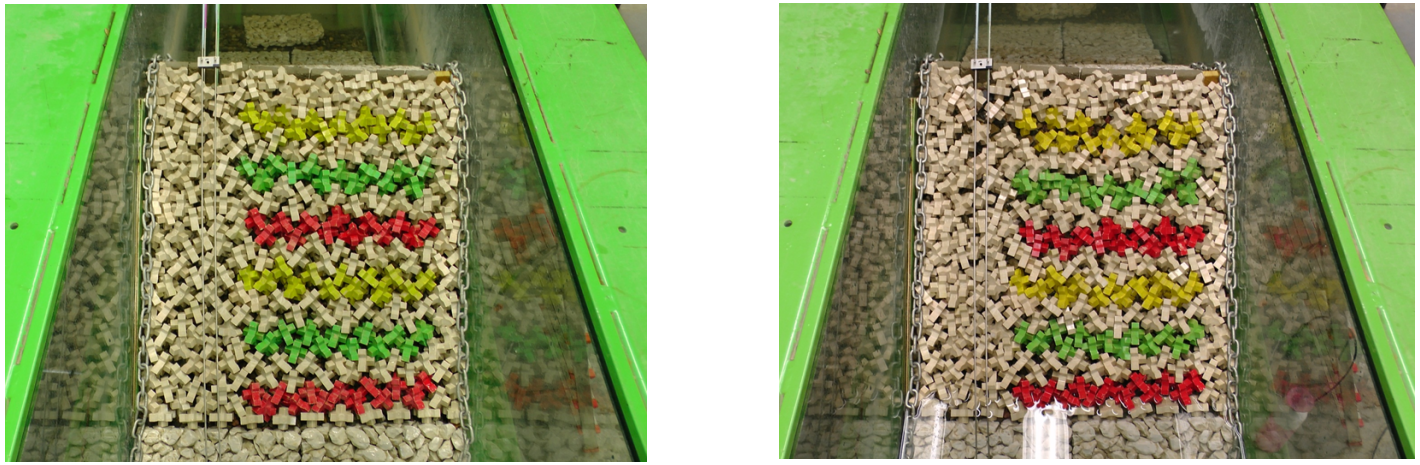

Fig. G.12: Test BB repetition 2; start and 100% picture

Fig. G.13: Test BB repetition 3; start and 100% picture

Impermeable core

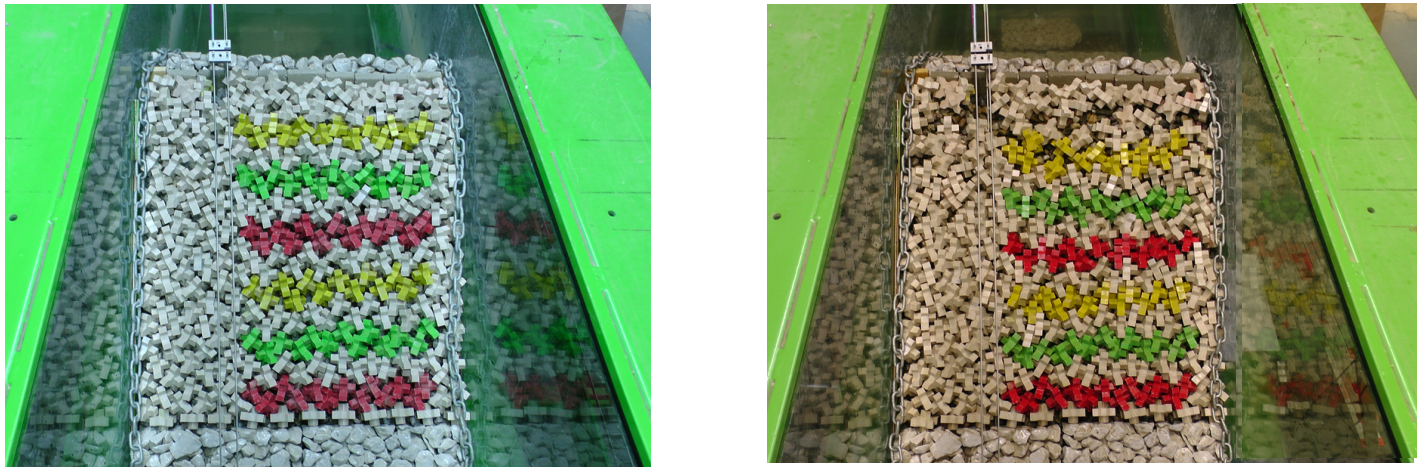

Fig. G.14: Test FA repetition 1; start and 100% picture

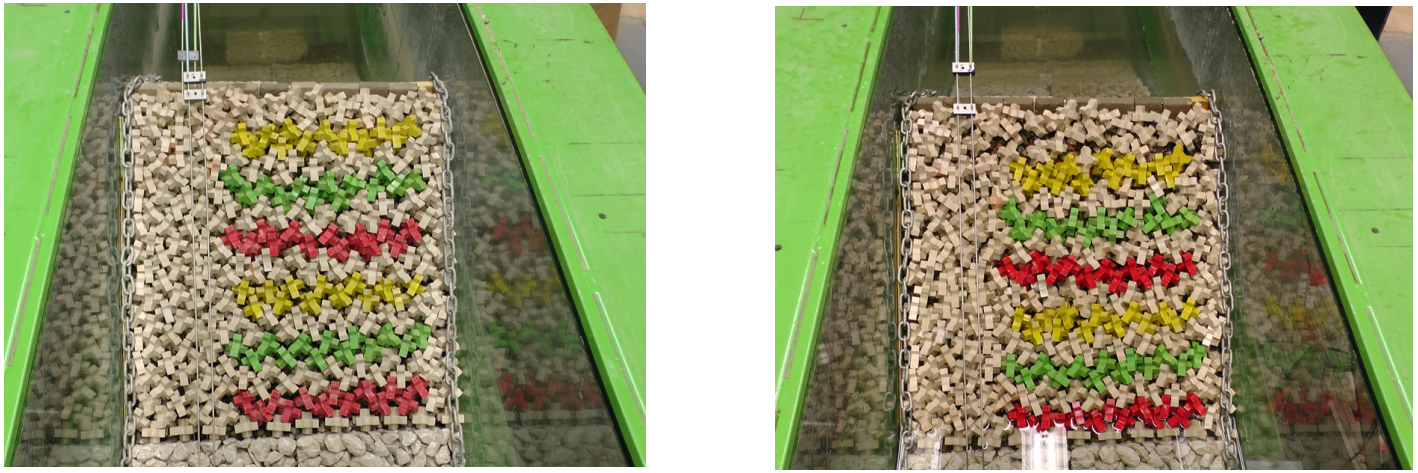

Fig. G.15: Test FA repetition 2; start and 100% picture

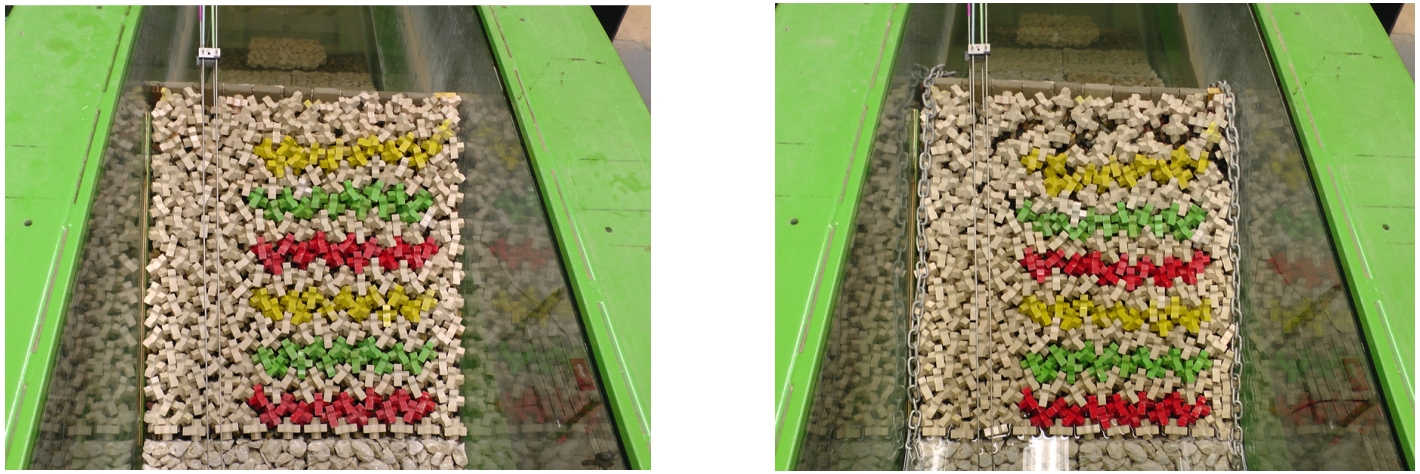

Fig. G.16: Test FA repetition 3; start and 100% picture

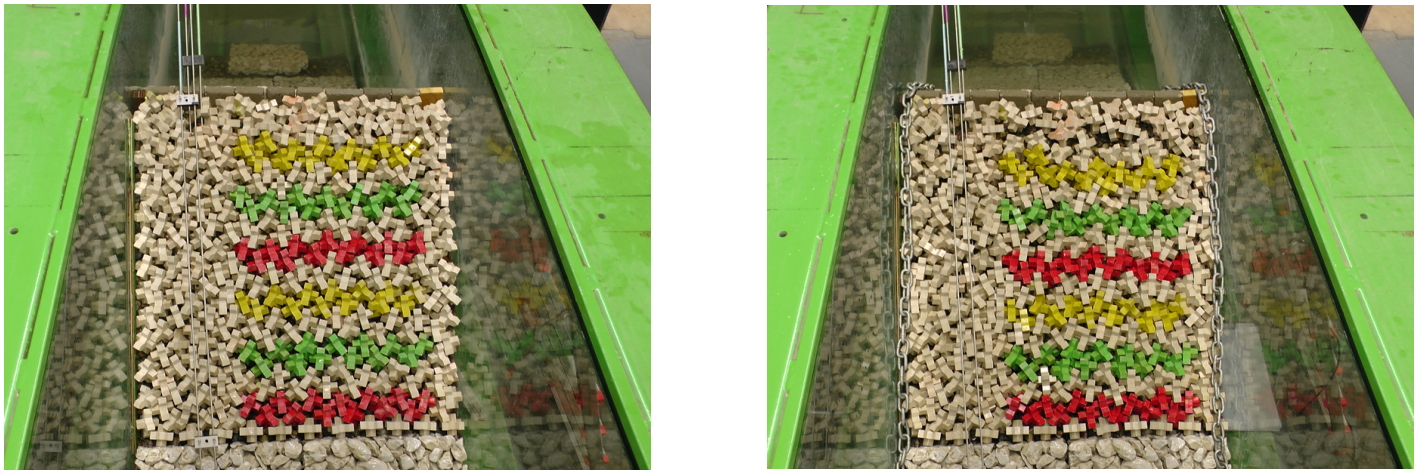

Fig. G.17: Test FB repetition 1; start and 100% picture

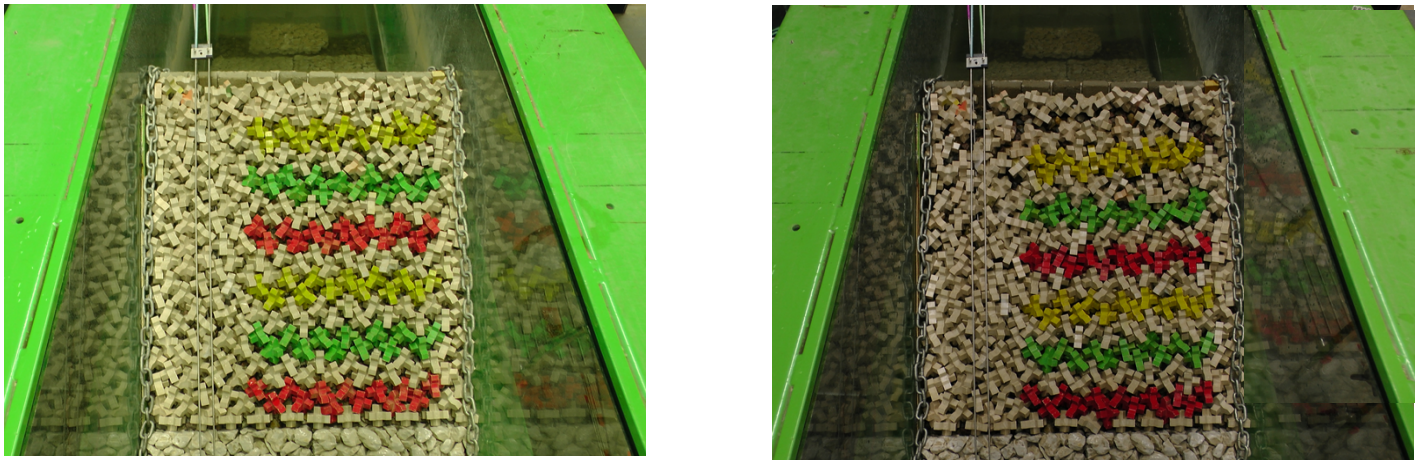

Fig. G.18: Test FB repetition 2; start and 100% picture

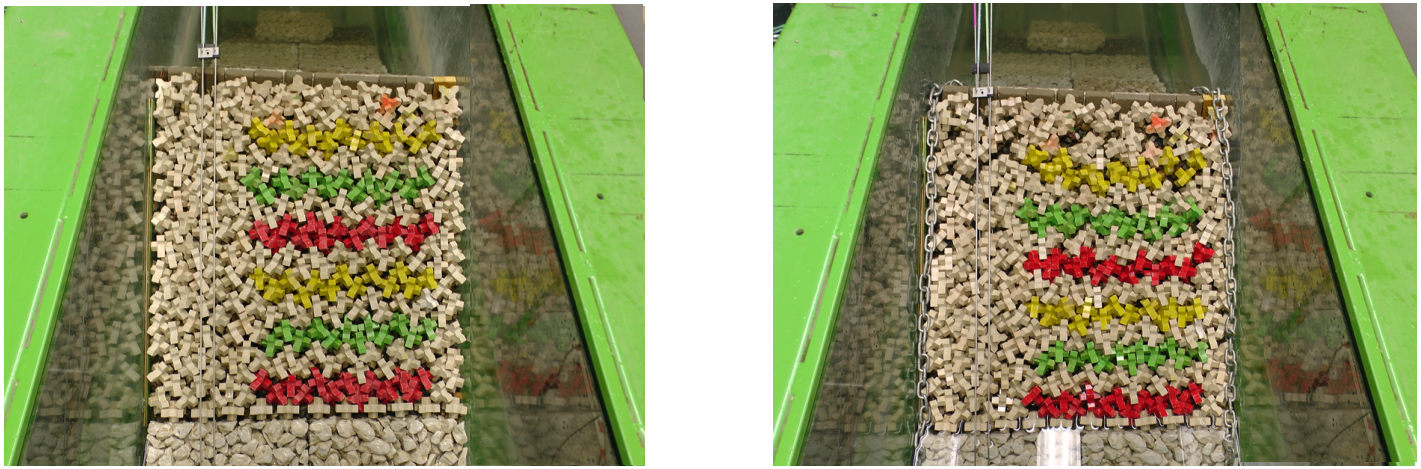

Fig. G.19: Test FB repetition 3; start and 100% picture

H. DAMAGE OBSERVATIONS TEST SERIES

The observed damage is summarised in this chapter. Occurrence of damage is separated in rocking, lifting of units and settlement. Rocking units are small movements of armour units around sea water level. Lifting of armour units has two appearance; units is lifted less than $0.5D_n$ or unit is lifted more than $0.5D_n$. Settlements is taken separately to indicate failure at the crest. Initial settlement is not taken into account in the damage levels.

* Several units are thrown over the breakwater.
** Extraction of an unit
*** Total extraction of the armour slope.
√ Great settlement.

H.1 Open core

CA1	**Damage observations of**				H_s **[mm]**		H_{max}
	Rocking	**Lifting of units**		**Settlement**			
Wave height	**<0.5** $\cdot D_n$**, > 2% of the waves**	**<0.5** $\cdot D_n$**, > 2% of the waves**	**>0.5**$\cdot D_n$	**>0.5**$\cdot D_n$	H_i	H_r	C_r
60%	-	-	-	-	61.2	17.4	0.354
80%	-	-	-	-	80.9	25.0	0.285
100%	2	-	-	-	101.4	34.0	0.387
120%	3	2	-	-	121.6	45.7	0.427
140%	1	1	-	-	142.0	58.5	-
160%	2	-	3	5	168.1	68.0	-

CA2	**Damage observations of**				H_s **[mm]**		H_{max}
	Rocking	**Lifting of units**		**Settlement**			
Wave height	**<0.5** $\cdot D_n$**, > 2% of the waves**	**<0.5** $\cdot D_n$**, > 2% of the waves**	**>0.5**$\cdot D_n$	**>0.5**$\cdot D_n$	H_i	H_r	C_r
60%	-	-	-	-	61.5	17.7	0.371
80%	2	-	-	-	81.7	25.5	0.300
100%	1	-	-	-	101.9	34.4	0.370
120%	3	-	-	-	125.1	47.0	0.403
140%	2	-	1	1	144.6	59.3	-
160%	-	2	1	3	171.7	72.2	-
180%	-	2	-	-	193.9	83.2	-

CA4	**Damage observations of**				H_s **[mm]**		H_{max}
	Rocking	**Lifting of units**		**Settlement**			
Wave height	**<0.5** $\cdot D_n$**,** **> 2% of the waves**	**<0.5** $\cdot D_n$**,** **> 2% of the waves**	**>0.5**$\cdot D_n$	**>0.5**$\cdot D_n$	H_i	H_r	C_r
60%	-	-	-	-	60.3	18.1	-
80%	-	-	-	-	80.0	25.7	-
100%	2	-	-	-	97.9	34.4	-
120%	3	-	-	-	117.7	46.1	-
140%	2	-	-	-	136.3	58.5	-
160%	1	-	3	-	162.2	73.5	-

CA5	**Damage observations of**				H_s **[mm]**		H_{max}
	Rocking	**Lifting of units**		**Settlement**			
Wave height C_r	**<0.5** $\cdot D_n$**,** **> 2% of the waves**	**<0.5** $\cdot D_n$**,** **> 2% of the waves**	**>0.5**$\cdot D_n$	**>0.5**$\cdot D_n$	H_i	H_r	
60%	-	-	-	-	61.1	17.5	0.367
80%	1	-	-	-	81.9	25.4	0.288
100%	3	-	-	-	101.6	34.7	0.371
120%	2	-	-	-	121.9	47.4	0.465
140%	3	-	-	-	140.3	60.3	-
160%	2	-	-	-	168.2	76.1	-
180%	3	-	-	-	191.9	89.2	-

CB1	**Damage observations of**				H_s **[mm]**		H_{max}
	Rocking	**Lifting of units**		**Settlement**			
Wave height	**<0.5** $\cdot D_n$**,** **> 2% of the waves**	**<0.5** $\cdot D_n$**,** **> 2% of the waves**	**>0.5**$\cdot D_n$	**>0.5**$\cdot D_n$	H_i	H_r	C_r
60%	-	-	-	-	557.3	14.5	0.225
80%	3	-	-	-	76.7	19.9	0.288
100%	1	-	3**	-	97.3	26.8	0.270
120%	1	1	4	-	117.7	34.0	0.282
140%	1	-	-	-	135.6	41.0	-
160%	-	-	3	-	155.1	48.9	-
180%	-	-	-	-	173.5	57.6	-

CB2	**Damage observations of**				H_s **[mm]**		H_{max}
	Rocking	**Lifting of units**		**Settlement**			
Wave height	**<0.5** $\cdot D_n$**,** **> 2% of the waves**	**<0.5** $\cdot D_n$**,** **> 2% of the waves**	**>0.5**$\cdot D_n$	**>0.5**$\cdot D_n$	H_i	H_r	C_r
60%	-	-	-	-	57.8	13.9	0.215
80%	1	-	-	-	77.9	19.2	0.283
100%	-	-	2	-	98.9	25.5	0.306
120%	2	-	-	-	118.8	32.0	0.263
140%	3	-	-	-	136.9	38.5	-
160%	2	3	-	-	157.0	46.3	-
180%	-	2	-	3	176.2	55.1	-

CB4	**Damage observations of**				H_s **[mm]**		H_{max}
	Rocking	**Lifting of units**		**Settlement**			
Wave height	**<0.5** $\cdot D_n$**,** **> 2% of the waves**	**<0.5** $\cdot D_n$**,** **> 2% of the waves**	**>0.5**$\cdot D_n$	**>0.5**$\cdot D_n$	H_i	H_r	C_r
60%	-	-	-	-	57.4	14.3	0.213
80%	2	-	-	-	77.0	20.2	0.282
100%	2	-	1	-	97.2	27.2	0.289
120%	2	-	4	-	117.2	34.1	0.293
140%	1	2	9	5	133.8	39.8	-
160%	-	-	20***	-	155.0	46.9	-

H.2 Normal core

BA1	**Damage observations of**				H_s **[mm]**		H_{max}
	Rocking	**Lifting of units**		**Settlement**			
Wave height	**<0.5** $\cdot D_n$**,** **> 2% of the waves**	**<0.5** $\cdot D_n$**,** **> 2% of the waves**	**>0.5**$\cdot D_n$	**>0.5**$\cdot D_n$	H_i	H_r	C_r
60%	-	-	-	-	60.8	18.74	0.382
80%	1	-	-	-	81.2	27.58	0.328
100%	2	-	-	-	101.7	37,51	0.392
120%	2	-	-	-	123.0	50.88	0.40
140%	-	-	-	2	141.6	63.8	-
160%	1	-	3*	3	166.9	77.7	-

BA2	**Damage observations of**				H_s **[mm]**		H_{max}
	Rocking	**Lifting of units**		**Settlement**			
Wave height	**<0.5** $\cdot D_n$**,** **> 2% of the waves**	**<0.5** $\cdot D_n$**,** **> 2% of the waves**	**>0.5**$\cdot D_n$	**>0.5**$\cdot D_n$	H_i	H_r	C_r
40%	-	-	-	-	41.9	10.0	0.300
60%	-	-	-	-	61.8	17.8	0.361
80%	-	-	-	-	82.4	26.55	0.374
100%	1	-	-	-	103.0	36.39	0.374
120%	-	-	2	-	125.9	50.1	0.416
140%	-	4	-	-	145.9	64.1	-
160%	-	3	5*	-	172.3	79.15	-

BA3	**Damage observations of**				H_s **[mm]**		H_{max}
	Rocking	**Lifting of units**		**Settlement**			
Wave height	**<0.5** $\cdot D_n$**,** **> 2% of the waves**	**<0.5** $\cdot D_n$**,** **> 2% of the waves**	**>0.5**$\cdot D_n$	**>0.5**$\cdot D_n$	H_i	H_r	C_r
40%	-	-	-	-	39.6	10.0	0.289
60%	-	-	-	-	58.0	17.2	0.382
80%	-	-	-	-	77.1	25.4	0.310
100%	1	-	-	-	95.3	33.86	0.387
120%	1	3	-	-	115.5	45.6	0.415
140%	-	8	-	-	133.9	58.5	-
160%	-	4	-	-	158.6	73.7	-

BB1	**Damage observations of**				H_s **[mm]**		H_{max}
	Rocking	**Lifting of units**		**Settlement**			
Wave height	**<0.5** $\cdot D_n$**,** **> 2% of the waves**	**<0.5** $\cdot D_n$**,** **> 2% of the waves**	**>0.5**$\cdot D_n$	**>0.5**$\cdot D_n$	H_i	H_r	C_r
60%	-	-	-	-	57.5	13.9	0.215
80%	-	-	-	-	77.7	20.1	0.270
100%	1	1	-	-	97.4	27.2	0.294
120%	9	-	-	-	116.5	34.2	0.308
140%	-	-	-	4	143.2	40.9	-

BB2	**Damage observations of**				H_s **[mm]**		H_{max}
	Rocking	**Lifting of units**		**Settlement**			
Wave height	**<0.5** $\cdot D_n$**,** **> 2% of the waves**	**<0.5** $\cdot D_n$**,** **> 2% of the waves**	**>0.5**$\cdot D_n$	**>0.5**$\cdot D_n$	H_i	H_r	C_r
40%	-	-	-	-	41.7	8.4	0.159
60%	-	-	-	-	58.1	13.1	0.215
80%		-	-	-	80.5	19.8	0.274
100%	1	-	-	-	100.7	27.4	0.275
120%	-	1	-	-	121.8	25.6	0.268
140%	1	-	5	2	136.9	42.3	-
160%	1	5	-	3	156.4	50.3	-
180%	-	5	-	2	174.9	59.3	-

BB3	**Damage observations of**				H_s **[mm]**		H_{max}
	Rocking	**Lifting of units**		**Settlement**			
Wave height	**<0.5** $\cdot D_n$**,** **> 2% of the waves**	**<0.5** $\cdot D_n$**,** **> 2% of the waves**	**>0.5**$\cdot D_n$	**>0.5**$\cdot D_n$	H_i	H_r	C_r
40%	-	-	-	-	40.5	8.0	0.159
60%	0	-	-	-	57.2	12.3	0.193
80%	2	-	-	-	77.3	18.4	0.263
100%	-	-	4	-	97.5	35.9	0.282
120%	-	-	4	3	116.4	33.7	0.274
140%	-	-	9	-	133.2	40.7	-

H.3 Impermeable core

FA1	**Damage observations of**				H_s **[mm]**		H_{max}
	Rocking	**Lifting of units**		**Settlement**			
Wave height	**<0.5** $\cdot D_n$**,** **> 2% of the waves**	**<0.5** $\cdot D_n$**,** **> 2% of the waves**	**>0.5**$\cdot D_n$	**>0.5**$\cdot D_n$	H_i	H_r	C_r
60%	-	-	-	√	58.3	22.0	0.477
80%	-	-	-	-	78.1	33.0	0.394
100%	1	-	1	-	98.0	45.0	0.476
120%	-	-	2	-	118.0	57.7	0.458
140%	-	4	-	-	136.6	71.0	-
160%	3	-	5*	-	161.5	85.8	-

FA2	**Damage observations of**				H_s **[mm]**		H_{max}
	Rocking	**Lifting of units**		**Settlement**			
Wave height	**<0.5** $\cdot D_n$**,** **> 2% of the waves**	**<0.5** $\cdot D_n$**,** **> 2% of the waves**	**>0.5**$\cdot D_n$	**>0.5**$\cdot D_n$	H_i	H_r	C_r
40%	-	-	-	-	40.2	12.7	0.371
60%	-	-	-	√	59.0	22.2	0.479
80%	1	-	-	-	77.5	32.5	0.385
100%	-	2	2	-	97.2	44.7	0.482
120%	-	3	-	2	118.0	59.2	0.496
140%	-	3	-	5	136.6	73.3	-
160%	4	-	5*	-	185.7	85.7	-

FA3	**Damage observations of**				H_s **[mm]**		H_{max}
	Rocking	**Lifting of units**		**Settlement**			
Wave height	**<0.5** $\cdot D_n$**,** **> 2% of the waves**	**<0.5** $\cdot D_n$**,** **> 2% of the waves**	**>0.5**$\cdot D_n$	**>0.5**$\cdot D_n$	H_i	H_r	C_r
40%	-	-	-	-	40.3	11.6	0.343
60%	-	–	-	√	59.6	21.5	0.461
80%	2	-	-	-	79.2	32.8	0.407
100%	-	3	-	-	98.5	44.5	0.465
120%	-	3	-	2	120.3	59.3	0.490

FB1	**Damage observations of**				H_s **[mm]**		H_{max}
	Rocking	**Lifting of units**		**Settlement**			
Wave height	**<0.5** $\cdot D_n$**,** **> 2% of the waves**	**<0.5** $\cdot D_n$**,** **> 2% of the waves**	**>0.5**$\cdot D_n$	**>0.5**$\cdot D_n$	H_i	H_r	C_r
40%	-	-	-	-	40.8	9.9	0.196
60%	-	-	-	-	57.4	15.6	0.242
80%	1	-	-	-	78.1	24.0	0.339
100%	-	1	-	4	97.6	33.8	0.358
120%	-	4	-	-	116.4	42.9	0.348
140%	-	-	2	6	132.6	50.8	-
160%	-	4	-	-	153.3	60.0	-

FB2	**Damage observations of**				H_s **[mm]**		H_{max}
	Rocking	**Lifting of units**		**Settlement**			
Wave height	**<0.5** $\cdot D_n$**,** **> 2% of the waves**	**<0.5** $\cdot D_n$**,** **> 2% of the waves**	**>0.5**$\cdot D_n$	**>0.5**$\cdot D_n$	H_i	H_r	C_r
40%	-	-	-	-	44.6	10.1	0.195
60%	-	-	-	-	62.8	16.2	0.248
80%	-	-	-	-	84.6	25.3	0.307
100%	-	-	7	-	106.3	35.6	0.347
120%	-	-	9	-	127.8	46.2	0.329

FB3	**Damage observations of**				H_s **[mm]**		H_{max}
	Rocking	**Lifting of units**		**Settlement**			
Wave height	**<0.5** $\cdot D_n$**,** **> 2% of the waves**	**<0.5** $\cdot D_n$**,** **> 2% of the waves**	**>0.5**$\cdot D_n$	**>0.5**$\cdot D_n$	H_i	H_r	C_r
40%	-	-	-	-	41.7	9.4	0.188
60%	-	-	-	-	58.8	15.7	0.250
80%	1	-	-	-	79.0	24.2	0.329
100%	-	-	4	-	98.9	34.1	0.337
120%	-	-	-	8	118.3	44.1	0.330
140%	8	-	-	-	135.8	53.0	-

I. RELATIVE PLACEMENT DENSITIES

The placement density is an important parameter for the stability of interlocking armour units. The packing density is a trade of between stability and the volume of concrete. A packing density of $1.2/D2$ is determined as optimum packing density. The packing density of the armour layer is calculated as relative packing density from $1.2/D^2$.

$$RPD = \frac{(N_x - 1)(N_y - 1) \cdot D_x \cdot D_y \cdot D^2}{L_x \cdot L_y} \cdot 100\% \tag{I.1}$$

$N_x N_y$	= number of units in the x-direction and y-direction
$D_x D_y$	= distance between the centre of gravity of two neighbouring units in the x-direction and y-direction
D	= the width of the unit
$L_x L_y$	= the measured length in the x-direction and y-direction

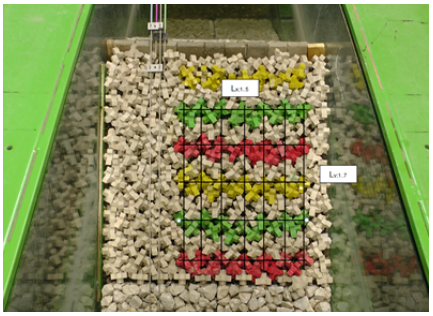

Fig. I.1: Area within RPD is measured

The relative packing density is determined after each placing and after various test. It is experienced that the RPD is sensitive to small measurement inaccuracies. The horizontal distance is therefore measured five times and the vertical distance seven, illustrated in figure I.1, to generate an average value. Despite of this measure the relative packing density measured during testing differs significant from the relative packing density measured from the picture that are taken during testing. The same trend was observed but with values that greatly differs from the measurements during testing.

Repetition	**Placing RPD** [%]		**Average RPD** [%]
	Testing	**Photo**	
CA1		105.2	
CA2		102.9	
CA4	100.6	97.7	99.2
CA5	104.5	102.0	103.8
CB1	102.5	97.3	99.9
CB2	100.6	99.2	99.9
CB4	101.6	99.4	100.5
BA1	104.0	100.4	102.3
BA2	102.1	99.1	100.6
BA3	105.6	102.3	104.0
BB1	106.2	99.9	103.1
BB2	100.3	98.6	99.5
BB3	100.0	96.6	98.3
FA1	103.2	99.8	101.5
FA2	103.4	98.7	101.1
FA3	104.7	102.1	103.4
FB1	105.0	102.6	103.8
FB2	103.5	100.3	101.9
FB3	103.2	100.2	101.7

J. DATA ANALYSE

J.1 General

In section 2.3 of this thesis is the water oscillation on and inside of the breakwater under wave attack explained regarding core permeability. Following from the literature, it is expected that low water penetration into the core induces the run-up levels on top of the core. The external wave oscillation is to a lesser extent influenced by the permeability resulting in a change in the hydraulic gradient, flow velocity, flow direction and flow forces on the armour units. This section will discuss the influence of the core permeability on the run-up level, hydraulic gradient, flow velocity and wave reflection using measured data from the model tests. The trend-line of the run-up level, run-down level and reflection coefficient has been compared to existing formulae for rock armour layers, resulting in fundamental difference in water motion between rock and single layer interlocking armour layers. This is also explained in section 6.6 of this thesis.
It must be noted that several empirical formulae contain the 'notional' permeability of Van der Meer (1988b). In this section is assumed that the impermeable core is equivalent to P=0.1, the normal core is equivalent to P=0.4 and the open core is equivalent to P=0.5. The assumption that the normal core is equivalent to P=0.4 is not based on the prescribed configurations by Van der Meer (1988b) but on the common use in practise to apply P=0.4 for a normal core.

The run-up levels on and under the armour layer are obtained from the run-up gauges. The hydraulic gradient and flow velocity can be calculated using the water levels from the run-up gauges. The reflective wave is measured by three wave gauges in front of the breakwater and separated from the incident wave by the method of Mansard and Funke (1980). The run-up gauges and wave gauges measured "continuously", 32 times per second, the water level around the armour layer.

J.2 Accuracy and reliability

The wave and run-up gauges measure the water level using the conductivity of the water. Conductivity of water is sensitive for change in water temperature. To obtain accurate measurements of the water levels, the gauges are calibrated before each test series.
The normal calibration method for the wave gauges is elevation and lowering of the wave probes using prefabricated pinholes. This method has a high accuracy but could not be applied for the run-up gauge that was fixed inside the breakwater. The used calibration method in the model tests was elevation and lowering of the water level in the wave flume. This method is sensitive for errors as the water level is measured by hand and may have lead to errors in the data.
Other errors that might have occurred is deviation of the water temperature leading to deviations in the conductivity of the water. The allowable relative error is calculated in subsequent section and used to check the accuracy and reliability of the test series.

Relative error

In order to calculate the accuracy and reliability of the measured data, the relative error is calculated. It is assumed that the variables are normal distributed with a standard deviation equal to the absolute error, as defined in table **??**.

The gauges are calibrated by lowering the water level approximately 150 mm. During the calibration, the water level is measured twice by hand with a maximum reading accuracy of 2 mm due to fluctuations in the water level. The accuracy of the data processing instrument is according to the manufacturer of the instruments less than 0.1%. Unfortunately, the error due to changes in water temperature and thereby in conductivity of water is not known. According to literature the conductivity of water increases with approximately 2% for an increase of 1 degree in water temperature around 10 degrees. It can be concluded that deviations in the water temperature influenced the accuracy significant. The effect of water temperature on the calibration can in general be described as illustrated in figure J.1.

Variable	Mean value	St. deviation	Relative error
a. Reading error	150mm	3mm	2.0%
b. Processing error	-	-	0.1%

Tab. J.1: Measuring errors

	absolute error at 150 mm from SWL	Relative error
Run-up	9.0 mm	3.0%
Water level diff.	6.0 mm	4%
Velocity	6.0 mm	4%

The relative error of a function h(a,b,...) with two or measured variable a, b,... is calculated as follows:

$$\mathcal{R}_h^2 = \frac{\sigma_a}{\mu_a} + \frac{\sigma_b}{\mu_b}^2 \qquad \textit{if variable are multiplied or divided} \tag{J.1}$$

$$\sigma_h^2 = \sigma_a^2 + \sigma_b^2 \qquad \textit{if variable are added or subtracted} \tag{J.2}$$

σ	standard deviation of the measurement error	[-]
μ	mean value of the measurement error	[-]
$\mathcal{R}$	relative error of the experiment	[-]

The influence of the water temperature and the reading error on the measurements should be limited to obtain the required accuracy for the data processing. The accuracy has been evaluated by comparing the measured wave height in front of the breakwater of each repetition with the calibrated wave spectra. The calibrated wave spectra was not subjected to deviations in water conductivity or reading errors. This is due to calibration by lifting and lowering of the wave probes in prefabricated pinholes and the tests were performed within a short duration after calibration. Furthermore, the waves were calibrated without a structure in the wave flume allowing to neglect the effect of the reflective wave.

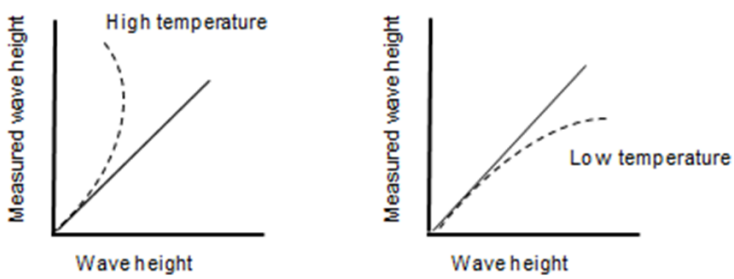

Fig. J.1: Influence of water temperature on the calibration

Data evaluation

The data of the wave gauges and run-up gauges are evaluated on large errors, which would make the data unusable for the analyse. This is done by comparing the calibrated wave spectrum with the measured spectrum for each individual repetition. It was observed that from the 120% wave height the

largest waves of the spectrum over-topped the breakwater resulting in disturbed data for i.e. the wave run-up and flow velocity. The accuracy of the repetitions is therefore evaluated till the 120% wave height.

The measured significant wave height for each repetition is plotted against the calibrated wave spectrum in figure J.2. The two lines in the graphs indicate the deviation of 3% of the calibrated wave height. From the right graph can be observed that the wave series are rather accurate calibrated, when test FB2 is neglected from the data set. Observing the left figure, more scatter in the data can be observed. The dispersion of the data might be caused due the relative short distance between the wave gauges in front of the breakwater and structure itself. The wave gauges were located within a meter of the structure were the wave height fluctuates to a certain extent and can influence the measurements. The fluctuations become negligible from a distance of one wave length of the breakwater. This supports the observation that the short wave encounter less fluctuations of the wave height than the longer waves. To overcome this problem it is chosen the compare the data series of the long waves with each other for a single configuration, illustrated in figure J.3.

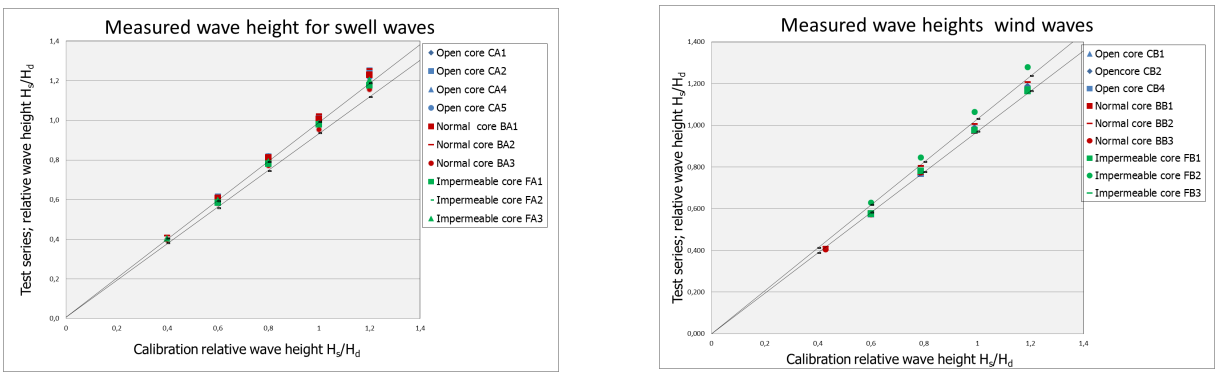

Fig. J.2: Data accuracy with 3% deviation lines.

The measured significant wave height of each repetition is plotted against the calibrated wave spectrum in figure J.3. From the left figure can be observed that the impermeable core shows negligible scatter and only an elevation of the average wave height. The calibration of the individual repetitions of the impermeable core are as reliable adopted.
Observing the centre and right figure it can be concluded that the normal and open core show more scatter. Two aberrant data series are indicated being BA3 and CA4. It is chosen to remove these data series from the data set as they show a consequently lower wave height than the other data sets.

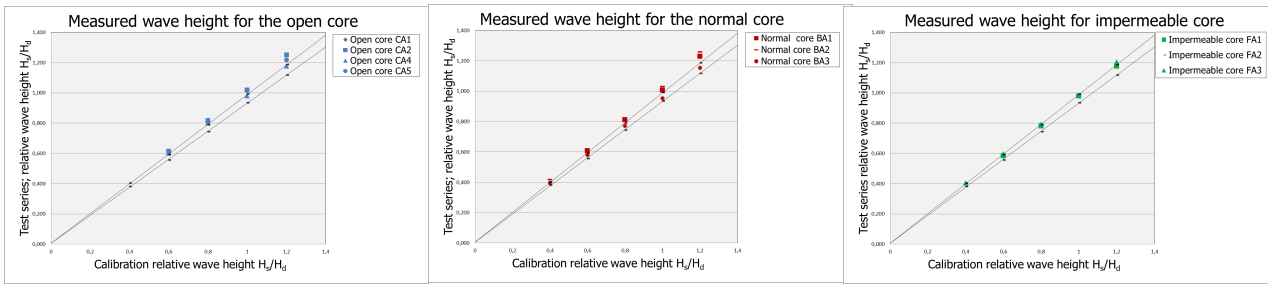

Fig. J.3: Data analyse

The following three data series are omitted from the data set for in the subsequent analyse:

- FB2; Second repetition of the impermeable core with wind waves.
- BA3; Third repetition of the normal core with swell waves.
- CA4; Fourth repetition fo the open core with swell waves.

J.3 Run-up and run-down level

Measured data

The run-up gauges measured the water levels on and under the breakwater. The run-up level represents the potential energy before the water moves downward. It is expected that run-up parameter level decreases with core permeability as more energy is dissipated inside the core.
The measured maximum run-up level on the armour layer for each individual test is presented in figure J.4. From the figure can be observed that repetition BA2 shows an apparent trend-line. A comparison of the run-up levels with the relative free-board of the breakwater (200mm) showed that the measured run-up level is higher than the relative free-board. It is concluded that the calibration of the run-up gauge on top of the armour layer failed.
Figure J.4 illustrates also a slight trend of lower run-up levels for the impermeable core and larger run-up levels for the open core. This is not expected but might due to the run-down level in front of the maximum run-up, which is lower for the impermeable core. However, no significant difference in trend-line of the run-up level on the armour layer is observed.

Van Boekhoven (2011) mentioned that the difference in run-up level on the armour layer would be smaller than under the armour layer. Figure J.5 illustrates the run-up levels under the armour layer for swell and wind waves. It can be observed that in both figures the impermeable core encounters the greatest run-up levels and the permeable core encounters the smallest run-up levels. The normal core is omitted from this figure to obtain a better overview of the difference in run-up level. The measured

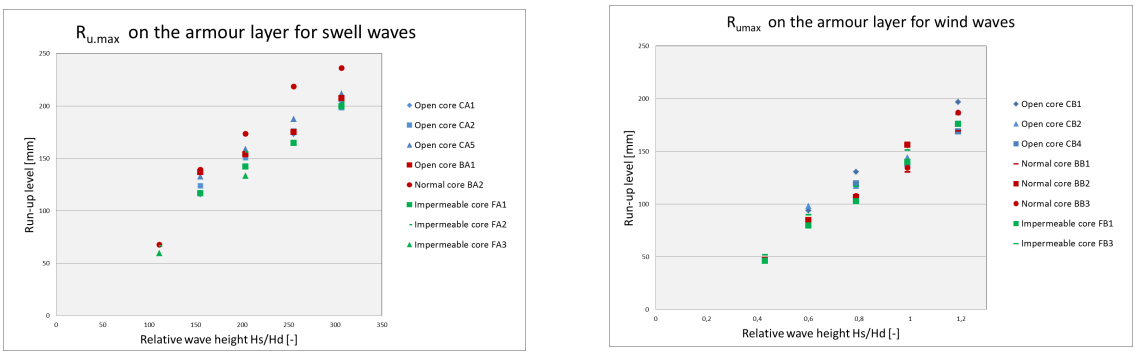

Fig. J.4: The R_{u_max} on the armour layer.

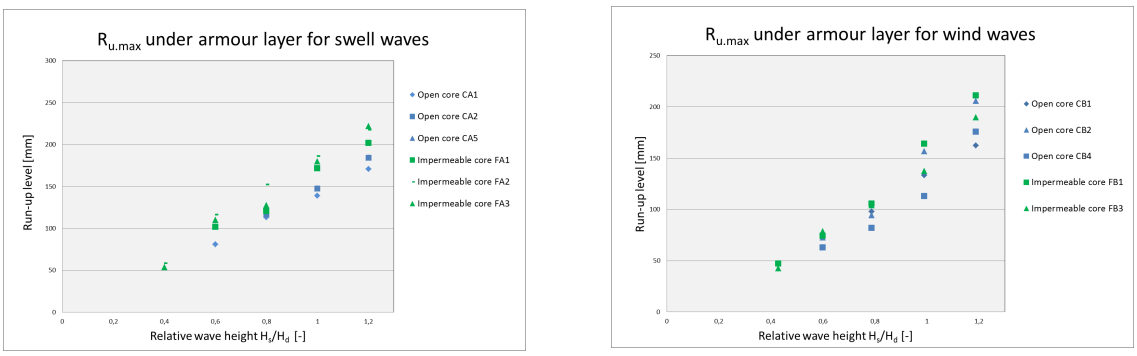

Fig. J.5: The R_{u_max} under the armour layer.

maximum run-down level for each individual test is presented in figure J.6. The left figure presents the run-down level for swell waves and the right figure the run-down level for wind waves. From the figures can be observed that both the swell and wind waves encounter lower run-down levels for an impermeable core. For swell waves is the run-down level also lower for the normal core.
It can be concluded that the run-down level become lower with decreasing core permeability or under attack of waves with a larger water volume. Both an impermeable core as a larger wave volume tend

to lead to a larger water volume in the armour layer during the downrush. This observation suggest the that run-down level on armour layer is affected by the water volume in the armour layer during the downrush. It is assumed that the run-down level is limited for a specific wave period by the maximum velocity parallel to the slope. This would explain the similarity between the run-down level of the impermeable and normal core for swell waves.

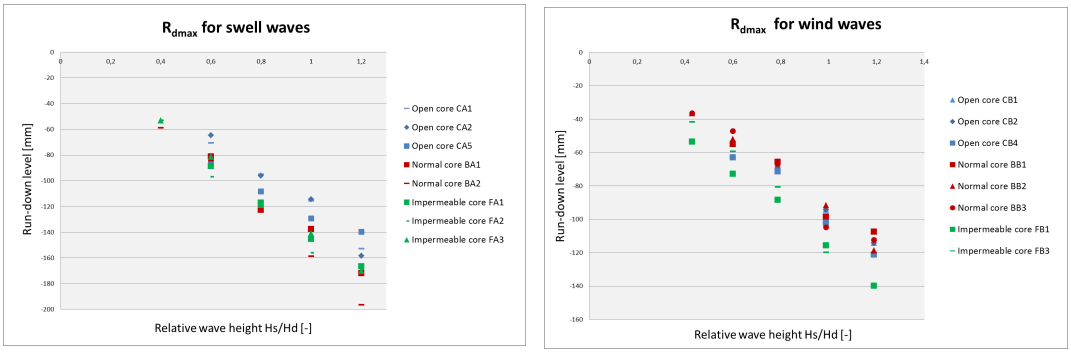

Fig. J.6: The R_{d_max} on the armour layer

The water oscillation on the slope of the structure is plotted against time in figure J.7 for the open, normal and impermeable core. The swell waves are presented in the left figure and the wind waves in the right figure. From the figures can be observed that due the increased run-down level of the impermeable core the water motion at the underside shows a sharper peak than for an open core. This peaked angle suggests that the backflow in the armour layer is forced to rotate fast in upward direction generating larger inertia forces on the armour units. Furthermore, the figure confirms the comparable run-up level for the core configurations.

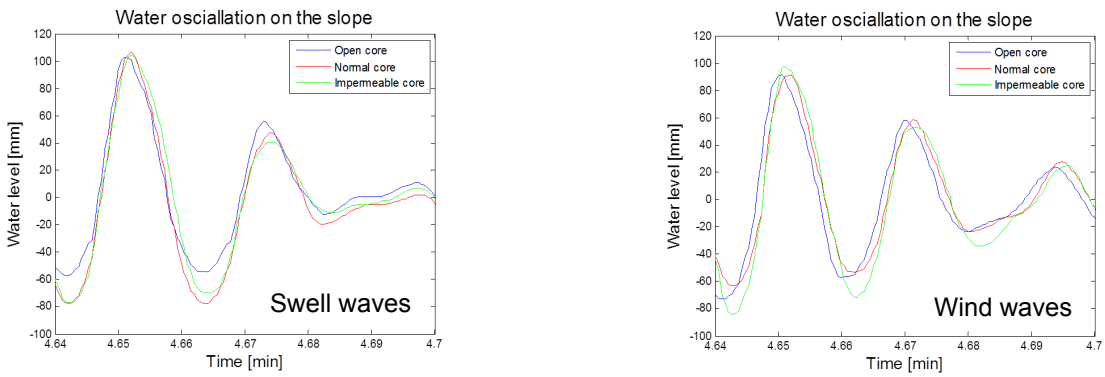

Fig. J.7: Water motion on the slope of the structure during the 100% wave height.

Empirical formulae

The water elevation on the slope of the breakwater is described by the formulae of Van der Meer and Stam (1992) for rock armour units (section 2.3). Two formulae are proposed for the run-up trend-line (equation J.3 and equation J.4) and an additional formula for the upper boundary of permeable structures (equation J.4). Expression J.4 is used as all tests are conducted with a surf similarity parameter (ξ_m) larger than 1.5.

$$R_{u.n\%}/H_s = a\xi_m \qquad \text{for} \xi_m \leq 1.5 \tag{J.3}$$

$$R_{u.n\%}/H_s = b\xi_m^c \qquad \text{for} \xi_m \geq 1.5 \tag{J.4}$$

$$R_{u.n\%}/H_s = d \qquad \text{Upper boundary for P} \geq 0.4 \tag{J.5}$$

The coefficients for a, b and c are expressed in table J.2. Both equation J.4 and equation J.5 are used in the evaluation of the run-up levels. The maximum measured run-up level is plotted in figure J.8 against

Run-up level n%	a	b	c	d
0.1	1.12	1.34	0.55	2.58
1	1.01	1.24	0.48	2.15
2	0.96	1.17	0.46	1.97
5	0.86	1.05	0.44	1.69
10	0.77	0.94	0.42	1.45
Significant	0.72	0.88	0.41	1.35
Mean	0.47	0.60	0.34	0.82

Tab. J.2: Coefficients for equation J.4, J.3 and J.5 CIRIA (2007)

the theoretical run-up level Van der Meer and Stam (1992). The black solid line presents the theoretical 0.1% run-up level that is equivalent to the maximum run-up level, as the tests are conducted with 1000 waves.
From the figures can be observed that the theoretical values has a resembled trend-line as the measured run-up levels. However, the values of the measured data differ significantly from the expected values for the 0.1% run-up level, which follows from the formulae of Van der Meer and Stam (1992). According to Van der Meer and Stam (1992) equation J.5 is valid for permeable structures under attack of swell waves. This formula is therefore applied for the normal and open core by swell waves.

The left figure presents the data of swell waves, in which the green and red dotted line are the theoretical values for the permeable and impermeable structure following from equation J.5 and equation J.4. Observations showed that the measured maximum run-up level for the permeable structure has a better fit with the theoretical run-up level of 2% using equation J.4. The maximum run-up level for impermeable structures shows a better fit with the theoretical run-up level of 10%.
The black dotted line in the right figure represent the 10% theoretical values from equation J.4. The measured data shows a better fit with the theoretical 10% run-up level than the 0.1% run-up level obtained from J.4.

Overall, it can be concluded that equation J.5 is not necessarily due the negligible difference in run-up level between the permeable and impermeable structures. Furthermore, the maximum run-up levels measured during the model tests show a better fit with the 10% run-up level obtained from equation J.4 for wind waves and the impermeable core of swell waves.

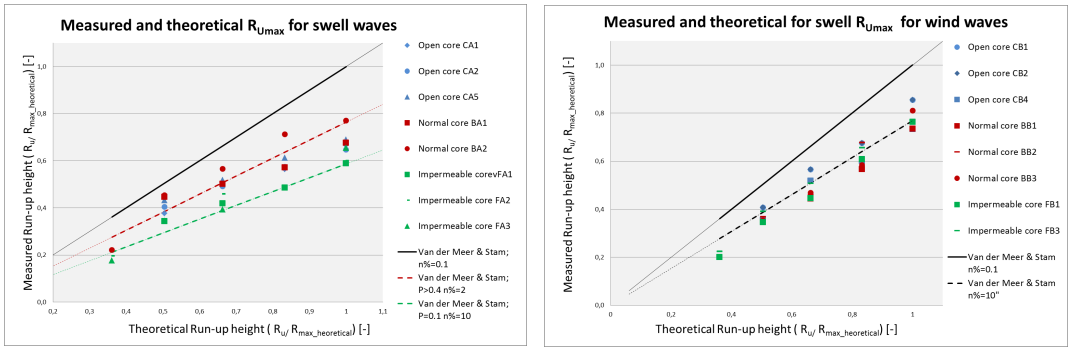

Fig. J.8: The R_{u_max} for s=0.023 (left figure) and s=0.04 (right figure) using equation J.4 and equation J.5

The run-down level is found equally important for the forces on the armour layer as the run-up level. Analysis of the run-down data of Van der Meer (1988b) resulted in a run-down formula that includes the slope angle α, 'notional' permeability P, and fictitious wave steepness s_{om}

$$R_{d2\%}/H_s = 2.1\sqrt{tan\alpha} - 1.2P^{0.15} + 1.5exp(-60s_{om}) \tag{J.6}$$

The theoretical values from equation J.6 is plotted against the measured $R_{d2\%}$ in figure J.9. The theoretical value is presented by the black solid line in both figures. From the figures can be observed that the theoretical values show a comparable trend-line and size of the run-down levels. The right figure

illustrates a small overestimation of the run-down level by equation J.6 for the normal and impermeable core and a good approximation of the run-down level of the open core.
The left figure presents the run-down values for swell waves. The theoretical data of the run-down levels show a underestimation for the normal core while the impermeable and the open core show good resembles with the theoretical values. Overall, it can be concluded that equation J.6 has a good fit with the measured data except for the normal core of swell waves.

The deviating result for the normal core between the measured data and equation J.6, suggests that the run-down level for single layered concrete armour units are more affected by the wave length than double layered rock armour units. However, Van der Meer (1988b) performed no physical model test with P=0.4. This means that no data was available of configuration P=0.4 and therefore the statement cannot be confirmed.

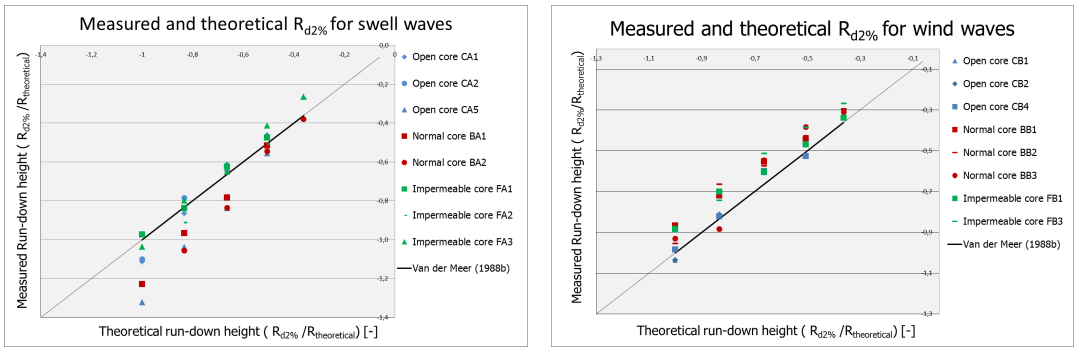

Fig. J.9: The $R_{d2\%}$ for s=0.023 (left figure) and s=0.04 (right figure) with formula J.6 (Green= impermeable core, Red= normal core and blue= open core)

Summary

The core permeability does not influence the run-up levels on the armour layer significantly. This observation suggest that the additional formula of Van der Meer and Stam (1992) for the upper boundary for permeable structures is not necessarily. The formulae of Van der Meer and Stam (1992) for the 0.1% run-up level result in larger run-up levels than measured with the run-up gauges. The theoretical 10% run-up level using equation J.4 shows a better fit with the measured maximum run-up level for wind waves and impermeable core of swell waves.
From these observations can be concluded that the run-up level on the slope is determined by the roughness of the slope (γ_f) and not on the core permeability. The overtopping method by TAW (2002) for impermeable structures (CIRIA, 2007) used such slope roughness factors. A greater surface roughness is specified for Xbloc than for rock armour in the TAW method. The relation of surface roughness is also valid for the run-up level as it is generally known that the run-up levels is closely related to the overtopping. The larger armour roughness of Xblocs lead to more energy dissipation and less energy conversion from kinetic energy into potential energy. This explains the lower run-up levels for Xblocs than for rock armour layers found by Van der Meer and Stam (1992).

The run-down levels are affected by the permeability of the core. The overall trend suggest that the water volume in the armour layer during the downrush determines the run-down level. The maximum run-down level is bounded by the time period before the next incident wave enters.
The theoretical values of the 2% run-down level of the formula of Van der Meer (1988b) show good resembles with the measured data, except for the normal core for swell waves. This might indicate that less energy is dissipated in a single layered normal breakwater with concrete armour units. However, Van der Meer (1988b) performed no physical model test with P=0.4. This means that no data was available of configuration P=0.4 and therefore the statement cannot be confirmed.

J.4 Hydraulic gradient

According to the literature is the size and direction of the flow forces in the armour layer is important for the armour stability. The hydraulic gradient in the armour layer is an important parameter to indicate the size and the direction of the water flow in the armour layer.
Figure J.10 illustrates the hydraulic gradient around maximum run-down for a low and high permeable core. The expected larger hydraulic gradient in the armour layer for a low permeable core induces the outflow velocity and changes the direction of the outflow parallel to the slope. The larger hydraulic gradient induces also the outflow velocity, which can be confirmed with the two formulae; the Forchheimer formula and the Bernoulli formula. The Forchheimer model is based on the relation between the hydraulic gradient and flow velocity in porous media. The principle of the model is that larger hydraulic gradients lead to larger velocities and otherwise. The formula is formulated for flow that encounters large resistance forces. However, the water flow in the armour layer encounters minimum resistance forces from the Xbloc units due high porosity. It can therefore be assumed that the water experienced a free fall and the velocity can be calculated with the simplified formula of Bernoulli $V = \sqrt{2 \cdot g\Delta H}$.

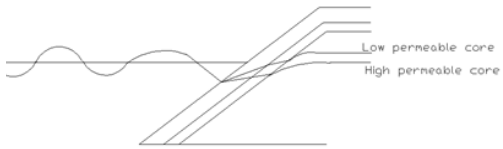

Fig. J.10: Water level difference around the armour layer at maximum run-down

Figure J.11 illustrates the expected reduced hydraulic gradient at maximum run-up for low permeable core due large water accumulation in the armour layer. The reduced hydraulic gradient at maximum run-up indicates the size of the water inflow into the core. The relation between hydraulic gradient and inflow velocity is similar as described before for the hydraulic gradient at maximum run-down.

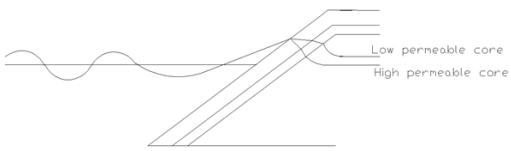

Fig. J.11: Water level difference around the armour layer at maximum run-up

Measured data

The hydraulic gradient in the armour layer can be evaluated using the data of the run-up gauges on and under the armour layer. Figure J.12 illustrates the run-up gauges on (A) and under (B) the armour layer. The water levels were subtracted from each other (water level at point A minus the water level at point B) at a specific time in order to give an indication of the hydraulic gradient in the armour layer.

The maximum water level difference during the downrush for the three core configurations are summarized in figure J.13. The left figure presents the data for swell and the right figure for wind waves. From the figures can be observed that the hydraulic gradient in the armour layer depends on the core permeability, wave height and wave period. The impermeable core shows a consequent larger water level difference for both wave steepness. The water decay in the armour layer shows a larger deviation between permeable and impermeable structures than the run-down level in figure J.6. This indicates that the run-down level under the armour layer are smaller for impermeable structures than for permeable structures.
The right figure presents the data for wind waves and illustrate an increase in water level difference with

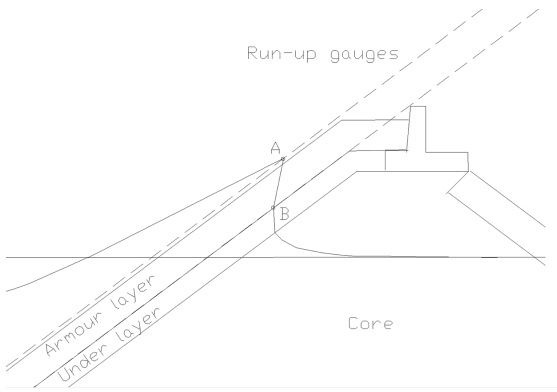

Fig. J.12: Representation of the measurement of the hydraulic gradient during the run-up.

wave height till the largest waves start to overtop the breakwater. The maximum hydraulic gradient seems to be affected by the overtopping. This is not the case for swell waves. From figure J.13 can also be observed that the normal core encounters a larger water level difference than the open core for swell waves and not for wind waves.

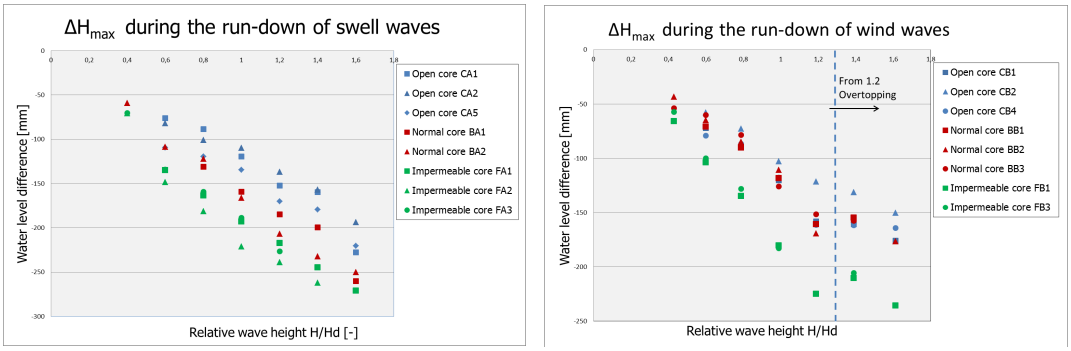

Fig. J.13: Maximum water level difference during run-down

The water level difference during the uprush is plotted against the relative wave height in figures J.14. From the figures can be observed that the maximum water level difference increases with wave height and wave period and exceeds the angle of vertical inflow, which is approximately 80mm. This suggests that the water flow on the armour layer has a larger velocity than the water can flow into the core. The run-up velocity increases with wave height leading to larger hydraulic gradients in the armour layer. It is difficult to draw more conclusions based on the maximum hydraulic gradient in the armour layer during the uprush.

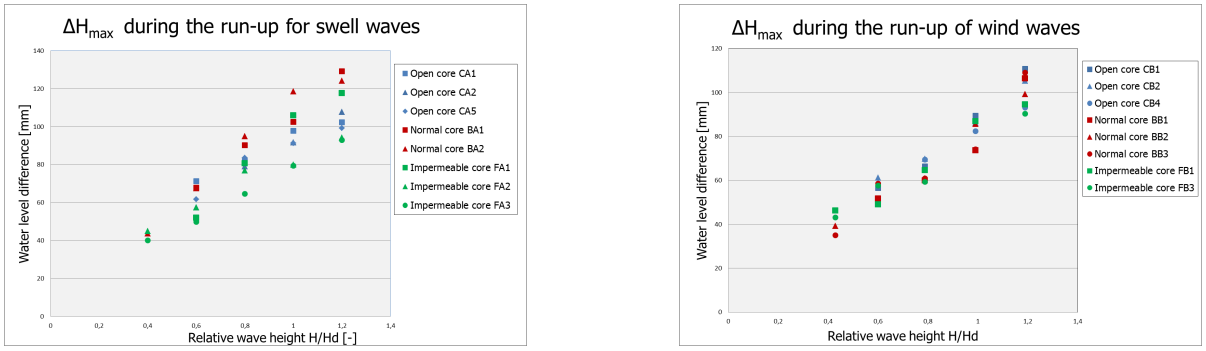

Fig. J.14: Maximum water level difference during run-up

The hydraulic gradient and water motion on the slope of the structure is plotted against time in figure

J.15. In the figure is the maximum run-down level indicated with a horizontal line and the location of the maximum hydraulic gradient with a vertical line. The distance in time between the maximum hydraulic and maximum run-down is indicated with a red horizontal line. It can be observed that the duration between the occurrence of the maximum hydraulic gradient and maximum run-down level becomes shorter with decreasing core permeability.

The consequence of a shorter duration between maximum hydraulic gradient and maximum run-down level can be related to the forces on the armour units. The backflow in the armour layer is maximum downward directed near the incident wave. This means that the backflow in the armour layer is forced to turn quickly into upward direction over a large angle within a short time. This results in large flow accelerations and inertia forces.

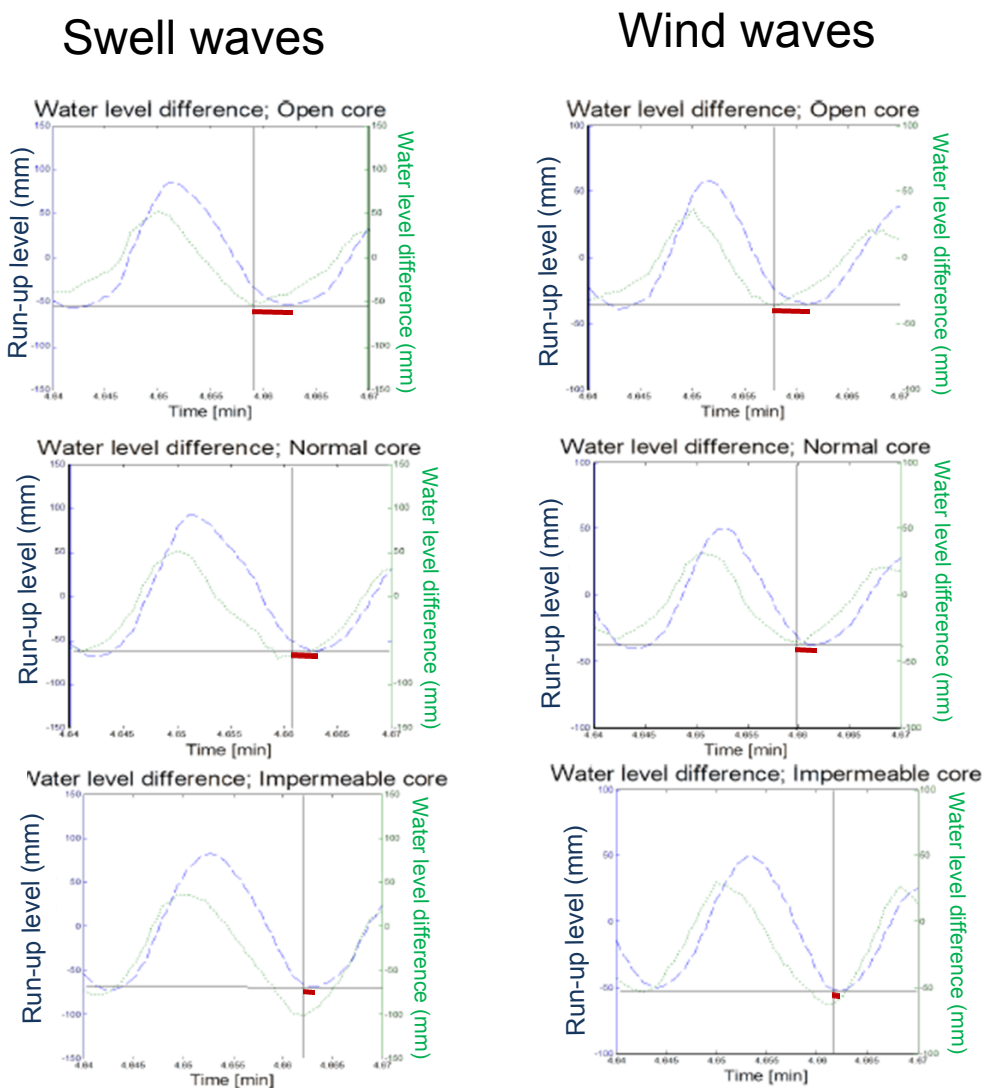

Fig. J.15: The water level difference versus wave run-up for the open, normal and impermeable core.

Empirical formula

Muttrray (2000) studied the hydraulic gradient in the armour layer, filter layer and core under regular waves in a rock armoured breakwater. The hydraulic gradient in the armour layer for in-flowing water is defined to be negative in the study of Muttray and positive for out-flowing water.
Muttray (2000) assumed that the hydraulic gradient ($\Delta\eta/\Delta x$) in the armour layer depends on horizontal particle velocity in shallow water, which corresponds to Rgk/ω with $R = H_i(1 + C_r)$. By multiplication

with $\sqrt{gd_{n50}}$ the following dimensional number was obtained:

$$\kappa_r = H_i(1 + C_r)\frac{k}{\omega}\sqrt{\frac{g}{d_{n50}}} \tag{J.7}$$

The hydraulic gradient is expressed in gradients, which is multiplied by 2 and divided by π resulting in $\arctan(\Delta\eta/\Delta x)2/\pi$.
The relation found by Muttrray (2000) between $\Delta\eta/\Delta x$ and κ_r is illustrated in figure J.16. From the figure can be observed that the greatest hydraulic gradients in the armour layer occur during the run-up (negative values) and the smallest during the run-down due the difference in Δx.
The negative values are bounded by the vertical inflow of water into the armour layer (value of 1). The positive gradient in the armour layer has also an upper boundary of 0.3, which is significant smaller than the negative values. The relation for a rock armour layer is defined by $\arctan(\Delta\eta/\Delta x)2/\pi$=0.129$\kappa_r$.

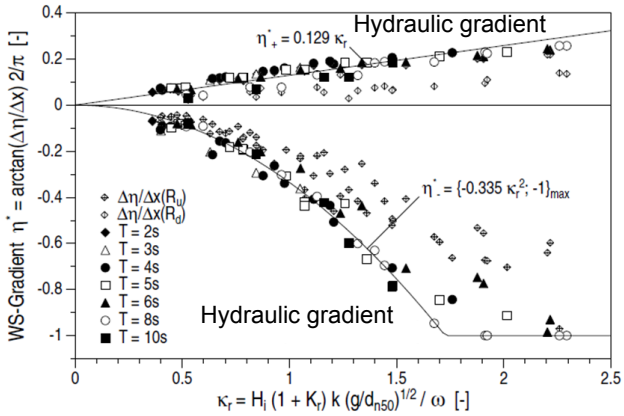

Fig. J.16: Hydraulic gradient in the armour layer found by Muttrray (2000) for rock armoured breakwaters

The positive hydraulic gradient in the study of Muttrray (2000) has been compared with the maximum hydraulic gradient in the armour layer during the run-down of this study. This comparison is not entirely correct as the model tests of Muttrray (2000) were conducted with a regular wave spectrum instead of the JONSWAP wave spectrum used in this study. Variations in wave height and wave period affect the hydraulic gradient. To obtain a significant difference between the theoretical data from equation J.7 and the measured data it was chosen to use the wave period and reflection coefficient related to the H_{max}.
The hydraulic gradient for the model test is calculated using the shortest distance between the run-up gauges, which is measured on 45 mm.

Figure J.17 presents both the obtained relation of Muttrray (2000) as the data of the model tests. From the figure can be observed that the theoretical trend-line for the hydraulic gradient show a good resembles with the measured values. However, the size of the theoretical and measured values show large differences. This might be adjusted to a key parameter in the equation J.7, which is the relation between wave length and wave height or wave steepness (s).
The model tests of Muttrray (2000) were conducted with three wave steepness between s=0.04 and s=0.1 on a slope of 1V:2H. This results in surf similarity parameters between ξ=2.5 and ξ=1.6, which are lower than the surf similarity parameter of the maximum wave height in this study, which are ξ=3.4 for swell waves and ξ=2.4 for wind waves.

In figure J.17 are the values related to swell waves illustrated with black borders around the marks. These marks fall outside the range in which the relation of Muttrray (2000) is applicable. This might explain the great difference between measured and theoretical gradient in the armour layer for ξ=3.4. The values related to swell waves hereafter omitted from the analysis.
The values related to wind waves are also presented in figure J.17 without a black border. It can be observed that the measured values are larger than theoretical values. The measured hydraulic gradients for the permeable core shows a better fit with 0.15κ_r instead of 0.129κ_r, which means an increase of

approximately 20%. The impermeable structure shows a better with $0.17\kappa_r$ instead of $0.129\kappa_r$, which is an increase of approximately 30%.

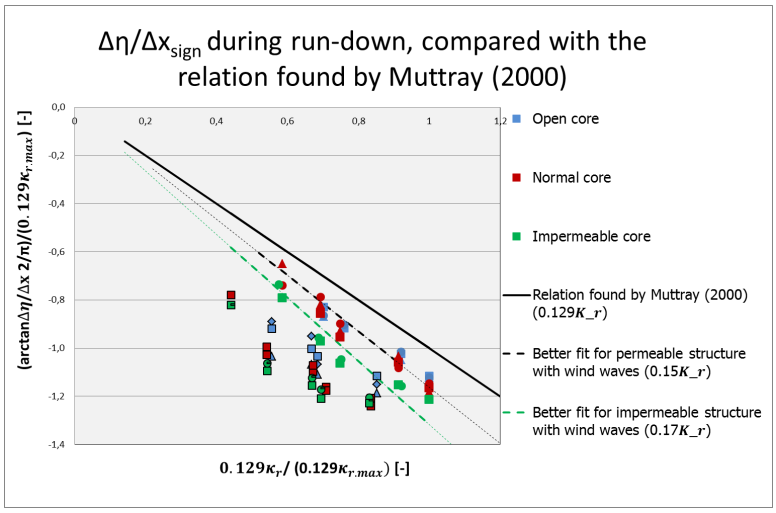

Fig. J.17: Measured significant hydraulic gradient in the armour layer during run-down compared with the equation found by Muttrray (2000) for rock armoured breakwaters under regular wave attack.

The increase of the hydraulic gradient can be adjusted to the single layer of armour units and steep slope angle in this study. Both the thickness of the armour layer as the slope angle influence the Δx, which determines the hydraulic gradient for a great part.
The hydraulic gradient can be a good indication of the size and the direction of the forces. The size and direction of the flow forces are important for the failure mechanism of the armour layer. An increase of the hydraulic gradient means an increase in flow velocity and flow forces. This means that single layer interlocking armour units encounter larger flow forces. However, the relative direction of this force is even of greater importance for the armour stability. The relative direction of the force on the armour units depend on the relation between slope angle and hydraulic gradient. The slope used in this study was 3V:4H, which is 40% steeper than used by Muttrray (2000). This means that the slope angle increases more than the hydraulic gradient for single layer interlocking armour units. It is therefore not possible to draw any conclusions on the difference in the relative direction of the flow forces between rock and interlocking armour units.

Overall, it can be concluded that a single layer armour units encounters larger hydraulic gradients in the armour layer during the run-down than rock armour units. This means that larger flow velocities occur and thereby larger flow forces on the armour units. However, it cannot be confirmed that the relative direction of the flow force on the armour units change due to the increased slope angle for single layer interlocking armour units.

Summary

The maximum hydraulic gradient during downrush increases with decreasing permeability. The consequence of this phenomena are larger flow velocities and thereby flow forces. The location of the maximum hydraulic gradient shifts in time towards the location of maximum run-down level. The combination of phase shift and increasing hydraulic gradient result in a larger rotation angle for the backflow within a shorter time period increasing the inertia forces on the armour units.
The measured hydraulic gradient during the run-down is compared with the empirical formula of Muttrray (2000) for rock armour layers. It was concluded that single layered armour units encounter larger hydraulic gradients in the armour layer than rock armour layer. It is concluded that interlocking armour units encounter larger forces than rock armour units. Despite the increase of the hydraulic gradient, no conclusions can be drawn on the relative direction of the force due to the increased slope angle of interlocking units.

J.5 Velocity

Measured data

The flow velocity is identified by various researcher (Izbash, 1930, Shield, 1936 and Morison, 1950) as an important parameter to express stone stability. Changes in the flow velocity along the slope due to decreased core permeability might also influence the damage progression of a Xbloc armour layer. The influence of the core permeability on the up- and downrush velocities are therefore analysed in this section of the thesis.

The maximum uprush velocity is plotted against the relative wave height in figure J.18. The maximum downrush is plotted against the relative wave height in figure J.19. From the figures follows that the maximum flow velocity on the armour layer is not influenced by the core permeability during the uprush and downrush. The swell waves are illustrated in the left figure and wind waves in the right figure. It can be observed that the maximum downrush of swell waves reaches a plateau, suggesting that the maximum downrush velocity has reached its upper boundary around the 80% wave height.

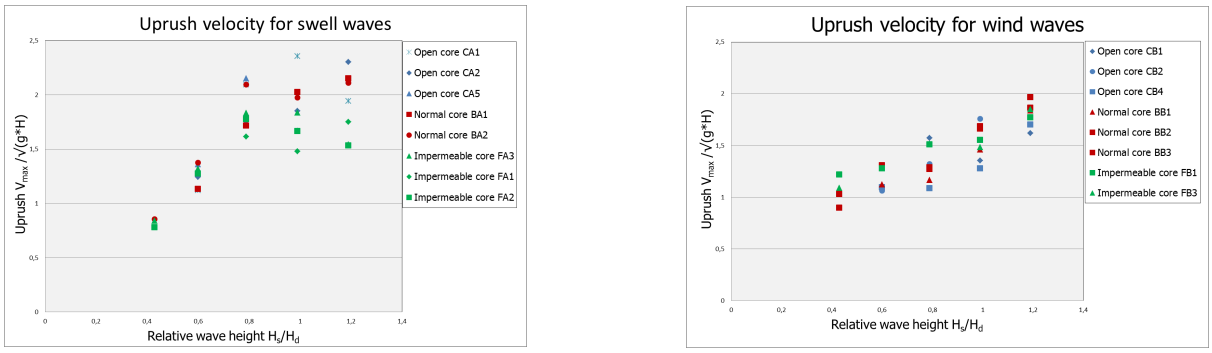

Fig. J.18: Water level difference around the armour layer at maximum run-up

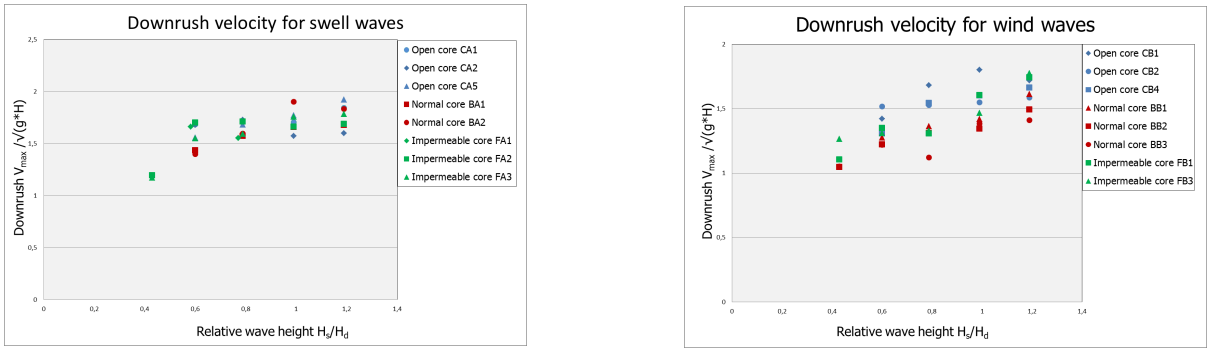

Fig. J.19: Water level difference around the armour layer at maximum run-up

The flow velocity along the slope is plotted against time in figure J.20. Irregular fluctuations in time in the flow velocity indicate turbulence. Turbulence is negative for the armour stability as a wake behind the unit is created generating a force in the direction of the flow. From the figure can be observed that not the maximum velocity differs but the rate of velocity change differs. The red line in the figure indicates the acceleration of the flow during the uprush.
It can be observed that the impermeable core encounters a larger flow acceleration or inertia forces than the open core. The difference in flow acceleration can be explained by the small storage area for the impermeable core in contrast to the open core. This reduces the inflow and therefore the increase in water level in the armour layer.

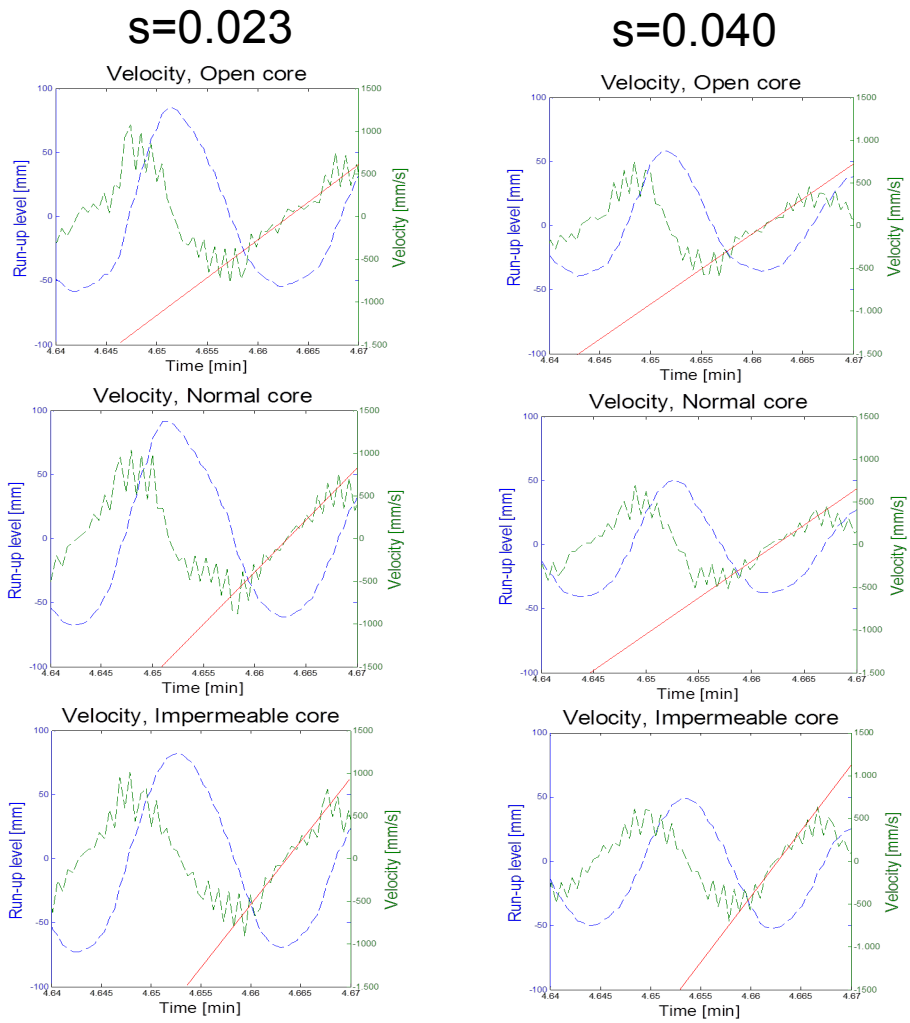

Fig. J.20: Flow velocity and water motion on the slope of the structure. The red line represents the rate that the flow velocity changes in time (60% wave height).

Summary

The maximum flow velocities parallel to the slope show no significant differences between the three core configurations. However, the acceleration shows an increase with decreasing permeability increasing inertia forces on the armour layer.

J.6 Wave reflection

Measured data

The reflected wave from the breakwater towards the sea is a characteristic of the wave structure interaction. The ratio H_r/H_i is the representation of the proportion of wave energy that flows back to the sea, identified as C_r as mentioned in section 2.3.

During the model tests the reflective wave is distinguished from the incoming wave using the method of Mansard and Funke (1980). The measured reflected coefficient is plotted against the relative wave height in figure J.21. From the figure can be concluded that the reflection coefficient depends on wave height, wave length and structural permeability. The dependence of the reflection coefficient on the wave length and wave height can be observed in figure J.22 were the reflection coefficient set-out against the wave length.

In figure J.22 can be observed that an impermeable core gives larger reflection coefficients, which was expected. The reflection coefficients for normal core start to vary from the open core for longer waves, which carry a larger water volume.

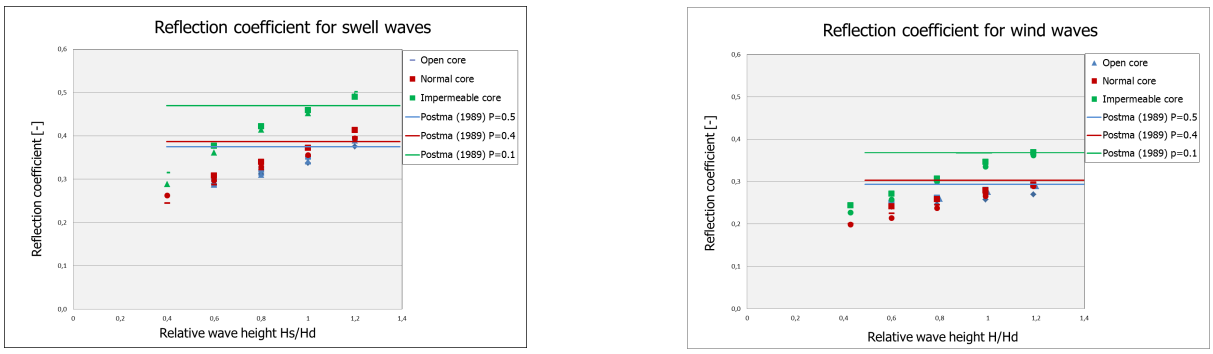

Fig. J.21: Reflection coefficient versus percentage of the design wave height

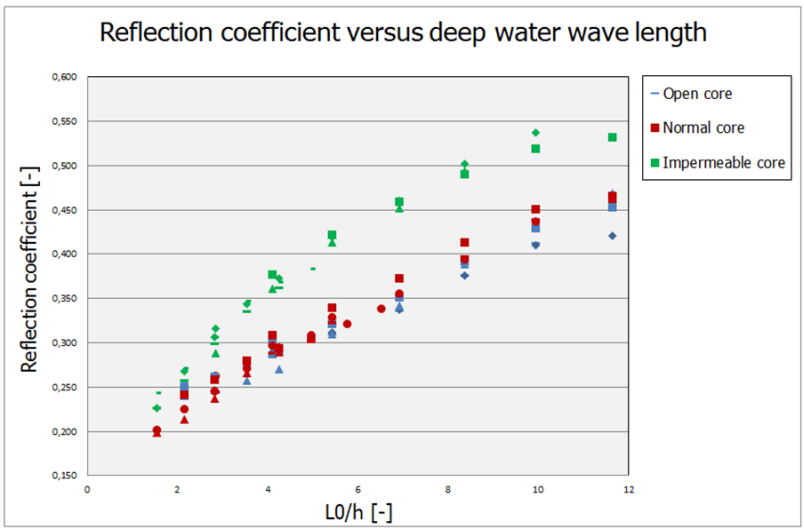

Fig. J.22: Reflection coefficient versus the deep water wave length

Empirical formula

The reflection coefficient regarding core permeability has been studied by Postma (1989) (CIRIA, 2007). According to Postma (1989), the reflection coefficient depends on the slope angle (α), fictitious wave steepness (s_{op}) and permeability of the construction (P). The parameters are related to each other as in the following formula.

$$C_r = \frac{0.081}{P^{0.14}(cot\alpha)^{0.78}s_{op}^{0.44}} \tag{J.8}$$

Besides the measured data in figure J.21, the figures present the theoretical reflection coefficient from the formula of Postma (1989). The horizontal lines in figure J.21 illustrate the theoretical coefficients for P=0.1 (green), P=0.4 (red) and P=0.5 (blue) obtained from equation J.8. From figure J.21 and equation J.8 can be observed that Postma (1989) suggest a constant reflection coefficient for an individual wave steepness. The relation between wave steepness and reflection coefficient cannot be confirmed by the measured reflection coefficients.
The theoretical reflection coefficient shows a good indication of the size of the reflection coefficient of the 100% and 120% wave height. The ratio between the open, normal and impermeable core is also good predicted for these wave heights. This means that equation J.8 is applicable for the most important wave heights and therefore usable for practical use but not for research.

Proposed relation

Both the swell as the wind waves in figure J.21 illustrate a linear relation (Ax+B) between the reflection coefficient and the relative wave height (H_s/H_d). The design wave height that is incorporated in the relative wave height on the horizontal axis is taken into account to make the wave height dimensionless. However, it might also indicate the relative thickness of the armour layer regarding the wave height. The relative thickness of the armour layer is of importance for the energy dissipation and thereby wave reflection.

The term B is constant for a single wave steepness and relates only on the fictitious wave steepness (s_{op}). The relation found from the data in this study is $\sqrt{0.0009/s_{op}}$.
The term A depends on both the permeability and fictitious wave steepness in the relation $0.33 - 3s_{op} - 0.2P$. The relation between the wave steepness, 'notional' Permeability (P) and the thickness of the armour layer is as follows:

$$C_r = 0.33 - 3s_{op} - 0.2P \cdot \frac{H_s}{H_d} + \sqrt{\frac{0.0009}{s_{op}}} \tag{J.9}$$

The fit between the measured data obtained from the model tests and equation J.9 is illustrated in figure J.23.

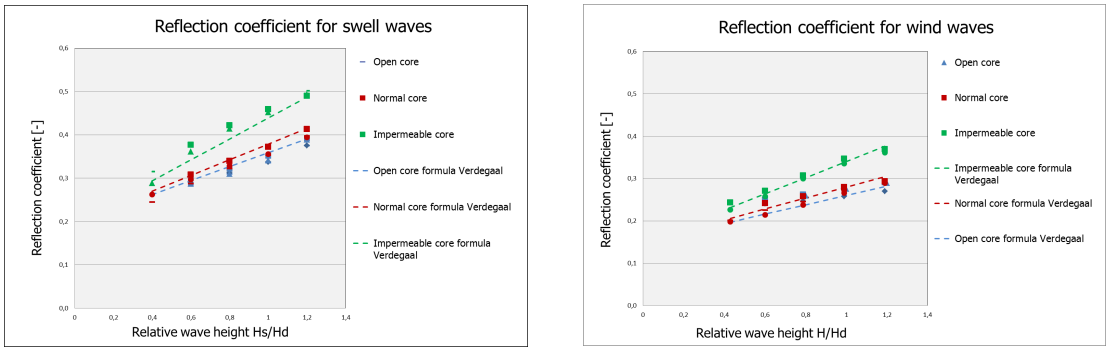

Fig. J.23: Fit between equation J.9 and data from the model tests

Summary

The influence of the core permeability is visible on the reflection coefficient. An impermeable core reflects a significant larger proportion of the wave than a normal or open core. This was expected by the fact that no water can penetrate into the core and must flow back into the sea.
Although the difference in reflection is smaller between the normal and open core, this difference increases with the length of the wave. From a theoretical point of view this can be explained by the larger water volume for longer waves and limited storage area in the core.

The empirical formula prescribed by Postma (1989) for rock armour layer is not valid for single layer interlocking armour layers. The suggested relation by Postma (1989) depends on the fictitious wave steepness and is independent of the wave height, which is in particular of importance.
A new formula is set-up that encounters the fictious wave steepness, structural permeability and wave height.

$$C_r = 0.33 - 3s_{op} - 0.2P \cdot \frac{H_s}{H_d} + \sqrt{\frac{0.0009}{s_{op}}} \tag{J.10}$$